

UNIVERSITY OF CALIFORNIA
Santa Barbara

Dynamics and Control in Power Grids and
Complex Oscillator Networks

A Dissertation submitted in partial satisfaction
of the requirements for the degree of

Doctor of Philosophy

in

Mechanical Engineering

by

Florian Anton Dörfler

Committee in Charge:

Professor Francesco Bullo, Chair

Professor Bassam Bamieh

Professor Igor Mezic

Professor Jeff Moehlis

Professor João Hespanha

September 2013

The Dissertation of
Florian Anton Dörfler is approved:

Professor Bassam Bamieh

Professor Igor Mezic

Professor Jeff Moehlis

Professor João Hespanha

Professor Francesco Bullo, Committee Chairperson

May 2013

Dynamics and Control in Power Grids and Complex Oscillator Networks

Copyright © 2013

by

Florian Anton Dörfler

To my family and my friends.

Acknowledgements

First and foremost, I must thank my advisor Francesco Bullo for his guidance and support and for serving as a role model in research and life in general. He taught me many invaluable lessons and was a constant source of inspiration. It was his enthusiasm for science that gave me the confidence and persistence to tackle my research problems. Finally, I truly appreciate that he gave me all the flexibility I needed to pursue my own agenda in research and other “extra-curricular” projects.

I am very grateful to my committee members Bassam Bamieh, João Hespanha, Igor Mezic, and Jeff Moehlis for their great lectures and for our constructive interactions when discussing my research problems. They are true scholars who understand to ask the right questions which reveal the weaknesses in my research.

I am indebted to my previous advisors Bruce Francis and Frank Allgöwer who taught me the fundamentals of control theory and dynamical systems. They sparked my interest in science, they encouraged me to pursue my graduate studies, and they have been supportive and a constant source of advice ever since.

I extremely benefitted from interactions with various people at the Center for Control, Dynamical Systems, and Computation. I must thank Petar Kokotovic for his advice on my research and life outside academia. Thanks to Brad Paden for his lessons on how to deliver an enthusiastic talk, thanks to Sandro Zampieri for sharing many small lessons, and thanks to Andy Teel for being a great instructor.

I have been fortunate to work with several wonderful collaborators. Thanks to Misha Chertkov for hosting me in Los Alamos, where I was able to simultaneously pursue my research “outside the box” as well as my personal objectives. Thanks to John Simpson-Porco for being a source of creativity, for his innovative ideas, and for his persistence and hard work in our common projects. Thanks to Fabio Pasqualetti for being a great friend, for teaching me lots of beautiful geometry, and for his enthusiasm driving our common work. Thanks to Mihailo Jovanovic for his help that I needed when exploring new terrain. Thanks to Diego Romeres and Hedi Bouattour for all the great interactions, fun times, and for teaching me many lessons on advising. Finally, I want to thank all permanent and visiting members of Francesco’s group for many great discussions and all the good times.

My thanks for my family will never be enough. This achievement and many past ones live on the support, the comforting words, and the care of my dear ones. Thanks to my housemates in Santa Barbara, Goleta, and Los Alamos, and thanks to my friends in the old and in the new world. Thanks for your support, your loyalty, and for grounding me whenever I was drifting away in my academic projects. Finally, a special thanks to Phillip Fanchon for being a great mentor, a true role model, and for providing me with his mountain retreat to write this thesis.

Finally, thank you Katrin, for your incredible patience, all your support, your sweet smile, and all the great shared memories and experiences.

Curriculum Vitæ Florian Anton Dörfler

Education

2008 Diplom in Engineering Cybernetics, University of Stuttgart

Honors and Awards

2013 Top Five Finalist for Best Student Paper Award at European Control Conference (as co-author and co-advisor)
2011 – 2012 Peter J. Frenkel Foundation Fellowship (institutional award)
2011 O. Hugo Schuck Best Paper Award (awarded by American Automatic Control Council for theoretical contributions)
2010 Best Student Paper Award at American Control Conference
2009 – 2013 Regent’s Special International Fellowship (institutional award)
2008 Baden-Württemberg Stipendium Renewed (national scholarship)
2007–2008 Baden-Württemberg Stipendium (national scholarship)
2007–2008 Ontario Baden-Württemberg Program Fellow (national scholarship)

Research Interests

1. Synchronization and dynamic phenomena in complex networks
2. Control, monitoring, optimization in energy systems and smart grids
3. Distributed control, monitoring, and security in cyber-physical systems
4. Cooperative control and coordination in multi-agent systems

Research Experience

2009 – 2013 Graduate Research Assistant, University of California Santa Barbara
2011 – 2013 Visiting Student Researcher, Los Alamos National Laboratories
2009 Visiting Scholar, University of California Santa Barbara
2008 Corporate Research Intern, EADS Astrium
2007 – 2008 Graduate Student Researcher, University of Toronto
2007 Student Research Assistant, University of Stuttgart

Teaching Experience and Mentoring

2011 – 2013 **Graduate Student Mentor**, University of California Santa Barbara
Students: Diego Romeres, Hedi Bouattour, and John W. Simpson-Porco

- 2011 – 2012 **Teaching Assistant**, University of California at Santa Barbara
 Teaching assistant for Engineering Mechanics: Dynamics
 Guest lecturer for course Distributed Systems and Control
- 2005 – 2008 **Teaching Assistant**, University of Stuttgart
 Teaching assistant for Advanced Mathematics II
 Teaching assistant for Simulation Engineering Scientific Computing
- 2006 **Course Instructor**, Study Guards, Stuttgart
 Summer school instructor for Advanced Mathematics I & II

Research Awards

I have contributed to the writing of the following award:

- 2011 NSF CPS Medium: *The Cyber-Physical Challenges of Transient Stability and Security in Power Grids*

Professional Service

Technical Reviewer

- Journals IEEE Transactions on Automatic Control, Automatica, IEEE Transactions on Control Systems Technology, Systems and Control Letters, European Journal of Control, Control Systems Magazine, Robotics and Autonomous Systems, Nonlinear Analysis: Hybrid Systems, Communications in Mathematical Sciences, Journal of Mathematical Physics, Physica D, SIAM Journal on Applied Dynamical Systems, International Journal of Electrical Power and Energy Systems, Journal of Process Control, IEEE Transactions on Power Systems
- Conferences American Control Conference, IEEE Conference on Decision and Control, IFAC World Congress, European Control Conference, IFAC Workshop on Distributed Estimation and Control in Networked Systems, Multi-conference on Systems and Control, Mediterranean Conference on Control and Automation

Organizer/Co-organizer

- 2011 Santa Barbara Control Workshop 2011

Chair/Co-Chair

- 2011 Session on *Electrical Power Systems I* at IEEE Conference on Decision and Control and European Control Conference, Orlando, FL, USA, December 2011.

Invited Workshops and Tutorials

- 2011 Workshop on *Control Systems Security: Challenges and Directions* at IEEE Conference on Decision and Control and European Control Conference, Orlando, FL, USA, December 2011.
- 2012 Tutorial on *Synchronization in Coupled Oscillators: Theory and Applications* at IEEE Conference on Decision and Control, Maui, HI, USA, December 2012.

Professional Affiliations

- 2009 – Student Member, Institute for Electrical and Electronics Engineers (IEEE)
IEEE Societies: Control Systems Society and Power and Energy Society
- 2009 – Student Member, Society for Industrial and Applied Mathematics (SIAM)

Invited Talks

- Jul 2013 Center for Nonlinear Studies, Los Alamos National Laboratories
- Jun 2013 Hybrid Control Systems Workshop, Technical University München
- Jun 2013 Symposium on Complex Systems Control, ETH Zürich
- Mar 2013 Department of Electrical Engineering, UC Los Angeles
- Mar 2013 Electrical and Computer Engineering, Georgia Institute of Technology
- Feb 2013 Center for Nonlinear Studies, Los Alamos National Laboratories
- Oct 2012 Automatic Control Laboratory, ETH Zürich
- Jul 2012 Institute for Systems Theory and Automatic Control, University of Stuttgart
- Jul 2012 Siemens Colloquium, Siemens AG, Munich
- Apr 2012 Department of Mathematics, UI Urbana-Champaign
- Feb 2012 Department of Electrical Engineering, UC Los Angeles
- Oct 2011 Institute for Energy Efficiency, UC Santa Barbara
- Jun 2011 Center for Nonlinear Studies, Los Alamos National Laboratories
- Sep 2010 Systems Control Group, University of Toronto
- Aug 2010 Institute of Automatic Control Engineering, Technical University Munich
- May 2010 Control and Dynamical Systems, California Institute of Technology

Publications

Journal Publications

- [J1] F. Dörfler, M. Jovanović, M. Chertkov, and F. Bullo. Sparsity-promoting optimal wide-area control of power networks. *IEEE Transactions on Power Systems*, July 2013. Note: submitted.

- [J2] F. Dörfler and F. Bullo. Synchronization in complex oscillator networks: A survey. *Automatica*, April 2013. Note: submitted.
- [J3] F. Dörfler, F. Pasqualetti, and F. Bullo. Continuous-time distributed observers with discrete communication. *IEEE Journal of Selected Topics in Signal Processing*, 7(2):296–304, April 2013.
- [J4] F. Dörfler, M. Chertkov, and F. Bullo. Synchronization in complex oscillator networks and smart grids. *Proceedings of the National Academy of Sciences*, 110(6):2005–2010, February 2013.
- [J5] F. Dörfler and F. Bullo. Kron reduction of graphs with applications to electrical networks. *IEEE Transactions on Circuits and Systems I: Regular Papers*, 60(1):150–163, January 2013.
- [J6] J. W. Simpson-Porco, F. Dörfler, and F. Bullo. Synchronization and power sharing for droop-controlled inverters in islanded microgrids. *Automatica*, 49(9): 2603–2611, September 2013.
- [J7] F. Pasqualetti, F. Dörfler, and F. Bullo. Attack detection and identification in cyber-physical systems. *IEEE Transactions on Automatic Control*, August 2012. Note: to appear.
- [J8] F. Dörfler and F. Bullo. Synchronization and transient stability in power networks and non-uniform Kuramoto oscillators. *SIAM Journal on Control and Optimization*, 50(3):1616–1642, 2012.
- [J9] F. Dörfler and F. Bullo. On the critical coupling for Kuramoto oscillators. *SIAM Journal on Applied Dynamical Systems*, 10(3):1070–1099, 2011.
- [J10] F. Dörfler and B. Francis. Geometric Analysis of the Formation Problem for Autonomous Robots. *IEEE Transactions on Automatic Control*, 55(10):2379–2384, October 2010.
- [J11] F. Dörfler, J. K. Johnsen, and F. Allgöwer. An Introduction to Interconnection and Damping Assignment Passivity-Based Control in Process Engineering. *Journal of Process Control*, 19(9):1413–1426, October 2009.

Refereed Conference Proceedings

- [C1] F. Dörfler and F. Bullo. Novel Insights into Lossless AC and DC Power Flow. In *IEEE Power & Energy Society General Meeting*, July 2013. Note: to appear.
- [C2] D. Romeres, F. Dörfler, and F. Bullo. Novel results on slow coherency in consensus and power networks. In *European Control Conference, Zürich, Switzerland*, July 2013. Note: to appear.
- [C3] J. W. Simpson-Porco, F. Dörfler, Q. Shafiee, J. M. Guerrero, and F. Bullo. Stability, power sharing, & distributed secondary control in droop-controlled microgrids. In *IEEE Int. Conf. on Smart Grid Communications*, October 2013. Note: to appear.

- [C4] F. Dörfler, M. Jovanovic, M. Chertkov, and F. Bullo. Sparse and optimal wide-area damping control in power networks. In *American Control Conference*, Washington, DC, USA, June 2013. Note: to appear.
- [C5] H. Bouattor, J. W. Simpson-Porco, F. Dörfler, and F. Bullo. Further results on distributed secondary control in microgrids. In *IEEE Conf. on Decision and Control*, March 2013. Note: to appear.
- [C6] J. W. Simpson-Porco, F. Dörfler, and F. Bullo. Voltage stabilization in microgrids using quadratic droop control. In *IEEE Conf. on Decision and Control*, February 2013. Note: to appear.
- [C7] F. Dörfler and F. Bullo. Exploring synchronization in complex oscillator networks. In *IEEE Conf. on Decision and Control*, pages 7157–7170, Maui, HI, USA, December 2012.
- [C8] F. Dörfler, M. Chertkov, and F. Bullo. Synchronization assessment in power networks and coupled oscillators. In *IEEE Conf. on Decision and Control*, pages 4998–5003, Maui, HI, USA, December 2012.
- [C9] F. Pasqualetti, F. Dörfler, and F. Bullo. Cyber-physical security via geometric control: Distributed monitoring and malicious attacks. In *IEEE Conf. on Decision and Control*, pages 3418–3425, Maui, HI, USA, December 2012.
- [C10] J. W. Simpson-Porco, F. Dörfler, and F. Bullo. Droop-controlled inverters are Kuramoto oscillators. In *IFAC Workshop on Distributed Estimation and Control in Networked Systems*, pages 264–269, Santa Barbara, CA, USA, September 2012.
- [C11] F. Dörfler and F. Bullo. Topological equivalence of a structure-preserving power network model and a non-uniform Kuramoto model of coupled oscillators. In *IEEE Conf. on Decision and Control and European Control Conference*, pages 7099–7104, Orlando, FL, USA, December 2011.
- [C12] F. Pasqualetti, F. Dörfler, and F. Bullo. Cyber-physical attacks in power networks: Models, fundamental limitations and monitor design. In *IEEE Conf. on Decision and Control and European Control Conference*, pages 2195–2201, Orlando, FL, USA, December 2011.
- [C13] F. Dörfler, F. Pasqualetti, and F. Bullo. Distributed detection of cyber-physical attacks in power networks: A waveform relaxation approach. In *Allerton Conf. on Communications, Control and Computing*, pages 1486–1491, September 2011.
- [C14] F. Dörfler and F. Bullo. On the critical coupling strength for Kuramoto oscillators. In *American Control Conference*, pages 3239–3244, San Francisco, CA, USA, June 2011.
- [C15] F. Dörfler and F. Bullo. Spectral Analysis of Synchronization in a Lossless Structure-Preserving Power Network Model. In *Proceedings of the 1st IEEE Conference on Smart Grid Communications in Gaithersburg, Maryland, USA*, pages 179–184, October 2010.

- [C16] F. Dörfler and F. Bullo. Synchronization of Power Networks: Network Reduction and Effective Resistance. In *Proceedings of the 2nd IFAC Workshop on Distributed Estimation and Control in Networked Systems in Annecy, France*, pages 197–202, September 2010.
- [C17] F. Dörfler and F. Bullo. Synchronization and Transient Stability in Power Networks and Non-Uniform Kuramoto Oscillators. In *Proceedings of the American Control Conference in Baltimore, Maryland, USA*, pages 930–937, June 2010.
- [C18] T. D. Krøvel, F. Dörfler, M. Berger, and J. M. Rieber. High-Precision Spacecraft Attitude and Manoeuvre Control Using Electric Propulsion. In *Proceedings of the 60th International Astronautical Congress in Seoul, Korea*, October 2009.
- [C19] F. Dörfler and B. Francis. Formation control of autonomous robots based on cooperative behavior. In *European Control Conference in Budapest*, pages 2432–2437, Budapest, Hungary, August 2009.
- [C20] J. K. Johnsen, F. Dörfler, and F. Allgöwer. \mathcal{L}_2 -gain of Port-Hamiltonian systems and application to a biochemical fermenter. In *American Control Conference*, pages 153–158, Seattle, Washinton, USA, June 2008.

Theses

- [T1] F. Dörfler. *Geometric Analysis of the Formation Problem for Autonomous Robots*. Diploma thesis, University of Toronto, Canada, August 2008.
- [T2] F. Dörfler. *Port-Hamiltonian Systems – Stability Analysis and Application in Process Control*. Student thesis, University of Stuttgart, Germany, July 2007.

Miscellaneous

- [M1] F. Dörfler, M. Jovanović, M. Chertkov, and F. Bullo. Sparsity-promoting optimal wide-area control of power networks, July 2013. Note: available at <http://arxiv.org/abs/1307.4342>.
- [M2] J. W. Simpson-Porco, F. Dörfler, and F. Bullo. Synchronization and power sharing for droop-controlled inverters in islanded microgrids, November 2012. Note: available at <http://arxiv.org/abs/1206.5033>.
- [M3] F. Dörfler and F. Bullo. Exploring synchronization in complex oscillator networks, September 2012. Extended version including proofs. Note: available at <http://arxiv.org/abs/1209.1335>.
- [M4] F. Dörfler, M. Chertkov, and F. Bullo. Synchronization in complex oscillator networks and smart grids, July 2012. Note: available at <http://arxiv.org/abs/1208.0045>.

- [M5] J. W. Simpson-Porco, F. Dörfler, and F. Bullo. Droop-controlled inverters are Kuramoto oscillators, June 2012. Note: available at <http://arxiv.org/pdf/1206.5033v1.pdf>.
- [M6] F. Pasqualetti, F. Dörfler, and F. Bullo. Attack detection and identification in cyber-physical systems – Part I: Models and fundamental limitations, February 2012. Note: available at <http://arxiv.org/abs/1202.6144>.
- [M7] F. Pasqualetti, F. Dörfler, and F. Bullo. Attack detection and identification in cyber-physical systems – Part II: Centralized and distributed monitor design, February 2012. Note: available at <http://arxiv.org/abs/1202.6049>.
- [M8] F. Pasqualetti, F. Dörfler, and F. Bullo. Cyber-physical attacks in power networks: Models, fundamental limitations and monitor design, September 2011. Note: available at <http://arxiv.org/abs/1103.2795>.
- [M9] F. Dörfler and F. Bullo. Kron reduction of graphs with applications to electrical networks, February 2011. Note: available at <http://arxiv.org/abs/1102.2950>.
- [M10] F. Dörfler and F. Bullo. On the critical coupling for Kuramoto oscillators, November 2010. Note: available at <http://arxiv.org/abs/1011.3878>.
- [M11] F. Dörfler and B. Francis. Geometric Analysis of the Formation Problem for Autonomous Robots, January 2010. Note: available at <http://arxiv.org/abs/1001.4494>.
- [M12] F. Dörfler and F. Bullo. Synchronization and transient stability in power networks and non-uniform Kuramoto oscillators, October 2009. Note: available at <http://arxiv.org/abs/0910.5673>.

Abstract

Dynamics and Control in Power Grids and Complex Oscillator Networks

Florian Anton Dörfler

The efficient production, transmission and distribution of electrical power underpins our technological civilization. Public policy and environmental concerns are leading to an increasing adoption of renewable energy sources and the deregulation of energy markets. These trends, together with an ever-growing power demand, are causing power networks to operate increasingly closer to their stability margins. Recent scientific advances in complex networks and cyber-physical systems along with the technological re-instrumentation of the grid provide promising opportunities to handle the challenges facing our future energy supply. In this thesis, we discuss the synchronization problem in power networks, which is central to their operation and functionality. We identify and exploit a close connection between the mathematical models for power networks and complex oscillator networks. Our main contributions are concise, sharp, and purely-algebraic conditions that relate synchronization in a power grid to graph-theoretical properties of the underlying electric network. Our novel conditions hold for arbitrary interconnection topologies and network parameters, and they significantly improve upon

previously-available tests. We illustrate how our results help in the analysis of large-scale transmission systems and lead to novel control strategies and their implementation in microgrids. Our approach combines traditional power engineering methods, synchronization theory for coupled oscillators, and control in multi-agent dynamical systems. Beside their applications in power networks, our mathematically-appealing results are also broadly applicable in synchronization phenomena ranging from natural and life sciences to engineering disciplines.

Professor Francesco Bullo
Dissertation Committee Chair

Contents

Acknowledgements	v
Curriculum Vitæ	vii
Abstract	xiv
List of Figures	xix
1 Introduction	1
1.1 Literature Synopsis	5
1.1.1 Synchronization in Complex Oscillator Networks	5
1.1.2 Synchronization and Stability in Power Networks	10
1.2 Contributions and Organization	15
2 Preliminaries, Models, and Synchronization Notions	20
2.1 Preliminaries in Algebraic Graph Theory	20
2.2 Oscillator Network Models and Synchronization Problems	25
2.2.1 Electric Power Networks	25
2.2.2 Additional Examples of Complex Oscillator Networks	33
2.3 Synchronization Notions and Concepts	41
2.3.1 Synchronization Notions	41
2.3.2 A Simple yet Illustrative Example	47
2.4 Consensus, Convexity, & Contraction	50
2.4.1 Consensus Protocols	50
2.4.2 Homogeneous Oscillator Networks as Nonlinear Consensus Protocols	53

3	Mechanical and Kinematic Oscillator Networks	57
3.1	Introduction	58
3.1.1	Relevant Literature	58
3.1.2	Contributions and Organization	61
3.2	Hamiltonian and Gradient Formulation	64
3.2.1	Classic Transient Stability Analysis Approaches	65
3.2.2	Potential Landscape and Jacobian Analysis	68
3.3	Topological Conjugacy	72
3.3.1	A One-Parameter Family of Dynamical Systems and its Properties	72
3.3.2	Equivalence of Local Synchronization Conditions	78
3.3.3	Phase Synchronization in Oscillator Networks	84
3.3.4	The Role of Inertia and Dissipation for Transient and Non-Symmetric Dynamics	87
3.4	Approximation by Singular Perturbation Methods	91
3.4.1	Symmetry Reduction and Grounded Variables	92
3.4.2	Singular Perturbation Analysis	97
3.4.3	Discussion of the Perturbation Assumption	104
3.5	Comparison and Alternative Relations	106
4	The Critical Coupling for Kuramoto Oscillators	108
4.1	Introduction	109
4.1.1	Relevant Literature	109
4.1.2	Contributions and Organization	111
4.2	Infinite-Dimensional Kuramoto Oscillator Networks	114
4.2.1	The Continuum Limit Model	115
4.2.2	Synchronization Phenomenology in the Continuum-Limit Model	116
4.2.3	Estimates on the Critical Coupling Strength	118
4.3	Finite-Dimensional Kuramoto Oscillator Networks	122
4.3.1	Synchronization Metrics in Kuramoto Oscillator Networks	122
4.3.2	Estimates on the Critical Coupling Strength	125
4.4	Explicit and Tight Conditions on the Critical Coupling	133
4.4.1	Boundedness and Contraction Analysis Insights	134
4.4.2	The Contraction Property and the Main Synchronization Result	138
4.4.3	Comparison and Statistical Analysis	149
4.4.4	Frequency Synchronization of Multi-Rate Kuramoto Oscillators	152

4.5	Applications to Network-Reduced Power System Models	155
5	Synchronization in Complex Oscillator Networks	159
5.1	Introduction	160
5.1.1	Relevant Literature	160
5.1.2	Contributions and Organization	162
5.2	Some Necessary or Sufficient Conditions	165
5.2.1	Absolute and Incremental Boundedness	165
5.2.2	Sufficient Synchronization Conditions	166
5.3	Towards an Exact Synchronization Condition	177
5.3.1	Norm and Cycle Constraints	177
5.3.2	Synchronization Assessment for Specific Networks	182
5.3.3	Statistical Synchronization Assessment	196
5.4	Applications to Structure-Preserving Power System Models	200
5.4.1	Synchronization and Security Assessment	200
5.4.2	Monitoring and Contingency Screening	206
5.4.3	Further Applications	209
6	Conclusions	212
6.1	Summary	212
6.2	Tangential and Related Contributions	215
6.3	Future Research Directions	217
	Bibliography	224

List of Figures

1.1	Mechanical analog of a coupled oscillator network	3
1.2	Dynamics of mechanical spring network	5
2.1	Illustration of different power network diagrams	26
2.2	Illustration of the power network devices as circuit elements . . .	26
2.3	Illustration of controlled planar particle dynamics	35
2.4	Schematic illustration of diffusion-based clock synchronization . .	38
2.5	Illustration of synchronization concepts	41
2.6	Illustration of the geometric concepts in the configuration space \mathbb{T}^2	47
2.7	Graphical analysis of two coupled oscillators	49
3.1	Topological conjugacy of first and second-order oscillator dynamics	81
3.2	Region of attraction of the forced pendulum dynamics	89
3.3	Illustration of the grounded map	93
3.4	Illustration of the singular perturbation approximation	103
4.1	Synchronization in the continuum limit model	117
4.2	Extremal distributions of the natural frequencies and phases . . .	123
4.3	Arc invariance and order parameter	124
4.4	Illustration of the contraction Lyapunov function	139
4.5	Kuramoto oscillators with time-varying natural frequencies	150
4.6	Statistical analysis of the critical coupling estimates	152
5.1	Energy landscape interpretation of the synchronization condition .	186
5.2	Cycle graph with $n = 5$ nodes and non-symmetric choice of ω . . .	194
5.3	Synchronization threshold in a complex Kuramoto oscillator network	201
5.4	Histogram of the prediction errors	205
5.5	Illustration of contingencies the RTS 96 power network.	207
5.6	The RTS 96 dynamics at the transition to instability	210

Chapter 1

Introduction

On 1 March 1665, Sir Robert Moray read to the Royal Society a letter from Christiaan Huygens, dated 27 February 1665, reporting of

[...] an odd kind of sympathy perceived by him in these watches.

(A comment on the interaction of two maritime pendulum clocks suspended by the side of each other [26].)

Synchronization in networks of coupled oscillators is a pervasive topic in various scientific disciplines ranging from biology, physics, and chemistry to social networks and technological applications. A coupled oscillator network is characterized by a population of heterogeneous oscillators and a graph describing the interaction among the oscillators. These two ingredients give rise to a rich dynamic behavior that keeps on fascinating the scientific community.

Within the rich modeling phenomenology on synchronization among coupled oscillators, this thesis focuses on the canonical model of a continuous-time limit-cycle oscillator network with continuous, bidirectional, and sinusoidal coupling.

We consider a system of n oscillators, each characterized by a phase angle $\theta_i \in \mathbb{S}^1$ and a natural rotation frequency $\omega_i \in \mathbb{R}$. We assume that the set of oscillators $\mathcal{V} = \{1, \dots, n\}$ is partitioned into the sets \mathcal{V}_1 and \mathcal{V}_2 , which we will later identify with mechanical and kinematic oscillators, respectively. The interaction topology and coupling strength among the oscillators are modeled by a connected, undirected, and weighted graph $G = (\mathcal{V}, \mathcal{E}, A)$ with nodes $\mathcal{V} = \{1, \dots, n\}$, edges $\mathcal{E} \subset \mathcal{V} \times \mathcal{V}$, and positive weights $a_{ij} = a_{ji} > 0$ for each undirected edge $\{i, j\} \in \mathcal{E}$. The interaction between neighboring oscillators is assumed to be additive, anti-symmetric, diffusive,¹ and proportional to the coupling strengths a_{ij} . In this case, the simplest 2π -periodic interaction function between neighboring oscillators $\{i, j\} \in \mathcal{E}$ is $a_{ij} \sin(\theta_i - \theta_j)$, and the overall model of coupled oscillators reads

$$M_i \ddot{\theta}_i + D_i \dot{\theta}_i = \omega_i - \sum_{j=1}^n a_{ij} \sin(\theta_i - \theta_j), \quad i \in \mathcal{V}_1, \quad (1.1a)$$

$$D_i \dot{\theta}_i = \omega_i - \sum_{j=1}^n a_{ij} \sin(\theta_i - \theta_j), \quad i \in \mathcal{V}_2, \quad (1.1b)$$

where $\theta_i \in \mathbb{S}^1$ and $\dot{\theta}_i \in \mathbb{R}^1$ are the phase and frequency of oscillator $i \in \mathcal{V}$, $\omega_i \in \mathbb{R}^1$ and $D_i > 0$ are the natural frequency and damping coefficient of oscillator $i \in \mathcal{V}$, and $M_i > 0$ is the inertial constant of a mechanical oscillator $i \in \mathcal{V}_1$.

Despite its apparent simplicity, this coupled oscillator model gives rise to rich dynamic behavior, and it is encountered in ubiquitous scientific disciplines rang-

¹The interaction between two oscillators is *diffusive* if its strength depends on the corresponding phase difference; such interactions arise for example in the discretization of the Laplace operator in diffusive partial differential equations.

ing from natural and life sciences to engineering. In particular, the models encountered in power network stability studies can be cast as variations and special instances of the oscillator network (1.1). In the following, we present a mechanical analog of the coupled oscillator model (1.1) to illustrate its basic phenomenology.

Mechanical Analog and Basic Phenomenology

A mechanical analog of a coupled oscillator network is the spring network shown in Figure 1.1. This network consists of a group of kinematic particles constrained to move on the unit circle \mathbb{S}^1 and assumed to move without colliding. Each particle is characterized by its angle $\theta_i \in \mathbb{S}^1$, its inertia coefficient $M_i > 0$, a

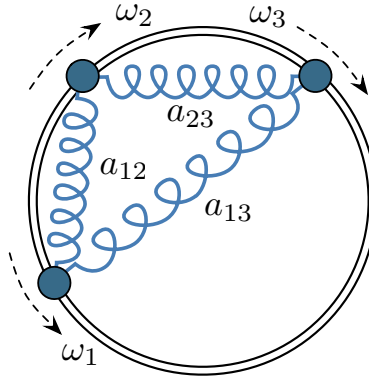


Figure 1.1: Mechanical analog of a coupled oscillator network

viscous damping force $D_i \dot{\theta}_i$ (with $D_i > 0$) opposing the direction of motion, and it is subject to an external driving torque $\omega_i \in \mathbb{R}$. Pairs of interacting particles i and j are coupled through a linear-elastic spring with stiffness $a_{ij} > 0$. The overall

spring network is modeled by a graph, whose nodes are the kinematic particles, whose edges are the linear-elastic springs, and whose edge weights are the positive stiffness coefficients $a_{ij} = a_{ji}$. Under these assumptions, it can be shown that the system of spring-interconnected particles obeys the coupled oscillator dynamics (1.1a) with $\mathcal{V}_2 = \emptyset$, see [89, Supplementary Information] for a detailed derivation.

The mechanical analog in Figure 1.1 illustrates the basic phenomenology displayed by the oscillator network (1.1). The spring-interconnected particles are subject to a competition between the external driving forces ω_i and the internal restoring torques $a_{ij} \sin(\theta_i - \theta_j)$. Hence, the interesting coupled oscillator dynamics (1.1) arise from a trade-off between each oscillator's tendency to align with its natural frequency ω_i and the synchronization-enforcing coupling $a_{ij} \sin(\theta_i - \theta_j)$ with its neighbors. Intuitively, a weakly coupled and strongly heterogeneous (that is, with strongly dissimilar natural frequencies) network does not display any coherent behavior, whereas a strongly coupled and sufficiently homogeneous network is amenable to synchronization, where all frequencies $\dot{\theta}_i(t)$ or even all phases $\theta_i(t)$ become aligned. For the spring network in Figure 1.1, these two qualitatively distinct regimes are illustrated in a dynamic simulation in Figure 1.2.

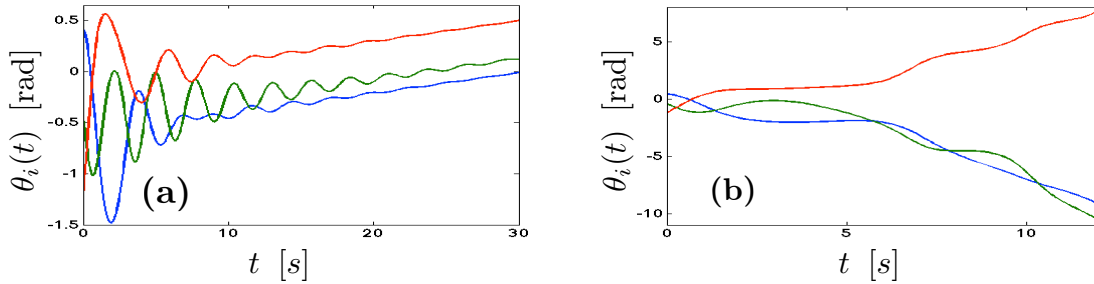


Figure 1.2: Dynamics of mechanical spring network

The two subfigures display a dynamic simulation of the spring-interconnected particles in Figure 1.1. With exception of the coupling weights (stiffness constants) a_{ij} , all parameters and the initial conditions in both simulations (a) and (b) are identical. In the case of strong coupling in Subfigure (a), the particles synchronize their frequencies. In the case of weak coupling in Subfigure (b), the oscillators do not show any coherent behavior.

1.1 Literature Synopsis

In this section we give an overview of the existing literature for the problems considered in this thesis.

1.1.1 Synchronization in Complex Oscillator Networks

In this subsection, we consider the complex oscillator network (1.1) and review its history, related applications, and theoretical developments.

A Brief Historical Account

The scientific interest in synchronization of coupled oscillators can be traced back to the work by Huygens [134] on “an odd kind of sympathy” between cou-

pled pendulum clocks, locking phenomena in circuits and radio technology [4], the analysis of brain waves and self-organizing systems [290, 291], and it still fascinates the scientific community nowadays [260, 295]. A variation of the considered coupled oscillator model (1.1) was first proposed by Winfree [294]. Winfree considered general (not necessarily sinusoidal) interactions among the oscillators. He discovered a phase transition from incoherent behavior with dispersed phases to synchrony with aligned frequencies and coherent (i.e., nearby) phases. Winfree found that this phase transition depends on the trade-off between the heterogeneity of the oscillator population and the strength of the mutual coupling, which he could formulate by parametric thresholds. However, Winfree's model was too general to be analytically tractable. Inspired by these works, Kuramoto [158] simplified Winfree's model and arrived at the coupled oscillator dynamics (1.1b) with purely kinematic oscillators $\mathcal{V} = \mathcal{V}_2 = \{1, \dots, n\}$, with unit time constants $D_i = 1$, with a complete interaction graph, and with uniform weights $a_{ij} = K/n$:

$$\dot{\theta}_i = \omega_i - \frac{K}{n} \sum_{j=1}^n \sin(\theta_i - \theta_j), \quad i \in \{1, \dots, n\}. \quad (1.2)$$

In an insightful and ingenious analysis, Kuramoto [158, 159] showed that synchronization occurs in the model (1.2) if the coupling strength K exceeds a certain critical threshold K_{critical} depending on the distribution of the natural frequencies ω_i . The dynamics (1.2) are nowadays known as *Kuramoto model* of coupled oscillators, and Kuramoto's original work initiated a broad stream of research. A

compelling historical perspective is offered by Strogatz [258]. We also recommend the surveys by Acebrón et al. [3] and Arenas et al. [18, Section 3]. A recent survey by the author provides a systems and control perspective [88].

Related Applications in Sciences

The coupled oscillator model (1.1) and its variations appear in the study of biological synchronization and rhythmic phenomena. Example systems include pacemaker cells in the heart [182], circadian cells in the brain [168], coupled cortical neurons [70], Hodgkin-Huxley neurons [34], brain networks [280], yeast cells [106], flashing fireflies [36, 96], chirping crickets [284], central pattern generators for animal locomotion [152], particle models mimicking animal flocking behavior [117, 120], and fish schools [209], among others. The coupled oscillator model (1.1) also appears in physics and chemistry in modeling and analysis of spin glass models [72, 141, 245], flavor evolution of neutrinos [210], coupled Josephson junctions [292], coupled metronomes [211], Huygen's coupled pendulum clocks [26, 144], micromechanical oscillators with optical [303] or mechanical [246] coupling, and in the analysis of chemical oscillations [147, 159]. Finally, oscillator networks of the form (1.1) also serve as phenomenological models for synchronization phenomena in social networks, such as rhythmic applause [196],

opinion dynamics [216,217], pedestrian crowd synchrony on London's Millennium bridge [261], and decision making in animal groups [163].

Related Applications in Engineering

Some technological applications of the coupled oscillator model (1.1) include deep brain stimulation [195,267], locking in solid-state circuit oscillators [1,186], planar vehicle coordination [148,149,209,242,243], carrier synchronization without phase-locked loops [220], synchronization in semiconductor laser arrays [155], and microwave oscillator arrays [301]. Since alternating current (AC) circuits are naturally modeled by equations similar to (1.1), some electric applications are found in structure-preserving [27,236] and network-reduced power system models [50,85], and droop-controlled inverters in microgrids [249]. Algorithmic applications of the coupled oscillator model (1.1) include limit cycle estimation through particle filters [272], clock synchronization in decentralized computing networks [23,247,288], central pattern generators for robotic locomotion [15,135,224], decentralized maximum likelihood estimation [25], and human-robot interaction [187]. Further envisioned applications of oscillator networks obeying equations similar to (1.1) include generating music [133], signal processing [246], and neuro-computing through micro-mechanical [131] or laser [130,285] oscillators.

Canonical Model and Prototypical Example

The importance of the coupled oscillator model (1.1) does not stem only from the various examples listed above. Even though this model appears to be quite specific (a phase oscillator with constant driving term and diffusive sinusoidal coupling), it is the *canonical model* for coupled limit-cycle oscillators [129]. This fact is established, for example, in work by the computational neuroscience community which has developed different approaches [97, 129, 137, 138] to reduce general oscillator and interaction models to phase oscillator networks of the form (1.1). Finally, the coupled oscillator model (1.1) serves as the prototypical example for synchronization in complex networks [18, 31, 203, 259, 264], and its linearization is the well-known consensus protocol studied in networked control, see the surveys and monographs [37, 104, 180, 200, 221]. Indeed, numerous control scientists explored the coupled oscillator model (1.1) as a nonlinear generalization of the consensus protocol [58, 139, 166, 191, 199, 233, 238, 241].

Theoretical investigations

Coupled oscillator models of the form (1.1) are studied from a purely theoretical perspective in the physics, dynamical systems, and control communities. At the heart of the coupled oscillator dynamics is the transition from incoherence to synchrony. Here, different notions and degrees of synchronization can be distin-

gushed, and the apparently incoherent state features rich dynamics, as well. In this thesis, we will be particularly interested in the notion of frequency synchronization, that is, in the property of certain solutions to reach equal frequencies $\dot{\theta}_i(t)$ among all oscillators. We will also establish conditions under which the angles $\theta_i(t)$ synchronize. We refer to the surveys and tutorials [3, 18, 31, 84, 88, 160, 177, 258, 259] for an incomplete set of recent theoretical research activities. We will review and attribute relevant results throughout the course of this thesis.

1.1.2 Synchronization and Stability in Power Networks

Electrical energy is the underpinning of our civilization as we know it. Virtually all infrastructures critical to our daily lives heavily rely on it. Despite its large scale, heterogeneity, and complexity, the power grid has been able to reliably provide energy making it arguably “the most valuable engineering achievement”² as well as as “the largest and most complex machine” engineered by humankind.³

The Importance of Power Network Stability – Today and Tomorrow

The interconnected power grid is a complex and large-scale system with rich nonlinear dynamic behavior. Local instabilities arising in such a power network

²We refer the reader to the book [66] and also to the website <http://www.greatachievements.org/> for a list of the greatest engineering achievements of the 20th century. This list is compiled by the National Academy of Engineering and led by “Electrification.”

³This statement is attributed to the renowned electrical engineer Charles Steinmetz [156].

can trigger cascading failures and ultimately result in wide-spread blackouts [13, 68, 197, 219]. The detection and rejection of such instabilities is one of the major challenges faced by the power system operators and control system designers. Stability is a classical topic in power systems engineering [12, 48, 156, 157, 207, 236, 276], but it is also of major importance in the envisioned *smart power grid*.

Recent political and societal developments are leading to the deregulation of energy markets and the increasing adoption of renewables. In face of the ever-increasing power demand, these developments are also leading to more stressed power networks operating near their stability margins, as documented by recent outages and the accompanying economic losses. Additional expected developments in future smart power grids include the paradigm of autonomously managed microgrids, the coordination of distributed sources and loads through a communication infrastructure, and the deployment of power electronics control devices (for example, inverters and flexible AC transmission system) and new measurement technologies (for example, phasor measurement units and smart meters).

In face of the increasing complexity of future smart grids, the volatility of deregulated energy markets, the ever-increasing power demand, and the integration challenges posed by renewable energy sources, a deeper understanding of the dynamical network phenomena as well as their control is increasingly important.

Synchronization in Electric Power Networks

Power system stability is broadly subdivided into *rotor angle stability* and *voltage stability*, see [157] for a comprehensive classification of power system stability. Here, we are particularly interested in *rotor angle stability*, which is the ability of the power system to remain in synchronism when subjected to disturbances. Rotor angle stability is further classified as *transient stability* for large disturbances and contingencies such as severe fluctuations in generation or load, faults on transmission elements, or loss of system components such as transformers or transmission lines. For example, a recent major blackout in 2003 was caused by tripping of a tie-line and resulted in a cascade of events leading to the loss of synchronism of the Italian power grid with the rest of Europe [219].

The mechanism by which interconnected synchronous machines are able to maintain and restore synchronism depends on the balance between the electromagnetic and the mechanical torque of each machine [12, 156, 236]. Even if each machine achieves such a balance, but the overall power generation and consumption (including demand at the loads and dissipation in the transmission network) are not balanced, then the power system frequency drifts away from its nominal frequency (60 Hz in North America). Since each component connected to an AC power grid is designed to operate in synchrony with the nominal carrier frequency, long-term frequency deviations may result in *frequency instabilities* [122].

At this point, it is instructive to point out that the mathematical models used for the analysis of synchronization problems in power networks can be cast as variations of the coupled oscillator model (1.1). Notice that both the transient stability problem and the frequency stability problem are aspects of the synchronization problem in complex oscillator networks. In a classic power systems setting, both problems are analyzed separately and typically on different time scales. We will detail the modeling of power networks in Subsection 2.2.1.

Transient stability analysis is mainly concerned with the problem of estimating the region of attraction of a given synchronous solution (or operating point) of the power grid, which arises after a fault is restored. To solve this problem, a direct numerical integration of a detailed power system model is often computationally too expensive and not feasible in real-time. Thus, various sophisticated analysis methods and numerical algorithms have been developed as alternatives. Reviews, tutorials, and survey articles on transient stability analysis can be found in [48, 50, 61, 207, 278]. Typically, the synchronization problem is recast as a stability problem in relative (or incremental) coordinates, the dynamics are cast as Hamiltonian or gradient-like systems, and computational methods are employed to compute or approximate the separatrices and the level sets of potential functions. These approaches are termed *energy function methods* or *direct methods* and will be reviewed throughout the course of this thesis. Unfortunately, the existing ap-

proaches do not provide simple conditions to check if a power system synchronizes for a given system state and parameters. In particular, an open problem recognized by the power system community and not resolved yet by classical methods is the quest for explicit and concise conditions relating transient stability to the parameters and graph-theoretical properties of the underlying network [123].

In comparison to transient stability, frequency stability is primarily concerned with the existence, local exponential stability, and robustness of solutions to the steady state power flow equations (possibly formulated in a rotating frame to include the frequency drift). A central question is “under which conditions on the network parameters and topology and the current load and generation profile, does there exist an optimal [162], stable [47,234], and robust [16,136,140,298,299] synchronous operating point”. A more general concern is whether the power flow equations admit any solution [53,164] or an existing solution vanishes in a saddle node bifurcation [78,112]. Various security indices have been proposed to quantify the robustness margin of a particular operating condition [121]. In comparison to transient stability analysis, these approaches rely on network and circuit-theory, algebraic problem formulations, and analytic solution approaches.

Historically, power systems were designed and operated conservatively in a region where the system behavior was fairly linear. With the steadily growing power demand, the deployment of renewables in remote areas, and the increasing

deregulation of energy markets, power networks are forced to operate near their stability and capacity margins. For heavily loaded and stressed power networks, the system nonlinearities and nonlocal network effects play a dominant role and the complex dynamics are only poorly understood [124]. The assessment of an acceptable synchronous operating point, the computation of its region of attraction, and the quantification of its robustness margin will become more and more important in an increasingly complex, volatile, and stressed power grid.

1.2 Contributions and Organization

The contents of this thesis are organized into four main chapters, followed by a shared conclusion. In the following, we briefly outline the contents of each chapter.

Chapter 2 – Preliminaries, Models, and Synchronization Notions: In this chapter, we present some tools from algebraic graph theory which are essential for the analysis of interconnected dynamical systems. We introduce different dynamic models of electric power systems and show how they can be naturally cast as instances of the coupled oscillator model (1.1). We briefly review further applications of the coupled oscillator model (1.1), we justify its importance as a canonical model, and we discuss different synchronization notions. Additionally, we introduce a few basic analysis methods from consensus protocols, we state

some basic insights and results, and we illustrate the basic phenomenology of the coupled oscillator dynamics (1.1) with a simple two-dimensional example.

Chapter 3 – Mechanical and Kinematic Oscillator Networks: In this chapter, we study the relationships between mechanical oscillator models (1.1a) with second-order dynamics and purely kinematic oscillator models (1.1b) with first-order dynamics. The bulk of the literature on synchronization and the theoretic analysis methods have been developed mainly for first-order oscillator networks (1.1b). On the other hand, many interesting applications of complex oscillator networks include oscillators with second-order mechanical dynamics, for instance, electric power networks. In this chapter, we show under which assumptions the two models can be related, and also demonstrate when their dynamic behavior is qualitatively different. In particular, we present two approaches that allow to extend the analysis methods and results from first-order kinematic oscillator models to second-order mechanical oscillator models.

Our first approach is based on topological equivalence and shows that both models share the same equilibria, the same local stability properties, as well as all local bifurcations. As a consequence, all local synchronization conditions hold equivalently for both models and without any further assumptions, but the results are only locally valid and restricted to forced gradient and Hamiltonian systems.

On the other hand, our second approach applies to general vector fields and allows to relate the dynamics and trajectories of the two models. This approach relies on singular perturbation methods and additionally requires that each mechanical oscillator is strongly overdamped. We discuss the applicability of these two approaches to electric power systems and relate them to the existing literature.

Throughout this chapter, we also develop important insights into the potential landscape of the coupled oscillator model (1.1), we state some key lemmas, and present a result on phase synchronization in homogeneous oscillator networks.

Chapter 4 – The Critical Coupling for Kuramoto Oscillators: In this chapter, we study the classic Kuramoto model (1.2) with a heterogeneous oscillator population and a complete and uniformly weighted network. We consider both finite and infinite oscillator populations. We review different synchronization notions, relate different performance metrics for synchronization, and present a comprehensive review of estimates on the critical coupling strength in a unified language. In our review, we cover necessary, sufficient, explicit, and implicit bounds on the critical coupling. In this effort, we collect contributions from several references and arrive at novel results within a unified perspective.

By making use of recently developed tools in the consensus literature, we also arrive at new estimates of the critical coupling as well as new insights into the

transient dynamics. Our approach relies on the contraction property and Jacobian arguments and results in a novel and explicit bound on the critical coupling. In particular, we require the coupling to dominate the worst-case dissimilarity in natural frequencies. The proposed bound is tight and thus necessary and sufficient when evaluated over arbitrary distributions with compact support of the natural frequencies. Additionally, we state tight bounds on the region of attraction for a synchronized solution and on the asymptotic performance metrics. We compare our result to the existing literature and present statistical studies for a uniform sampling distribution of the natural frequencies. We also present extensions of our result to second-order Kuramoto oscillators and time-varying natural frequencies.

We conclude this chapter by extending our analysis framework to so-called network-reduced power system models and non-uniform Kuramoto oscillators.

Chapter 5 – Synchronization in Complex Oscillator Networks: In this chapter, we study heterogeneous oscillator populations with distinct natural frequencies and a nontrivial coupling topology. We review the extensive literature proposing synchronization conditions based on different metrics for coupling and heterogeneity. Similar to every review article on complex oscillator networks, we conclude that the existing synchronization conditions are either not concise or only conservative estimates on the threshold from incoherence to synchrony.

Here, we present a set of necessary and a set of sufficient conditions for synchronization in complex oscillator networks. To the best of the author's knowledge, these are the sharpest explicit conditions known to date. The sufficient conditions are based on analysis approaches using two-norm-type metrics, Lyapunov methods, and fixed-point theorems. Additionally, we develop a novel algebraic analysis approach emphasizing the crucial role of cut-sets and cycles in the graph. As a result, we propose a concise and sharp synchronization condition, which can be stated elegantly in terms of the network topology and parameters. Our results significantly improve upon the existing conditions advocated thus far, they are provably exact for various interesting network topologies and parameters, and they are statistically correct for a broad range of nominal random network models.

We illustrate the validity, the accuracy, and the practical applicability of our results in complex networks scenarios and in smart grid applications including a set of standard IEEE power system test cases. Finally, we illustrate the utility of our approach through a contingency screening case study in the RTS 96 power network and conclude by summarizing further applications.

Chapter 6 – Conclusions: This chapter concludes the thesis and discusses some aspects for future research in the area of complex oscillator networks and applications to electric power grids.

Chapter 2

Preliminaries, Models, and Synchronization Notions

In this chapter, we recall some preliminaries, introduce different models, and review the synchronization notions of interest. Additionally, we introduce a few basic analysis methods and state some basic results.

2.1 Preliminaries in Algebraic Graph Theory

In this section, we introduce some notation and preliminary results from algebraic graph theory. Algebraic graph theory provides a link between matrix theory and graph theory, and it is an essential tool for the analysis and control of large-scale interconnected systems. Our notation is mostly standard, and we only introduce the essential concepts necessary to develop the results in this thesis.

We refer to [29, 30, 107] for further details on algebraic graph theory and to the monographs [37, 103, 180] for connections with distributed control systems.

Vector and matrix notation: The following notation for vectors and matrices will be used throughout this thesis. Let $\mathbf{1}_n \in \mathbb{R}^n$ and $\mathbf{0}_n \in \mathbb{R}^n$ be the n -dimensional vectors of unit and zero entries, and let $\mathbf{1}_n^\perp$ be the orthogonal complement of $\mathbf{1}_n$ in \mathbb{R}^n , that is, $\mathbf{1}_n^\perp \triangleq \{x \in \mathbb{R}^n \mid x \perp \mathbf{1}_n\}$. Accordingly, let $\mathbf{0}_{n \times n}$ and $\mathbf{1}_{n \times n}$ denote the $(n \times n)$ -dimensional matrix with unit entries, respectively. We denote the $(n \times n)$ -dimensional identity matrix by I_n . Given an n -tuple (x_1, \dots, x_n) , let $x \in \mathbb{R}^n$ be the associated vector with maximum and minimum elements x_{\max} and x_{\min} .

For $p \in \mathbb{N}$, a vector x , and a matrix A , let $\|x\|_p$ be the p -norm of x , and $\|A\|_p$ denotes the induced p -norm of A . The nullspace and image of A are denoted by $\text{Ker}(A)$ and $\text{Im}(A)$, respectively. The *inertia* of a matrix $A \in \mathbb{R}^{n \times n}$ is given by the triple $\{\nu_s, \nu_c, \nu_u\}$, where ν_s (respectively ν_u) denotes the number of stable (respectively unstable) eigenvalues of A in the open left (respectively right) complex half plane, and ν_c denotes the number of center eigenvalues with zero real part. Given an ordered index set \mathcal{I} of cardinality $|\mathcal{I}|$ and a one-dimensional array $\{x_i\}_{i \in \mathcal{I}}$, let $\text{diag}(\{x_i\}_{i \in \mathcal{I}}) \in \mathbb{R}^{|\mathcal{I}| \times |\mathcal{I}|}$ be the associated diagonal matrix. For a symmetric matrix $A = A^T \in \mathbb{R}^{n \times n}$, we implicitly assume that its eigenvalues $\lambda_i(A)$ are arranged in increasing order, that is, $\lambda_1(A) \leq \dots \leq \lambda_n(A)$.

Digraphs, associated matrices, and their properties: A *weighted directed graph* (or simply *digraph*) with n nodes is a triple $G(\mathcal{V}, \mathcal{E}, A)$, where $\mathcal{V} = \{1, \dots, n\}$ is the set of nodes, $\mathcal{E} \subset \mathcal{V} \times \mathcal{V}$ is the set of directed edges, and $A \in \mathbb{R}^{n \times n}$ is the *adjacency matrix*. The entries of A satisfy $a_{ij} > 0$ for each directed edge $(i, j) \in \mathcal{E}$ and are zero otherwise. Any nonnegative matrix A induces a weighted directed graph G . Unless stated otherwise, we restrict ourselves to digraphs without self-loops, that is, $(i, i) \notin \mathcal{E}$ and $a_{ii} = 0$ for all $i \in \mathcal{V}$. If for any two distinct nodes $i, j \in \mathcal{V}$, we have that $(i, j) \in \mathcal{E}$, then G is referred to as a *complete graph*.

A directed path on a digraph G of length ℓ from node v_{i_0} to node v_{i_ℓ} is an ordered set of distinct nodes $\{v_{i_0}, v_{i_1}, \dots, v_{i_\ell}\} \subset \mathcal{V}$ such that $(v_{i_{j-1}}, v_{i_j}) \in \mathcal{E}$ for $j \in \{1, \dots, \ell\}$. If there is a directed path in G from one node $i \in \mathcal{V}$ to another node $j \in \mathcal{V}$, then j is *reachable* from i . If a node $i \in \mathcal{V}$ is reachable from any other node $j \in \mathcal{V} \setminus \{i\}$ in the digraph, then we say it is *globally reachable*.

For each node $i \in \mathcal{V}$, we define the weighted out-degree by $\deg_i = \sum_{j=1}^n a_{ij}$, and the associated out-degree matrix $\text{diag}(\{\deg_i\}_{i=1}^n) \in \mathbb{R}^{n \times n}$. Define the *Laplacian matrix* by $L = \text{diag}(\{\deg_i\}_{i=1}^n) - A \in \mathbb{R}^{n \times n}$. Since the Laplacian matrix L can be identified with the adjacency matrix A (up to self-loops), we say the L also induces the graph $G(\mathcal{V}, \mathcal{E}, A)$. By construction, we have that $\text{Ker}(L) = \mathbf{1}_n$, by the Geršgorin disk theorem [28,132] we have that all eigenvalues of L have nonnegative

real part, and additionally the zero eigenvalue is simple if and only if the digraph features a globally reachable node [165, Lemma 2].

Undirected graphs, associated matrices, and their properties: Of particular interest in this thesis are undirected and weighted graphs $G(\mathcal{V}, \mathcal{E}, A)$. A weighted digraph is said to be undirected if $(i, j) \in \mathcal{E}$ and $a_{ij} > 0$ implies that $(j, i) \in \mathcal{E}$ and $a_{ji} = a_{ij}$. Equivalently, the unordered pair $\{i, j\} \in \mathcal{E}$ is in the edge set and will simply be referred to as *edge*, the adjacency matrix $A = A^T$ and the Laplacian matrix $L = L^T$ are symmetric, and node k is reachable from node ℓ if and only if ℓ is reachable from k . If each node $i \in \mathcal{V}$ is reachable from any other node $j \in \mathcal{V} \setminus \{i\}$, then the graph G is said to be *connected*. Unless stated otherwise, we assume throughout this thesis that all graphs are undirected and connected.

If a unique number $\ell \in \{1, \dots, |\mathcal{E}|\}$ and an arbitrary direction are assigned to each edge $\{i, j\} \in \mathcal{E}$, the (oriented) *incidence matrix* $B \in \mathbb{R}^{n \times |\mathcal{E}|}$ is defined component-wise by $B_{k\ell} = 1$ if node k is the sink node of edge ℓ and by $B_{k\ell} = -1$ if node k is the source node of edge ℓ ; all other elements are zero. The associated orthogonal vector spaces $\text{Ker}(B)$ and $\text{Ker}(B)^\perp = \text{Im}(B^T)$ are spanned by vectors associated to cycles and cut-sets in the graph, see [29, Section 4]. In the following, we refer $\text{Ker}(B)$ and $\text{Im}(B^T)$ as the *cycle space* and the *cut-set space*, respectively.

If $\mathcal{A} = \text{diag}(\{a_{ij}\}_{\{i,j\} \in \mathcal{E}})$ is the diagonal matrix of edge weights, then one can show

$$L = BAB^T.$$

If the graph is connected, then $\text{Ker}(B^T) = \text{Ker}(L) = \text{span}(\mathbf{1}_n)$, and all $n - 1$ non-zero eigenvalues of L are strictly positive. The second-smallest eigenvalue $\lambda_2(L)$ and is a spectral connectivity measure termed the *algebraic connectivity* [98, 188].

Since the Laplacian L is singular, we will frequently use its *Moore-Penrose pseudo inverse* [181] denoted by L^\dagger . If $V \in \mathbb{R}^{n \times n}$ is an orthonormal matrix of eigenvectors of L , its singular value decomposition is $L = V \text{diag}(0, \{\lambda_i\}_{i \in \{2, \dots, n\}}) V^T$, and its Moore-Penrose pseudo inverse L^\dagger is given by

$$L^\dagger = V \text{diag}(0, \{1/\lambda_i\}_{i \in \{2, \dots, n\}}) V^T.$$

A direct consequence of the singular value decomposition are the identities $L \cdot L^\dagger = L^\dagger \cdot L = I_n - \frac{1}{n} \mathbf{1}_{n \times n}$. For any two nodes $i, j \in \mathcal{V}$, we define their *effective resistance*

$$R_{ij} = L_{ii}^\dagger + L_{jj}^\dagger - 2L_{ij}^\dagger.$$

If a resistive circuit with conductance matrix L is associated to the graph, the effective resistance R_{ij} is the potential difference between the nodes i and j when a unit current is injected in i and extracted in j . We refer to [86, 94, 105, 114] for further information on Laplacian inverses and on the resistance distance.

2.2 Oscillator Network Models and Synchronization Problems

In this section, we detail the mathematical models used in this thesis. We demonstrate that a variety of power network models can be cast as special instances or variations of the coupled oscillator model (1.1). We further justify the importance of the coupled oscillator (1.1) through other examples, and we show that it is the canonical model of coupled limit cycle oscillators.

2.2.1 Electric Power Networks

For our purposes, an AC power network is a large-scale circuit, with different types of power sources and loads attached, see Figure 2.1. We model this circuit as an undirected, connected, and complex-weighted weighted graph with the n buses forming the node set $\mathcal{V} = \{1, \dots, n\}$, the transmission lines forming the undirected edge set $\mathcal{E} \subset \mathcal{V} \times \mathcal{V}$, and with each edge $\{i, j\}$ we associate the nonzero complex-valued admittance $Y_{ij} \in \mathbb{C}$. Here, the real part $\Re(Y_{ij})$ is the conductance and the imaginary part $\Im(Y_{ij})$ is the susceptance of the transmission line. We also allow for self-loops in the graph corresponding to nonzero shunt admittances, that is, loads modeled as impedances to ground. Typically, a high-voltage transmission network can be regarded as a lossless and purely inductive circuit.

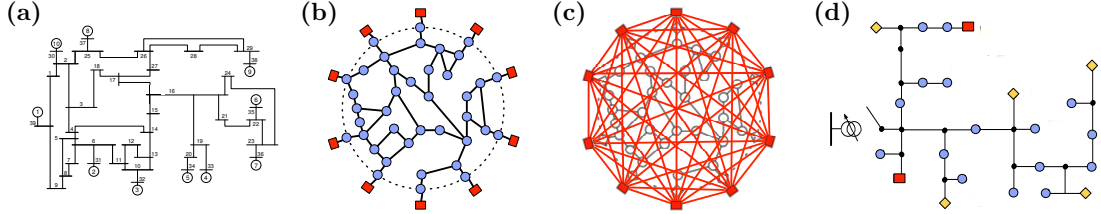


Figure 2.1: Illustration of different power network diagrams
 Subfigures (a), (b), and (c) show the IEEE 39 New England power grid [207]. Subfigure (a) shows the single line diagram, Subfigure (b) shows an equivalent schematic illustration, where the (red) squares depict synchronous generators and the (blue) circles are load buses, and Subfigure (c) shows the corresponding network-reduced model, where the load buses have been removed through Kron reduction [86]. Finally, Subfigure (d) shows a microgrid based on the IEEE 37 feeder [145], where the (yellow) diamonds depict DC/AC inverters and the (black) circles are passive junctions.

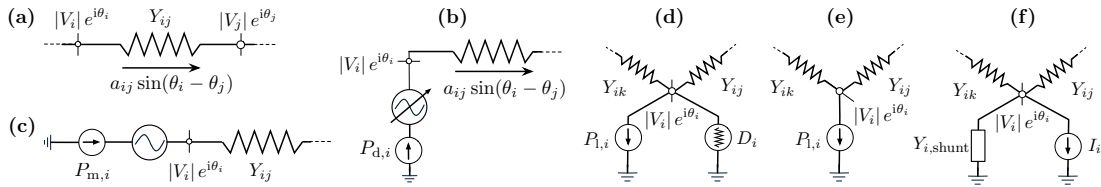


Figure 2.2: Illustration of the power network devices as circuit elements
 Subfigure (a) shows a transmission element connecting nodes i and j . Subfigure (b) shows an inverter controlled according to (2.2). Subfigure (c) shows the synchronous generator model (2.1). Subfigure (d) shows the frequency-dependent load model (2.3). Subfigure (e) shows the constant power load model (2.4). Finally, Subfigure (f) shows a constant current and constant impedance load.

For each node, consider the voltage phasor $V_i = |V_i|e^{i\theta_i}$ corresponding to the phase $\theta_i \in \mathbb{S}^1$ and magnitude $|V_i| \geq 0$ of the sinusoidal solution to the circuit equations. For a lossless network, the active power flow from node i to j is $a_{ij} \sin(\theta_i - \theta_j)$, where we adopt the shorthand $a_{ij} = |V_i| \cdot |V_j| \cdot \Im(Y_{ij})$ for the maximum active power transfer, see Figure 2.2.(a). The node set is partitioned as $\mathcal{V} = \mathcal{V}_1 \cup \mathcal{V}_2 \cup \mathcal{V}_3$, where \mathcal{V}_1 are synchronous generators, \mathcal{V}_2 are grid-connected direct current (DC) power sources, and \mathcal{V}_3 are load buses. We assume that all voltage levels $|V_i|$ are constant, see Remark 2.2.1 for a discussion of this assumption.

Synchronous generators: We use the conventional of model a synchronous generator as a *constant voltage source behind a transient reactance*, see Figure 2.2(c) for a circuit diagram and [156, 236] for a detailed derivation. If the generator transient reactances are absorbed into the network admittance matrix, then the electromechanical swing dynamics of the synchronous generators are obtained as

$$M_i \ddot{\theta}_i + D_i \dot{\theta}_i = P_{m,i} - \sum_{j=1}^n a_{ij} \sin(\theta_i - \theta_j), \quad i \in \mathcal{V}_1, \quad (2.1)$$

where $\theta_i \in \mathbb{S}^1$ and $\dot{\theta}_i \in \mathbb{R}^1$ are the generator rotor angle and frequency, $P_{m,i} > 0$ is the mechanical power input from the prime mover, and $M_i > 0$, and $D_i > 0$ are the inertia and damping coefficients, respectively.

DC/AC inverters: We assume that each DC source \mathcal{V}_2 is connected to the AC grid via a DC/AC inverter. For the purposes of this work, and as widely adopted in the microgrid literature, we will consider the class of voltage controlled *voltage source inverters* with purely sinusoidal voltage output, see Figure 2.2(b). We assume the inverter output impedances are absorbed into the network admittance matrix, and each inverter is controlled with a conventional frequency droop control law [46, 275]. For a droop-controlled inverter $i \in \mathcal{V}_2$ with droop-slope $1/D_i > 0$, the deviation of the inverter power output $\sum_{j=1}^n a_{ij} \sin(\theta_i - \theta_j)$ from its nominal value $P_{d,i} > 0$ is proportional to the frequency deviation $D_i \dot{\theta}_i$. As shown in [249], the droop-controlled inverter then obeys the closed-loop dynamics

$$D_i \dot{\theta}_i = P_{d,i} - \sum_{j=1}^n a_{ij} \sin(\theta_i - \theta_j), \quad i \in \mathcal{V}_2. \quad (2.2)$$

In the following, we complete our list of power network components with different load models, and we show that in each case the overall network dynamics can be cast as a special instance or a variation of the coupled oscillator model (1.1).

Load models: We consider the following load models illustrated in Figure 2.2.

1) *PV buses with frequency-dependent loads:* All load buses are *PV buses*, that is, the active power demand $P_{l,i}$ and the voltage magnitude $|V_i|$ are specified for each bus. The active power drawn by load i consists of a constant term $P_{l,i} > 0$ and a frequency dependent term $D_i \dot{\theta}_i$ with $D_i > 0$, as illustrated in Figure 2.2(d).

The resulting real power balance equation is

$$D_i \dot{\theta}_i + P_{1,i} = - \sum_{j=1}^n a_{ij} \sin(\theta_i - \theta_j), \quad i \in \mathcal{V}_3. \quad (2.3)$$

The dynamics (2.1), (2.2), (2.3) are known as the *structure-preserving power network model*. The model has been proposed in [27] for bulk power systems, and a derivation from first principles can be found in [236, Chapter 7]. Observe that the power network dynamics (2.1), (2.2), (2.3) are obtained as the coupled oscillator model (1.1) with $\omega_i \in \{P_{m,i}, P_{d,i}, -P_{1,i}\}$ as power injections and with the coupling coefficients a_{ij} corresponding to the maximum active power transfers.

2) *PV buses with constant power loads*: All load buses are *PV buses* and each load demands a constant amount of active power $P_{1,i} > 0$, that is,

$$P_{1,i} = - \sum_{j=1}^n a_{ij} \sin(\theta_i - \theta_j), \quad i \in \mathcal{V}_3. \quad (2.4)$$

The corresponding circuit-theoretic model is shown in Figure 2.2(e). If the angular distances $|\theta_i(t) - \theta_j(t)| < \pi/2$ are bounded for each transmission line $\{i, j\} \in \mathcal{E}$ (these conditions will be precisely established in the next chapters), then it is known that the resulting differential-algebraic system (2.1), (2.2), (2.4) has the same local stability properties as the dynamics (2.1), (2.2), (2.3) with frequency-dependent loads [234, 249]. Additionally, as shown in [234], the transient dynamics of the ODE system (2.1), (2.2), (2.3) and the DAE system (2.1), (2.2), (2.4) can be mapped to another through a singular perturbation analysis for D_{\max} sufficiently

small. Hence, all results derived for the coupled oscillator model (1.1) apply locally also to the differential-algebraic power network model (2.1), (2.2), (2.4).

3) *Constant current and constant admittance loads:* Assume that each load $i \in \mathcal{V}_3$ is modeled as a constant current demand I_i and a shunt admittance $Y_{i,\text{shunt}}$, as illustrated in Figure 2.2(f). In this case, the current-balance equations are $I = LV$, where $I \in \mathbb{C}^n$ and $V \in \mathbb{C}^n$ are the vectors of nodal current injections and voltages, and L is the network admittance matrix with off-diagonal elements $L_{ij} = -Y_{ij}$ and diagonal elements $L_{ii} = \sum_{j=1}^n Y_{ij} + Y_{i,\text{shunt}}$. After elimination of the bus variables V_i (for $i \in \mathcal{V}_3$) through *Kron reduction*, we obtain the reduced current balance equations as $I_{\text{red}} = L_{\text{red}}V_{\text{red}}$. We will not detail the reduced quantities here and refer to the author's article [86] for details. We want to remark two crucial properties of the reduced network. First, even if the original transmission network is lossless, then the presence of resistive shunt loads leads to a lossy reduced network, that is, the resistive loads in the original network are absorbed in the form of line losses in the reduced network. Second, even if the original topology is sparse, then the topology induced by the reduced admittance matrix Y is dense, see Figures 2.1(b) and 2.1(c). In fact, for most power networks the subgraph induced by the load buses \mathcal{V}_3 is connected, and it follows that the topology of the reduced network is complete in this case [86, Theorem 3.4].

After Kron reduction, the generator and inverter dynamics take the form

$$M_i \ddot{\theta}_i + D_i \dot{\theta}_i = \tilde{P}_i - \sum_{j=1}^n \tilde{a}_{ij} \sin(\theta_i - \theta_j - \varphi_{ij}), \quad i \in \mathcal{V}_1, \quad (2.5)$$

$$D_i \dot{\theta}_i = \tilde{P}_i - \sum_{j=1}^n \tilde{a}_{ij} \sin(\theta_i - \theta_j - \varphi_{ij}), \quad i \in \mathcal{V}_2. \quad (2.6)$$

Here, $\tilde{a}_{ij} = |V_i| \cdot |V_j| \cdot \Im(Y_{\text{red},ij})$ are the maximal active power flows in the reduced network, and the phase shifts $\varphi_{ij} = -\arctan(\Re(Y_{\text{red},ij})/\Im(Y_{\text{red},ij})) \in [0, \pi/2[$ reflect the transfer conductance in the reduced network. The effective power injections \tilde{P}_i take the form $\tilde{P}_i = P_{m,i} - P_{\text{red},1} - \Re(Y_{\text{red},ii})|V_i|^2$ for $i \in \mathcal{V}_1$, and $\tilde{P}_i = P_{d,i} - P_{\text{red},2} - \Re(Y_{\text{red},ii})|V_i|^2$ for $i \in \mathcal{V}_2$, where the terms $P_{\text{red},1}$ and $P_{\text{red},2}$ result from the constant current and possibly constant inductance loads in the original network, and $\Re(Y_{\text{red},ii})|V_i|^2$ reflects the constant impedance loads.

The model (2.5)-(2.6) is known as *network-reduced power system model*. We refer to [86, 156, 236] for a detailed derivation of the network-reduced model and an analysis of the reduced circuit and graph-theoretic properties. Observe that, with exception of the phase shifts φ_{ij} , the network-reduced model (2.5)-(2.6) is again an instance of the coupled oscillator model (1.1).

4) *Synchronous motor loads*: Synchronous motors are synchronous machines which are modeled as synchronous generators (2.1) with a mechanical load, that is, the term $P_{m,i}$ in (2.1) is negative [156], see Figure 2.2(a). The resulting power network model is a perfect electrical analog of the coupled oscillator model (1.1).

Finally, combinations of the different load models are possible as well.

Remark 2.2.1 (Voltage dynamics). *To conclude this modeling paragraph, we want to state a word of caution regarding the assumption of constant voltage magnitudes. This assumption is well justified for synchronous generators, motor loads, and inverters, where the voltage magnitudes $|V_i|$ are tightly controlled.*

Under normal operating conditions, the active power flow $a_{ij} \sin(\theta_i - \theta_j) = |V_i| \cdot |V_j| \cdot \Im(Y_{ij}) \cdot \sin(\theta_i - \theta_j)$ between two nodes $i, j \in \mathcal{V}_1 \cup \mathcal{V}_2$ is primarily governed by the angular difference $\theta_i - \theta_j$ and not by the voltage magnitudes $|V_i|, |V_j|$. The latter assumption is known as “decoupling assumption” in the power systems community. Whereas the PV load models 1) and 2) are well-adopted for power systems stability studies, the assumption of constant load voltage magnitudes at these buses ceases to hold in a heavily stressed grid (near a bifurcation point), where additional dynamic phenomena can occur such as voltage collapse at the loads [78]. In short, the coupling weights a_{ij} are not necessarily constant. Likewise, if the shunt admittance loads in the load model model 3) are not constant (e.g., constant power loads can be transformed to voltage-dependent shunt admittances), then the Kron reduction process may be ill-posed, or the elements of the admittance matrix of the network-reduced model depend on the load voltages. In the latter case, the coupling weights a_{ij} are again not constant but depend on the load voltages.

To explicitly account for such unmodeled voltage dynamics affecting the coupling weights a_{ij} , the coupled oscillator model (1.1) can be studied with interval-valued parameters, where each a_{ij} takes value in the range $0 < \underline{a}_{ij} \leq a_{ij} \leq \overline{a}_{ij}$. We refer to the author's article [89, Supplementary Information] for details. Throughout this thesis, we assume that all parameters a_{ij} are constant and known. \square

Synchronization is central to the operation and functionality of power networks. All generating units of an interconnected grid must remain in strict frequency synchronism while continuously following demand and rejecting disturbances. The power network dynamics presented here are all instances of the coupled oscillator model (1.1). Thus, it is not surprising that scientists from different disciplines recently advocated coupled oscillator approaches to analyze synchronization in power networks, see [40, 99, 100, 123, 193, 228, 263, 266, 296] among others. The theoretical tools presented in this thesis establish how *synchronization* in power networks depends on the nodal parameters $(P_{l,i}, P_{m,i}, P_{d,i})$ as well as the interconnecting electrical network with weights a_{ij} .

2.2.2 Additional Examples of Complex Oscillator Networks

In this subsection, we briefly review two additional examples of the coupled oscillator model (1.1), and we justify its importance as a canonical model.

Flocking, Schooling, and Vehicle Coordination

A recent research field in control is the coordination of autonomous vehicles based on locally available information and inspired by biological flocking phenomena. Consider a set of n particles in the plane \mathbb{R}^2 , which we identify with the complex plane \mathbb{C} . Each particle $i \in \mathcal{V} = \{1, \dots, n\}$ is characterized by its position $r_i \in \mathbb{C}$, its heading angle $\theta_i \in \mathbb{S}^1$, and a steering control law $u_i(r, \theta)$ depending on the position and heading of itself and other vehicles, see Figure 2.3.(a) for a schematic illustration of the model. For simplicity, we assume that all particles have unit speed. The particle kinematics are then given by [142]

$$\begin{aligned}\dot{r}_i &= e^{i\theta_i}, \\ \dot{\theta}_i &= u_i(r, \theta),\end{aligned}\tag{2.7}$$

where $i \in \{1, \dots, n\}$ and $i = \sqrt{-1}$ is the imaginary unit. If no control is applied, then particle i travels in a straight line with orientation $\theta_i(0)$, and if $u_i = \omega_i \in \mathbb{R}$ is a nonzero constant, then particle i traverses a circle with radius $1/|\omega_i|$.

The interaction among the particles is modeled by a possibly time-varying interaction graph $G(\mathcal{V}, \mathcal{E}(t), A(t))$ determined by communication and sensing patterns. Interesting motion patterns emerge if the controllers use only relative phase information between neighboring particles, that is, $u_i = \omega_0(t) + f_i(\theta_i - \theta_j)$ for $\{i, j\} \in \mathcal{E}(t)$ and $\omega_0 : \mathbb{R}_{\geq 0} \rightarrow \mathbb{R}$. For example, the steering control $u_i =$

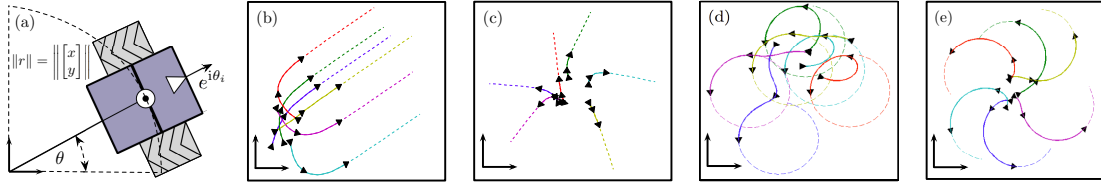


Figure 2.3: Illustration of controlled planar particle dynamics

Panel (a) illustrates the particle kinematics (2.7). Panels (b)-(e) illustrate the controlled dynamics (2.7)-(2.8) with $n=6$ particles, a complete interaction graph, and identical and constant natural frequencies: $\omega_0(t) = 0$ in panels (b) and (c) and $\omega_0(t) = 1$ in panels (d) and (e). The values of K are $K = 1$ in panel (b) and (d) and $K = -1$ in panel (c) and (e). The arrows depict the orientation, the dashed curves show the long-term position dynamics, and the solid curves show the initial transient position dynamics. As illustrated, the resulting motion displays “synchronized” or “balanced” heading angles for $K = \pm 1$, and translational motion for $\omega_0(t) = 0$, respectively circular motion for $\omega_0(t) = 1$.

$\omega_0(t) - K \cdot \sum_{j=1}^n a_{ij}(t) \sin(\theta_i - \theta_j)$ with gain $K \in \mathbb{R}$ results in the phase dynamics

$$\dot{\theta}_i = \omega_0(t) - K \cdot \sum_{j=1}^n a_{ij}(t) \sin(\theta_i - \theta_j), \quad i \in \{1, \dots, n\}. \quad (2.8)$$

The controlled phase dynamics (2.8) form a network of purely kinematic oscillators (1.1b) with a time-varying interaction graph with weights $K \cdot a_{ij}(t)$ and identically time-varying natural frequencies $\omega_i = \omega_0(t)$. The controlled phase dynamics (2.8) give rise to elegant and useful coordination patterns that mimic animal flocking behavior [163] and fish schools [209]. A few representative trajectories are illustrated in Figure 2.3. Inspired by these biological phenomena, scientists have studied the controlled phase dynamics (2.8) and their variations in the context of tracking and formation controllers in swarms of autonomous vehicles. We refer to [148, 149, 163, 209, 237, 242, 243] for further control laws and motion patterns.

Clock Synchronization in Decentralized Networks

Another emerging technological application of oscillator networks is clock synchronization in decentralized computing networks. A natural approach to clock synchronization is to treat each clock as an oscillator and follow a diffusion-based (or pulse-coupling) protocol to synchronize them, see the surveys [167, 247] and the interesting recent results [23, 128, 174, 287, 288].

For illustration, consider a set of distributed processors $\mathcal{V} = \{1, \dots, n\}$ connected by a (possibly directed) communication network. Each processor is equipped with an internal clock. These clocks need to be synchronized for distributed computing and network routing tasks. As discussed in the surveys [167, 247], we consider only analog clocks with continuous coupling since digital clocks are essentially discretized analog clocks, and pulse-coupled clocks can be modeled continuously after a phase reduction and averaging analysis. For our purposes, the clock of processor i is a voltage-controlled oscillator (VCO) generating a harmonic waveform $s_i(t) = \sin(\theta_i(t))$, where $\theta_i(t)$ is the accumulated instantaneous phase. For uncoupled clocks, each phase $\theta_i(t)$ evolves according to

$$\theta_i(t) = \left(\theta_i(0) + \frac{2\pi}{T_{\text{nom}} + T_i} t \right) \bmod(2\pi), \quad i \in \{1, \dots, n\}.$$

where $T_{\text{nom}} > 0$ is the nominal period, $T_i \in \mathbb{R}$ is an offset (or skew), and $\theta_i(0) \in \mathbb{S}^1$ is the initial phase. To synchronize their internal clocks, the processors follow a

diffusion-based protocol. In a first step, neighboring oscillators communicate their respective waveforms $s_i(t)$ to another. Second, through a phase detector (PD) each node measures a convex combination of phase differences

$$\text{cvx}_i(\theta(t)) = \sum_{j=1}^n a_{ij} f(\theta_i(t) - \theta_j(t)), \quad i \in \{1, \dots, n\},$$

where $f : \mathbb{S}^1 \rightarrow \mathbb{R}$ is an odd 2π -periodic function, and $a_{ij} \geq 0$ are detector-specific convex weights satisfying $\sum_{j=1}^n a_{ij} = 1$. Finally, $\text{cvx}_i(\theta(t))$ is fed to a phase-locked loop filter (PLL) whose output drives the local phase. A first-order and constant PLL with gain K results in

$$\dot{\theta}_i(t) = \frac{2\pi}{T_{\text{nom}} + T_i} + K \cdot \text{cvx}_i(\theta(t)), \quad i \in \{1, \dots, n\}. \quad (2.9)$$

The diffusion-based synchronization protocol (2.9) is illustrated in Figure 2.4, and its objective is to synchronize the frequencies $\dot{\theta}_i(t)$ and possibly also the phases $\theta_i(t)$ in the processor network. For an undirected communication protocol, symmetric weights $a_{ij} = a_{ji}$, and a sinusoidal coupling function $f(\cdot) = \sin(\cdot)$, the synchronization protocol (2.9) equals the coupled oscillator model (1.1).

Canonical Coupled Oscillator Model

In the preceding subsections we have seen how the coupled-oscillator model (1.1) appears naturally in various applications. We now illustrate how this apparently specific model can be derived as a *canonical model* of coupled limit-cycle

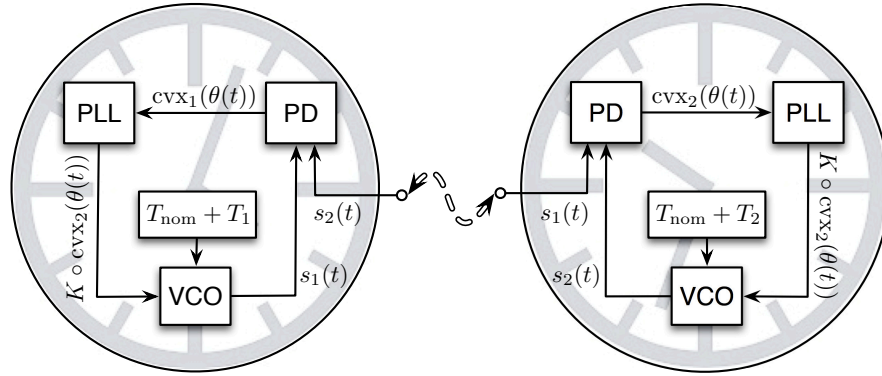


Figure 2.4: Schematic illustration of diffusion-based clock synchronization. The figure shows a schematic illustration of the diffusion-based synchronization protocol (2.9) for two coupled analog clocks.

oscillators [129] through a standard reduction procedure from general limit-cycle oscillator and interaction models. Our presentation is informal, we schematically follow the approaches developed in the computational neuroscience community, and we refer to the textbooks [129,137], the tutorials [138,177], and the pioneering papers [97,294] for further details.

Consider a limit-cycle oscillator modeled as a dynamical system with state $x \in \mathbb{R}^m$ and nonlinear dynamics $\dot{x} = f(x)$. Assume that this system admits a locally exponentially stable periodic orbit $\mathcal{S} \subset \mathbb{R}^m$ with period $T > 0$. By a local change of variables, any trajectory in a neighborhood of \mathcal{S} can be characterized by a phase variable $\varphi \in \mathbb{S}^1$ with dynamics $\dot{\varphi} = \Omega$, where $\Omega = 2\pi/T$. Now consider a weakly-forced oscillator of the form

$$\dot{x}(t) = f(x(t)) + \epsilon g(t), \quad (2.10)$$

where $\epsilon > 0$ is sufficiently small and $g(t)$ is a time-dependent external forcing term. For sufficiently small forcing $\epsilon g(t)$, the attractive limit cycle \mathcal{S} persists, and the local phase dynamics are obtained as

$$\dot{\varphi}(t) = \Omega + \epsilon Q(\varphi(t))g(t),$$

where $\varphi \mapsto Q(\varphi)$ is the *infinitesimal phase response curve* (iPRC) and we dropped higher order terms $\mathcal{O}(\epsilon^2)$. The iPRC is a linear response function that associates to each point on the periodic orbit \mathcal{S} (parameterized by the phase φ) the phase shift induced by the input $\epsilon g(t)$.

Now consider n such limit-cycle oscillators. Let $x_i \in \mathbb{R}^m$ be the state of oscillator i with limit cycle $\mathcal{S}_i \subset \mathbb{R}^m$ and period $T_i > 0$. We assume that the oscillators are weakly coupled with interaction graph $G(\mathcal{V}, \mathcal{E})$ and dynamics

$$\dot{x}_i = f_i(x_i) + \epsilon \sum_{\{i,j\} \in \mathcal{E}} g_{ij}(x_i, x_j), \quad i \in \{1, \dots, n\}, \quad (2.11)$$

where g_{ij} is the coupling function for the pair $\{i, j\} \in \mathcal{E}$. This coupling function may be continuous or impulsive. The weak coupling in (2.11) can be identified with the weak forcing in (2.10), and a transformation to phase coordinates yields

$$\dot{\varphi}_i = \Omega_i + \epsilon \sum_{\{i,j\} \in \mathcal{E}} Q_i(\varphi_i) g_{ij}(x_i(\varphi_i), x_j(\varphi_j)),$$

where $\Omega_i = 2\pi/T_i$. The local change of variables $\theta_i(t) = \varphi_i(t) - \Omega_i t$ then yields the coupled phase dynamics

$$\dot{\theta}_i = \epsilon \sum_{\{i,j\} \in \mathcal{E}} Q_i(\theta_i + \Omega_i t) g_{ij}(x_i(\theta_i + \Omega_i t), x_j(\theta_j + \Omega_j t)).$$

An averaging analysis applied to the θ -dynamics yields

$$\dot{\theta}_i = \epsilon\omega_i + \epsilon \sum_{\{i,j\} \in \mathcal{E}} h_{ij}(\theta_i - \theta_j), \quad (2.12)$$

where the averaged coupling functions h_{ij} are

$$h_{ij}(\chi) = \lim_{T \rightarrow \infty} \frac{1}{T} \int_0^T Q_i(\Omega_i \tau) g_{ij}(x_i(\Omega_i \tau), x_j(\Omega_j \tau - \chi)) d\tau,$$

and $\omega_i = h_{ii}(0)$. Notice that the averaged coupling functions h_{ij} are 2π -periodic and the coupling in (2.12) is diffusive. If the interaction among the oscillators is anti-symmetric, then all functions h_{ij} are odd, and a first-order Fourier series expansion yields $h_{ij}(\cdot) \approx a_{ij} \sin(\cdot)$ as first harmonic with coefficient a_{ij} . In this case, the dynamics (2.12) in the slow time scale $\tau = \epsilon t$ reduce exactly to the coupled oscillator model (1.1). This analysis justifies calling (1.1) the *canonical model* for coupled limit-cycle oscillators. It also explains the widespread adoption of the oscillator network (1.1) as phenomenological model in synchronization studies.

For example, for two coupled van der Pol oscillators (with parameters in the quasi-harmonic limit) the above procedure results exactly in the coupled oscillator model (1.1), see the elegant analysis in [177]. In general, the coupling functions h_{ij} depend on the iPRC, may not be sinusoidal or antisymmetric, and include higher-order harmonics. Hence, the iPRC serves as a natural analysis [35, 231] and design [287, 288] tool for general limit-cycle oscillator models.

2.3 Synchronization Notions and Concepts

In this section, we introduce different notions of synchronization illustrated in Figure 2.5. We address various commonly-studied notions of synchronization associated with coherent behavior, cohesive phases, and aligned frequencies. We relate these concepts and synchronization notions to our enabling application of interest – synchronization in power networks. We do not touch upon related concepts such as phase balancing, splay state stabilization, and pattern formation since they are not relevant to our particular application.

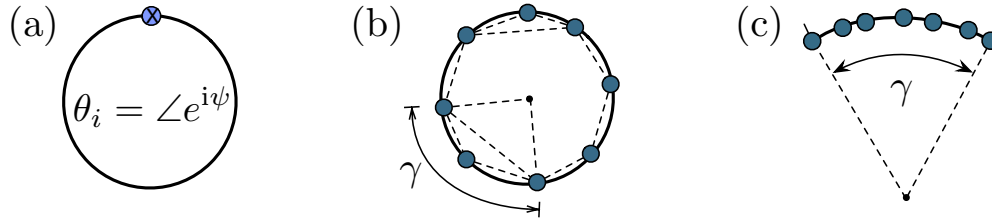


Figure 2.5: Illustration of synchronization concepts

Frequency-synchronized solutions of the oscillator network (1.1) can exhibit different phase configurations: (a) phase synchronization, (b) phase cohesiveness, and (c) arc invariance.

2.3.1 Synchronization Notions

Before beginning our discussion, we review some terminology and geometric concepts: The set \mathbb{S}^1 denotes the *unit circle*, an *angle* is a point $\theta \in \mathbb{S}^1$, and an *arc* is a connected subset of \mathbb{S}^1 . The *n-torus* is the Cartesian product $\mathbb{T}^n = \mathbb{S}^1 \times \cdots \times \mathbb{S}^1$.

The *geodesic distance* between two angles θ_1, θ_2 is the minimum of the counter-clockwise and the clockwise arc lengths connecting θ_1 and θ_2 . With slight abuse of notation, let $|\theta_1 - \theta_2|$ denote the *geodesic distance* between the angles $\theta_1, \theta_2 \in \mathbb{S}^1$.

The coupled oscillator model (1.1) evolves on $\mathbb{T}^n \times \mathbb{R}^{|\mathcal{V}_1|}$ and features an important symmetry, namely, the rotational invariance of the angular variable θ , that is, the oscillator network dynamics (1.1) remain invariant under a rotation of all oscillators by the same constant angle. This symmetry gives rise to the structure of the state space and the different synchronization properties that the model (1.1) can display. All notions of synchronized solutions share the common property that the frequencies are equal to a constant synchronization frequency.

Definition 2.3.1 (Frequency synchronization). *A solution $(\theta, \dot{\theta}): \mathbb{R}_{\geq 0} \rightarrow (\mathbb{T}^n, \mathbb{R}^{|\mathcal{V}_1|})$ achieves frequency synchronization if all frequencies $\dot{\theta}_i(t)$ converge to a common constant frequency $\omega_{\text{sync}} \in \mathbb{R}$ as $t \rightarrow \infty$.*

The explicit synchronization frequency $\omega_{\text{sync}} \in \mathbb{R}$ of the coupled oscillator model (1.1) can be obtained by exploiting its rich symmetry properties.

Lemma 2.3.2 (Explicit synchronization frequency). *If a solution of the coupled oscillator model (1.1) achieves frequency synchronization, then it does so with synchronization frequency equal to $\omega_{\text{sync}} = \frac{\sum_{i=1}^n \omega_i}{\sum_{i=1}^n D_i}$.*

Proof. By summing over all equations in (1.1), we obtain $\sum_{j=1}^{|\mathcal{V}_1|} M_j \ddot{\theta}_j + \sum_{i=1}^n D_i \dot{\theta}_i = \sum_{i=1}^n \omega_i$. In the frequency-synchronized case, this sum simplifies to $\sum_{i=1}^n D_i \omega_{\text{sync}} = \sum_{i=1}^n \omega_i$, and we obtain the synchronization frequency stated in the lemma. \square

By transforming to a rotating frame with frequency ω_{sync} and by replacing ω_i with $\omega_i - D_i \omega_{\text{sync}}$, we obtain $\omega_{\text{sync}} = 0$ (or equivalently $\omega \in \mathbf{1}_n^\perp$). In what follows, without loss of generality, we assume that $\omega \in \mathbf{1}_n^\perp$ so that $\omega_{\text{sync}} = 0$.

Remark 2.3.3 (Synchronization frequency in power networks). *For the considered lossless power network models in Subsection 2.2.1, the assumption $\omega_{\text{sync}} = 0$ translates to balanced power injections $\sum_{i \in \mathcal{V}_1} P_{m,i} + \sum_{i \in \mathcal{V}_2} P_{d,i} + \sum_{i \in \mathcal{V}_2} P_{l,i} = 0$. If this assumption is not satisfied, for example, the total load exceeds the total generation, then the network frequency drifts away from the nominal frequency.*

In the presence of losses, as in the model (2.5)-(2.6), the arguments in the proof of Lemma 2.3.2 lead to an additional term depending on the losses and the steady state power flows, and we obtain the synchronization frequency

$$\omega_{\text{sync}}^{\text{lossy}} = \frac{\sum_{i \in \mathcal{V}_1} \tilde{P}_{m,i} + \sum_{i \in \mathcal{V}_2} \tilde{P}_{d,i} - \sum_{i,j \in \mathcal{V}_1 \cup \mathcal{V}_2} \tilde{a}_{ij} \sin(\theta_i^* - \theta_j^* - \varphi_{ij})}{\sum_{i \in \mathcal{V}_1 \cup \mathcal{V}_2} D_i},$$

where $\theta^ \in \mathbb{T}^n$ is the steady state angle defined modulo rotational symmetry. Compared to the lossless synchronization frequency ω_{sync} , the additional term in $\omega_{\text{sync}}^{\text{lossy}}$ arises from the impedance loads or losses in the reduced transmission network.*

These losses need to be balanced by the generation such that $\omega_{\text{sync}}^{\text{lossy}} = 0$. \square

The definition of a frequency-synchronized solution allows for multiple phase configurations, for example, synchronized phases, see Figure 2.5(a).

Definition 2.3.4 (Phase synchronization). *A solution $(\theta, \dot{\theta}) : \mathbb{R}_{\geq 0} \rightarrow (\mathbb{T}^n, \mathbb{R}^{|\mathcal{V}_1|})$ to the coupled oscillator model (1.1) achieves phase synchronization if all phases $\theta_i(t)$ become identical as $t \rightarrow \infty$.*

Remark 2.3.5 (Terminology). *Alternative terminologies for phase synchronization include full, exact, or perfect synchronization. For a frequency-synchronized solution all phase distances $|\theta_i(t) - \theta_j(t)|$ are constant, and the terminology phase locking is sometimes used instead of frequency synchronization. Other commonly used terms instead of frequency synchronization include frequency locking, frequency entrainment, or also partial synchronization. \square*

It can be easily verified that for non-zero and dissimilar natural frequencies $\omega \in \mathbf{1}_n^\perp$, the coupled oscillator model (1.1) does not admit a phase-synchronized solution of the form $\theta_i(t) = \theta_j(t)$ for all $i, j \in \{1, \dots, n\}$. If the natural frequencies are dissimilar, then each pairwise distance $|\theta_i(t) - \theta_j(t)|$ can converge to a constant but not necessarily zero value. The concept of phase cohesiveness formalizes this possibility. For $\gamma \in [0, \pi[$, let $\bar{\Delta}_G(\gamma) \subset \mathbb{T}^n$ be the closed set of angle arrays $(\theta_1, \dots, \theta_n)$ with the property $|\theta_i - \theta_j| \leq \gamma$ for all $\{i, j\} \in \mathcal{E}$, that is, each pairwise phase distance is upper bounded by γ . Also, let $\Delta_G(\gamma)$ be the interior of $\bar{\Delta}_G(\gamma)$.

Definition 2.3.6 (Phase cohesiveness). *A solution $(\theta, \dot{\theta}) : \mathbb{R}_{\geq 0} \rightarrow (\mathbb{T}^n, \mathbb{R}^{|\mathcal{V}_1|})$ of the coupled oscillator model (1.1) is said to be phase cohesive if there exists a length $\gamma \in [0, \pi[$ such that $\theta(t) \in \bar{\Delta}_G(\gamma)$ for all $t \geq 0$.*

Notice that a phase cohesive solution is also phase synchronous when $\gamma = 0$.

The main object under study in most applications and theoretic analyses are phase-cohesive and frequency-synchronized solutions, where all oscillators rotate with the same frequency and all the pairwise phase distances are upper bounded. In the following, we restrict our attention to synchronized solutions with sufficiently small phase distances $|\theta_i - \theta_j| \leq \gamma < \pi/2$ for $\{i, j\} \in \mathcal{E}$. Of course, there may exist other synchronized solutions with larger phase distances, but these are not necessarily stable (see Lemma 3.2.1) and not relevant in our application of interest, see Remark 2.3.7 below. In what follows, in the interest of brevity, we call a solution *synchronized* if it is frequency synchronized and phase cohesive.

Remark 2.3.7 (Steady state phase distances in power networks). *In power network applications the coupling terms $a_{ij} \sin(\theta_i - \theta_j)$ are the active power flows along transmission lines $\{i, j\} \in \mathcal{E}$. Hence, the case of phase synchronization is not of interest since there is no active power flow in steady state. Also, for a transmission line $\{i, j\} \in \mathcal{E}$, the steady state phase distances $|\theta_i^* - \theta_j^*|$ need to be bounded well below $\pi/2$ due to thermal constraints. The bounds on the angular*

differences are known as security constraints and play an important role in the operation of a power system [297], for example, in power flow optimization. \square

A geometric object of interest is the synchronization manifold. Given a point $r \in \mathbb{S}^1$ and an angle $s \in [0, 2\pi]$, let $\text{rot}_s(r) \in \mathbb{S}^1$ be the rotation of r counterclockwise by the angle s . For $(r_1, \dots, r_n) \in \mathbb{T}^n$, define the equivalence class

$$[(r_1, \dots, r_n)] = \{(\text{rot}_s(r_1), \dots, \text{rot}_s(r_n)) \in \mathbb{T}^n \mid s \in [0, 2\pi]\}.$$

Clearly, if $(r_1, \dots, r_n) \in \bar{\Delta}_G(\gamma)$ for some $\gamma \in [0, \pi/2[$, then $[(r_1, \dots, r_n)] \subset \bar{\Delta}_G(\gamma)$.

Definition 2.3.8 (Synchronization manifold). *Given $\theta_{\text{sync}} \in \bar{\Delta}_G(\gamma)$ for some $\gamma \in [0, \pi/2[$, the set $([\theta_{\text{sync}}], \omega_{\text{sync}} \mathbf{1}_{|\mathcal{V}_1|}) \subset \mathbb{T}^n \times \mathbb{R}^{|\mathcal{V}_1|}$ is a synchronization manifold of the coupled oscillator model (1.1).*

Note that a synchronized solution takes value in a synchronization manifold due to rotational symmetry, and for $\omega \in \mathbf{1}_n^\perp$ (implying $\omega_{\text{sync}} = 0$) a synchronization manifold is also an equilibrium manifold of the coupled oscillator model (1.1). These geometric concepts are illustrated in Figure 2.6 for the two-dimensional case.

To conclude our list of synchronization notions, we introduce the concept of arc invariance. For $\gamma \in [0, 2\pi[$, let $\overline{\text{Arc}}_n(\gamma) \subset \mathbb{T}^n$ be the closed set of angle arrays $\theta = (\theta_1, \dots, \theta_n)$ with the property that there exists an arc of length γ containing all $\theta_1, \dots, \theta_n$. Thus, an angle array $\theta \in \overline{\text{Arc}}_n(\gamma)$ satisfies $\max_{i,j \in \{1, \dots, n\}} |\theta_i - \theta_j| \leq \gamma$. Finally, let $\text{Arc}_n(\gamma)$ be the interior of the set $\overline{\text{Arc}}_n(\gamma)$. Notice that $\overline{\text{Arc}}_n(\gamma) \subseteq$

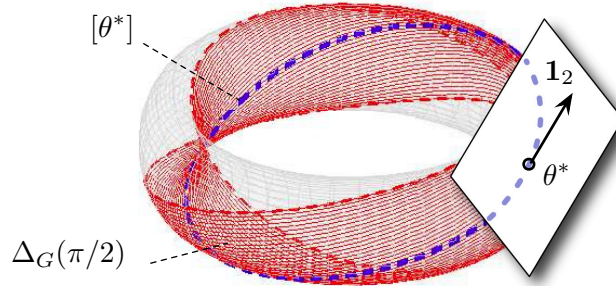


Figure 2.6: Illustration of the geometric concepts in the configuration space \mathbb{T}^2 . Illustration of the state space \mathbb{T}^2 , the set $\Delta_G(\pi/2)$ (red set), the synchronization manifold $[\theta^*]$ associated to a phase-synchronized angle array $\theta^* = (\theta_1^*, \theta_2^*) \in \bar{\Delta}_G(0)$ (blue curve), and the tangent space with translation vector $\mathbf{1}_2$ at θ^* .

$\bar{\Delta}_G(\gamma)$ but the two sets are generally not equal. For a complete coupling graph, sufficiently many oscillators, and for sufficiently small γ , the two sets become equal, and arc invariance is an appropriate synchronization notion.

Definition 2.3.9 (Arc invariance). *A solution $(\theta, \dot{\theta}) : \mathbb{R}_{\geq 0} \rightarrow (\mathbb{T}^n, \mathbb{R}^{|\mathcal{V}_1|})$ to the coupled oscillator model (1.1) said to be arc invariant if there exists a length $\gamma \in [0, 2\pi[$ such that $\theta(t) \in \overline{\text{Arc}_n(\gamma)}$ for all $t \geq 0$.*

2.3.2 A Simple yet Illustrative Example

The following example illustrates different notions of synchronization and points out various important geometric subtleties occurring on the compact state space \mathbb{T}^2 . Consider $n = 2$ oscillators with first-order dynamics $\mathcal{V}_1 = \emptyset$ and $\omega_2 \geq 0 \geq \omega_1 = -\omega_2$. We restrict our attention to angles contained in $\text{Arc}_n(\pi)$: for

angles θ_1, θ_2 with $|\theta_2 - \theta_1| < \pi$, the *angular difference* $\theta_2 - \theta_1$ is the number in $] -\pi, \pi[$ with magnitude equal to the geodesic distance $|\theta_2 - \theta_1|$ and with positive sign if and only if the counter-clockwise path length from θ_1 to θ_2 is smaller than the clockwise path length. With this definition the two-dimensional oscillator dynamics can be reduced to the scalar dynamics of the angular difference $\theta_2 - \theta_1$. After scaling time as $t \mapsto t(\omega_2 - \omega_1)$ and introducing $\kappa = 2a_{12}/(\omega_2 - \omega_1)$, we obtain

$$\frac{d}{dt}(\theta_2 - \theta_1) = f_\kappa(\theta_2 - \theta_1) \triangleq 1 - \kappa \sin(\theta_2 - \theta_1). \quad (2.13)$$

The dynamics (2.13) can be analyzed graphically by plotting the scalar vector field $f_\kappa(\theta_2 - \theta_1)$, for $\theta_2 - \theta_1 \in [0, \pi]$, see Figure 2.7(a). Figure 2.7 displays a saddle-node bifurcation at $\kappa = 1$. For $\kappa < 1$ no equilibria exist. For $\kappa > 1$ we have an asymptotically stable equilibrium $\theta_{\text{stable}} = \arcsin(\kappa^{-1}) \in]0, \pi/2[$ together with an unstable equilibrium $\theta_{\text{unstable}} = \arcsin(\kappa^{-1}) \in]\pi/2, \pi[$. For $\kappa > 1$ and $\theta(0) \in [0, \theta_{\text{unstable}}[$, all trajectories converge to θ_{stable} , that is, the oscillators synchronize and remain phase cohesive (or arc invariant). For $\theta(0) \notin [0, \theta_{\text{unstable}}]$ the difference $\theta_2(t) - \theta_1(t)$ increases beyond π , and $\theta_2(t) - \theta_1(t)$ converges asymptotically to the equilibrium θ_{stable} in the set where $\theta_2 - \theta_1 < 0$. Equivalently in the configuration space \mathbb{S}^1 , the oscillators revolve once around the circle before converging to $[\theta_{\text{stable}}]$. Since $\sin(\theta_{\text{stable}}) = \sin(\theta_{\text{unstable}}) = \kappa^{-1}$, in the limit $\kappa \rightarrow \infty$ the oscillators achieve phase synchronization from every initial condition in an open semi-circle $\text{Arc}_2(\pi)$.

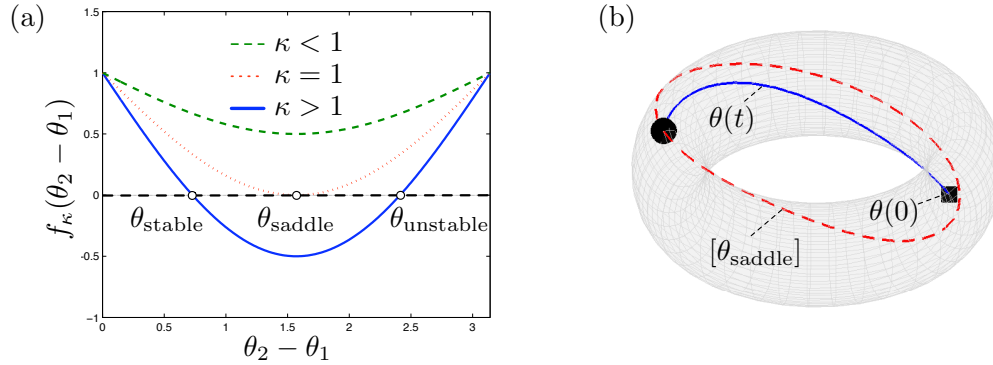


Figure 2.7: Graphical analysis of two coupled oscillators

Subfigure (a) shows a plot of the vector field (2.13) for $\theta_2 - \theta_1 > 0$ and different values of κ . Subfigure (b) displays a trajectory $\theta(t) \in \mathbb{T}^2$ for the critical case $\kappa = 1$. Here, the dashed line is the saddle equilibrium manifold and \blacksquare and \bullet depict the initial angles $\theta(0)$ and the asymptotic angles $\lim_{t \rightarrow \infty} \theta(t)$.

In the critical case, $\kappa = 1$, the saddle equilibrium manifold at $[\theta_{\text{saddle}}]$ is globally attractive but not stable, see the trajectory in Figure 2.7(b).

In conclusion, the simple but already rich 2-dimensional case shows that two oscillators are phase cohesive and synchronize if and only if $\kappa > 1$, that is, if and only if the coupling dominates the heterogeneity as $2a_{12} > \omega_2 - \omega_1$. The ratio $1/\kappa$ determines the asymptotic phase cohesiveness as well as the set of admissible initial conditions. More general oscillator networks display the same phenomenology, but the threshold from incoherence to synchrony is generally unknown. Finally, we remark that for oscillator networks of dimension $n \geq 3$, this loss of synchrony via a saddle-node bifurcation is only the starting point of a series of bifurcations occurring if the coupling is further decreased, see [172, 218, 264, 273].

2.4 Consensus, Convexity, & Contraction

In this section, we present the consensus protocol as a linear counterpart to the coupled oscillator model (1.1). We review some properties and analysis methods for the linear consensus protocol, and we show how these methods extend to networks of identical first-order oscillators.

2.4.1 Consensus Protocols

In a system of n *autonomous agents*, each characterized by a state variable $x_i \in \mathbb{R}$, a basic task is to achieve a consensus on a common state value. Given a digraph $G(\mathcal{V}, \mathcal{E}, A)$ with adjacency matrix $A \in \mathbb{R}^{n \times n}$ describing the interaction between agents, this consensus objective can be achieved by the *consensus protocol*

$$\dot{x}_i = - \sum_{j=1}^n a_{ij}(x_i - x_j), \quad i \in \{1, \dots, n\}. \quad (2.14)$$

The consensus protocol (2.14) is well-studied in the control literature [37, 104, 180, 200, 221], and it can be regarded as linear counterpart to the coupled oscillator model (1.1b) with first-order dynamics evolving on a Euclidean state space \mathbb{R}^n , without drift terms, and with identical and unit rates $D_i = 1$ for all $i \in \{1, \dots, n\}$.

In vector notation the consensus protocol (2.14) takes the form $\dot{x} = -Lx$. Due to the properties of the Laplacian matrix L listed in Section 2.1, the consensus dynamics (2.14) are translationally invariant, that is, $\mathbf{1}_n$ is an equilibrium subspace

and the change of variables $x \mapsto x + c\mathbf{1}_n$, where $c \in \mathbb{R}$, does not alter the consensus protocol (2.14). Additionally, the equilibrium subspace $\mathbf{1}_n$ is exponentially stable if and only if the graph G has a globally reachable node. The equilibrium subspace $\mathbf{1}_n$ is sometimes termed *agreement subspace* or the *consensus space*.

Consensus can also be established for digraphs with time-varying and non-negative weights $a_{ij} : \mathbb{R}_{\geq 0} \rightarrow \mathbb{R}_{\geq 0}$ for all $i, j \in \{1, \dots, n\}$. Of particular interest here is a *union δ -digraph*: given an interval $T > 0$ and a threshold $\delta > 0$, the union δ -digraph is the graph induced by the matrix $\tilde{A} = \int_t^{t+T} A(\tau) d\tau$, where we additionally set $\tilde{a}_{ij} = 0$ if $\tilde{a}_{ij} \leq \delta$. Under a joint connectivity assumption on the union δ -digraph for some $T > 0$ and $\delta > 0$, we can state the following result.

Theorem 2.4.1. (Convergence of the consensus protocol, [190, Theorems 1], [166, Theorem 3.6 and 3.7]) *Consider the time-varying consensus protocol*

$$\dot{x}_i(t) = - \sum_{j=1}^n a_{ij}(t)(x_i(t) - x_j(t)), \quad i \in \{1, \dots, n\}, \quad (2.15)$$

where each $a_{ij}(t) \geq 0$ is a bounded and piecewise continuous function of time for all $i, j \in \{1, \dots, n\}$. If there is $T > 0$ and $\delta > 0$ such that for each $t \geq 0$ the union δ -digraph induced by $\int_t^{t+T} A(\tau) d\tau$ has a globally reachable node, the time-varying consensus protocol (2.14) features the uniformly exponentially stable equilibrium subspace $\mathbf{1}_n$, the convex hull of all states $x_i(t)$ is non-increasing, and all states $x_i(t)$ will exponentially reach a consensus value $x_\infty \in [x_{\min}(0), x_{\max}(0)]$.

The proof of Theorem 2.4.1 relies on the *contraction Lyapunov function*

$$V(x(t)) = \max_{i,j \in \{1, \dots, n\}} |x_i(t) - x_j(t)|, \quad (2.16)$$

which is a measure for the size of the convex hull of all agents' states at time t . If $V(x(t))$ is a decreasing function of time, then the agents will asymptotically reach consensus. The technical analysis showing the decay of $V(x(t))$ is slightly more subtle since the function $V(x(t))$ is continuous but not necessarily differentiable when the maximum distance is attained by more than one pair of agents. The proof strategies rely on non-smooth analysis. The linear continuous-time case can be found in [190, Theorems 1], the linear discrete-time case can be found in [191, Theorems 1 and 2], the nonlinear case can be found in [166, Theorem 3.6 and 3.7], and we also recommend the review in [244, Section 2].

If the graph G is undirected and connected, then further conclusions can be drawn by symmetry considerations. In this case, $\mathbf{1}_n^T \dot{x}(t) = \mathbf{1}_n^T Lx(t) = \mathbf{0}_n$, and we conclude that $\sum_{i=1}^n x_i(t)$ is a conserved quantity for all $t \geq 0$. By applying this argument for $t = 0$ and $t \rightarrow \infty$, we conclude that, if the consensus protocol is convergent to $x_\infty \in [x_{\min}(0), x_{\max}(0)]$, we have that the asymptotic consensus value is the average of the initial values $x_\infty = \sum_{i=1}^n x_i(0)/n$. The appropriate error coordinate is then given by the *disagreement vector* $\delta = x - x_\infty \mathbf{1}_n$ living in the *disagreement space* $\mathbf{1}_n^\perp$. The quadratic disagreement Lyapunov function $\|\delta\|_2^2$ can

be adopted to show that the rate of convergence is no worse than $\lambda_2(L)$, that is, $\|\delta(t)\|_2 \leq \|\delta(0)\|_2 e^{-\lambda_2(L)t}$ for all $t \geq 0$, see [201, Theorem 8] and [200, Corollary 1].

2.4.2 Homogeneous Oscillator Networks as Nonlinear Consensus Protocols

The interest of the control community in oscillator networks (1.1) was initially sparked by the articles [139] and [191], which analyzed networks of identical oscillators as nonlinear extensions of the consensus protocol (2.14). Indeed, for identical oscillators with first-order dynamics $\mathcal{V} = \mathcal{V}_2 = \{1, \dots, n\}$, with zero natural frequencies $\omega = \mathbf{0}_n$, and with unit speeds $D_i = 1$ for all $i \in \{1, \dots, n\}$, the coupled oscillator model (1.1) simplifies to

$$\dot{\theta}_i = - \sum_{j=1}^n a_{ij} \sin(\theta_i - \theta_j), \quad i \in \{1, \dots, n\}. \quad (2.17)$$

If all angles are contained in an open semicircle $\theta \in \text{Arc}_n(\pi)$, the dynamics (2.17) can be projected onto the real line via the local coordinate map $\varphi :] - \pi/2, \pi/2[^n \rightarrow \mathbb{R}^n$ defined by $x_i = \varphi_i(\theta_i) = \tan(\theta_i)$. With this projection proposed in [191], the dynamics (2.17) are rewritten as the consensus-type model

$$\dot{x}_i = - \sum_{j=1}^n b_{ij}(x)(x_i - x_j), \quad (2.18)$$

where $b_{ij}(x) = a_{ij} \sqrt{(1+x_i^2)/(1+x_j^2)} \geq 0$. In particular, for $\theta \in \overline{\text{Arc}_n}(\gamma)$ for some $\gamma \in [0, \pi[$, we have that $b_{ij}(x) \geq a_{ij}/\sec(\gamma/2) > 0$ is strictly positive for $\{i, j\} \in \mathcal{E}$.

A similar viewpoint is taken in [139], where the coupled oscillator model (2.17) is equivalently written as

$$\dot{\theta}_i = - \sum_{j=1}^n c_{ij}(\theta)(\theta_i - \theta_j), \quad (2.19)$$

where $c_{ij}(\theta) = a_{ij} \operatorname{sinc}(\theta_i - \theta_j) \geq 0$. Again, we have that $c_{ij}(\theta) \geq a_{ij} \operatorname{sinc}(\gamma) > 0$ for $\{i, j\} \in \mathcal{E}$ and $\theta \in \overline{\operatorname{Arc}_n(\gamma)}$, $\gamma \in [0, \pi[$. Further consensus-theoretical derivations of the oscillator network (2.17) can be found in [199, 233, 241].

In both formulations (2.18) and (2.19), the dynamics (2.17) are regarded as a consensus protocol (2.14) with strictly positive weights whose values are time-varying or state-dependent. This interpretation is well defined provided that $\theta(t) \in \overline{\operatorname{Arc}_n(\gamma)}$ for all $t \geq 0$ and for some $\gamma \in [0, \pi[$. Different Lyapunov functions can be used to assure this boundedness. One natural Lyapunov function relying upon the contraction property is simply the length of the shortest arc containing all oscillators. We will revisit these ideas in detail in Chapter 4.

The following result follows from the analysis of nonlinear consensus protocols, see [166, Theorem 3.6 and 3.7] and [191, Theorems 1 and 2], and the convergence rate estimate can be obtained along the lines of [139, Theorem 1].

Theorem 2.4.2 (Contraction in Open Semicircle $\operatorname{Arc}_n(\pi)$). *Consider the coupled oscillator model (2.17) with a weighted digraph $G(\mathcal{V}, \mathcal{E}, A)$ and $\omega = \mathbf{0}_n$, and assume that G has a globally reachable node. Then each set $\overline{\operatorname{Arc}_n(\gamma)}$, for $\gamma \in [0, \pi[$,*

is positively invariant, and each trajectory originating in $\overline{\text{Arc}}_n(\gamma)$ achieves exponential phase synchronization. Moreover, if G is undirected then

$$\|\theta(t) - \theta_{\text{avg}} \mathbf{1}_n\|_2 \leq \|\theta(0) - \theta_{\text{avg}} \mathbf{1}_n\|_2 e^{\lambda_{\text{ps}} t}, \quad (2.20)$$

where $\lambda_{\text{ps}} = -\lambda_2(L) \text{sinc}(\gamma)$ and $\theta_{\text{avg}} = \sum_{i=1}^n \theta_i(0)/n$ is the average initial phase.¹

Theorem 2.4.2 also applies to more general interaction functions, and it can be extended to time-delays and time-varying graphs. Applications to oscillator networks and extensions can be found in [116, 116, 166, 191, 194, 232, 240]. In Chapter 4, we revisit this literature and adopt the contraction Lyapunov function and the quadratic disagreement Lyapunov function to complex oscillator networks.

Remark 2.4.3 (A control-theoretical perspective on synchronization). *As established in Theorems 2.4.2, the phase-synchronized set $\bar{\Delta}_G(0) = \overline{\text{Arc}}_n(0)$ is locally exponentially stable provided all natural frequencies are identical. While phase synchronization is not possible for dissimilar natural frequencies, a certain degree of phase cohesiveness can still be achieved. Indeed, the coupled oscillator model (1.1) can be regarded as an exponentially stable system subject to the disturbance $\omega \in \mathbf{1}_n^\perp$ and synchronization can be studied using classic control-theoretical concepts such as input-to-state stability, practical stability, ultimate boundedness [146]*

¹This “average” of angles (points on \mathbb{S}^1) is well-defined for angles in an open semi-circle. If the parametrization of θ has no discontinuity inside the arc containing all angles, then the average can be obtained by the usual formula.

or their incremental versions [14]. In control-theoretical terminology, phase cohesiveness can then be described as “practical phase synchronization.” Compared to prototypical nonlinear control examples, additional challenges arise in the analysis of the oscillator network (1.1) due to the bounded and non-monotone sinusoidal coupling, the compact state space, and the coexistence of multiple equilibria. \square

Chapter 3

Mechanical and Kinematic Oscillator Networks

Inertia is a mixed blessing.

(An apparently common insight in economics and rediscovered here.)

The bulk of the literature on synchronization of coupled oscillators considers a particular instance of the coupled oscillator model (1.1), namely first-order oscillator models with identical unit time-scales, that is, $\mathcal{V} = \mathcal{V}_2 = \{1, \dots, n\}$ and $D_i = 1$ for all $i \in \{1, \dots, n\}$. The resulting dynamics take the form

$$\dot{\theta}_i = \omega_i - \sum_{j=1}^n a_{ij} \sin(\theta_i - \theta_j), \quad \{1, \dots, n\}. \quad (3.1)$$

The first-order oscillator network model (3.1) is studied primarily in the dynamics, control, and physics communities, but also many approaches to transient stability analysis in power networks rely on the first-order model (3.1). On the other hand, many interesting applications of coupled oscillator networks include oscillators

with second-order mechanical dynamics, for instance, the power system models developed in Subsection 2.2.1.

The theoretic analysis methods for coupled oscillators have been developed mainly for first-order models of the form (3.1) and cannot be extended in a straightforward way to second-order models or only under conservative conditions. Nevertheless, the results and insights gained from the first-order oscillator network (3.1) carry over to the coupled oscillator model (1.1). In this chapter, we build bridges between the original coupled oscillator model (1.1) and its first-order variant (3.1). We show under which assumptions the two models can be related, and we also demonstrate when their dynamic behavior is qualitatively different.

3.1 Introduction

3.1.1 Relevant Literature

The coupled oscillator model (1.1) with both first and second-order dynamics appears directly in structure-preserving power network models [27,47,234]. Purely second-order oscillator networks (1.1a) appear in synchronization phenomena in populations of fireflies [96], in coupled Josephson junctions [292], in network-reduced power system models [49, 50], in animal flocking behavior [117, 120], in

laser oscillators [130], in micromechanical oscillators [246, 303], in coupled pendulum clocks [26, 144], in metronomes [211], and in crowd synchrony [261].

Multiple disciplines study the relationships between the first-order kinematic systems and the associated second-order Newtonian system, such as the coupled oscillator model (1.1) and its first-order variant (3.1). Clearly, both systems have the same equilibria. If the first-order vector field is a gradient system and admits a finite number of isolated and hyperbolic equilibria, then various similarities between the first-order gradient flow and the second-order dissipative Newtonian systems are known in mechanical control systems [150, 151], in dynamic optimization [10, 20, 109], and in transient stability studies for power networks [49, 51, 61]. These results do generally not extend to the coupled oscillator model (1.1) and its first-order variant (3.1). In order to overcome these difficulties in transient stability analysis, the dynamics are formulated in relative coordinates, for example, by pinning one generator angle to a fixed value or by assuming a uniform inertia over damping ratio for all generators. We remark that these mathematical assumptions are not necessarily physically justified. Additionally, the cited results do not extend to symmetry-breaking transfer conductances, or do so only for sufficiently small conductances. We will detail these shortcomings in Subsection 3.2.1.

The Kuramoto model (1.2) is a particular instance of the first-order coupled oscillator model (3.1). Likewise, a particular instance of the coupled oscillator

model (1.1) is given by the *multi-rate Kuramoto model*:

$$\begin{aligned} M_i \ddot{\theta}_i + D_i \dot{\theta}_i &= \omega_i - \frac{K}{n} \sum_{i=1}^n \sin(\theta_i - \theta_j), & i \in \mathcal{V}_1, \\ D_i \dot{\theta}_i &= \omega_i - \frac{K}{n} \sum_{i=1}^n \sin(\theta_i - \theta_j), & i \in \mathcal{V}_2. \end{aligned} \tag{3.2}$$

For $\mathcal{V}_2 = \emptyset$, unit damping $D_i = 1$, and uniform inertia $M_i = M > 0$, the second-order Kuramoto system (3.2) has received some attention in the recent literature [2, 3, 57, 126, 127, 265, 266]. The cited results on the inertial effects on synchronization are controversial and report that synchronization is either enhanced or inhibited by sufficiently large (or also sufficiently small) inertial coefficients.

In [57] two sufficient synchronization conditions are derived via second-order Gronwall's inequalities resulting in an explicit bound on the critical coupling together with conditions on sufficiently small inertia or sufficiently large inertia [57, Theorems 5.1 and 5.2]. In [57, Theorem 4.1 and 4.2] phase synchronization was also found to depend on the inertia, whereas phase synchronization was found to be independent of the inertia in the corresponding continuum limit model [2, 3]. References [265, 266] observe a discontinuous first-order phase transition (where the incoherent state loses its stability), which is independent of the distribution of the natural frequencies when the inertia M is sufficiently large. This result is also confirmed in [2, 3]. In [127] a second-order Kuramoto model with time delays is analyzed, and a correlation between the inertia and the asymptotic synchronization frequency and asymptotic magnitude of the order parameter magnitude

Chapter 3. Mechanical and Kinematic Oscillator Networks

is observed. In [2, 3, 126] it is reported that inertia suppress synchronization for an externally driven or noisy second-order Kuramoto model, and [2, 3] explicitly show that the critical coupling K_{critical} increases with the inertia coefficient M for a Lorentzian or a bipolar distribution of the natural frequencies.

The cited results [2, 3, 57, 126, 127, 265, 266] on the inertial effects on synchronization appear conflicting. Possible reasons for this controversy include that the cited articles consider slightly different scenarios (time delays, noise, external forcing), the cited results are only sufficient, the analyses are based on the infinite-dimensional continuum-limit approximation of the finite-dimensional model (3.2), and some results stem from insightful but partially incomplete numerical observations and physical intuition.

3.1.2 Contributions and Organization

In the following sections, we present different methods to relate the coupled oscillator model (1.1) and its first-order variant (3.1).

Section 3.2: We begin our discussion by introducing a forced Hamiltonian and forced gradient formulation of the coupled oscillator model (1.1). We find that this formulation is very versatile for the latter analysis. Since the classic transient stability analysis literature also makes use of Hamiltonian methods, we present a brief review in Subsection 3.2.1. Additionally, we state some key prop-

erties resulting from a potential landscape and Jacobian analysis of the first-order coupled oscillator model (3.1), see Lemma 3.2.1.

Section 3.3: In this section, we prove a general result that relates the equilibria and local stability properties of forced gradient systems to those of dissipative Hamiltonian systems together with gradient-like dynamics and external forcing, see Theorem 3.3.1. Our method of proof relies on homotopy methods, topological conjugacy arguments, and matrix theory. As a special case, we are able to show that the coupled oscillator model (1.1) is locally topologically conjugate to its first-order variant (3.1), see Theorem 3.3.3. As a corollary of this topological conjugacy and our analysis of the potential landscape, we are able to state a result on phase synchronization in the coupled oscillator model (1.1), see Theorem 3.3.4.

Our results show that the inertial coefficients M_i *do not affect* the local synchronization conditions in the coupled oscillator model (1.1). In particular, the location and local stability properties of all equilibria are independent of the inertial coefficients M_i and so are all local bifurcations. Rather, these quantities depend on the viscous damping parameters D_i and the natural frequencies ω_i . These interesting and provably correct findings contradict prior observations on the role of inertia inhibiting or enhancing synchronization in second-order multi-rate Kuramoto models (3.2). Of course, these conclusions are valid only locally, and the inertial terms still affect the transient synchronization behavior. Addition-

ally, the topological conjugacy results strongly rely on the fact that the coupled oscillator model (1.1) can be formulated as a forced gradient and Hamiltonian system. The equivalence of local stability conditions may not be true otherwise. We conclude Section 3.3 by highlighting the role of inertia and damping terms in transient stability analysis in power networks.

Section 3.4: In this section, we present a reduction method that allows to relate transient dynamics and the trajectories of first and second-order oscillator networks. We consider a system of coupled oscillators with second-order dynamics and with phase shifts in the coupling functions. This model is found in the description of network-reduced power system models (2.5). The symmetry-breaking phase shifts imply that the model is not Hamiltonian, and the topological conjugacy results cannot be applied. We assume that each oscillator is strongly overdamped, that is, the ratio of inertia and damping is sufficiently small. This assumption allows us to relate the second-order oscillator dynamics to an associated first-order oscillator model through a singular perturbation analysis.

In order to apply a singular perturbation analysis by Tikhonov's method, we reformulate the first and second-order oscillator networks in grounded coordinates, which take value in Euclidean space and remove the rotational symmetry. Our main result, Theorem 3.4.2, shows that for a sufficiently overdamped oscillators, the trajectories of the first and second-order oscillator network can be related up

to an error of the order of the perturbation parameter. We illustrate the quality of the singular perturbation approximation through a simulation study, and discuss the validity of the singular perturbation assumption in power network models.

Section 3.5: This section concludes this chapter by comparing the singular perturbation and topological conjugacy approaches as well as alternative approaches suggested in the literature.

3.2 Hamiltonian and Gradient Formulation

Recall the mechanical analog in Figure 1.1. The potential energy $U : \mathbb{T}^n \rightarrow \mathbb{R}$ of the elastic springs is, up to an additive constant,

$$U(\theta) = \sum_{\{i,j\} \in \mathcal{E}} a_{ij} (1 - \cos(\theta_i - \theta_j)). \quad (3.3)$$

For the complete graph with uniform weights K/n , the magnitude r of the order parameter and the potential energy $U(\theta)$ are related by $\frac{2}{n}U(\theta) = 1 - r^2$. One can easily verify that the phase-synchronized state is a local minimum of the potential.

In general, for an *undirected* graph, the coupled oscillator model (1.1) can be rewritten as a mixed gradient and Newtonian (or second-order Hamiltonian) system with dissipation and external forcing terms:

$$\begin{aligned} M_i \ddot{\theta}_i + D_i \dot{\theta}_i &= \omega_i - \frac{\partial}{\partial \theta_i} U(\theta), & i \in \mathcal{V}_1, \\ D_i \dot{\theta}_i &= \omega_i - \frac{\partial}{\partial \theta_i} U(\theta), & i \in \mathcal{V}_2. \end{aligned} \quad (3.4)$$

Likewise, the first-order coupled oscillator model (3.1) can be reformulated as the forced gradient flow

$$\dot{\theta}_i = \omega_i - \frac{\partial}{\partial \theta_i} U(\theta), \quad i \in \{1, \dots, n\}. \quad (3.5)$$

3.2.1 Classic Transient Stability Analysis Approaches

As discussed in Subsection 3.1.1, non-gradient-like vector fields and non-isolated equilibria pose challenges in the analysis of the coupled oscillator model (1.1) and its first-order variant (3.1). In the following, we show how the transient stability literature circumvents these obstacles and which assumptions are typically made.

In order to remove the rotational symmetry and to render the synchronization problem to a stability problem, the power system dynamics are usually formulated in relative coordinates. Sometimes, the existence of an *infinite bus* (a stationary bus with fixed angle and without dynamics) as reference is postulated [52, 278]. Some other times, the *center of angle coordinates* $\theta_i - (\sum_j M_j \theta_j / \sum_j M_j)$ are chosen or machine n is selected as reference in the coordinates $\theta_i - \theta_n$, $i \in \{1, \dots, n - 1\}$ [6, 268]. Since the resulting dynamics under these approaches are not self-contained, a common (and historically debated [206]) assumption is that of uniform damping, that is, D_i/M_i is assumed to be constant for all generators. We remark that the assumption of uniform damping and the existence of an infinite bus are mathematical simplifications that are not necessarily physically justified.

For dissimilar forcing terms, the vector field (3.5) is not a gradient system, and the second-order vector field (3.4) is not a Hamiltonian system. Dissimilar forcing terms correspond to the distinct natural frequencies in a heterogeneous oscillator network or to active power injections (positive for sources and negative for sinks) in a power network. In the transient stability literature, the forcing terms are usually absorbed into the potential energy, such that it reads

$$\tilde{U}(\theta) = U(\theta) - \sum_{i=1}^n \omega_i \cdot \theta_i.$$

Notice that $\tilde{U}(\theta)$ is not a 2π -periodic function, it is only locally defined on \mathbb{T}^n , and its level sets are not necessarily compact. Hence, even though $\tilde{U}(\theta)$ is decreasing along solutions of (3.1), it cannot be used as a standard Lyapunov function whose level sets guarantee a bounded evolution. On the other hand, it can be used within the *energy function* framework [8, 48, 50, 207, 278], which led to the development of various sophisticated analytic and computational methods.

In presence of transmission line losses or impedance load models, the power network equations feature nontrivial (transfer) conductances $\Re(Y_{ij}) > 0$ (or equivalently nonzero phase shifts $\varphi_{ij} > 0$) and read as in (2.5)-(2.6). Since Hamiltonian formulations for lossy power network models do not exist [62], early analysis approaches neglect the conductances [52, 278]. While this assumption is fairly realistic for the line losses in high-voltage transmission networks, it cannot be made for

transfer conductances arising from impedance loads. These obstacles led to the development of structure-preserving models and their analysis [27, 48, 50, 274, 305].

Finally, we highlight the *PEBS* [52] and the *BCU* [49] analysis methods, which relate the first and second-order systems (3.4)-(3.5) under the above assumptions. We list the following results: $(\theta^*, \mathbf{0}_{|\mathcal{V}_1|})$ is a hyperbolic type- k equilibrium of (3.4), that is, the Jacobian has k stable eigenvalues, if and only if θ^* is a hyperbolic type- k equilibrium of (3.5). Additionally, if a generic transversality condition holds, then the regions of attractions of both equilibria are bounded by the stable manifolds of the same unstable equilibria [52, Theorems 6.2-6.3]. By means of structural stability arguments, these results can also be extended for “sufficiently small” phase shifts φ_{ij} [49, Theorem 5.7]. Based on these results, sophisticated computational methods were developed to approximate the stability boundaries of (3.4) by level sets of energy functions and separatrices of (3.5).

We remark that for sufficiently large conductances and sufficiently small damping, the local stability properties do not translate between the two models (3.4)-(3.5), see [252]. Additionally, power network models sometimes feature “degenerate” vector fields, where the generic transversality conditions fail, and sufficiently large damping is required to relate the regions of attractions of the two models (3.4)-(3.5), see [7, 9, 63, 205, 208]. We revisit these issues in Subsection 3.3.4.

3.2.2 Potential Landscape and Jacobian Analysis

In this subsection, we review a few fundamental insights, we state some key properties, and we introduce some analysis methods which will be exploited in this section and throughout the rest of this thesis.

The formulation (3.5) of the first-order oscillator network (3.1) as a forced gradient system clarifies the competition between the synchronization-enforcing coupling through $U(\theta)$ and the synchronization-inhibiting heterogeneous natural frequencies ω_i . The unforced system (3.5) with $\omega = \mathbf{0}_n$ is simply a negative gradient flow $\dot{\theta} = -\partial U(\theta)/\partial\theta$ with $U(\theta)$ as natural Lyapunov function.

Since the Jacobian $J(\theta)$ is the negative Hessian of the potential $U(\theta)$, we continue by drawing some insights from a Jacobian analysis. The following results are known in the synchronization literature [85, 139] as well as in power systems, where the saturation of a transmission line corresponds to a singularity of the load flow Jacobian and results in a saddle node bifurcation [16, 27, 47, 78, 112, 136, 234, 235, 269, 270, 298, 299]. To the best of the author's knowledge the following insights date back to in [269, 270] and have been rediscovered several times.

Lemma 3.2.1 (Stable synchronization in $\Delta_G(\pi/2)$). *Consider the coupled oscillator model (1.1) with an undirected, connected, and weighted graph $G(\mathcal{V}, \mathcal{E}, A)$ and frequencies $\omega \in \mathbf{1}_n^\perp$. If there exists an equilibrium $\theta^* \in \Delta_G(\pi/2)$, then*

(i) The Jacobian $J(\theta^*)$ is a negative Laplacian matrix:

$$J(\theta) = -B \operatorname{diag}(\{a_{ij} \cos(\theta_i^* - \theta_j^*)\}_{\{i,j\} \in \mathcal{E}}) B^T; \quad (3.6)$$

(ii) the equilibrium manifold $[\theta^*] \subset \Delta_G(\pi/2)$ is locally exponentially stable (modulo rotational symmetry).

Proof. The right-hand side of (1.1) defines the vector field $f : \mathbb{T}^n \rightarrow \mathbb{R}^n$ with components

$$f_i(\theta) = \omega_i - \sum_{j=1}^n a_{ij} \sin(\theta_i - \theta_j), \quad i \in \{1, \dots, n\}. \quad (3.7)$$

Since we have that $\frac{\partial}{\partial \theta_i} f_i(\theta) = -\sum_{j=1}^n a_{ij} \cos(\theta_i - \theta_j)$ and $\frac{\partial}{\partial \theta_j} f_i(\theta) = a_{ij} \cos(\theta_i - \theta_j)$, the negative Jacobian $-J(\theta)$ of the coupled oscillator model (1.1) equals the Laplacian of the connected graph $G(\mathcal{V}, \mathcal{E}, \tilde{A})$ where $\tilde{a}_{ij} = a_{ij} \cos(\theta_i - \theta_j)$. Equivalently, in compact notation the Jacobian is given by $J(\theta)$ in (3.6).

The Jacobian $J(\theta)$ evaluated at an equilibrium point $\theta^* \in \bar{\Delta}_G(\gamma)$ is negative semidefinite with rank $n - 1$. Its nullspace $\mathbf{1}_n$ arises from the rotational symmetry, see Figure 2.6. Consequently, the equilibrium $\theta^* \in \bar{\Delta}_G(\gamma)$ is locally (transversally) exponentially stable, and the corresponding equilibrium manifold $[\theta^*] \subset \bar{\Delta}_G(\gamma)$ is locally exponentially stable. This completes the proof of statement 2). \square

Remark 3.2.2 (Uniqueness in $\bar{\Delta}_G(\pi/2)$). *In earlier work [89], we also stated that the equilibrium manifold $[\theta^*]$ is unique in $\bar{\Delta}_G(\pi/2)$ (modulo rotational symmetry).*

The proof of this statement was based on [16, Corollary 1], which states that the vector field $f - \omega$ is a one-to-one function on $\bar{\Delta}_G(\pi/2)$ modulo rotational symmetry, that is, for $\theta_1 \in \bar{\Delta}_G(\pi/2)$ and $\theta_2 \in \bar{\Delta}_G(\pi/2)$, we have that $f(\theta_1) = f(\theta_2)$ if and only if $[\theta_1] = [\theta_2]$. However, the result [16, Corollary 1] is erroneous when carefully treating the angles as elements on the unit circle \mathbb{S}^1 rather than numbers on the real axis \mathbb{R} . A simple counter-example is given by a ring graph with $n \geq 5$ nodes, with identical unit weights, and with $\omega = \mathbf{0}_n$. In this case, the phase-synchronized set $\bar{\Delta}_G(0) \subset \bar{\Delta}_G(\pi/2)$ is one stable solution in $\bar{\Delta}_G(\pi/2)$. Yet another stable solution in $\bar{\Delta}_G(\pi/2)$ is given by a loop flow [154], that is, the set of uniformly spaced angles $[\theta^*] = [(0, 2\pi/n, \dots, (n-1) \cdot 2\pi/n)] \in \bar{\Delta}_G(2\pi/n) \subset \bar{\Delta}_G(\pi/2)$. \square

These basic results in Lemma 3.2.1 are fundamental to various analysis approaches. Further consequences of the particular form of the Jacobian (3.6) in $\Delta_G(\pi/2)$ are collected in Chapter 4. The results in Lemma 3.2.1 are applicable only to angles inside the phase cohesive set $\Delta_G(\pi/2)$, where all weights $\tilde{a}_{ij}(\theta^*) = a_{ij} \cos(\theta_i^* - \theta_j^*)$ are strictly positive for $\{i, j\} \in \mathcal{E}$ and the Laplacian properties of the Jacobian $J(\theta)$ can be exploited. Outside the set $\Delta_G(\pi/2)$, the weights $\tilde{a}_{ij}(\theta^*) = a_{ij} \cos(\theta_i^* - \theta_j^*)$ can be zero or negative for $\{i, j\} \in \mathcal{E}$, and the associated state-dependent graph (induced by $\tilde{A}(\theta^*)$) may be disconnected. In this more general setting, the standard methods from algebraic and spectral graph theory cannot be applied and many puzzling examples are known [16]. A

necessary condition for stability of arbitrary equilibrium manifolds $[\theta^*] \subset \mathbb{T}^n$ is that the graph induced by the Jacobian $J(\theta^*)$ possesses a spanning tree with strictly positive weights $\tilde{a}_{ij}(\theta^*) > 0$ along its edges [77]. Sufficient stability and instability conditions can be derived if the graph induced by $J(\theta^*)$ admits certain cutsets [16, 27, 47, 173]. Finally, for the complete graph with uniform weights (see the Kuramoto model (1.2)), additional insights and identities related to the Jacobian (3.6) can be found in [5, 33, 185, 281].

Since the Jacobian matrix $J(\theta)$ is the negative Hessian matrix of the potential $U(\theta)$, Lemma 3.2.1 implies that any equilibrium in $\Delta_G(\pi/2)$ is a local minimizer of $U(\theta)$. Of particular interest are so-called \mathbb{S}^1 -*synchronizing graphs* for which all critical points of (3.3) are hyperbolic, the phase-synchronized state is the global minimum of $U(\theta)$, and all other critical points are local maxima or saddle points. The class of \mathbb{S}^1 -synchronizing graphs includes, among others, complete graphs and acyclic graphs [42–44, 189, 232]. These basic results motivated the study of the critical points and of the curvature of the potential energy $U(\theta)$ in the literature on the theory and applications of synchronization, including, for example, the study of transient stability in power systems and the design of motion coordination controllers for planar vehicles, see Subsections 2.2.2 and 2.2.1.

3.3 Topological Conjugacy

In this section we show that the location, local stability conditions, and local bifurcations are identical in the coupled oscillator model (1.1) and its first-order variant (3.1). In Subsection 3.3.1, we prove a general theorem that relates the local stability properties of first-order gradient-like systems and second-order dissipative Hamiltonian systems. In Subsection 3.3.2, we specialize this result to complex oscillator networks. In Subsection 3.3.3, we further refine this result for homogeneous oscillator networks. As a consequence, the local synchronization conditions are independent of the inertiae, but transient dynamics and non-gradient-like dynamics strongly depend on the inertial terms, as discussed in Subsection 3.3.4.

The treatment in this section slightly differs from the author's article [83] and contains a simpler problem setup and more compact proof methods.

3.3.1 A One-Parameter Family of Dynamical Systems and its Properties

In this subsection, we apply homotopy methods to link the coupled oscillator model (1.1) and its first-order variant (3.1) through a parametrized system.

Consider for $n_1, n_2 \geq 0$ and $\lambda \in [0, 1]$ the following one-parameter family \mathcal{H}_λ of dynamical systems combining dissipative Hamiltonian and gradient-like dynamics

together with external forcing as

$$\begin{aligned}
 (\lambda I_{n_1} + (1 - \lambda)D_1)\dot{x}_1 &= F_1 - \frac{\partial H(x)}{\partial x_1}, \\
 \mathcal{H}_\lambda : \begin{bmatrix} I_{n_2} & \mathbf{0} \\ \mathbf{0} & (\lambda I_{n_2} + (1 - \lambda)M) \end{bmatrix} \begin{bmatrix} \dot{x}_2 \\ \dot{x}_3 \end{bmatrix} &= \begin{bmatrix} \lambda F_2 \\ (1 - \lambda)F_2 \end{bmatrix} + \\
 &\left((1 - \lambda) \begin{bmatrix} \mathbf{0} & I_{n_2} \\ -I_{n_2} & \mathbf{0} \end{bmatrix} - \begin{bmatrix} \lambda I_{n_2} & \mathbf{0} \\ \mathbf{0} & (\lambda I_{n_2} + (1 - \lambda)D_2) \end{bmatrix} \right) \begin{bmatrix} \frac{\partial H(x)}{\partial x_2} \\ \frac{\partial H(x)}{\partial x_3} \end{bmatrix},
 \end{aligned} \tag{3.8}$$

where $x = (x_1, x_2, x_3) \in \mathcal{X}_1 \times \mathcal{X}_2 \times \mathbb{R}^{n_2} = \mathcal{X}$. Here, \mathcal{X}_1 and \mathcal{X}_2 are smooth manifolds of dimensions n_1 and n_2 , respectively. The matrices $D_1 \in \mathbb{R}^{n_1 \times n_1}$, $D_2 \in \mathbb{R}^{n_2 \times n_2}$, and $M \in \mathbb{R}^{n_2 \times n_2}$ are positive definite. The symbol $\mathbf{0}$ denotes zero matrices of appropriate dimension¹, $F_1 \in \mathbb{R}^{n_1}$ and $F_2 \in \mathbb{R}^{n_2}$ are constant forcing terms, and $H : \mathcal{X} \rightarrow \mathbb{R}$ is a smooth potential function with gradient $\nabla H(x) = (\partial H(x)/\partial x)^T \in \mathbb{R}^{(n_1+2n_2) \times 1}$ and Hessian matrix $\nabla^2 H(x) = \partial^2 H(x)/\partial x^2 \in \mathbb{R}^{(n_1+2n_2) \times (n_1+2n_2)}$.

The parameterized system (3.8) continuously interpolates, as a function of $\lambda \in [0, 1]$, between gradient and mixed dissipative Hamiltonian/gradient-like dynamics. For $\lambda = 0$, the dynamics (3.8) reduce to gradient-like dynamics for x_1

¹In this subsection, we do not index the zero matrices according to their dimension to avoid notational clutter.

and dissipative Hamiltonian (or Newtonian) dynamics for (x_2, x_3) written as

$$D_1 \dot{x}_1 = F_1 - \frac{\partial H(x)}{\partial x_1},$$

$$\mathcal{H}_0 : \begin{bmatrix} I_{n_2} & \mathbf{0} \\ \mathbf{0} & M \end{bmatrix} \begin{bmatrix} \dot{x}_2 \\ \dot{x}_3 \end{bmatrix} = \begin{bmatrix} \mathbf{0} \\ F_2 \end{bmatrix} + \left(\begin{bmatrix} \mathbf{0} & I_{n_2} \\ -I_{n_2} & \mathbf{0} \end{bmatrix} - \begin{bmatrix} \mathbf{0} & \mathbf{0} \\ \mathbf{0} & D_2 \end{bmatrix} \right) \begin{bmatrix} \frac{\partial H(x)}{\partial x_2} \\ \frac{\partial H(x)}{\partial x_3} \end{bmatrix}. \quad (3.9)$$

For $\lambda=1$, (3.8) reduces to gradient dynamics with external forcing $\mathbf{F} = (F_1, F_2, \mathbf{0}_{n_2})$:

$$\mathcal{H}_1 : \quad \dot{x} = \mathbf{F} - \nabla H(x). \quad (3.10)$$

It turns out that, independently of $\lambda \in [0, 1]$, all parameterized systems of the form (3.8) have the same equilibria with the same local stability properties determined by potential function $H(x)$. The following theorem summarizes these facts.

Theorem 3.3.1 (Properties of the \mathcal{H}_λ family). *Consider for $\lambda \in [0, 1]$ the one-parameter family \mathcal{H}_λ of dynamical systems (3.8) with arbitrary positive definite matrices D_1 , D_2 , and M . The following statements hold:*

(i) **Invariance of equilibria:** *For all $\lambda \in [0, 1]$, the equilibria of \mathcal{H}_λ are given*

by the set $\mathcal{E} \triangleq \{x \in \mathcal{X} : \nabla H(x) = \mathbf{F}\}$; and

(ii) **Invariance of local stability:** *For any equilibrium $x^* \in \mathcal{E}$ and for all*

$\lambda \in [0, 1]$, the inertia of the Jacobian of \mathcal{H}_λ equals the inertia of $-\nabla^2 H(x^)$*

and the corresponding center-eigenspace is the nullspace of $\nabla^2 H(x^)$.*

Statements 1) and 2) assert that normal hyperbolicity of the critical points of $H(x)$ can be directly related to local exponential (set) stability for any $\lambda \in [0, 1]$. This implies that all vector fields \mathcal{H}_λ , $\lambda \in [0, 1]$, are *locally topologically conjugate* [226] near a hyperbolic equilibrium point $x^* \in \mathcal{E}$. In particular, near $x^* \in \mathcal{E}$, trajectories of the gradient vector field (3.10) can be continuously deformed to match trajectories of the Hamiltonian vector field (3.9) while preserving parameterization of time. This topological conjugacy holds also for hyperbolic equilibrium trajectories [65, Theorem 6] considered in synchronization. The similarity between second-order Hamiltonian systems and the corresponding first-order gradient flows is well-known in mechanical control systems [150, 151], in dynamic optimization [10, 20, 109], and in transient stability studies for power networks [49, 51, 61], but we are not aware of any result as general as Theorem 3.3.1. In [49, 51, 61], statements 1) and 2) are proved under the more stringent assumptions that \mathcal{H}_λ has a finite number of isolated and hyperbolic equilibria.

Remark 3.3.2 (Extensions on Euclidean state spaces). If the dynamical system \mathcal{H}_λ is analyzed on the Euclidean space $\mathbb{R}^{n_1+2n_2}$, then it can be verified that the modified potential function $\tilde{H} : \mathbb{R}^{n_1+2n_2} \rightarrow \mathbb{R}$, $\tilde{H}(x) = -F_1^T x_1 - F_2^T x_2 + H(x_1, x_2, M^{1/2} x_3)$ is non-increasing along any forward-complete solution $x : \mathbb{R}_{\geq 0} \rightarrow \mathbb{R}^{n_1+2n_2}$ and for all $\lambda \in [0, 1]$. Furthermore, if the sublevel set $\Omega_c = \{x \in \mathcal{X} : \tilde{H}(x) \leq c\}$ is compact, then every solution initiating in Ω_c is

bounded and forward-complete, and by the invariance principle [146, Theorem 4.4] it converges to the set $\mathcal{E} \cap \Omega_c$, independently of $\lambda \in [0, 1]$. These statements can be refined under further structural assumptions on the potential function $\tilde{H}(x)$, and various other minimizing properties can be deduced, see [10, 20, 109]. Additionally, if $\tilde{H}(x)$ constitutes an *energy function*, if all equilibria are hyperbolic, and if a one-parameter transversality condition is satisfied, then the separatrices of system (3.8) can be characterized accurately [49, 51, 61]. For zero forcing $\mathbf{F} = \mathbf{0}_{n_1+2n_2}$, these convergence statements also hold on the possibly non-Euclidean space \mathcal{X} , see Theorem 3.3.4 for an analysis of phase synchronization. \square

Proof of Theorem 3.3.1: For notational simplicity, consider the matrices $D_{\lambda,1} = (\lambda I_{n_1} + (1 - \lambda)D_1)$, $D_{\lambda,2} = (\lambda I_{n_2} + (1 - \lambda)D_2)$, and $M_\lambda = (\lambda I_{n_2} + (1 - \lambda)M)$. Notice that for all $\lambda \in [0, 1]$, the matrices $D_{\lambda,1}$, $D_{\lambda,2}$, and M_λ are positive definite.

To prove statement 1), we reformulate the parameterized dynamics (3.8) as

$$\begin{bmatrix} D_{\lambda,1}\dot{x}_1 \\ \dot{x}_2 \\ M_\lambda\dot{x}_3 \end{bmatrix} = \underbrace{\begin{bmatrix} I_{n_1} & \mathbf{0} & \mathbf{0} \\ \mathbf{0} & \lambda I_{n_2} & (\lambda - 1)I_{n_2} \\ \mathbf{0} & (1 - \lambda)I_{n_2} & D_{\lambda,2} \end{bmatrix}}_{\triangleq W_\lambda} \underbrace{\begin{bmatrix} F_1 - \frac{\partial H(x)}{\partial x_1} \\ F_2 - \frac{\partial H(x)}{\partial x_2} \\ -\frac{\partial H(x)}{\partial x_3} \end{bmatrix}}_{=\mathbf{F} - \nabla H(x)}.$$

It follows from the *Schur determinant formula* [302] that $\det(W_\lambda) = \det(\lambda D_{\lambda,2} + (1 - \lambda)^2 I_{n_2})$ is positive for all $\lambda \in [0, 1]$. Hence, W_λ is nonsingular for all $\lambda \in [0, 1]$, and the equilibria of (3.8) are given by the set $\mathcal{E} = \{x \in \mathcal{X} : \nabla H(x) = \mathbf{F}\}$.

For the proof of statement 2), consider the Jacobian $J_\lambda(x^*)$ of \mathcal{H}_λ at an equilibrium $x^* \in \mathcal{E}$, which is given by

$$J_\lambda(x^*) = \underbrace{\begin{bmatrix} D_{\lambda,1}^{-1} & 0 & 0 \\ 0 & \lambda I_{n,2} & (\lambda - 1)M_\lambda^{-1} \\ 0 & (1 - \lambda)M_\lambda^{-1} & M_\lambda^{-1}D_{\lambda,2}M_\lambda^{-1} \end{bmatrix}}_{\triangleq S_\lambda} \underbrace{\begin{bmatrix} -I_{n_1+n_2} & \mathbf{0} \\ \mathbf{0} & -M_\lambda \end{bmatrix}}_{\triangleq S(x^*)} \nabla^2 H(x^*). \quad (3.11)$$

Again, we obtain $\det(S_\lambda) = \det(D_{\lambda,1}^{-1}) \det(\lambda \cdot M_\lambda^{-1} D_{\lambda,2} M_\lambda^{-1} + (1 - \lambda)^2 I_{n_2})$. Thus, for all $\lambda \in [0, 1]$, the matrix S_λ is nonsingular and the nullspace of $J_\lambda(x^*)$ equals $\text{Ker}(\nabla^2 H(x^*))$. To show that the stability properties of the equilibrium $x^* \in \mathcal{E}$ are independent of $\lambda \in [0, 1]$, we prove that the inertia of the Jacobian $J_\lambda(x^*)$ depends only on $S(x^*)$ and not on $\lambda \in [0, 1]$. For the invariance of the inertia we invoke the *main inertia theorem for positive semi-definite matrices* [45, Theorem 5]. Note that $J_\lambda(x^*)$ and $J_\lambda(x^*)^T$ have the same eigenvalues. Let $A \triangleq J_\lambda(x^*)^T$ and $P \triangleq S(x^*)$, and consider the matrix Q defined via Lyapunov's equation as

$$Q \triangleq \frac{1}{2} (AP + PA^T) = P \begin{bmatrix} D_{\lambda,1}^{-1} & 0 & 0 \\ 0 & \lambda I_{n,2} & 0 \\ 0 & 0 & M_\lambda^{-1} D_{\lambda,2} M_\lambda^{-1} \end{bmatrix} P.$$

Note that Q is positive semidefinite for $\lambda \geq 0$, and for $\lambda \neq 0$ the nullspaces of Q and P coincide, that is, $\text{Ker}(Q) = \text{Ker}(P)$. Hence, for $\lambda \in]0, 1]$ the assumptions of [45, Theorem 5] are satisfied, and it follows that the non-zero

inertia of $A = J_\lambda(x^*)^T$ (restricted to image of A) corresponds to the non-zero inertia of P . Hence, the non-zero inertia of $J_\lambda(x^*)$ is *independent* of $\lambda \in]0, 1]$, and possible zero eigenvalues correspond to $\text{Ker}(J_\lambda(x^*)) = \text{Ker}(\nabla^2 H(x^*))$.

To handle the case $\lambda = 0$ we invoke continuity arguments. Since the eigenvalues of $J_\lambda(x^*)$ are continuous functions of the matrix elements and the inertia of $J_\lambda(x^*)$ is constant for all $\lambda \in]0, 1]$, the inertia of $J_0(x^*)$ is either the same as the inertia of $J_\lambda(x^*)$ for $\lambda > 0$ sufficiently small or at least one eigenvalue becomes zero. The latter case is not possible since the zero eigenspace of the Jacobian $J_\lambda(x^*)$ is given by $\text{Ker}(\nabla^2 H(x^*))$ and remains unchanged as $\lambda \downarrow 0$. It follows that the inertia of $J_\lambda(x^*)$ equal the inertia of P for all $\lambda \in [0, 1]$.

Finally, since $\text{blkdiag}(I_{n_1+n_2}, M)$ is positive definite, *Sylvester's inertia theorem* [45] asserts that the inertia of $P = \text{blkdiag}(I_{n_1+n_2}, M)(-\nabla^2 H(x^*))$ equals the inertia of $-\nabla^2 H(x^*)$. In conclusion, the inertia and the nullspace of $J_\lambda(x^*)$ equal the inertia of $-\nabla^2 H(x^*)$ and $\text{Ker}(\nabla^2 H(x^*))$, and the proof is complete. \square

3.3.2 Equivalence of Local Synchronization Conditions

As a consequence of Theorem 3.3.1, we can link synchronization in the coupled oscillator model (1.1) and its first-order variant (3.1). Since Theorem 3.3.1 is valid only for equilibria, we change coordinates to a rotating frame. By Lemma 2.3.2, the explicit synchronization frequency of the coupled oscillator model (1.1)

is given by $\omega_{\text{sync}} = \sum_{i=1}^n \omega_i / \sum_{i=1}^n D_i$, that is, it depends only on the natural frequencies and damping coefficients of the oscillators. As discussed in Subsection 2.3.1, by transforming to a rotating frame with frequency ω_{sync} , stable synchronization is equivalent to stability of a synchronization (or equilibrium) manifold. Equivalently, assume that each ω_i is replaced $\omega_i - D_i \omega_{\text{sync}}$, such that $\omega \in \mathbf{1}_n^\perp$.

In the following, we consider the coupled oscillator model (1.1) and its first-order variant (3.1) with $\omega \in \mathbf{1}_n^\perp$. Additionally, we consider the the globally exponentially stable, linear, and fully decoupled *frequency dynamics*

$$\frac{d}{dt} \dot{\theta}_i = -\dot{\theta}_i, \quad i \in \{1, \dots, m\}, \quad (3.12)$$

Notice that the coupled oscillator model (1.1) and its first-order variant (3.1) together with frequency dynamics (3.12) are instances of the parameterized system (3.8) with x_1 being associated with the angles θ_i for $i \in \mathcal{V}_2$, (x_2, x_3) being associated with $(\theta_i, \dot{\theta}_i)$ for $i \in \mathcal{V}_1$, the forcing terms $\mathbf{F} = (\omega, \mathbf{0}_{|\mathcal{V}_1|})$, and the potential $H : \mathbb{T}^n \times \mathbb{R}^{|\mathcal{V}_1|} \rightarrow \mathbb{R}$, $H(\theta, \dot{\theta}) = \frac{1}{2} \dot{\theta}^T \dot{\theta} + U(\theta)$ defined up to a constant value. The following result is obtained by applying Theorem 3.3.1 to these two models.

Theorem 3.3.3 (Synchronization Equivalence). *Consider the coupled oscillator model (1.1) and its first-order variant (3.1) together with frequency dynamics (3.12) with an undirected, connected, and weighted graph $G(\mathcal{V}, \mathcal{E}, A)$. Assume*

that $\omega \in \mathbf{1}_n^\perp$, and let $\gamma \in [0, \pi[$. The following statements are equivalent for any $\gamma \in [0, \pi/2[$ and any synchronization manifold $([\theta], \mathbf{0}_{|\mathcal{V}_1|}) \subset \bar{\Delta}_G(\gamma) \times \mathbb{R}^{|\mathcal{V}_1|}$.

(i) $([\theta], \mathbf{0}_{|\mathcal{V}_1|})$ is a locally exponentially stable synchronization manifold of the coupled oscillator model (1.1); and

(ii) $[\theta]$ is a locally exponentially stable synchronization manifold of the first-order coupled oscillator model (3.1).

If the equivalent statements (i) and (ii) are true, then, locally near their respective synchronization manifolds, the coupled oscillator model (1.1) and its first-order variant (3.1) together with frequency dynamics (3.12) are topologically conjugate.

For purely second-order oscillator networks (1.1) ($\mathcal{V} = \mathcal{V}_1$), Theorem 3.3.1 and Theorem 3.3.3 essentially state that the locations and stability properties of the *foci* of second-order oscillators (with damped oscillatory dynamics) are equivalent to those of the *nodes* of the first-order oscillator network (3.1) and the frequency dynamics (3.12) (with overdamped dynamics), as illustrated in Figure 3.1. Loosely speaking, the topological conjugacy result means that the trajectories of the two phase space plots in Figure 3.1 can be continuously deformed to match each other while preserving parameterization of time.

Proof of Theorem 3.3.3: Recall from Subsection 2.3.1 that a synchronized trajectory of the coupled oscillator model (1.1) with $\omega \in \mathbf{1}_n^\perp$ takes value in a synchroniza-

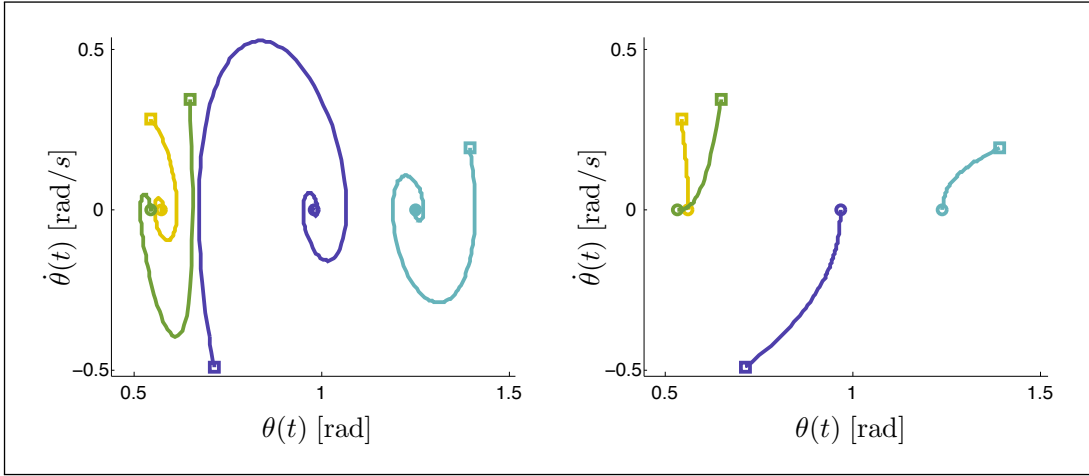


Figure 3.1: Topological conjugacy of first and second-order oscillator dynamics. The left plot shows the phase space dynamics of a network of $n = 4$ second-order multi-rate Kuramoto oscillators (3.2) with $\mathcal{V}_2 = \emptyset$ and Kuramoto-type coupling $a_{ij} = K/n$ for all distinct $i, j \in \mathcal{V}_1 = \{1, \dots, 4\}$ and for $K \in \mathbb{R}$. The right plot shows the phase space dynamics corresponding to first-order Kuramoto oscillators (1.2) together with the frequency dynamics (3.12). The natural frequencies ω_i and the coupling strength K are chosen such that $\omega_{\text{sync}} = 0$ and $K = 1.1 \cdot \max_{i,j \in \{1, \dots, 4\}} |\omega_i - \omega_j|$. From the same initial configuration $\theta(0)$ (denoted by \blacksquare) both first and second-order oscillators converge exponentially to the same synchronized equilibria (denoted by \bullet), as predicted by Theorem 3.3.3.

tion manifold of the form $([\theta_{\text{sync}}], \mathbf{0}_{|\mathcal{V}_1|}) \subset \mathbb{T}^n \times \mathbb{R}^{|\mathcal{V}_1|}$ for some for some $\gamma \in [0, \pi/2[$ and $\theta_{\text{sync}} \in \bar{\Delta}_G(\gamma)$. The synchronization manifold is also an equilibrium manifold.

In the quotient space $\mathbb{T}^n \setminus \mathbb{S}^1 \times \mathbb{R}^{|\mathcal{V}_1|}$, after factoring out the rotational invariance of the angular variable θ , the synchronization manifold $([\theta_{\text{sync}}], \mathbf{0}_{|\mathcal{V}_1|})$ is an isolated equilibrium point of the coupled oscillator model (1.1). Recall that an isolated equilibrium of a smooth nonlinear system with bounded and Lipschitz Jacobian is exponentially stable if and only if the Jacobian is a Hurwitz matrix [146, Theorem

4.15]. Therefore, the synchronization manifold is hyperbolic in the quotient space $\mathbb{T}^n \setminus \mathbb{S}^1 \times \mathbb{R}^m$ if and only if the Jacobian of the coupled oscillator model (1.1) evaluated in $([\theta_{\text{sync}}], \mathbf{0}_{|\mathcal{V}_1|}) \subset \mathbb{T}^n \times \mathbb{R}^{|\mathcal{V}_1|}$, has exactly $|\mathcal{V}_1| + 2 \cdot |\mathcal{V}_2| - 1$ stable eigenvalues and one zero eigenvalue due to rotational symmetry. Equivalently, the synchronization manifold $([\theta_{\text{sync}}], \mathbf{0}_{|\mathcal{V}_1|})$ is locally exponentially stable if and only if the inertia of the Jacobian is $\{|\mathcal{V}_1| + 2 \cdot |\mathcal{V}_2| - 1, 0, 1\}$. By an analogous reasoning we reach the same conclusion for the first-order coupled oscillator model (3.1): the synchronization manifold $[\theta_{\text{sync}}] \subset \mathbb{T}^n$ is exponentially stable if and only if the inertia of the Jacobian evaluated in $[\theta_{\text{sync}}]$ is $\{|\mathcal{V}_1| + |\mathcal{V}_2| - 1, 0, 1\}$.

Finally, recall that the coupled oscillator model (1.1) and its first-order variant (3.1) together with frequency dynamics (3.12) are instances of the parameterized system (3.8). Therefore, by Theorem 3.3.1, both systems have the same equilibria and the corresponding Jacobians (evaluated at these equilibria) have the same inertia. Thus, the equilibrium manifold $([\theta_{\text{sync}}], \mathbf{0}_{|\mathcal{V}_1|}) \subset \mathbb{T}^n \times \mathbb{R}^{|\mathcal{V}_1|}$ is locally exponentially stable for the system (1.1) if and only if it is locally exponentially stable for the system (3.1),(3.12). This concludes the proof of the equivalence (i) \Leftrightarrow (ii).

We now prove the final conjugacy statement. By the *generalized Hartman-Grobman theorem* [65, Theorem 6], the trajectories of the coupled oscillator model (1.1) and its first-order variant (3.1) together with frequency dynamics (3.12) are topologically conjugate to the flow generated by their respective linearized vec-

tor fields locally near the exponentially stable equilibrium $([\theta_{\text{sync}}], \mathbf{0}_{|\mathcal{V}_1|})$. Since the two vector fields (1.1) and (3.1),(3.12) are hyperbolic with respect to $([\theta_{\text{sync}}], \mathbf{0}_{|\mathcal{V}_1|})$ and their respective Jacobians have the same hyperbolic inertia (besides the common one-dimensional center eigenspace arising from the rotational symmetry), the corresponding two linearized dynamics are topologically conjugate [226, Theorem 7.1]. In summary, the two vector fields (1.1) and (3.1),(3.12) are locally topologically conjugate near the equilibrium manifold $([\theta_{\text{sync}}], \mathbf{0}_{|\mathcal{V}_1|})$. \square

The following remarks concerning Theorem 3.3.3 are in order. The above results are valid only for equilibria. Thus, the coupled oscillator model (1.1) and its first-order variant (3.1) possibly have to be transformed to a rotating frame by replacing ω_i by $\omega_i - D_i\omega_{\text{sync}}$. The existence and location of equilibria, their local stability properties, as well as all local bifurcations in the coupled oscillator model (1.1) are then independent of the inertial coefficients M_i since they can be analyzed by means of the first-order variant (3.1). Rather they depend only on the nodal parameters $\omega_i - D_i\omega_{\text{sync}}$ and the interaction topology among the oscillators with coupling gains a_{ij} . Theorem 3.3.3 is also in perfect agreement with the results derived in [126] for the case of two second-order Kuramoto oscillators, which arrives at the same synchronization conditions as our analysis of two first-order oscillators in Subsection 2.3.2. In Theorem 3.3.4 (respectively, Theorem 4.4.4),

we also show that the synchronization conditions of homogeneous (respectively, heterogeneous) oscillator networks are independent of the inertial terms $M_i\ddot{\theta}_i$.

3.3.3 Phase Synchronization in Oscillator Networks

In this subsection, we consider homogeneous oscillator networks with identical natural frequencies and study the problem of phase synchronization. In this case, an elegant analysis of the coupled oscillator model (2.17) follows the insights from the potential function and Jacobian analysis in Subsection 3.2.2 and the topological conjugacy results developed in Subsection 3.3.2. In the following theorem, we adopt the more general notion of a phase-synchronized solution with not necessarily zero synchronization frequency. We do so to emphasize the homogeneity aspect, and we will not use this concept outside of this subsection.

Theorem 3.3.4 (Phase synchronization). *Consider the coupled oscillator model (1.1) with a connected, undirected, and weighted graph $G(\mathcal{V}, \mathcal{E}, A)$, with natural frequencies $\omega \in \mathbb{R}^n$, and positive inertial and damping coefficients $M_i > 0$ and $D_i > 0$, respectively. The following statements are equivalent:*

- (i) **Homogeneity:** *there exists a constant $\omega_0 \in \mathbb{R}$ such that $\omega_i/D_i = \omega_0$ for all $i \in \{1, \dots, n\}$; and*

(ii) **Local phase synchronization:** *there exists a locally exponentially stable phase-synchronized solution with constant frequency $\omega_{\text{sync}} \in \mathbb{R}$.*

If the two equivalent cases (i) and (ii) are true, then $\omega_{\text{sync}} \equiv \omega_0$, and the following statements hold:

- 1) **Global convergence:** *For all initial conditions, the frequencies $\dot{\theta}(t)$ converge to $\omega_0 \mathbf{1}_n$ and the phases $\theta(t)$ converge to $\{\theta \in \mathbb{T}^n \mid \partial U(\theta)/\partial \theta = \mathbf{0}_n\}$; and*
- 2) **Almost global stability:** *If $G(\mathcal{V}, \mathcal{E}, A)$ is \mathbb{S}^1 -synchronizing, the region of attraction of the phase synchronized solution is almost all of $\mathbb{T}^n \times \mathbb{R}^{|\mathcal{V}_1|}$.*

Proof. We first prove the implication (ii) \implies (i). By assumption, $\theta_i = \theta_j$ for all $i, j \in \mathcal{V}$ and $\dot{\theta}_i = \omega_0$ for $i \in \mathcal{V}$. In the phase-synchronized case, the dynamics (1.1) then read as $\omega_i = D_i \omega_{\text{sync}}$ for all $i \in \{1, \dots, n\}$. Hence, a necessary condition for the existence of phase-synchronized solutions is that all ratios ω_i/D_i are identical.

In order to prove the converse implication (i) \implies (ii), notice that by Lemma 2.3.2 and under the assumption $\omega_i/D_i = \omega_0$ for all $i \in \{1, \dots, n\}$, we obtain the explicit synchronization frequency by $\omega_{\text{sync}} = \omega_0$. Now, consider the coupled oscillator model (1.1) written in a rotating frame with frequency $\omega_0 = \omega_i/D_i$:

$$\begin{aligned} M\ddot{\theta}_i + D_i\dot{\theta}_i &= - \sum_{j=1}^n a_{ij} \sin(\theta_i - \theta_j), & i \in \mathcal{V}_1, \\ D_i\dot{\theta}_i &= - \sum_{j=1}^n a_{ij} \sin(\theta_i - \theta_j), & i \in \mathcal{V}_2. \end{aligned} \tag{3.13}$$

Note that (3.13) is a dissipative Hamiltonian system, and the corresponding energy function $H : \mathbb{T}^n \times \mathbb{R}^{|\nu_1|} \rightarrow \mathbb{R}$, $H(\theta, \dot{\theta}) = \frac{1}{2}\dot{\theta}^T \dot{\theta} + U(\theta)$, is non-increasing along trajectories. Since the sublevel sets of $H(\theta, \dot{\theta})$ are compact, the invariance principle [146, Theorem 4.4] asserts that every solution converges to set of equilibria.

By Theorem 3.3.3, we conclude that the phase synchronization manifold of the homogeneous oscillator network (3.13), given by $(\bar{\Delta}_G(0), \mathbf{0}_{|\nu_1|})$, is locally exponentially stable if and only if the phase-synchronized equilibrium $\bar{\Delta}_G(0)$ of the corresponding first-order oscillator network (3.1) with $\omega_i = 0$ is exponentially stable. From the Jacobian arguments in Lemma 3.2.1 it follows again that the phase-synchronized equilibrium manifold $\bar{\Delta}_G(0)$ is locally exponentially stable. Moreover, for an \mathbb{S}^1 -synchronizing graph, all other equilibria are unstable. This concludes the proof of the implication (i) \implies (ii) as well as of statements 1) and 2), which are stated in the original (non-rotating) coordinate frame. \square

Theorem 3.3.4 has been presented for first-order oscillator networks (3.1) in [139, 189, 238, 242], and we followed the respective proof strategies. The corresponding discrete-time analog to Theorem 3.3.4 for first-order oscillators can be found in [148, 149, 238]. If higher order models with dynamic coupling are considered, then almost global stable phase synchronization can be achieved for arbitrary connected (and also directed) graphs, see [170, 238, 243].

With regards to multi-rate Kuramoto oscillators (3.2) (with a complete and uniformly weighted graph), Theorem 3.3.4 shows that phase synchronization is independent of the inertial coefficients M_i , thereby improving the sufficient conditions presented in [57, Theorems 4.1 and 4.2] and confirming the results in [2, 3] derived for a continuum limit model with infinitely many oscillators. Furthermore, since the complete and uniformly weighted graph is \mathbb{S}^1 -synchronizing, Theorem 3.3.4 guarantees almost global phase synchronization, which improves upon the estimate of the region of attraction presented in [57] and in Theorem 2.4.2.

3.3.4 The Role of Inertia and Dissipation for Transient and Non-Symmetric Dynamics

Based on Theorem 3.3.3 we conclude that the inertial terms do not affect the location and local stability properties of synchronized trajectories in the coupled oscillator model (1.1). However, the inertial terms may still affect the transient synchronization behavior, for example, the convergence rates, the shape of separatrices and basins of attractions, and the qualitative (possibly oscillatory) transient dynamics. These points will be briefly discussed in this subsection.

Kinetic energy is a mixed blessing. The inertial terms in the coupled oscillator model (1.1) are sometimes beneficial, for example, disturbances acting on the second-order dynamics (1.1a) will be integrated twice before affecting the

angles, and stable oscillator networks with large inertial terms will not be affected by minor disturbances. At other times the kinetic energy associated with the inertial terms leads to adverse affects, for example, the region of attraction of a synchronized solution heavily depends on the ratio of damping and inertial coefficients, and can diminish significantly if this ratio is too small. To illustrate the latter point consider the forced pendulum equation with dissipation given by

$$m\ddot{\theta} + d\dot{\theta} = p - a \sin(\theta), \quad (3.14)$$

where m , d , and a are positive scalar constants and $p \in \mathbb{R}$ is an external forcing term. The forced pendulum dynamics (3.14) can be thought of as a single oscillator coupled to a stationary reference oscillator. An electrical analog of the forced-pendulum dynamics (3.14) is the single machine infinite bus model in the power systems literature [156]. We assume that $a > p$, such that the forced pendulum dynamics admit a stable and an unstable stationary solution given by $(\theta^*, \dot{\theta}^*) = (\arcsin(p/a), 0)$, where the arcsin function takes value in $[0, \pi/2[$ for the stable solution and in $]\pi/2, \pi]$ for the unstable solution.

The first-order kinematics associated to the pendulum dynamics (3.14) are

$$\dot{\theta} = p - a \sin(\theta). \quad (3.15)$$

By Theorem 3.3.1, the first-order kinematics (3.15) feature the same equilibria with the same stability properties as the forced pendulum dynamics (3.14). How-

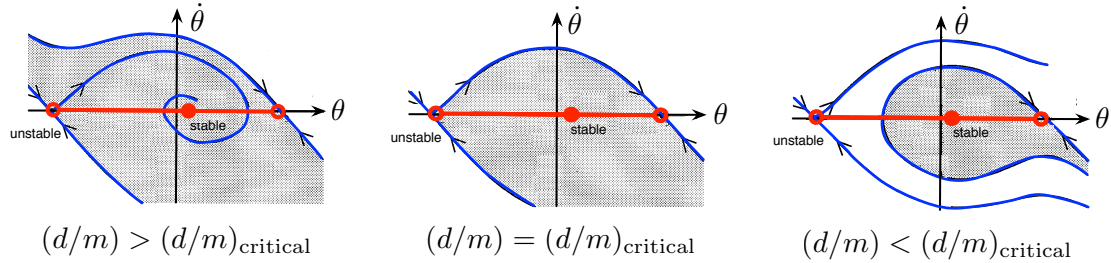


Figure 3.2: Region of attraction of the forced pendulum dynamics

The subfigures illustrate the state space topology for the forced pendulum dynamics (3.14) under different parametric settings and in the lifted state space \mathbb{R}^2 , where the vector field is 2π -periodic in the θ -direction. The lifted state space of the first-order kinematics is simply the θ -axis. The stable (respectively, unstable) equilibrium of the forced pendulum dynamics (3.14) and its associated first-order kinematics (3.1) is shown as solid red disc (respectively, red circle). For the first-order kinematics (3.1) the region of attraction of the stable equilibrium (and its 2π -periodic multiples) is the entire θ -axis (marked in red) with exception of the unstable equilibrium (and its 2π -periodic multiples). In comparison, for the second-order forced pendulum dynamics (3.15), the region of attraction (displayed as grey shaded area) depends heavily on d/m , the ratio of inertia and damping. At the critical value $(d/m)_{\text{critical}} > 0$, the basin of attraction qualitatively changes.

ever, the global behavior and the region of attraction is different. It can be verified, that the equilibrium $\arcsin(p/a) \in [0, \pi/2[$ is almost globally stable for the first-order kinematics (3.15). As shown in Figure 3.2, the region of attraction for the second-order pendulum dynamics (3.14) severely depends on the ratio d/m .

The non-local bifurcation phenomena illustrated in Figure 3.2 is analyzed extensively in the power systems community [7, 9, 63, 205, 208] and shows that the basin of attraction of the coupled oscillator model (1.1) and its first-order variant (3.1) can be qualitatively different unless the damping is sufficiently large.

We emphasize that the conclusions of Theorem 3.3.1 require the coupling among the oscillators to be the gradient of a potential function. Indeed, the application to oscillator networks in Theorem 3.3.3 applies only for undirected graphs and symmetric coupling. It may not be true for directed graphs and asymmetric coupling functions. For example, the lossy network-reduced power system model (2.5)-(2.6) features the coupling terms $a_{ij} \sin(\theta_i - \theta_j - \varphi_{ij})$ and $a_{ij} \sin(\theta_j - \theta_i - \varphi_{ij})$ between oscillators i and j . These coupling terms are not antisymmetric and the overall model is not of Hamiltonian nature. If the phase shifts are zero, then the equilibrium $(\theta^*, \mathbf{0}_{|\mathcal{V}_1|})$ is stable provided that $|\theta_i^* - \theta_j^*| < \pi/2$ for all $\{i, j\} \in \mathcal{E}$, by Lemma 3.2.1. Surprisingly, there are parametric instances (with sufficiently large phase shifts and sufficiently small damping), where the corresponding condition $|\theta_i^* - \theta_j^* - \varphi_{ij}| < \pi/2$ does not guarantee local stability of the second-order system (2.5) while it does guarantee stability of a pure first-order system (2.6).

The above examples show that the transient dynamics in of the coupled oscillator model (1.1) and its first-order variant (3.1) can be severely different in the case of small damping, large inertia, and in presence of symmetry-breaking phase shifts. On the other hand, for overdamped systems with small inertia and large damping, the following subsection shows that the trajectories of the two models can be related, even in the presence of symmetry-breaking terms.

3.4 Approximation by Singular Perturbation Methods

Motivated by the lossy network-reduced power system model (2.5)-(2.6), we study the following instance of the coupled oscillator model (1.1):

$$M_i \ddot{\theta}_i + D_i \dot{\theta}_i = \omega_i - \sum_{j=1}^n a_{ij} \sin(\theta_i - \theta_j - \varphi_{ij}). \quad (3.16)$$

We refer to (3.16) as *second-order lossy oscillator network* and repeat the parametric assumptions for the reader's convenience: $M_i > 0$, $D_i > 0$, and $\omega_i \in \mathbb{R}$ for all $i \in \{1, \dots, n\}$, $\varphi_{ij} \in [0, \pi/2[$ and $a_{ij} = a_{ji} \geq 0$ for all $\{i, j\} \in \mathcal{E}$, and the weights a_{ij} induce an undirected and connected graph. By convention, $a_{ii} = 0$ for all $i \in \{1, \dots, n\}$. Associated to the second-order lossy oscillator network (3.16), we define the first-order *non-uniform Kuramoto model* by

$$D_i \dot{\theta}_i = \omega_i - \sum_{j=1}^n a_{ij} \sin(\theta_i - \theta_j - \varphi_{ij}), \quad i \in \{1, \dots, n\}, \quad (3.17)$$

where the parameters take the same values as in (3.16).

For zero phase shifts φ_{ij} , the non-uniform Kuramoto model (3.17) coincides with the first-order coupled oscillator model (3.1) up to the system metric D . Additionally, for zero phase shifts φ_{ij} and by Theorem 3.3.3, the two models (3.16) and (3.17) are topologically conjugate locally near their respective equilibrium manifolds. As shown in the previous subsection, this connection is only locally

valid and for zero phase shifts. Under the assumption that the second-order lossy oscillator network (3.16) is strongly overdamped, its dynamics can be related to the non-uniform Kuramoto dynamics (3.17) via a singular perturbation analysis.

3.4.1 Symmetry Reduction and Grounded Variables

The singular perturbation analysis by Tikhonov's method [146, 202] requires a system evolving on Euclidean space and an exponentially stable and isolated fixed point. In order to satisfy these assumptions, we introduce two concepts.

As first concept, we introduce a map from a suitable subset of \mathbb{T}^n to a compact subset of the Euclidean space \mathbb{R}^{n-1} . For $\gamma \in [0, \pi[$, define the *grounded map*

$$\begin{aligned} \text{grnd} : \text{Arc}_n(\gamma) &\rightarrow \text{Arc}_{\text{grnd}}(\gamma) \\ &\triangleq \{ \bar{\delta} \in \mathbb{R}^{n-1} : |\bar{\delta}_i| < \gamma, \max_{i,j} |\bar{\delta}_i - \bar{\delta}_j| < \gamma, i, j \in \{1, \dots, n-1\} \} \end{aligned} \quad (3.18)$$

that associates to the array of angles $(\theta_1, \dots, \theta_n) \in \text{Arc}_n(\gamma)$ the array of angle differences $\bar{\delta}$ with components $\bar{\delta}_i = \theta_i - \theta_n$, for $i \in \{1, \dots, n-1\}$. This map is well defined, that is, $\bar{\delta} \in \text{Arc}_{\text{grnd}}(\gamma)$ since $|\bar{\delta}_i| = |\theta_i - \theta_n| < \gamma$ and $|\bar{\delta}_i - \bar{\delta}_j| = |\theta_i - \theta_j| < \gamma$ for all distinct $i, j \in \{1, \dots, n-1\}$. Also, this map is smooth because $\gamma < \pi$ implies that all angles take value in an open semi-circle and their pairwise differences are smooth functions. In the spirit of circuit theory, we refer to the angle differences $\bar{\delta}$ as *grounded angles*. The map $\theta \mapsto \bar{\delta} = \text{grnd}(\theta)$ is illustrated in Figure 3.3.

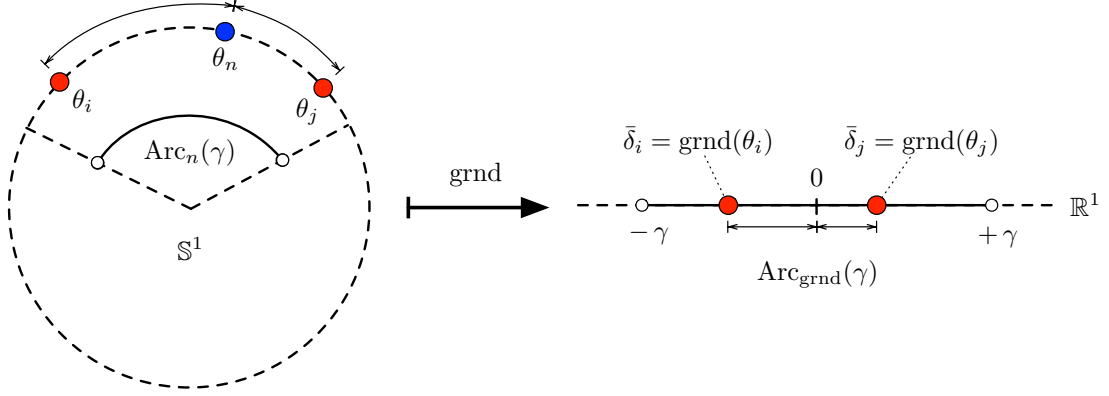


Figure 3.3: Illustration of the grounded map

Illustration of the map $\text{grnd} : \text{Arc}_n(\gamma) \rightarrow \text{Arc}_{\text{grnd}}(\gamma)$. The map grnd can be thought of as a symmetry-reducing projection from $\text{Arc}_n(\gamma)$ (illustrated as subset of \mathbb{S}^1) to $\text{Arc}_{\text{grnd}}(\gamma)$ (illustrated as subset of \mathbb{R}^1), where θ_n is projected to the origin 0. The set $\text{Arc}_n(\gamma)$ and the map grnd are invariant under translations on \mathbb{T}^n that is, under maps of the form $(\theta_1, \dots, \theta_n) \mapsto (\theta_1 + \alpha, \dots, \theta_n + \alpha)$.

As second concept, by formally computing the difference between the angles

$\dot{\theta}_i$ and $\dot{\theta}_n$, we define *grounded Kuramoto model* with state $\delta \in \mathbb{R}^{n-1}$ by

$$\begin{aligned} \dot{\delta}_i = & \frac{\omega_i}{D_i} - \frac{\omega_n}{D_n} - \sum_{j=1, j \neq i}^{n-1} \left(\frac{a_{ij}}{D_i} \sin(\delta_i - \delta_j - \varphi_{ij}) + \frac{a_{nj}}{D_n} \sin(\delta_j + \varphi_{jn}) \right) \\ & - \left(\frac{a_{in}}{D_i} \sin(\delta_i - \varphi_{in}) + \frac{a_{in}}{D_n} \sin(\delta_i + \varphi_{in}) \right), \quad i \in \{1, \dots, n-1\}. \end{aligned} \quad (3.19)$$

The grounded Kuramoto model (3.19) with solution $\delta(t)$ and the non-uniform Kuramoto model (3.17) with solution $\theta(t)$ appear to be directly related via $\delta(t) = \text{grnd}(\theta(t))$ – provided that the grounded map (involving angular differences) is indeed well-defined for all $t \geq 0$. The following lemma shows that the equality $\delta(t) = \text{grnd}(\theta(t))$ holds under an arc invariance assumption. Furthermore, the lemma establishes the equivalence of exponential synchronization in the non-

uniform Kuramoto model (3.17) and exponential stability of equilibria in the grounded Kuramoto model (3.19). These equivalences will put us in a convenient position to apply Tikhonov's theorem.

Lemma 3.4.1 (Properties of grounded Kuramoto model). *Let $\gamma \in [0, \pi[$ and let $\theta : \mathbb{R}_{\geq 0} \rightarrow \mathbb{T}^n$ be a solution to the non-uniform Kuramoto model (3.17) satisfying $\theta(0) \in \text{Arc}_n(\gamma)$. Let $\delta : \mathbb{R}_{\geq 0} \rightarrow \mathbb{R}^{n-1}$ be the solution to the grounded Kuramoto model (3.19) with initial condition $\delta(0) = \text{grnd}(\theta(0)) \in \text{Arc}_{\text{grnd}}(\gamma)$. Then, $\delta(t) = \text{grnd}(\theta(t))$ for all $t \geq 0$, if any one of the two following equivalent conditions holds:*

- 1) **arc invariance:** *the angles $\theta(t)$ take value in $\text{Arc}_n(\gamma)$ for all $t \geq 0$; and*
- 2) **well-posedness:** *the grounded angles $\delta(t)$ take value in $\text{Arc}_{\text{grnd}}(\gamma)$ for all $t \geq 0$.*

Moreover, the following two statements are equivalent for any $\gamma \in [0, \pi[$:

- 3) **exponential frequency synchronization:** *every trajectory of the non-uniform Kuramoto model satisfying the arc invariance property 1) achieves exponential frequency synchronization; and*
- 4) **exponential convergence to equilibria:** *each trajectory of the grounded Kuramoto model satisfying the well-posedness property 2) converges exponentially to an equilibrium point.*

Finally, each trajectory of the grounded Kuramoto model as in 4) satisfying property 2) with $\gamma \in [0, \pi/2 - \varphi_{\max}]$ converges to an isolated exponentially stable equilibrium point.

Proof. Since both vector fields (3.17) and (3.19) are locally Lipschitz, existence and uniqueness of the corresponding solutions follow provided that the corresponding evolutions are bounded. Now, assume that 1) holds, that is, $\theta(t) \in \text{Arc}_n(\gamma)$ (bounded) for all $t \geq 0$. Therefore, $\bar{\delta}(t) = \text{grnd}(\theta(t)) \in \text{Arc}_{\text{grnd}}(\gamma)$ for all $t \geq 0$. Also recall that the map grnd is smooth over $\text{Arc}_n(\gamma)$. These facts and the definition of the grounded Kuramoto model (3.19) imply that $\frac{d}{dt} \text{grnd}(\theta(t))$ is well defined and identical to $\dot{\bar{\delta}}(t)$ for all $t \geq 0$. In turn, this implies that $\delta(t) = \text{grnd}(\theta(t)) \in \text{Arc}_{\text{grnd}}(\gamma)$ holds for all $t \geq 0$.

Conversely, assume that 2) holds, that is, $\delta(t) \in \text{Arc}_{\text{grnd}}(\gamma)$ (bounded) for all $t \geq 0$. Due to existence and uniqueness and since $\delta(0) = \text{grnd}(\theta(0))$ with $\theta(0) \in \text{Arc}_n(\gamma)$, a set of angles $\theta(t) \in \text{Arc}_n(\gamma)$ can be associated to $\delta(t) \in \text{Arc}_{\text{grnd}}(\gamma)$ such that $\delta(t) = \text{grnd}(\theta(t))$ for all $t \geq 0$. By construction of the grounded Kuramoto model (3.19), we have that $\theta(t)$ is identical to the solution to the non-uniform Kuramoto model (3.17). Thus, statement 2) implies statement 1) and $\delta(t) = \text{grnd}(\theta(t))$ for all $t \geq 0$. Having established the equivalence of 1) and 2), we do not further distinguish between $\delta(t)$ and $\text{grnd}(\theta(t))$.

Assume that 3) holds, that is, all $\dot{\theta}_i(t)$ converge exponentially fast to some $\dot{\theta}_\infty \in \mathbb{R}$. It follows that each $\dot{\delta}_i(t) = \dot{\theta}_i(t) - \dot{\theta}_n(t)$ converges exponentially fast to zero, and $\delta(t) = \delta(0) + \int_0^t \dot{\delta}(\tau) d\tau$ converges exponentially fast to some $\delta_\infty \in \text{Arc}_{\text{grnd}}(\gamma)$ due to property 2). Since the vector field (3.19) is continuous and $\lim_{t \rightarrow \infty} (\delta(t), \dot{\delta}(t)) = (\delta_\infty, \mathbf{0}_{n-1})$, the vector δ_∞ is necessarily an equilibrium of (3.19), and property 4) follows.

Assume that 4) holds, that is, all angular differences $\delta_i(t) = \theta_i(t) - \theta_n(t)$ converge exponentially fast to constant values $\delta_{i,\infty}$ for $i \in \{1, \dots, n-1\}$. This fact and the continuity of the vector field in equation (3.19) imply that the array with entries $\delta_{i,\infty}$ is an equilibrium for (3.19) and that each frequency difference $\dot{\delta}_i(t) = \dot{\theta}_i(t) - \dot{\theta}_n(t)$ converges to zero. Moreover, because the vector field in equation (3.19) is analytic and the solution converges exponentially fast to an equilibrium point, the right-hand side of equation (3.19) converges exponentially fast to zero and thus also the time-derivative of the solution, that is, the array of frequency differences, converges exponentially fast.

To prove the final statement, assume that the non-uniform Kuramoto model (3.17) achieves frequency synchronization and arc invariance in $\text{Arc}_n(\pi/2 - \varphi_{\max})$. Thus, when formulated in a rotating coordinate frame, all trajectories converge exponentially to an *equilibrium manifold* $[\theta^*] \in \text{Arc}_n(\pi/2 - \varphi_{\max})$. In the following, we additionally establish local exponential *stability* of this equilibrium manifold

by Jacobian arguments. The negative Jacobian of the non-uniform Kuramoto model evaluated at $[\theta^*]$ is given by the Laplacian matrix with weights $\tilde{a}_{ij}(\theta^*) = (a_{ij}/D_i) \cos(\theta_i^* - \theta_j^* - \varphi_{ij})$. Since the weights a_{ij} induce a connected graph, it follows, for $\theta^* \in \text{Arc}_n(\pi/2 - \varphi_{\max})$, that the weights $\tilde{a}_{ij}(\theta^*)$ are positive for $\{i, j\} \in \mathcal{E}$ and induce a directed graph with a globally reachable node. From the Laplacian properties in Subsection 2.1, we conclude that $[\theta^*]$ is locally exponentially stable with respect to the non-uniform Kuramoto dynamics (3.17). Because of this and due to property 4), the corresponding *point* $\delta^* = \text{grnd}(\theta^*(t)) \in \text{Arc}_{\text{grnd}}(\pi/2 - \varphi_{\max})$ (the rotational symmetry is removed by the grounded map) is an exponentially stable and thus isolated equilibrium of the grounded Kuramoto model (3.19). \square

3.4.2 Singular Perturbation Analysis

The nonuniform Kuramoto model (3.17) may be seen as a long-time approximation of the second-order lossy oscillator network(3.16), or spoken differently, it is the reduced system obtained by a singular perturbation analysis. A physically reasonable singular perturbation parameter is the worst-case choice of M_i/D_i , that is, $\epsilon = M_{\max}/D_{\min}$. The dimension of ϵ is in seconds, which makes sense since time still has to be normalized with respect to ϵ . If we reformulate (3.16) in grounded angular coordinates with the state $(\delta, \dot{\theta}) \in \mathbb{R}^{n-1} \times \mathbb{R}^n$, then we obtain

the following system in singular perturbation standard form

$$\frac{d}{dt}\delta_i = f_i(\dot{\theta}) \triangleq \dot{\theta}_i - \dot{\theta}_n, \quad i \in \{1, \dots, n-1\}, \quad (3.20)$$

$$\begin{aligned} \epsilon \frac{d}{dt}\dot{\theta}_i = g_i(\delta, \dot{\theta}) &\triangleq -F_i \dot{\theta}_i + \frac{F_i}{D_i} \left(\omega_i - \sum_{j=1}^n a_{ij} \sin(\delta_i - \delta_j - \varphi_{ij}) \right), \\ i &\in \{1, \dots, n\}, \end{aligned} \quad (3.21)$$

where $F_i = (D_i/D_{\min})/(M_i/M_{\max})$ and $\delta_n = 0$ in equation (3.21). For ϵ sufficiently small, the long-term dynamics of (3.20)-(3.21) can be approximated by the grounded Kuramoto model (3.19) and the frequencies of the non-uniform Kuramoto model (3.17) written in δ -coordinates:

$$h_i(\delta) \triangleq \frac{\omega_i}{D_i} - \sum_{j=1}^n \frac{a_{ij}}{D_i} \sin(\delta_i - \delta_j - \varphi_{ij}) \equiv 0, \quad i \in \{1, \dots, n\}. \quad (3.22)$$

Theorem 3.4.2 (Singular Perturbation Approximation). *Consider the second-order lossy oscillator network(3.16) written as the singular perturbation problem (3.20)-(3.21) with bounded initial conditions $(\delta(0), \dot{\theta}(0))$, and the grounded non-uniform Kuramoto model (3.19) with initial condition $\delta(0)$ and solution $\bar{\delta}(t)$. Assume that there exists an exponentially stable fixed point δ_∞ of (3.19) and $\delta(0)$ is in a compact subset Ω_δ of its region of attraction. Then, for each Ω_δ*

- 1) *there exists $\epsilon_* > 0$ such that for all $\epsilon < \epsilon_*$, the system (3.20)-(3.21) has a unique solution $(\delta(t, \epsilon), \dot{\theta}(t, \epsilon))$ for all $t \geq 0$, and for all $t \geq 0$ it holds uniformly in t that*

$$\delta(t, \epsilon) - \bar{\delta}(t) = \mathcal{O}(\epsilon), \quad \text{and} \quad \dot{\theta}(t, \epsilon) - h(\bar{\delta}(t)) - y(t/\epsilon) = \mathcal{O}(\epsilon), \quad (3.23)$$

where $y_i(t/\epsilon) \triangleq (\dot{\theta}_i(0) - h_i(\delta(0))) e^{-F_i t/\epsilon}$ and $h_i(\delta)$ is given in (3.22).

2) For any $t_b > 0$, there exists $\epsilon^* \leq \epsilon_*$ such that for all $t \geq t_b$ and whenever $\epsilon < \epsilon^*$

it holds uniformly that

$$\dot{\theta}(t, \epsilon) - h(\bar{\delta}(t)) = \mathcal{O}(\epsilon). \quad (3.24)$$

3) Additionally, there exist ϵ and φ_{\max} sufficiently small such that the approximation errors (3.23)-(3.24) converge exponentially to zero as $t \rightarrow \infty$.

Proof. To prove statements 1) and 2) we will follow *Tikhonov's theorem* [146, Theorem 11.2] and show that the singularly perturbed system (3.20)-(3.21) satisfies all assumptions of [146, Theorem 11.2] when analyzing it on $\mathbb{R}^{n-1} \times \mathbb{R}^n$.

Exponential stability of the reduced system: The *quasi-steady-state* of (3.20)-(3.21) is obtained by solving $g_i(\delta, \dot{\theta}) = 0$ for $\dot{\theta}$, resulting in the unique (and thus isolated) root $\dot{\theta}_i = h_i(\delta)$ for $i \in \{1, \dots, n\}$. The *reduced system* is obtained as $\dot{\delta}_i = f_i(h(\delta)) = h_i(\delta) - h_n(\delta)$, $i \in \{1, \dots, n-1\}$, which is equivalent to the grounded non-uniform Kuramoto model (3.19). The reduced system is smooth, evolves on \mathbb{R}^{n-1} , and by assumption its solution $\bar{\delta}(t)$ is bounded and converges exponentially to the stable equilibrium δ_∞ . Define the error coordinates $x(t) \triangleq \bar{\delta}(t) - \delta_\infty$ and the resulting system $\dot{x} = f(h(x + \delta_\infty))$ with state in \mathbb{R}^{n-1} and initial value $x(0) = \delta(0) - \delta_\infty$. Notice that $x(t)$ is bounded and converges exponentially to the stable equilibrium $x = \mathbf{0}_{n-1}$.

Exponential stability of the boundary layer system: Consider the error coordinate $y_i = \dot{\theta}_i - h_i(\delta)$, which shifts the error made by the quasi-stationarity assumption $\dot{\theta}_i(t) \approx h_i(\delta(t))$ to the origin. After stretching time to the dimensionless variable $\tau = t/\epsilon$, the quasi-steady-state error obeys the dynamics

$$\frac{d}{d\tau} y_i = g_i(\delta, y + h(\delta)) - \epsilon \frac{\partial h_i}{\partial \delta} f(y + h(\delta)) = -F_i y_i - \epsilon \frac{\partial h}{\partial \delta} f_i(y + h(\delta)), \quad (3.25)$$

where $y_i(0) = \dot{\theta}_i(0) - h_i(\delta(0))$. For $\epsilon = 0$, (3.25) reduces to the *boundary layer model*

$$\frac{d}{d\tau} y_i = -F y_i, \quad y_i(0) = \dot{\theta}_i(0) - h_i(\delta(0)). \quad (3.26)$$

The boundary layer model (3.26) is globally exponentially stable with solution $y_i(t/\epsilon) = y_i(0)e^{-F_i t/\epsilon}$ and bounded $y_i(0)$. In summary, the singularly perturbed system (3.20)-(3.21) is smooth on $\mathbb{R}^{n-1} \times \mathbb{R}^n$, and the origins of the reduced system (in error coordinates) $\dot{x} = f(h(x + \delta_\infty))$ and the boundary layer model (3.26) are exponentially stable (Lyapunov functions are readily existent by converse arguments [146, Theorem 4.14]). Thus, all assumptions of [146, Theorem 11.2] are satisfied and statements 1)-2) follow.

To prove statement 3), note that $\bar{\delta}(t)$ converges to an exponentially stable equilibrium point δ_∞ , and $(\delta(t, \epsilon), \dot{\theta}(t, \epsilon))$ converges to an $\mathcal{O}(\epsilon)$ neighborhood of $(\delta_\infty, h(\bar{\delta}_\infty))$, where $h(\bar{\delta}_\infty) = \mathbf{0}_n$. We now invoke topological equivalence arguments [49, 52]. Both the second-order system (3.20)-(3.21) as well as the reduced system $\dot{\delta} = f(h(\delta))$ correspond to the perturbed Hamiltonian system (8)-(9) in [49] and

the perturbed gradient system (10) in [49], where the latter is considered with unit damping $D_i = 1$ in [49]. Consider for a moment the case when all $\varphi_{ij} = 0$. In this case, the reduced system has a locally exponentially stable fixed point δ_∞ (for any $D_i > 0$ due to [52, Theorem 3.1]), and by [49, Theorem 5.1] we conclude that $(\delta_\infty, \mathbf{0}_n)$ is also a locally exponentially stable fixed point of the second order system (3.20)-(3.21). Furthermore, due to structural stability [49, Theorem 5.7, R1], this conclusion holds also for sufficiently small φ_{ij} . Thus, for sufficiently small ϵ and φ_{\max} , the solution of (3.20)-(3.21) converges exponentially to $(\delta_\infty, \mathbf{0}_n)$. In this case, the approximation errors $\delta(t, \epsilon) - \bar{\delta}(t)$ and $\dot{\theta}(t, \epsilon) - h(\bar{\delta})$ as well as the boundary layer error $y(t/\epsilon)$ vanish exponentially. \square

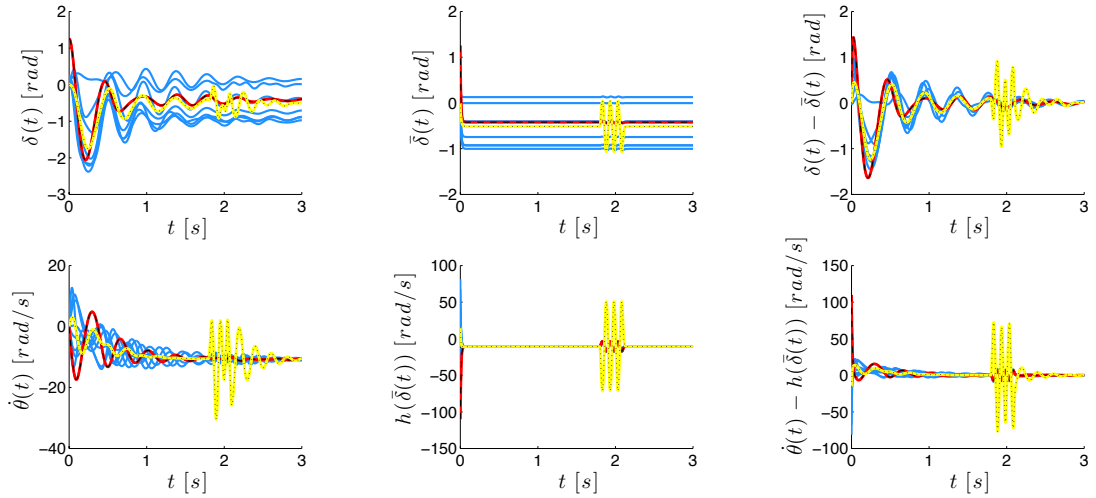
It is instructive to note that the reduced slow system (3.19) and the fast boundary layer model (3.26) in the singular perturbation approach correspond to the first-order oscillator dynamics (3.1) and the frequency dynamics (3.12) (in the time-scale t/ϵ) in the topological conjugacy approach.²

We illustrate the singular perturbation approximation in Theorem 3.4.2 through a simulation study. Figure 3.4 shows a simulation of the second-order lossy oscillator network (3.16) with $n = 10$ oscillators and the corresponding non-uniform Kuramoto model (3.17), where all initial angles $\theta(0)$ are tightly clustered with

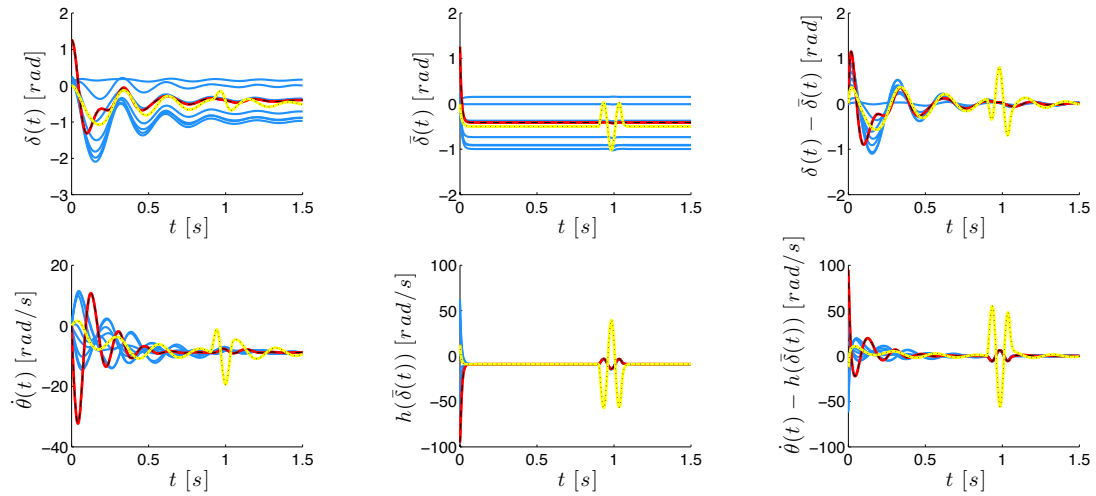
²This analogy is perfect only if $D_{\lambda,1}$, $D_{\lambda,2}$, and M_λ in (3.8) are replaced by D_1 , D_2 , and M , respectively. It can be verified, that the proofs of all results in Section 3.3 still hold without major modifications, see [83] for further details.

exception of the first one (red dashed curves) and the initial frequencies $\dot{\theta}(0)$ are drawn from a uniform distribution over $[-0.1, 0.1]$ rad/s, which we denote by $\text{unif}(-0.1, 0.1)$ rad/s. Additionally, at two-third of the simulation interval a time-varying high frequency disturbance is introduced at ω_{n-1} (yellow dotted curve). For illustration, relative angular coordinates are defined as $\delta_i(t) = \theta_i(t) - \theta_n(t)$, $i \in \{1, \dots, n-1\}$. The network parameters are chosen randomly $\omega_i \in \text{unif}(-5, 5)$, $a_{ij} \in \text{unif}(0.7, 1.2)$, and $\tan(\varphi_{ij}) \in \text{unif}(0, 0.25)$, which match typical line and generation data for network-reduced power system models [11, 156, 207].

For the simulation in Figure 3.4(a), we chose $M_i \in \text{unif}(2, 12)/(2\pi 60)$ s and $D_i \in \text{unif}(20, 30)/(2\pi 60)$ resulting in the rather large perturbation parameter $\epsilon = 0.58$. The angles $\bar{\delta}(t)$ of the non-uniform Kuramoto model synchronize very fast from the non-synchronized initial conditions (within 0.05 s), and the transient disturbance around $t = 2$ s does not severely affect the synchronization dynamics. The same findings hold for the quasi-steady state $h(\bar{\delta}(t))$ depicting the frequencies of the non-uniform Kuramoto model, where the disturbance acts directly without being integrated. Since ϵ is large the trajectories $(\delta(t), \dot{\theta}(t))$ show the expected underdamped behavior and synchronize with oscillatory dynamics. As expected, the disturbance at $t = 2$ s does not affect the second-order power network δ -dynamics as much as the first-order non-uniform Kuramoto $\bar{\delta}$ -dynamics. Nevertheless, after



(a) Weakly damped simulation with $\epsilon = 0.58$ s



(b) Strongly damped simulation with $\epsilon = 0.18$ s

Figure 3.4: Illustration of the singular perturbation approximation. The simulation shows the second-order lossy oscillator network (3.16) and the non-uniform Kuramoto model (3.17) in a weakly damped case (subfigure (a)) and a strongly damped (yet oscillatory) case (subfigure (b)).

the initial and mid-simulation transients the singular perturbation errors $\delta(t) - \bar{\delta}(t)$ and $\theta(t) - h(\bar{\delta}(t))$ quickly become small and ultimately converge.

Figure 3.4(b) shows the exact same simulation as in Figure 3.4(a), except that the simulation time is halved, the inertiae are $M_i \in \text{unif}(2, 6)/(2\pi 60)$ s, and the damping is chosen uniformly as $D_i = 30/(2\pi 60)$, which gives the small perturbation parameter $\epsilon = 0.18$ s. The resulting second-order lossy oscillator dynamics $(\delta(t), \dot{\theta}(t))$ are strongly damped (note the different time scales), and the non-uniform Kuramoto dynamics $\bar{\delta}(t)$ and the quasi-steady state $h(\bar{\delta}(t))$ have smaller time constants. As expected, the singular perturbation errors remain smaller during transients and converge faster than in the weakly damped case in Figure 3.4(a).

3.4.3 Discussion of the Perturbation Assumption

By Theorem 3.4.2, the transient dynamics of the second-order lossy oscillator network (3.16) and the first-order grounded Kuramoto model (3.19) can be related up to an approximation error of order ϵ – even in the presence of the symmetry-breaking conductances. The key assumption is that each oscillator is strongly overdamped, which is captured by the smallness of the perturbation parameter $\epsilon = M_{\max}/D_{\min}$. This choice of the perturbation parameter is similar to the analysis of Josephson arrays [292], coupled overdamped mechanical pendula [73], flocking models [120], and also classic transient stability analysis [52, Theorem 5.2], [263].

In the linear case, this analysis resembles the well-known overdamped harmonic oscillator, which features one slow and one fast eigenvalue. The overdamped harmonic oscillator exhibits two time-scales and the fast eigenvalue corresponding to the frequency damping can be neglected in the long-term phase dynamics.

In the application to power network models one has to be careful under which operating conditions ϵ is indeed a small physical quantity. For synchronous generators, M_i is typically of the order $[2\text{s}, 12\text{s}]/(2\pi f_0)$ depending on the type of generator and the damping is poor: $D_i \in [1, 3]/(2\pi f_0)$. However, for the synchronization problem also the generator's internal excitation control have to be considered, which increases the damping torque to $D_i \in [10, 35]/(2\pi f_0)$ depending on the system load [11, 156, 236]. In this case, $\epsilon \in \mathcal{O}(0.1)$ is indeed a small quantity and a singular perturbation approximation is accurate. In fact, the recent power systems literature discusses the need for sufficiently large damping to enhance transient stability, see [7, 63] and references therein.

We note that our simulation studies in Figure 3.4 show an accurate approximation of the power network by the non-uniform Kuramoto model also for values of $\epsilon \in \mathcal{O}(1)$, which indicate that the threshold ϵ^* may be sizable. The theoretical reasoning is the topological equivalence between the power network model (3.16) and the non-uniform Kuramoto model (3.17), as discussed in Theorem 3.3.3, [52, Theorems 3.1-3.4], [49, Theorem 5.7], and [83, Theorem 4.1].

The analogies between the second-order lossy oscillator network (3.16) and the non-uniform Kuramoto model (3.17), are directly employed in the *PEBS* [52] and *BCU* algorithms [49]. These algorithms are not only scholastic but applied by the power industry [48], which additionally supports the validity of the singular perturbation approximation in power network models.

3.5 Comparison and Alternative Relations

In this chapter, we introduced two methods to relate coupled oscillator model (1.1) and its first-order variant (3.1). The first method in Section 3.3 built on local topological conjugacy and showed, among others, that synchronization conditions in the two models (1.1) and (3.1) are identical and independent of the inertial coefficients, as seen in our analysis of phase synchronization. On the other hand, this approach yields only local conclusions, and it is restricted to Hamiltonian and gradient systems, which excludes lossy power network models, among others.

Alternatively, the singular perturbation approach presented in Section 3.4 is applicable to non-Hamiltonian systems and it allows for a dynamic comparison between the trajectories of the coupled oscillator model (1.1) and its first-order variant (3.1). On the other hand, the singular perturbation approach relies on the assumption of a sufficiently small inertia over damping ratio. Even though simu-

lation studies suggest that the critical threshold may be sizable, this assumption may be restrictive in some applications.

Alternative methods to relate stability properties of the coupled oscillator model (1.1) and its first-order variant (3.1) include second-order Gronwall's inequalities [57] and strict Lyapunov functions for mechanical systems [150, 151]. It should be noted that the approaches [57, 150, 151] are limited to purely second-order systems, the second-order Gronwall inequality approach [57] has been carried out only for uniform inertia $M_i = M$ and unit damping $D_i = 1$. The Lyapunov approach [150, 151] is limited to potential-based Lyapunov functions, and it does not extend to the contraction-based Lyapunov functions which we use in Chapter 4.

In summary, the author's investigations showed that the topological conjugacy approach reveals strong connections between the coupled oscillator model (1.1) and its first-order variant (3.1). On the other hand, this approach is only locally valid, and a global connection between the two models necessarily requires strongly overdamped dynamics, as suggested by the one-dimensional example in Figure 3.2. In this case, the singular perturbation approximation is a feasible alternative.

Chapter 4

The Critical Coupling for Kuramoto Oscillators

Surprisingly enough, this seemingly obvious fact seems difficult to prove.

Yoshiki Kuramoto (1984)

(A comment on the rigorous mathematical treatment of the emergence of synchronization in a network of coupled oscillators.)

In this chapter, we study heterogeneous oscillators with first-order dynamics, unit time constants $D_i = 1$, and coupled in a complete and uniformly weighted graph.

In this case, the coupled oscillator model (1.1) reduces to the celebrated Kuramoto model (1.2). For the reader's convenience, we briefly reintroduce the Kuramoto model here. Consider $n \geq 2$ heterogeneous oscillators with distinct natural frequencies $\omega \in \mathbf{1}_n^\perp$ and coupled in a complete graph with uniform weights $a_{ij} = K/n$, where $K > 0$ is the coupling strength among the oscillators:

$$\dot{\theta}_i = \omega_i - \frac{K}{n} \sum_{j=1}^n \sin(\theta_i - \theta_j), \quad i \in \{1, \dots, n\},$$

The Kuramoto model will reach synchronization provided that the coupling K is larger than a critical value K_{critical} , which depends on the dissimilarity among the natural frequencies ω . Starting from Winfree's and Kuramoto's pioneering work [158, 159, 294], this trade-off has been characterized by parametric inequalities.

In this chapter, we present various estimates of the critical coupling strength K_{critical} to characterize the on-set of synchronization as well as the ultimate stage of synchronization. We consider both finite-dimensional as well as infinite-dimensional oscillator populations. We present a comprehensive review of the literature in a unified language. In this effort, we collect contributions from several references and arrive at novel results within a unified perspective. By making use of recently developed tools in the consensus literature, we arrive at new estimates of the critical coupling strength as well as new insights into the transient dynamics.

4.1 Introduction

4.1.1 Relevant Literature

An elegant and insightful analysis of the Kuramoto model (1.2) is based on the *order parameter* introduced by Kuramoto [158, 159] as

$$r e^{i\psi} = \frac{1}{n} \sum_{j=1}^n e^{i\theta_j}. \quad (4.1)$$

The order parameter (4.1) is the centroid of all oscillators represented as points on the unit circle in \mathbb{C}^1 . The magnitude $r \in [0, 1]$ of the order parameter is a synchronization measure whose extremal characteristics are as follows: if the oscillators are phase-synchronized, then $r = 1$, and if the oscillators are spaced equally on the unit circle, then $r = 0$. The latter case is referred to as phase balancing and is of importance in neuroscience applications [34, 70, 280], deep-brain stimulation [195, 267], vehicle coordination [148, 149, 209, 242, 243], and central pattern generators for locomotion purposes [15, 135, 224].

By means of the order parameter $re^{i\psi}$ defined in equation (4.1), the Kuramoto model (1.2) can be rewritten in the insightful form

$$\dot{\theta}_i = \omega_i - Kr \sin(\theta_i - \psi), \quad i \in \{1, \dots, n\}. \quad (4.2)$$

Equation (4.2) gives the intuition that the oscillators synchronize because of their coupling to a *mean field* represented by the order parameter $re^{i\psi}$, which itself is a function of $\theta(t)$. Intuitively, for small coupling strength K each oscillator rotates with its distinct natural frequency ω_i , whereas for large coupling strength K all angles $\theta_i(t)$ will entrain to the mean field $re^{i\psi}$, and the oscillators synchronize. The transition from incoherence to synchronization occurs at a critical threshold value of the coupling strength, denoted by K_{critical} .

This phase transition has been the source of numerous research papers starting with Kuramoto's own insightful and ingenious analysis [158, 159]. For instance,

since $r \leq 1$, no frequency-synchronized solution of (4.2) of the form $\dot{\theta}_i(t) = \dot{\theta}_j(t)$ can exist if $K < |\omega_i - \omega_j|/2$. Hence, $K \geq |\omega_i - \omega_j|/2$ provides a necessary synchronization condition and a lower bound for K_{critical} . Various necessary, sufficient, implicit, and explicit estimates of the critical coupling strength K_{critical} have been derived in the vast literature on the Kuramoto model both for oscillator networks of finite size as well in the continuum limit of infinitely many oscillators.

We will detail the existing results and analysis methods as well as their shortcomings throughout this chapter.

4.1.2 Contributions and Organization

The remainder of this chapter is organized as follows:

Section 4.2: In this section, we introduce the continuum limit model of an infinite-dimensional oscillator population and present its synchronization phenomenology including partial synchronization and full phase-locking. Furthermore, we present a set of implicit and explicit conditions on the critical coupling strength K_{critical} for the partial synchronization threshold and the full phase-locking threshold. In this effort, we collect contributions from several references in a unified language, which allows for a comparison of our latter results on finite-dimensional Kuramoto oscillator networks.

Section 4.3: In this section, we review the extensive literature on the Kuramoto model, and present various necessary, sufficient, implicit, and explicit estimates of the critical coupling strength for the finite and infinite-dimensional Kuramoto model in a unified language. Aside from the comparison of the different estimates of the critical coupling strength, the second purpose of this review is the comparison of the different analysis techniques. We collect contributions from several references and arrive at novel results within a unified perspective, see Lemma 4.3.3 and Theorem 4.3.4.

Section 4.4: In this section, we derive an explicit, necessary, and sufficient condition on the critical coupling strength to achieve exponential synchronization in the finite-dimensional Kuramoto model with an arbitrary distribution of the natural frequencies ω_i , see Theorem 4.4.2. Our technical approach is based on Jacobian insights on the transient dynamics, see Lemma 4.4.1, and an adoption of the contraction Lyapunov function (2.16) (originally developed for consensus protocols) to heterogeneous oscillator networks with dissimilar natural frequencies.

We show that synchronization occurs for $K > K_{\text{critical}} = \omega_{\text{max}} - \omega_{\text{min}}$, where ω_{max} and ω_{min} are the maximum and minimum natural frequency, respectively. The multiplicative gap K_{critical}/K determines the admissible initial and the guaranteed asymptotic level of arc invariance as well as the guaranteed asymptotic magnitude r of the order parameter. In particular, the asymptotic level of arc in-

variance can be made arbitrary small by increasing this multiplicative gap. This result resembles the concept of *practical stability* in dynamics and control if K and K_{critical} are understood as a synchronization-enhancing gain and as a measure for the desynchronizing dissimilar natural frequencies. Additionally, our main result includes estimates on the exponential rate of frequency synchronization, and our analysis also applies to switching and smoothly time-varying natural frequencies

We show that our proposed condition also provides a worst-case upper bound on the critical coupling, which is saturated in case of a bipolar distribution of the natural frequencies, see Corollary 4.4.3. In statistical studies, we compare our condition to other necessary and explicit or implicit and exact conditions proposed in the literature. Finally, we also extend our synchronization condition to frequency synchronization of multi-rate Kuramoto oscillators (3.2). Previously, no exact or tight synchronization conditions were known for the multi-rate Kuramoto model (3.2). Again, the inertial coefficients M_i do not affect the local synchronization conditions. These interesting and provably correct findings contradict prior observations on the role of inertia inhibiting or enhancing synchronization in second-order Kuramoto models, as summarized in Subsection 3.1.1.

Section 4.5: In this section, we show an application of the analysis methods in Section 4.4 and Section 3.4 to the network-reduced power system model (3.16) and the non-uniform Kuramoto model (3.17).

4.2 Infinite-Dimensional Kuramoto Oscillator Networks

The formulation (4.1)-(4.2) of the Kuramoto model by means of the order parameter suggests that the oscillators synchronize by coupling to a *mean field* represented by the order parameter $re^{i\psi}$. The analysis of this phase transition based on a mean-field and statistical mechanics viewpoint has been the subject of numerous investigations, starting with Kuramoto's own ingenious analysis in [158, 159]. As neatly described in [258], Kuramoto assumed the a priori existence of solutions to (4.2) which feature a stationary order parameter $r(t)e^{i\psi(t)} = \text{constant}$. Following this assumption and his intuition, Kuramoto derived a set of self-consistency equations. A rigorous mathematical underpinning to Kuramoto's mean-field approach can be established by a time-scale separation [119] or in the continuum limit as the number of oscillators tends to infinity, and the natural frequencies ω are sampled from a distribution function $g : \mathbb{R} \rightarrow \mathbb{R}_{\geq 0}$.

The continuum-limit model has enjoyed a considerable amount of attention by the physics and dynamics communities. Infinite-dimensional oscillator networks are surveyed in detail in [3, 24, 258] Related control-theoretical applications of the continuum limit can be found in [272, 300]. In this section, introduce the continuum limit model and describe its synchronization phenomenology. We do

not aim at a comprehensive treatment of infinite-dimensional oscillator networks and discuss them only briefly for the sake of comparing our latter results.

4.2.1 The Continuum Limit Model

In what follows, we present an informal Eulerian derivation of the continuum-limit model. We also remark that a treatment of (4.2) as a stochastic differential equation (in the limit of zero additive white noise) results in a Fokker-Planck equation analogous to the continuum-limit model [3, 69, 258].

Consider an infinite population of oscillators, and let $\rho : \mathbb{S}^1 \times \mathbb{R}_{\geq 0} \times \mathbb{R} \rightarrow \mathbb{R}_{\geq 0}$ be the probability density function of the oscillators, that is, $\int_0^\gamma \int_{\underline{\omega}}^{\bar{\omega}} \rho(\theta, t, \omega) g(\omega) d\omega d\theta$ denotes the fraction of oscillators in $\overline{\text{Arc}}_n(\gamma) \subseteq \mathbb{S}^1$, at time t , and with frequencies $\omega \in [\underline{\omega}, \bar{\omega}]$. Hence, the order parameter is given by

$$r(t)e^{i\psi(t)} = \int_0^{2\pi} \int_{-\infty}^{\infty} e^{i\theta} \rho(\theta, t, \omega) g(\omega) d\omega d\theta. \quad (4.3)$$

Notice that in the discrete (finite-dimensional) case $\rho(\theta, t, \omega) = \frac{1}{n} \sum_{j=1}^n \delta(\theta - \theta_j)$ (where δ is the Dirac δ -distribution) the order parameters (4.1) and (4.3) coincide. According to (4.2), the instantaneous velocity of an oscillator at position θ , at time t , and with natural frequency ω is given by $v(\theta, t, \omega) = \omega - Kr(t) \sin(\theta - \psi(t))$. The evolution of the probability density is then governed by the continuity equation

$$\frac{\partial}{\partial t} \rho + \frac{\partial}{\partial \theta} (\rho v) = 0, \quad (4.4)$$

subject to the conservation of the oscillators at time t and with frequency ω :

$$\int_0^{2\pi} \rho(\theta, t, \omega) d\theta = 1.$$

We remark that the continuum-limit model (4.3)-(4.4) is presented sometimes with the density $\tilde{\rho}(\theta, t, \omega) = \rho(\theta, t, \omega)g(\omega)$ satisfying $\int_0^{2\pi} \tilde{\rho}(\theta, t, \omega) d\theta = g(\omega)$.

4.2.2 Synchronization Phenomenology in the Continuum-Limit Model

Similar to the finite-dimensional model (4.1)-(4.2), the continuum-limit model (4.3)-(4.4) displays a rich set of symmetries [204] and dynamics [24, 175]. The saddle-node bifurcation from incoherence to synchrony in the finite-dimensional model (4.1)-(4.2) (see Subsection 2.3.2) manifests itself in the infinite-dimensional model (4.3)-(4.4) as a phase transition from the *uniform incoherent state* with density $\rho(\theta, t, \omega) = 1/(2\pi)$ to the so-called *partially synchronized state*. The partially synchronized state is characterized by a subset of phase-locked oscillators rotating in unison whereas the remaining oscillators are incoherent. The synchronized set of oscillators are those satisfying $Kr > |\omega|$ such that $v(\theta, t, \omega) = 0$, and the incoherent ones are uniformly spread over the circle, see Figures 4.1(a) and 4.1(b) for a schematic illustration. This phase transition occurs when K exceeds some critical value K_{critical} . When K is further increased, more and more oscil-

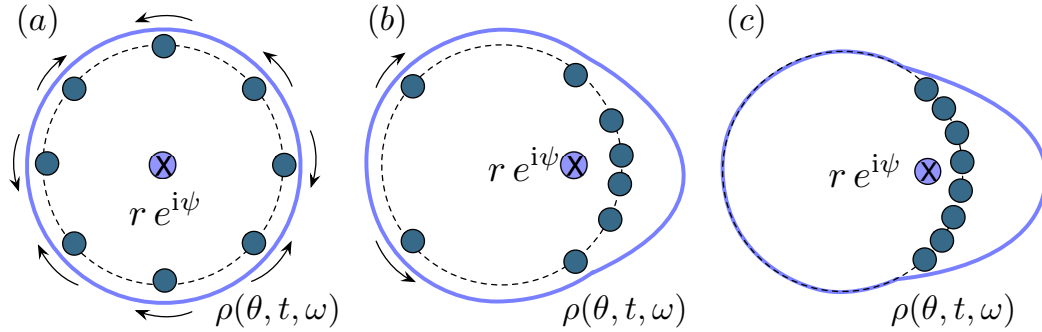


Figure 4.1: Synchronization in the continuum limit model

Subfigure (a) displays the uniform incoherent state $\rho(\theta, t, \omega) = 1/(2\pi)$. Subfigure (b) illustrates the partially synchronized state, where a subset of oscillators rotates in unison and the remaining oscillators are incoherent. Subfigure (c) illustrates the fully phase-locked state.

lators become entrained by the mean field (4.3) and join the set of phase-locked oscillators. For a frequency distribution $g(\omega)$ with bounded support, there exists a second critical parameter $K_{\text{lock}} \geq K_{\text{critical}}$, such that for $K > K_{\text{lock}}$ all oscillators are phase-locked. This final stage of synchronization is illustrated in Figure 4.1(c). It is often referred to as the *fully phase-locked state*, and it is reminiscent of frequency synchronization as displayed in the finite-dimensional model (4.1)-(4.2).

Whereas the majority of the literature on the continuum-limit model (4.3)-(4.4) focuses on the first phase transition and the calculation of K_{critical} , see [3, 24, 54, 69, 159, 183, 204, 258] and references therein, the articles [95, 183, 185, 225, 277, 283] discuss the fully phase-locked state and the calculation of K_{lock} . An extensive line of recent research in dynamics has been triggered by the work [204], which exploits the extensive symmetries of the continuum-limit model (4.3)-(4.4)

to construct simple solutions obeying low-dimensional ODE dynamics. Finally, we remark that the continuum-limit model and its analysis can be extended to second-order mechanical oscillator models [3].

4.2.3 Estimates on the Critical Coupling Strength

In his ingenious analysis of the continuum-limit model (4.3)-(4.4) Kuramoto considered continuous, even, and unimodal distributions $g(\omega)$ of the natural frequencies (achieving their maximum at $g(0)$), and found that phase-locked solutions (if existent) must satisfy the *self-consistency equation* [159, Eq. (5.4.26)]

$$r = Kr \int_{-\pi/2}^{\pi/2} \cos^2(\theta) g(Kr \sin(\theta)) d\theta. \quad (4.5)$$

One trivial solution to the self-consistency equation (4.5) is $r = 0$ corresponding to the uniform incoherent state shown in Figure 4.1(a). The second solution for $r > 0$ corresponds to the partially synchronized state illustrated in Figure 4.1(b). When canceling the variable r from both sides of (4.5) and taking the limit $r \searrow 0$, the self-consistency equation (4.5) delivers the bifurcation parameter

$$K_{\text{critical}} = \frac{2}{\pi g(0)}. \quad (4.6)$$

Kuramoto conjectured that the uniform incoherent state would become unstable for $K > K_{\text{critical}}$ and concluded famously that “surprisingly enough, this seemingly obvious fact seems difficult to prove.” The resolution of this long-standing

conjecture and Kuramoto's ingenious yet incomplete analysis inspired generations of scientists, see [258] for an historical account. We present the following general result taken from the recent article [54, Theorem 3.5].

Theorem 4.2.1 (Instability of the incoherent state). *Consider the infinite-dimensional Kuramoto model (4.3),(4.4) with coupling gain K and frequency distribution $g : \mathbb{R} \rightarrow \mathbb{R}_{\geq 0}$. Let $\{y_1, y_2, \dots\}$ be the roots of the equation*

$$\lim_{x \searrow 0} \int_{-\infty}^{\infty} \frac{\omega - y}{x^2 + (\omega - y)^2} g(\omega) d\omega = 0, \quad (4.7)$$

and assume $g(\omega)$ is continuous at $\{y_1, y_2, \dots\}$. If

$$K > K_{\text{critical}} = \frac{2}{\pi \sup_j g(y_j)},$$

then the incoherent state $\rho(\theta, t, \omega) = 1/(2\pi)$ is unstable.

It can be shown that for a continuous, even, and unimodal distribution $g(\omega)$, the unique root of (4.7) is given by $y_1 = 0$, see [54, Corollary 3.6]. This observation leads to the following corollary, which can be found in [3, 24, 54, 69, 175, 183, 204] and references therein.

Corollary 4.2.2 (Instability beyond Kuramoto's critical transition point). *Consider the infinite-dimensional Kuramoto model (4.3)-(4.4) with coupling gain K and frequency distribution $g : \mathbb{R} \rightarrow \mathbb{R}_{\geq 0}$. Suppose that $g(\omega)$ is continuous at the origin, even, and unimodal. If K is greater than K_{critical} as given in (4.6), then the incoherent state $\rho(\theta, t, \omega) = 1/(2\pi)$ is unstable.*

A linear stability analysis of the associated partially-synchronized state illustrated in Figure 4.1(b) is discussed in [183] and reveals linear neutral stability. To the best of the author's knowledge, a nonlinear stability analysis of the partially-synchronized state is still outstanding.

If the distribution $g(\omega)$ is restricted to have bounded support, then the fully phase-locked state (illustrated in Figure 4.1(c)) can be achieved when the coupling K is larger than the second critical threshold $K_{\text{lock}} \geq K_{\text{critical}}$. In this case, two distributions of interest are the uniform and the bipolar distribution given by

$$g_{\text{unif}} : [-\omega_0, +\omega_0] \rightarrow \mathbb{R}, \quad g_{\text{unif}}(\omega) = \frac{1}{2\omega_0},$$

$$g_{\text{bip}} : [\omega_{\min}, \omega_{\max}] \rightarrow \mathbb{R},$$

$$g_{\text{bip}}(\omega) = p \cdot \delta(\omega - \omega_{\max}) + (1 - p) \cdot \delta(\omega - \omega_{\min}),$$

where $\omega_0 > 0$, $\omega_{\max} > \omega_{\min}$, and $p \in [0, 1]$. These two distributions are particularly interesting since they yield the smallest and the largest threshold K_{lock} .

Theorem 4.2.3 (Full phase locking thresholds). *Consider the infinite-dimensional Kuramoto model (4.3),(4.4) with coupling gain K and frequency distribution $g : \mathbb{R} \rightarrow \mathbb{R}_{\geq 0}$ with bounded support. The following statements hold for the full phase-locking threshold K_{lock} :*

(i) **Lower bound:** For any continuous, even, and unimodal $g : [-\omega_0, +\omega_0] \rightarrow \mathbb{R}$, where $\omega_0 > 0$, we have $K_{\text{lock}} \geq 4\omega_0/\pi$. Moreover, for the uniform distribution $g_{\text{unif}}(\omega)$, we have $K_{\text{lock}} = 4\omega_0/\pi$.

(ii) **Upper bound:** For any $g : [\omega_{\min}, \omega_{\max}] \rightarrow \mathbb{R}_{\geq 0}$, where $\omega_{\max} > \omega_{\min}$, we have $K_{\text{lock}} \leq \omega_{\max} - \omega_{\min}$. Moreover, for the bipolar distribution $g_{\text{bip}}(\omega)$ we have $K_{\text{lock}} = \omega_{\max} - \omega_{\min}$.

A proof of the lower bound (i) can be found in [95, Corollary 2(b)] and in [183]. Notice that the two thresholds K_{critical} (reported in (4.6)) and K_{lock} coincide for the uniform distribution:

$$K_{\text{lock}} = \frac{2}{\pi g_{\text{unif}}(0)} = K_{\text{critical}}.$$

This remarkable identity was also observed in [183, 225, 277, 283]. The upper bound (ii) on bipolar distributions has been proved in [277] and earlier in [95] for the symmetric case ($p = 1/2$ and $\omega_{\max} = -\omega_{\min} = \omega_0$). Bipolar and more general bimodal frequency distributions $g(\omega)$ have attracted tremendous research interest by dynamicists thanks to their rich bifurcation diagram, see [3, 175]. The uniform and bipolar distributions are shown in Figure 4.2 together with the associated stationary phase distributions in the critical case $K \searrow K_{\text{lock}}$ (explicitly calculated in [277]). For later reference, Figure 4.2 also shows the tripolar distri-

bution $g_{\text{trip},n}(\omega) = \frac{1}{n}\delta(\omega - \omega_0) + \frac{n-2}{n}\delta(\omega_0) + \frac{1}{n}\delta(\omega + \omega_0)$ and its associated phase distribution (calculated by [58, Proof of Theorem 2.1]) for $n \rightarrow \infty$.

4.3 Finite-Dimensional Kuramoto Oscillator Networks

In this section, we present and compare different synchronization metrics tailored to the Kuramoto model (1.2), and we review a set of necessary, sufficient, implicit, and explicit estimates of the critical coupling strength. Finally, we also state a key lemma on the frequency synchronization of Kuramoto oscillators, which we will exploit in the following section.

4.3.1 Synchronization Metrics in Kuramoto Oscillator Networks

The notions of phase cohesiveness and arc invariance are performance measures for synchronization, and phase synchronization is the extreme case of phase cohesiveness with $\lim_{t \rightarrow \infty} \theta(t) \in \bar{\Delta}_G(0) = \overline{\text{Arc}_n(0)}$. An alternative performance measure is the magnitude of the order parameter $re^{i\psi}$ introduced in (4.1): if the oscillators are phase-synchronized, then $r = 1$, and if the oscillators are spaced equally on the unit circle, then $r = 0$. For a complete graph, the magnitude r of

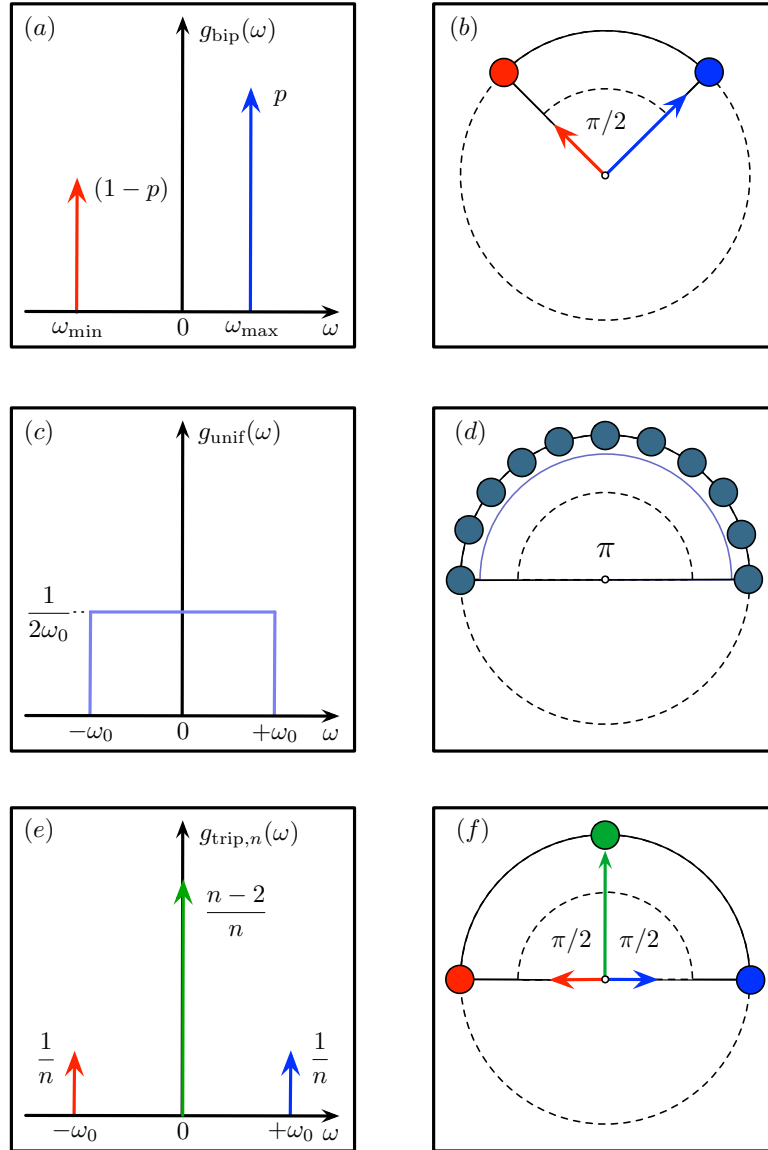


Figure 4.2: Extremal distributions of the natural frequencies and phases
 Extremal distributions $g(\omega)$ of the natural frequencies and their stationary phase distributions in the critical case $K \searrow K_{\text{lock}}$: Panels (a) and (b) show the non-symmetric bipolar distribution $g_{\text{bip}}(\omega) = p \cdot \delta(\omega - \omega_{\text{max}}) + (1 - p) \cdot \delta(\omega - \omega_{\text{min}})$ and its associated bipolar phase distribution. Panels (c) and (d) show the uniform $g_{\text{unif}}(\omega) = 1/(2\omega_0)$ and its associated uniform phase distribution. Finally, panels (e) and (f) show the tripolar distribution $g_{\text{trip},n}(\omega) = \frac{1}{n}\delta(\omega - \omega_0) + \frac{n-2}{n}\delta(\omega_0) + \frac{1}{n}\delta(\omega + \omega_0)$ and its associated tripolar phase distribution for $n \rightarrow \infty$.

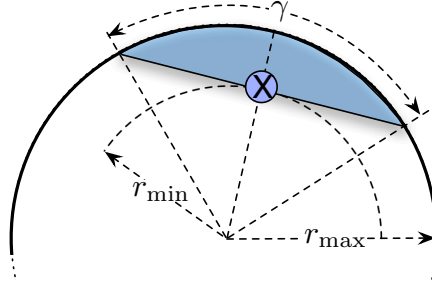


Figure 4.3: Arc invariance and order parameter

Schematic illustration of an arc of length $\gamma \in [0, \pi]$, its convex hull (shaded), and the value \otimes of the corresponding order parameter $re^{i\psi}$ with minimum magnitude $r_{\min} = \cos(\gamma/2)$ and maximum magnitude $r_{\max} = 1$.

the order parameter is an *average* performance index for synchronization, and arc invariance can be understood as a *worst-case* performance index.

The order parameter (4.1) is the centroid of the oscillators (when represented as points on the unit circle), and is contained in the convex hull (in the complex plane) of the smallest arc containing all oscillators, see Figure 4.3. Hence, the magnitude r of the order parameter can be related to the arc length γ as follows:

Lemma 4.3.1 (Shortest arc length and order parameter). *Given an angle array $\theta = (\theta_1, \dots, \theta_n) \in \mathbb{T}^n$ with $n \geq 2$, let $r(\theta) = \frac{1}{n} |\sum_{j=1}^n e^{i\theta_j}|$ be the magnitude of the order parameter, and let $\gamma(\theta)$ be the length of the shortest arc containing all angles, that is, $\theta \in \overline{\text{Arc}_n}(\gamma(\theta))$. The following statements hold:*

- 1) if $\gamma(\theta) \in [0, \pi]$, then $r(\theta) \in [\cos(\gamma(\theta)/2), 1]$; and
- 2) if $\theta \in \overline{\text{Arc}_n}(\pi)$, then $\gamma(\theta) \in [2 \arccos(r(\theta)), \pi]$.

Proof. The order parameter $re^{i\psi}$ is the centroid of all *phasors* $e^{i\theta_j}$ represented as points on the unit circle in \mathbb{C}^1 . Hence, for $\theta \in \overline{\text{Arc}}_n(\gamma)$, $\gamma \in [0, \pi]$, r is contained in the convex hull of the arc of length γ , as illustrated in Figure 4.3. Let $\gamma \in [0, \pi]$ be fixed and let $\theta \in \overline{\text{Arc}}_n(\gamma)$. It follows from elementary geometric arguments that $\cos(\gamma/2) = r_{\min} \leq r \leq r_{\max} = 1$, which proves statement 1). Conversely, if r is fixed and $\theta \in \overline{\text{Arc}}_n(\pi)$, then the centroid $re^{i\psi}$ is always contained within the convex hull of the semi-circle $\overline{\text{Arc}}_n(\pi)$ (centered at ψ). The smallest arc whose convex hull contains the centroid $re^{i\psi}$ is the arc of length $\gamma = 2 \arccos(r)$ (centered at ψ), as illustrated in Figure 4.3. This proves statement 2). \square

Appropriate definitions of the order parameter tailored to non-complete graphs have been proposed, among others, in [139, 209, 222, 238].

4.3.2 Estimates on the Critical Coupling Strength

In the finite-dimensional case, various necessary, sufficient, implicit, and explicit estimates of the critical coupling strength K_{critical} have been proposed.

Necessary, explicit, and tight conditions:

In the finite dimensional case, the following well known conditions show that the natural frequencies ω have to be absolutely and incrementally bounded for frequency synchronization to be feasible.

Lemma 4.3.2 (Necessary synchronization conditions). *Consider the Kuramoto model (1.2) with $\omega \in \mathbf{1}_n^\perp$. The following statements hold:*

1) **Absolute boundedness:** *If there exists a frequency-synchronized solution, then*

$$K \geq K_{\text{critical}} \triangleq \frac{n}{n-1} \cdot \max_{i \in \{1, \dots, n\}} |\omega_i|. \quad (4.8)$$

2) **Incremental boundedness:** *If there exists a frequency-synchronized solution, then*

$$K \geq K_{\text{critical}} \triangleq \frac{n}{2(n-1)} (\omega_{\max} - \omega_{\min}) \quad (4.9)$$

Proof. Recall from Subsection 2.3.1 that, if the Kuramoto model (1.2) synchronizes, then the explicit synchronization frequency is zero since $\omega \in \mathbf{1}_n^\perp$. Hence, the fixed-point equations of the Kuramoto model (1.2) read as

$$\omega_i = \frac{K}{n} \sum_{j=1}^n \sin(\theta_i - \theta_j), \quad i \in \{1, \dots, n\}. \quad (4.10)$$

Since the sinusoidal interaction between the oscillators is bounded, $\sin(\theta_i - \theta_j) \in [-1, +1]$ for all $\theta_i, \theta_j \in \mathbb{S}^1$, the fixed-point equations (4.10) have no solution if condition (5.1) is not satisfied. Alternatively, a subtraction of the i th and j th fixed-point equation (4.10), yields the following equation for all $\{i, j\} \in \mathcal{E}$:

$$\omega_i - \omega_j = \frac{K}{n} \sum_{\ell=1}^n (\sin(\theta_i - \theta_\ell) - \sin(\theta_j - \theta_\ell)). \quad (4.11)$$

Again, equation (4.11) has no solution if condition (4.9) is not satisfied. \square

By Lemma 4.3.2, the natural frequencies necessarily need to be supported on a compact interval, $\omega_i \in [\omega_{\max}, \omega_{\min}] \subset \mathbb{R}$ for all $i \in \{1, \dots, n\}$. The necessary condition (4.9) then states the critical coupling in terms of the width of the interval $[\omega_{\max}, \omega_{\min}]$. In the limit as $n \rightarrow \infty$, this bound reduces to $(\omega_{\max} - \omega_{\min})/2$, the simple bound derived in the introduction of this chapter. A looser but still insightful necessary condition is $K \geq 2\sigma$, where σ is the variance of the ω_i [277], [281, Corollary 2]. For bipolar distributions $\omega_i \in \{\omega_{\min}, \omega_{\max}\}$, necessary explicit conditions similar to (4.9) can be derived for non-complete and highly symmetric coupling topologies [40]. Of course, this often-reported lower bound (4.9) is generally conservative. The following tighter lower bound has been constructed in [58].

Lemma 4.3.3 (Explicit, necessary, and tight critical coupling). *Consider the Kuramoto model (1.2) with $n \geq 2$ oscillators, natural frequencies $\omega \in \mathbf{1}_n^\perp$, and coupling strength K . Define $\gamma \in [\pi/2, \pi]$ by*

$$\gamma = 2 \arccos \left(\frac{-(n-2) + \sqrt{(n-2)^2 + 32}}{8} \right). \quad (4.12)$$

The Kuramoto model has a frequency-synchronized solution only if the coupling strength K is larger than a critical value, that is,

$$K \geq K_{\text{critical}} \triangleq \frac{n \cdot (\omega_{\max} - \omega_{\min})}{2(\sin(\gamma) + (n-2)\sin(\gamma/2))}. \quad (4.13)$$

Moreover, condition (4.13) is tight: for $\omega = \omega_{\text{trip}} \triangleq \omega_0 \cdot (+1, -1, \mathbf{0}_{n-2})$ with $\omega_0 \in \mathbb{R}$ and for any of its permutations, there exists a synchronous solution if and only if $K \geq K_{\text{critical}}$.

Notice that the bound (4.13) equals the bound (4.9) for $n = 2$ and for $n \rightarrow \infty$, and it is a strict improvement otherwise. The bound (4.13) is reported in [58, Eqs. (8) and (11)] and is computed using optimization techniques. Though not explicitly stated in [58], it can be verified from the derivation that the lower bound (4.12)-(4.13) is tight for $\omega = \omega_{\text{trip}}$. In the critical case $K = K_{\text{critical}}$, the associated arc-invariant equilibrium manifold is given by $[\theta^*] = [(+\gamma/2, -\gamma/2, \mathbf{0}_{n-2})]$. In the limit $n \rightarrow \infty$ this choice of natural frequencies ω corresponds to the tripolar distribution in Figure 4.2(e), and the associated phases $[\theta^*]$ are shown in Figure 4.2(f).

Sufficient and explicit conditions:

Besides the necessary conditions in Lemmas 4.3.2 and 4.3.3, various bounds *sufficient* for synchronization have been derived including estimates of the region of attraction. Typically, these sufficient bounds are derived via incremental stability arguments and are of the form

$$K > K_{\text{critical}} = \|V\omega\|_p \cdot f(n, \gamma), \quad (4.14)$$

where $\|\cdot\|_p$ is the p -norm and V is a matrix (of yet unspecified row dimension) measuring the dissimilarity among the ω_i . For instance, $V = I_n - (1/n)\mathbf{1}_{n \times n}$ gives

the deviation from the average natural frequency, $V\omega = \omega - \omega_{\text{avg}}\mathbf{1}_n$. Finally, the function $f : \mathbb{N} \times [0, \pi/2[\rightarrow [1, \infty[$ captures the dependence of K_{critical} on the number of oscillators n and the scalar γ determining a bound on the admissible pairwise phase differences, which is, for instance, of the form $\|(\dots, |\theta_i^* - \theta_j^*|, \dots)\|_p \leq \gamma$.

Two-norm bounds, that is, $p = 2$ in condition (4.14) can be derived using quadratic Lyapunov functions in [58, proof of Theorem 4.2] and [85, Theorem 4.4] (see Theorem 5.2.2 in the next chapter) and fixed-point theorems [139, Condition (11)] and [84, Theorem 4.7] (see also Theorem 5.2.3 in the next chapter), where the matrix $V \in \mathbb{R}^{n(n-1)/2 \times n}$ is the incidence matrix of the complete graph, and $V\omega$ is the vector of $n(n-1)/2$ pairwise differences $\omega_i - \omega_j$. A sinusoidal Lyapunov function [102, Proposition 1] leads to a two-norm bound with $V = I_n - (1/n)\mathbf{1}_{n \times n}$. Similar two-norm bounds can be obtained by contraction mapping [139, Theorem 2] and by contraction analysis [64, Theorem 8], where $V \in \mathbb{R}^{n-1 \times n}$ is an orthonormal projector on $\mathbf{1}_n^\perp$. For all cited references the region of attraction is given by the $n(n-1)/2$ initial phase differences in two-norm or ∞ -norm balls satisfying $\|V\theta(0)\|_{2,\infty} < \pi$. Unfortunately, none of these bounds scales independently of n since $\|V\omega\|_2^2$ is a sum of at least $n-1$ terms in all cited references and $f(n, \gamma)$ is either an increasing [139] or a constant function of n [58, 64, 85, 102].

A scaling of condition (4.14) independently of n has been achieved only when considering the width $\omega_{\text{max}} - \omega_{\text{min}} = \|(\dots, \omega_i - \omega_j, \dots)\|_\infty$, that is, for $V\omega$ being

the vector of all $n(n-1)/2$ pairwise frequency differences and $p = \infty$ in condition (4.14). A quadratic Lyapunov function leads to $f(n, \gamma) = n/(2 \sin(\gamma))$ [58, proof of Theorem 4.1], a contraction argument leads to $f(n, \gamma) = n/((n-2) \sin(\gamma))$ [239, Lemma 9], and a geometric argument leads to the scale-free bound $f(\gamma) = 1/(2 \sin(\gamma/2) \cos(\gamma))$ [74, proof of Proposition 1]. In [116, Theorem 3.3] and in the author's work [85, Theorem 2.4] and [83, Theorem 4.1] (to be presented in the next section), the simple and scale-free bound $f(\gamma) = 1/\sin(\gamma)$ has been derived by analyticity and contraction arguments. In our notation, the region of attraction for synchronization in references [58, 74, 116, 239] is given as $\theta(0) \in \overline{\text{Arc}_n(\gamma)}$ for $\gamma \in [0, \pi/2[$ determined from condition (4.14).

Exact and implicit conditions:

The articles [5, 185, 281] derive a set of implicit consistency equations for the *exact* critical coupling strength K_{critical} for which frequency-synchronized solutions exist. The consistency equation can be easily motivated. Each equilibrium solution to the Kuramoto model (4.1),(4.2) is characterized by $[\theta^*] \in \mathbb{T}^n$ such that the left-hand side of (4.2) equals zero. We denote the corresponding value of the order parameter (4.1) by $r_\infty \in [0, 1]$ and, without loss of generality, we assume

that its phase ψ is zero. Hence, we arrive at the equations

$$\begin{aligned}\omega_i &= Kr_\infty \sin(\theta_i^*), \\ r_\infty &= \frac{1}{n} \sum_{j=1}^n \cos(\theta_j^*).\end{aligned}\tag{4.15}$$

The equations (4.15) are solvable only if $Kr_\infty \geq \|\omega\|_\infty$, and thus necessarily $r_\infty > 0$ unless $\omega = \mathbf{0}_n$. By eliminating θ^* from (4.15), we arrive at the often-stated *consistency equation*

$$r_\infty = \frac{1}{n} \sum_{j=1}^n \pm \sqrt{1 - (\omega_j/Kr_\infty)^2},\tag{4.16}$$

where the \pm signs are due to the equality: $\cos(\arcsin(x)) = \pm\sqrt{1-x^2}$ for $x \in]-1, 1[$. In fact, the consistency equation (4.16) is a set of 2^n equations corresponding to different possible equilibria θ^* in (4.15) and thus different choices of the \pm signs, although not all choices yield feasible solutions satisfying $r_\infty \geq 0$. We refer to [5] for a discussion of the consistency equation (4.16) and its infinite-dimensional counterpart (4.5). The implicit consistency equation (4.16) marks the starting point for the analyses in [5, 185, 281]. By collecting various results in these three references, we arrive at the following statement, which has not been presented in this complete and self-contained form so far.

Theorem 4.3.4 (Implicit formulae for the exact critical coupling). *Consider the Kuramoto model (1.2) with $n \geq 2$ oscillators, natural frequencies $\omega \in \mathbf{1}_n^\perp \setminus \{\mathbf{0}_n\}$, and coupling strength K . Compute $u^* \in [\|\omega\|_\infty, 2\|\omega\|_\infty]$ as unique solution to the*

equation

$$2 \sum_{i=1}^n \sqrt{1 - (\omega_i/u)^2} = \sum_{i=1}^n 1/\sqrt{1 - (\omega_i/u)^2}. \quad (4.17)$$

The following statements are equivalent:

(i) **Critical coupling:** the coupling strength K is larger than a critical value,

that is,

$$K > K_{\text{critical}} \triangleq nu^* / \sum_{i=1}^n \sqrt{1 - (\omega_i/u^*)^2}; \quad (4.18)$$

(ii) **Stable frequency synchronization:** there exists at least one locally exponentially stable equilibrium manifold $[\theta^*] \subset \mathbb{T}^n$.

The implicit formulae (4.17)-(4.18) have been established in [281, Theorem 3], who showed that K_{critical} is the smallest nonnegative value of the coupling strength for which the Kuramoto model (1.2) admits a frequency-synchronized solution. We remark that Verwoerd and Mason also extended the implicit formulae (4.17)-(4.18) to complete bipartite graphs [282, Theorem 3] and infinite-dimensional networks [283, Theorem 4]. Moreover, they provided bisection algorithms to compute K_{critical} with predefined precision in a finite number of iterations. Similar implicit formulae are found in [5] and [185], where additionally a local stability analysis is carried out [5, Theorems 1 and 3] and [185, Sections 3 and 4] showing a saddle-node bifurcation for $K = K_{\text{critical}}$: for $K < K_{\text{critical}}$ no frequency-synchronized solution (that is, equilibrium manifolds) exists and for $K > K_{\text{critical}}$ a locally stable (cor-

responding to all + signs in (4.16)) and multiple unstable phase-locked solutions co-exist. As shown in [225], the Kuramoto model (1.2) can be embedded into a higher-dimensional, linear, and complex-valued system, and the above stability results can also be elegantly established via linear systems theory, see [67].

4.4 Explicit and Tight Conditions on the Critical Coupling

In the finite dimensional case various necessary or sufficient explicit bounds on the coupling strength K_{critical} are known as well as the implicit formulae (4.17)-(4.18) to compute K_{critical} which is provably a threshold for local stability. For the purpose of analyzing and selecting a sufficiently strong coupling in applications, the exact conditions in Theorem 4.3.4 have three drawbacks. The stability results are local and the region of attraction of a synchronized solution is unknown. Second, the exact formulae (4.17)-(4.18) are implicit and thus not suited for performance estimates. For example, it is unclear which value of asymptotic arc invariance can be achieved if $K > c \cdot K_{\text{critical}}$ for some $c > 1$. Third and finally, the natural frequencies ω_i are often time-varying or uncertain in most applications. In this case, the exact value of K_{critical} needs to be estimated in continuous time, or a conservatively strong coupling $K \gg K_{\text{critical}}$ has to be chosen.

Recall from the two-dimensional example in Subsection 2.3.2 that two oscillators synchronize if and only if $K > K_{\text{critical}} \triangleq |\omega_2 - \omega_1|$, and the ratio $\kappa^{-1} = K_{\text{critical}}/K < 1$ determines the asymptotic arc invariance as well as the set of admissible initial conditions. In other words, practical phase synchronization is achieved for $K \gg K_{\text{critical}}$, and arc invariance occurs only for initial angles $\theta(0) \in \overline{\text{Arc}_n(\gamma)}$, where $\gamma = \arcsin(K_{\text{critical}}/K) \in]\pi/2, \pi[$. This set of admissible initial conditions $\overline{\text{Arc}_n(\gamma)}$ can be enlarged to an open semi-circle by increasing K/K_{critical} . Finally, synchronization is lost in a saddle-node bifurcation at $K = K_{\text{critical}}$. In this section, we will generalize all outcomes of this simple two-dimensional example to the case of n oscillators.

4.4.1 Boundedness and Contraction Analysis Insights

We start our analysis gaining further insights into the transient dynamics of first-order coupled oscillator systems. For the sake of generality and for later applications, we consider the first-order coupled oscillator model (3.1) here. We repeat the model for the reader's convenience:

$$\dot{\theta}_i = \omega_i - \sum_{j=1}^n a_{ij} \sin(\theta_i - \theta_j), \quad \{1, \dots, n\}.$$

The following lemma shows that frequency synchronization of first-order coupled oscillators can be achieved if the dynamics are confined to a subset of the phase cohesive set $\Delta_G(\pi/2)$.

Lemma 4.4.1 (Frequency sync and contraction in $\Delta_G(\pi/2)$). *Consider the first-order coupled oscillator model (3.1) with an undirected, connected, and weighted graph $G(\mathcal{V}, \mathcal{E}, A)$ and natural frequencies $\omega \in \mathbb{R}^n$. Assume that the phase cohesive set $\bar{\Delta}_G(\gamma)$ is forward invariant and $\theta(0) \in \bar{\Delta}_G(\gamma)$ for some $\gamma \in [0, \pi/2[$. Then all frequencies $\dot{\theta}_i(t)$ synchronize exponentially to the average frequency $\omega_{\text{avg}} = \sum_{i=1}^n \omega_i/n$ with convergence rate no worse than $\lambda_{\text{fe}} = -\lambda_2(L) \cos(\gamma)$, that is,*

$$\left\| \dot{\theta}(t) - \omega_{\text{sync}} \mathbf{1}_n \right\|_2 \leq \left\| \dot{\theta}(0) - \omega_{\text{avg}} \mathbf{1}_n \right\|_2 e^{\lambda_{\text{fe}} t}.$$

Proof. By differentiating the first-order coupled oscillator model (3.1), we obtain its frequency dynamics as

$$\frac{d}{dt} \dot{\theta}_i = - \sum_{j=1}^n \tilde{a}_{ij}(\theta(t)) (\dot{\theta}_i - \dot{\theta}_j), \quad i \in \{1, \dots, n\}, \quad (4.19)$$

where $\tilde{a}_{ij}(\theta(t)) = a_{ij} \cos(\theta_i(t) - \theta_j(t))$. The frequency dynamics (4.19) evolve on the tangent space of \mathbb{T}^n , that is, the Euclidean space \mathbb{R}^n . If the set $\bar{\Delta}_G(\gamma)$ is forward invariant and $\theta(0) \in \bar{\Delta}_G(\gamma)$ for some $\gamma \in [0, \pi/2[$, then $a_{ij}(\theta(t)) \geq a_{ij} \cos(\gamma) > 0$ for all $\{i, j\} \in \mathcal{E}$. Thus, the frequency dynamics (4.19) can be regarded as linear *consensus protocol* (2.14) with time-varying and strictly-positive weights. Based on this observation, it follows from the consensus convergence result (in Theorem 2.4.1) that all frequencies $\dot{\theta}_i(t)$ synchronize exponentially.

To obtain the explicit convergence rate, notice that for $\theta(t) \in \bar{\Delta}_G(\gamma)$ the frequency dynamics (4.19) read in vector form as

$$\frac{d}{dt}\dot{\theta} = J(\theta(t))\dot{\theta} = - \underbrace{B \operatorname{diag}(\{\tilde{a}_{ij}(\theta(t))\}_{\{i,j\} \in \mathcal{E}})}_{L(t)} B^T \dot{\theta}, \quad (4.20)$$

where $L(t)$ is a time-varying Laplacian matrix, as discussed in Lemma 3.2.1. By Lemma 2.3.2 and its proof, the explicit synchronization frequency is given by the average frequency ω_{avg} and $\sum_{i=1}^n \dot{\theta}_i(t) = \sum_{i=1}^n \omega_i = n \cdot \omega_{\text{avg}}$ is a conserved quantity for all $t \geq 0$. Consider the disagreement vector $\dot{\delta} = \dot{\theta} - \omega_{\text{avg}} \mathbf{1}_n$, as an error coordinate satisfying $\mathbf{1}_n^T \dot{\delta} = 0$, that is, $\dot{\delta}$ lives in the disagreement eigenspace of dimension $n - 1$ with normal vector $\mathbf{1}_n$. Since ω_{avg} is constant and $\operatorname{Ker}(L(t)) = \operatorname{Span}(\mathbf{1}_n)$ for all $t \geq 0$ the dynamics (4.20) read in $\dot{\delta}$ -coordinates as

$$\frac{d}{dt}\dot{\delta} = -L(t)\dot{\delta}. \quad (4.21)$$

Consider the disagreement function $\dot{\delta} \mapsto \|\dot{\delta}\|_2^2$ and its derivative along the disagreement dynamics (4.21): $\frac{d}{dt}\|\dot{\delta}\|_2^2 = -2\dot{\delta}^T L(t)\dot{\delta}$. By the Courant-Fischer Theorem [181], the derivative of the disagreement function can be upper-bounded (point-wise in time) by the second-smallest eigenvalue of the time-invariant Laplacian L :

$$\begin{aligned} \frac{d}{dt}\|\dot{\delta}\|_2^2 &= -2\dot{\delta}^T L(t)\dot{\delta} = -2(B^T \dot{\delta})^T \operatorname{diag}(\{a_{ij} \cos(\theta_i(t) - \theta_j(t))\}_{\{i,j\} \in \mathcal{E}}) (B^T \dot{\delta}) \\ &\leq -2 \min_{\{i,j\} \in \mathcal{E}} \{\cos(\theta_i - \theta_j) : \theta \in \bar{\Delta}_G(\gamma)\} \cdot \dot{\delta}^T L \dot{\delta} \leq 2\lambda_{\text{fe}} \|\dot{\delta}\|_2^2. \end{aligned}$$

The Bellman-Gronwall Lemma [146, Lemma A.1] yields that the disagreement vector $\delta(t)$ satisfies $\|\dot{\delta}(t)\| \leq \|\dot{\delta}(0)\| e^{\lambda_{\text{fe}} t}$. This concludes the proof. \square

The key ideas of Lemma 4.4.1 have first been presented in [58, Theorem 3.1], and we refer to [85, Theorem 4.1] and [240, Lemma 3.5] for extensions to digraphs, more general coupling functions, and time-delays.

Contraction Analysis

The proof of Lemma 4.4.1 is essentially based on the particular form of the Jacobian $J(\theta)$, which is negative semidefinite for $\theta \in \bar{\Delta}_G(\gamma)$. If $\bar{\Delta}_G(\gamma)$ is a forward invariant set, it also follows that the first-order coupled oscillator dynamics (3.1) are *contracting*¹ relative to the nullspace $\mathbf{1}_n$. Consequently, the dynamics (3.1) are incrementally exponentially stable (modulo symmetry), that is, given any two initial values $\theta(0), \tilde{\theta}(0) \in \bar{\Delta}_G(\gamma)$, there is a pseudo-metric $d : \mathbb{T}^n \times \mathbb{T}^n \rightarrow \mathbb{R}_{\geq 0}$ (a metric modulo symmetry)² and constants $c_1 \geq 1$ and $c_2 > 0$ such that

$$d(\theta(t), \tilde{\theta}(t)) \leq c_1 e^{-c_2 t} d(\theta(0), \tilde{\theta}(0)), \quad \forall t \geq 0. \quad (4.22)$$

The application of contraction analysis to the coupled oscillator model (1.1) yields the incremental exponential stability (4.22) in ℓ_2 -type metrics [64, Theorem 7] or in ℓ_∞ -type metrics [101, Example 6]. [55, Theorem 4.1] report the incremental stability (4.22) in an ℓ_1 -metric. Finally, for discontinuous and monotone coupling

¹We refer the reader to [169, 254] for a treatment of contraction analysis and to [101, 230, 286] for its extension to systems with symmetries.

²The pseudo-metric d is a nonnegative and symmetric function ($d(\theta_1, \theta_2) = d(\theta_2, \theta_1)$) satisfying the triangle inequality $d(\theta_1, \theta_2) \leq d(\theta_1, \theta_3) + d(\theta_3, \theta_2)$ and $d(\theta_1, \theta_1) = 0$ if and only if $[\theta_1] = [\theta_2]$. The pseudo-metric d is a proper distance function on the quotient manifold $\mathbb{T}^n/\mathbb{S}^1$.

functions and complete interaction graphs the total variation distance provides yet another ℓ_1 -type contraction metric [178].

4.4.2 The Contraction Property and the Main Synchronization Result

The results in the previous subsection show that frequency synchronization and incremental stability can be achieved if the dynamics are confined to a subset of the phase cohesive set $\Delta_G(\pi/2)$, respectively, a subset of the arc invariant set $\text{Arc}_n(\pi/2) \subseteq \Delta_G(\pi/2)$ for the complete graph case. In order to show this boundedness, different Lyapunov functions can be adopted which generally lead to only sufficient (and possibly conservative) conditions. Here, we adopt the contraction property presented for consensus networks in Subsection 2.4.1. Recall the geodesic distance on \mathbb{S}^1 and define the continuous function $V : \mathbb{T}^n \rightarrow [0, \pi]$ by

$$V(\psi) = \max\{|\psi_i - \psi_j| \mid i, j \in \{1, \dots, n\}\}. \quad (4.23)$$

If all angles at time t are contained in an arc of length strictly less than π , then the arc length $V(\theta(t)) = \max_{i,j \in \{1, \dots, n\}} |\theta_i(t) - \theta_j(t)|$ is a Lyapunov function candidate to show arc invariance, see Figure 4.4. Intuitively, the oscillators $\theta_\ell(t)$ and $\theta_r(t)$ at both boundaries are pulled towards their neighbors in the interior $\text{Arc}_n(V(\theta(t)))$, and the Lyapunov function $V(\theta(t))$ is non-increasing.

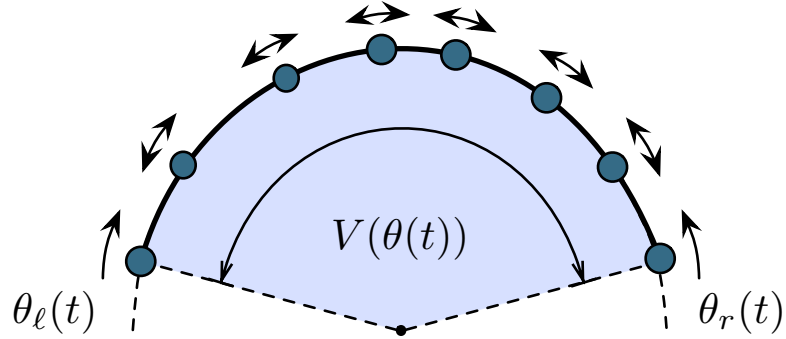


Figure 4.4: Illustration of the contraction Lyapunov function. The Lyapunov function candidate $V(\theta(t))$ is shown for angles in an open semi-circle $\theta(t) \in \text{Arc}_n(\pi)$. The oscillators at the boundaries of the arc containing all oscillators $\overline{\text{Arc}_n(V(\theta(t)))}$ are denoted by $\theta_\ell(t)$ and $\theta_r(t)$.

Based on these observations, the following theorem provides an explicit upper bound on the critical coupling together with performance estimates, convergence rates, and a guaranteed semi-global region of attraction. This bound is tight and thus necessary and sufficient when considering arbitrary distributions with compact support of the natural frequencies.

Theorem 4.4.2 (Explicit, sufficient, & tight critical coupling and practical phase sync). *Consider the Kuramoto model (1.2) with $n \geq 2$ oscillators, natural frequencies $\omega \in \mathbf{1}_n^\perp$ and coupling strength K . The following statements are equivalent:*

- (i) **Critical coupling:** *the coupling strength K is larger than a critical value, that is,*

$$K > K_{\text{critical}} \triangleq \omega_{\max} - \omega_{\min} ; \tag{4.24}$$

- (ii) **Admissible initial arc invariance:** *there exists $\gamma_{\max} \in]\pi/2, \pi]$ such that the Kuramoto model (1.2) synchronizes exponentially for all possible distributions of the natural frequencies ω_i supported on the compact interval $[\omega_{\min}, \omega_{\max}]$ and for all initial phases $\theta(0) \in \text{Arc}_n(\gamma_{\max})$; and*
- (iii) **Arc invariance of sync manifold:** *there exists $\gamma_{\min} \in [0, \pi/2[$ such that the Kuramoto model (1.2) has a locally exponentially stable synchronization manifold in $\overline{\text{Arc}}_n(\gamma_{\min})$ for all possible distributions of the natural frequencies ω_i supported on the compact interval $[\omega_{\min}, \omega_{\max}]$.*

If the equivalent conditions (i), (ii), and (iii) hold, then the ratio K_{critical}/K and the arc lengths $\gamma_{\min} \in [0, \pi/2[$ and $\gamma_{\max} \in]\pi/2, \pi]$ are related uniquely via $\sin(\gamma_{\min}) = \sin(\gamma_{\max}) = K_{\text{critical}}/K$, and the following statements hold:

- 1) **practical phase synchronization:** *the set $\overline{\text{Arc}}_n(\gamma)$ is positively invariant for every $\gamma \in [\gamma_{\min}, \gamma_{\max}]$, and each trajectory originating in $\text{Arc}_n(\gamma_{\max})$ approaches asymptotically $\overline{\text{Arc}}_n(\gamma_{\min})$;*
- 2) **order parameter:** *the asymptotic value of the magnitude of the order parameter denoted by $r_{\infty} \triangleq \lim_{t \rightarrow \infty} \frac{1}{n} |\sum_{j=1}^n e^{i\theta_j(t)}|$ is bounded as*

$$1 \geq r_{\infty} \geq \cos\left(\frac{\gamma_{\min}}{2}\right) = \sqrt{\frac{1 + \sqrt{1 - (K_{\text{critical}}/K)^2}}{2}};$$

3) **frequency synchronization:** *the asymptotic synchronization frequency is*

$$\omega_{\text{sync}} = \sum_{i=1}^n \omega_i/n, \text{ and, given arc invariance in } \overline{\text{Arc}}_n(\gamma) \text{ for some fixed } \gamma < \pi/2, \text{ the exponential synchronization rate is no worse than } \lambda_{\text{fe}}.$$

The proof of Theorem 4.4.2 relies on the contraction property. Since the proof of Theorem 4.4.2 is rather lengthy, we present a brief outline here. If all angles at time $t \geq 0$ belong to a closed arc of length $\gamma \in [0, \pi[$, that is, $\theta(t) \in \overline{\text{Arc}}_n(\gamma)$, then the arc length $t \mapsto V(\theta(t))$ is non-increasing provided that $K \sin(\gamma) \geq \omega_{\max} - \omega_{\min}$. This inequality holds true for $\gamma \in [\gamma_{\min}, \gamma_{\max}]$ if and only if condition (4.24) holds true. Additionally, $t \mapsto V(\theta(t))$ is strictly decreasing for $\gamma \in]\gamma_{\min}, \gamma_{\max}[$, the angles $\theta(t)$ reach the set $\overline{\text{Arc}}_n(\gamma_{\min}) \in \Delta_G(\pi/2)$, and frequency synchronization and stability follow from the results developed in Lemma 4.4.1. The converse implications follow since condition (4.24) is also necessary for synchronization with bipolar natural frequencies $\omega = \omega_{\text{bip}} \triangleq \omega_0 \cdot (-p \cdot \mathbf{1}_{n-p}, +(n-p) \cdot \mathbf{1}_p)$ with $\omega_0 \in \mathbb{R}$, $p \in \{1, \dots, n-1\}$, and for any of its permutations.

Proof of Theorem 4.4.2. Sufficiency (i) \implies (ii): We start by proving the positive invariance of $\overline{\text{Arc}}_n(\gamma)$, that is, arc invariance in $\overline{\text{Arc}}_n(\gamma)$ for some $\gamma \in [0, \pi]$. Recall the contraction Lyapunov function (4.23) depicting the length of the arc containing all angles. This arc has two boundary points: a counterclockwise maximum and a counterclockwise minimum. If we let $I_{\max}(\psi)$ (respectively, $I_{\min}(\psi)$)

denote the set indices of the angles ψ_1, \dots, ψ_n that are equal to the counterclockwise maximum (respectively, the counterclockwise minimum), then we may write

$$V(\psi) = |\psi_{m'} - \psi_{\ell'}|, \text{ for all } m' \in I_{\max}(\psi) \text{ and } \ell' \in I_{\min}(\psi).$$

By assumption, the angles $\theta_i(t)$ belong to the set $\overline{\text{Arc}}_n(\gamma)$ at time $t = 0$. We aim to show that they remain so for all subsequent times $t > 0$. Note that $\theta(t) \in \overline{\text{Arc}}_n(\gamma)$ if and only if $V(\theta(t)) \leq \gamma \leq \pi$. Therefore, $\overline{\text{Arc}}_n(\gamma)$ is positively invariant if and only if $V(\theta(t))$ does not increase at any time t such that $V(\theta(t)) = \gamma$. The *upper Dini derivative* of $V(\theta(t))$ along the Kuramoto dynamics (1.2) is [166, Lemma 2.2]

$$D^+V(\theta(t)) = \limsup_{h \downarrow 0} \frac{V(\theta(t+h)) - V(\theta(t))}{h} = \dot{\theta}_m(t) - \dot{\theta}_\ell(t),$$

where $m \in I_{\max}(\theta(t))$ and $\ell \in I_{\min}(\theta(t))$ are indices with the properties that $\dot{\theta}_m(t) = \max\{\dot{\theta}_{m'}(t) \mid m' \in I_{\max}(\theta(t))\}$ and $\dot{\theta}_\ell(t) = \min\{\dot{\theta}_{\ell'}(t) \mid \ell' \in I_{\min}(\theta(t))\}$.

Written out in components $D^+V(\theta(t))$ takes the form

$$D^+V(\theta(t)) = \omega_m - \omega_\ell - \frac{K}{n} \sum_{i=1}^n (\sin(\theta_m(t) - \theta_i(t)) + \sin(\theta_i(t) - \theta_\ell(t))).$$

Note that the index i in the upper sum can be evaluated for $i \in \{1, \dots, n\}$, and for $i = m$ and $i = \ell$ one of the two sinusoidal terms is zero and the other one achieves its maximum value in $\overline{\text{Arc}}_n(\gamma)$. The trigonometric identity $\sin(x) + \sin(y) =$

$2 \sin(\frac{x+y}{2}) \cos(\frac{x-y}{2})$ then leads to

$$D^+V(\theta(t)) = \omega_m - \omega_\ell - \frac{K}{n} \sum_{i=1}^n \left(2 \sin\left(\frac{\theta_m(t) - \theta_\ell(t)}{2}\right) \times \cos\left(\frac{\theta_m(t) - \theta_i(t)}{2} - \frac{\theta_i(t) - \theta_\ell(t)}{2}\right) \right). \quad (4.25)$$

The equality $V(\theta(t)) = \gamma$ implies that, measuring distances counterclockwise and modulo additional terms equal to multiples of 2π , we have $\theta_m(t) - \theta_\ell(t) = \gamma$, $0 \leq \theta_m(t) - \theta_i(t) \leq \gamma$, and $0 \leq \theta_i(t) - \theta_\ell(t) \leq \gamma$. Therefore, $D^+V(\theta(t))$ simplifies to

$$D^+V(\theta(t)) \leq \omega_m - \omega_\ell - \frac{K}{n} \sum_{i=1}^n \left(2 \sin\left(\frac{\gamma}{2}\right) \cos\left(\frac{\gamma}{2}\right) \right).$$

Reversing the identity from above as $2 \sin(x) \cos(y) = \sin(x-y) + \sin(x+y)$ yields

$$D^+V(\theta(t)) \leq \omega_m - \omega_\ell - \frac{K}{n} \sum_{i=1}^n \sin(\gamma) = \omega_m - \omega_\ell - K \sin(\gamma).$$

Therefore, the length of the arc formed by the angles is non-increasing in $\overline{\text{Arc}}_n(\gamma)$ if for any pair $\{m, \ell\}$ it holds that $K \sin(\gamma) \geq \omega_m - \omega_\ell$, which is true if and only if

$$K \sin(\gamma) \geq K_{\text{critical}}, \quad (4.26)$$

where K_{critical} is as stated in equation (4.24). For $\gamma \in [0, \pi]$ the left-hand side of (4.26) is a concave function of γ that achieves its maximum at $\gamma^* = \pi/2$. Therefore, there exists an open set of arc lengths $\gamma \in [0, \pi]$ satisfying equation (4.26) if and only if equation (4.26) is true with the strict equality sign at $\gamma^* = \pi/2$, which corresponds to inequality (4.24) in the statement of Theorem 4.4.2.

Additionally, if these two equivalent statements are true, then there exists a unique $\gamma_{\min} \in [0, \pi/2[$ and a unique $\gamma_{\max} \in]\pi/2, \pi]$ that satisfy equation (4.26) with the equality sign, namely $\sin(\gamma_{\min}) = \sin(\gamma_{\max}) = K_{\text{critical}}/K$. For every $\gamma \in [\gamma_{\min}, \gamma_{\max}]$ it follows that the arc-length $V(\theta(t))$ is non-increasing, and it is strictly decreasing for $\gamma \in]\gamma_{\min}, \gamma_{\max}[$.

Among other things, this reasoning shows that statement (i) implies statement 1). Additionally, the oscillators are asymptotically phase cohesive in $\overline{\text{Arc}}_n(\gamma_{\min})$. It follows from Lemma 4.3.1 that the asymptotic magnitude r of the order parameter satisfies $1 \geq r \geq \cos(\gamma_{\min}/2)$. The trigonometric identity $\cos(\gamma_{\min}/2) = \sqrt{(1 + \cos(\gamma_{\min}))/2}$ together with a Pythagorean identity yields then the bound in statement 2). Finally, since for $\theta(0) \in \text{Arc}_n(\gamma_{\max})$ and for all $\gamma \in]\gamma_{\min}, \gamma_{\max}]$ there exists a finite time $T \geq 0$ such that $\theta(t) \in \overline{\text{Arc}}_n(\gamma)$ for all $t \geq T$, the frequency synchronization statement 3) then follows directly from Lemma 4.4.1 This concludes the proof of the sufficiency (i) \implies (ii) and the statements 1), 2), and 3).

Necessity (ii) \implies (i): To show that the critical coupling in condition (4.24) is also necessary for synchronization, it suffices to construct a counter example for which $K \leq K_{\text{critical}}$ and the oscillators do not achieve exponential synchronization even though all $\omega_i \in [\omega_{\min}, \omega_{\max}]$ and $\theta(0) \in \text{Arc}_n(\gamma)$ for every $\gamma \in]\pi/2, \pi]$.

A basic instability mechanism under which synchronization breaks down is caused by a bipolar distribution of the natural frequencies. Let the index set

$\{1, \dots, n\}$ be partitioned by the two non-empty sets \mathcal{I}_1 and \mathcal{I}_2 . Let $\omega_i = \omega_{\min}$ for $i \in \mathcal{I}_1$ and $\omega_i = \omega_{\max}$ for $i \in \mathcal{I}_2$, and assume that at some time $t \geq 0$ it holds that $\theta_i(t) = -\gamma/2$ for $i \in \mathcal{I}_1$ and $\theta_i(t) = +\gamma/2$ for $i \in \mathcal{I}_2$ and for some $\gamma \in [0, \pi[$. By construction, at time t all oscillators are contained in an arc of length $\gamma \in [0, \pi[$. Assume now that $K < K_{\text{critical}}$ and the oscillators synchronize. Consider the evolution of the arc length $V(\theta(t))$ given as in (4.25) by

$$\begin{aligned} D^+V(\theta(t)) &= \omega_m - \omega_\ell - \frac{K}{n} \sum_{i \in \mathcal{I}_1} \left(2 \sin\left(\frac{\theta_m(t) - \theta_\ell(t)}{2}\right) \right. \\ &\quad \times \cos\left(\frac{\theta_m(t) - \theta_i(t)}{2} - \frac{\theta_i(t) - \theta_\ell(t)}{2}\right) \\ &\quad \left. - \frac{K}{n} \sum_{i \in \mathcal{I}_2} \left(2 \sin\left(\frac{\theta_m(t) - \theta_\ell(t)}{2}\right) \cos\left(\frac{\theta_m(t) - \theta_i(t)}{2} - \frac{\theta_i(t) - \theta_\ell(t)}{2}\right) \right) \right), \end{aligned}$$

where the summation is split according to the partition of $\{1, \dots, n\}$ into \mathcal{I}_1 and \mathcal{I}_2 . By construction, we have that $\ell \in \mathcal{I}_1$, $m \in \mathcal{I}_2$, $\omega_\ell = \omega_{\min}$, $\omega_m = \omega_{\max}$, $\theta_i(t) = \theta_\ell(t) = -\gamma/2$ for $i \in \mathcal{I}_1$, and $\theta_i(t) = \theta_m(t) = +\gamma/2$ for $i \in \mathcal{I}_2$. Thus, $D^+V(\theta(t))$ simplifies to

$$D^+V(\theta(t)) = \omega_{\max} - \omega_{\min} - \frac{K}{n} \sum_{i \in \mathcal{I}_1} \left(2 \sin\left(\frac{\gamma}{2}\right) \cos\left(\frac{\gamma}{2}\right) \right) - \frac{K}{n} \sum_{i \in \mathcal{I}_2} \left(2 \sin\left(\frac{\gamma}{2}\right) \cos\left(\frac{\gamma}{2}\right) \right).$$

Again, we reverse the trigonometric identity via $2 \sin(x) \cos(y) = \sin(x - y) + \sin(x + y)$, unite both sums, and arrive at

$$D^+V(\theta(t)) = \omega_{\max} - \omega_{\min} - K \sin(\gamma). \quad (4.27)$$

Clearly, for $K < K_{\text{critical}}$ the arc length $V(\theta(t)) = \gamma$ is increasing for any arbitrary $\gamma \in [0, \pi]$. Thus, the phases are not bounded in $\overline{\text{Arc}}_n(\gamma)$. This contradicts the assumption that the oscillators synchronize for $K < K_{\text{critical}}$ from every initial condition $\theta(0) \in \overline{\text{Arc}}_n(\gamma)$. Thus, K_{critical} provides the exact threshold. For $K = K_{\text{critical}}$, we know from [5, 185] that phase-locked equilibria have a zero eigenvalue with a two-dimensional Jacobian block, and thus synchronization cannot occur. This instability via a two-dimensional Jordan block is also visible in (4.27) since (for $K = K_{\text{critical}}$) $D^+V(\theta(t))$ is increasing for $\theta(t) \in \text{Arc}_n(\gamma)$, $\gamma \in]\pi/2, \pi]$ until all oscillators change orientation, just as in the two-dimensional example in Subsection 2.3.2. This concludes the proof of the necessity (ii) \implies (i).

Sufficiency (i),(ii) \implies (iii): Assume that (i) and (ii) hold and exponential synchronization occurs. When formulating the Kuramoto model (1.2) in a rotating frame with frequency ω_{avg} , statement 3) implies exponential convergence of the frequencies $\dot{\theta}_i(t)$ to zero. Hence, for all $\theta(0) \in \text{Arc}_n(\gamma_{\text{max}})$ every phase $\theta_i(t)$ converges exponentially to a constant limit phase given by $\theta_{i,\text{sync}} \triangleq \lim_{t \rightarrow \infty} \theta_i(t) = \theta_i(0) + \int_0^\infty \dot{\theta}_i(\tau) d\tau$, which corresponds to an equilibrium of the Kuramoto model (1.2) in a rotating frame. Furthermore, statement 1) implies that these equilibria $(\theta_{1,\text{sync}}, \dots, \theta_{n,\text{sync}})$ are contained in $\overline{\text{Arc}}_n(\gamma_{\text{min}})$. Finally, these equilibria are stable (modulo symmetry) by Lemma 3.2.1. Hence, if conditions (i)-(ii) hold, then there exists a locally exponentially stable synchronized solution $[\theta_{\text{sync}}] \subset \overline{\text{Arc}}_n(\gamma_{\text{min}})$.

Necessity (iii) \implies (i),(ii): Conversely, assume that condition (i) does not hold, that is, $K \leq K_{\text{critical}} = \omega_{\text{max}} - \omega_{\text{min}}$. We prove the necessity of (iii) again by invoking a bipolar distribution of the natural frequencies. In this case, it is known that for $K = K_{\text{critical}} = \omega_{\text{max}} - \omega_{\text{min}}$ there exists a unique equilibrium (in a rotating frame with frequency ω_{avg}), and for $K < K_{\text{critical}}$ there exists no equilibrium [277, Section 4]. In the latter case, synchronization cannot occur. In the former case, the equilibrium configuration corresponds to the phases arranged in two groups (sorted according to the bipolar distribution) which are exactly $\pi/2$ apart, see Figure 4.2(a). Finally, note that such an equilibrium configuration is unstable, as shown by equality (4.27). We remark that the same conclusions can alternatively be drawn from the implicit conditions (4.17)-(4.18) for the critical coupling. This proves the necessity (iii) \implies (i),(ii). \square

We make the following remarks concerning Theorem 4.4.2. Besides establishing a tight condition for K_{critical} , Theorem 4.4.2 establishes some properties of the transient evolution of the Kuramoto dynamics (1.2) and a practical stability result. The multiplicative gap K_{critical}/K in the bound (4.24) determines the admissible initial and the guaranteed asymptotic arc invariance as well as the guaranteed asymptotic magnitude of the order parameter. In view of this result, the asymptotic synchronization behavior of the Kuramoto model (1.2) is best described by the control-theoretic terminology *practical phase synchronization*.

Notice that Theorem 4.4.2 fully generalizes the observations from the two-dimensional example in Subsection 2.3.2 to the n -dimensional case. Moreover, Theorem 4.4.2 reduces to the phase synchronization result in Theorem 2.4.2 for identical natural frequencies. We remark that similar synchronization conditions are reported in [55, 74, 116, 240], the contraction Lyapunov function (4.23) can be partially extended to second-order oscillators [57] for sufficiently small or sufficiently large inertiae, and the bound γ_{\min} on the asymptotic phase distances can be improved for particular pairs of oscillators, see [55, Theorem 5.2] for details.

The proof of Theorem 4.4.2 uses the bipolar distribution ω_{bip} as a worst-case instance to show that the bound (4.24) is also saturated. The recent analysis [56] shows that ω_{bip} is indeed the worst-case selection of natural frequencies: if there are more than three distinct natural frequencies, then the bound (4.24) is not saturated and only sufficient. To compare the bound (4.24) to the bounds presented in Section 4.3, we note from the proof of Theorem 4.4.2 that condition (4.24) can be equivalently stated as $K > (\omega_{\max} - \omega_{\min})/\sin(\gamma)$ and thus improves upon the sufficient bounds [58, 64, 74, 102, 139, 239]. In the simple case $n = 2$ analyzed in Subsection 2.3.2, the bound (4.24) is exact and also equals the necessary bound (4.9). In the infinite-dimensional case the bound (4.24) is tight with respect to the necessary bound for a bipolar distribution $\omega_i \in \{\omega_{\min}, \omega_{\max}\}$ in Theorem 4.2.3.

Note that condition (4.24) also guarantees synchronization for arbitrary distributions of ω_i supported in $[\omega_{\min}, \omega_{\max}]$, which can possibly be uncertain or even unknown. Additionally, Theorem 4.4.2 also guarantees a larger region of attraction $\theta(0) \in \text{Arc}_n(\gamma_{\max})$ for synchronization than [58, 64, 74, 102, 116, 139, 239]. Finally, we remark that the proof strategy via the contraction Lyapunov function (4.23) can be adapted to more general cases, for example, the conclusions of Theorem 4.4.2 can be extended to time-varying natural frequencies, see the illustration in Figure 4.5. We refer to the author’s article [83] for further details. The authors of [71, 102] come to a similar conclusion when analyzing the effects of time-varying frequencies via input-to-state stability arguments or in simulations.

4.4.3 Comparison and Statistical Analysis

Theorem 4.4.2 states the tight and explicit upper bound (4.24) on the critical coupling strength K_{critical} . Likewise, Lemma 4.3.3 states the tight and explicit lower bound (4.13) on K_{critical} . The exact critical coupling lies somewhere in-between and can be obtained from the implicit formulae (4.17)-(4.18). By collecting these results, we can state the following corollary, which improves upon the explicit bounds proposed by [281, Corollary 7].

Corollary 4.4.3 (Tight explicit bounds). *Consider the Kuramoto model (1.2) with $n \geq 2$ oscillators, natural frequencies $\omega \in \mathbf{1}_n^\perp \setminus \{\mathbf{0}_n\}$, and coupling strength*

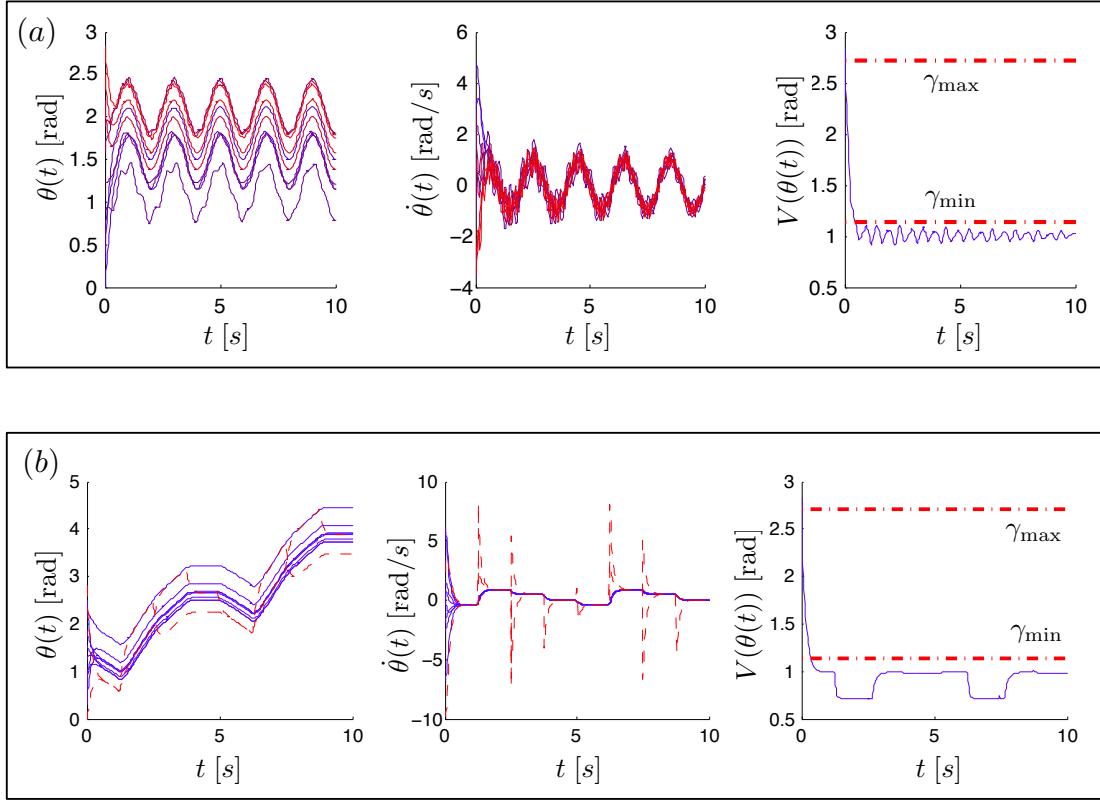


Figure 4.5: Kuramoto oscillators with time-varying natural frequencies. Simulation of a network of $n = 10$ Kuramoto oscillators (1.2) satisfying $K = 1.1 \cdot (\omega_{\max} - \omega_{\min})$. In panel (a), the natural frequencies $\omega_i : \mathbb{R}_{\geq 0} \rightarrow [\omega_{\min}, \omega_{\max}] = [0, 1]$ are smooth, bounded, and distinct sinusoidal functions. Each natural frequency $\omega_i(t)$ asymptotically converges to $\tilde{\omega}_i + \sin(\pi t)$ with constant and randomly chosen $\tilde{\omega}_i \in [0, 1]$. In panel (b), the natural frequencies $\omega_i(t)$ of oscillators 1 and 10 (displayed in red dashed lines) switch between constant values in $[\omega_{\min}, \omega_{\max}] = [0, 1]$. The simulations illustrate the phase cohesiveness of the angles $\theta(t)$ in $\text{Arc}_n(\gamma_{\min})$, the boundedness and convergence of the frequency variations (between consecutive switching instances) $\dot{\theta}(t) - \omega_{\text{avg}}(t)\mathbf{1}_n$, as well as the monotonicity of the Lyapunov function $V(\theta(t))$ in $\text{Arc}_n(\gamma)$ for $\gamma \in [\gamma_{\min}, \gamma_{\max}]$.

K. Compute the exact critical coupling K_{critical} according to (4.17)-(4.18). The explicit necessary condition (4.13) and sufficient condition (4.24) provide tight upper and lower bounds on the exact critical coupling K_{critical} , that is,

$$\frac{n \cdot (\omega_{\max} - \omega_{\min})}{2(\sin(\gamma) + (n-2)\sin(\gamma/2))} \leq K_{\text{critical}} \leq \omega_{\max} - \omega_{\min}, \quad (4.28)$$

where $\gamma \in [\pi/2, \pi]$ is defined in (4.12). Moreover, the lower bound is tight for $\omega = \omega_{\text{trip}} \triangleq \omega_0 \cdot (+1, -1, \mathbf{0}_{n-2})$, and the upper bound is tight for $\omega = \omega_{\text{bip}} \triangleq \omega_0 \cdot (-p \cdot \mathbf{1}_{n-p}, +(n-p) \cdot \mathbf{1}_p)$, where $\omega_0 \in \mathbb{R}$, $p \in \{1, \dots, n-1\}$, and both ω_{trip} and ω_{bip} are defined modulo index permutations.

Corollary 4.4.3 is the finite-dimensional counterpart to Theorem 4.2.3 and identifies bipolar and tripolar frequencies as the extreme choices for the resulting critical coupling K_{critical} . These two distributions of natural frequencies are illustrated in Figure 4.2(a) and 4.2(e). We remark that for natural frequencies sampled from a particular distribution $g(\omega)$ the critical quantity in Corollary 4.4.3, the support $\omega_{\max} - \omega_{\min}$, can be estimated by extreme value statistics, see [33] for details.

By Theorem 4.2.3, for infinite-dimensional models the uniform distribution $g_{\text{unif}}(\omega) = 1/2$ yields the smallest synchronization threshold $K_{\text{lock}} = 4\omega_0/\pi$ over all continuous, symmetric, and unimodal distributions $g(\omega)$ with bounded support $\omega \in [-\omega_0, +\omega_0]$. Hence, the uniform distribution is an interesting choice to compare the three conditions (4.13), (4.17)-(4.18), and (4.24) in a statistical

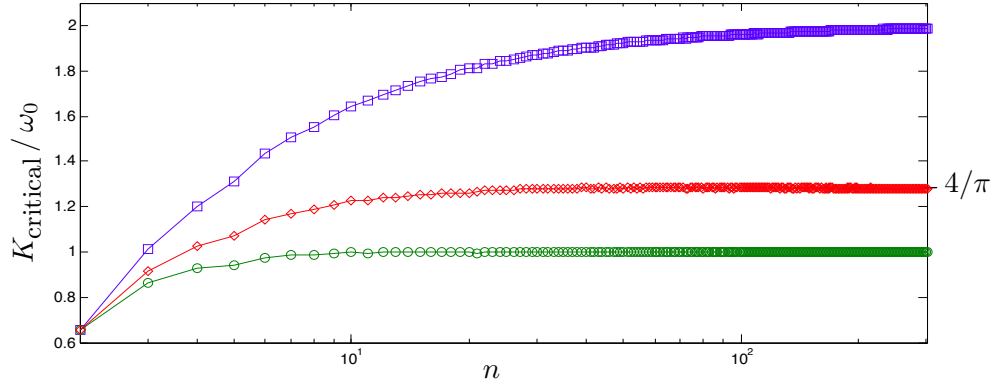


Figure 4.6: Statistical analysis of the critical coupling estimates. Statistical analysis of the necessary, tight, and explicit bound (4.13) (\diamond), the exact and implicit formulae (4.17)-(4.18) (\circ), and the sufficient, tight, and explicit bound (4.24) (\square) for $n \in [2, 300]$ oscillators, where the coupling gains for each n are averaged over 1000 samples of randomly uniformly generated frequencies.

analysis. Figure 4.6 reports our numerical findings. All three displayed conditions are identical for $n = 2$ oscillators. As n increases, the sufficient bound (4.24) converges to the width $\omega_{\max} - \omega_{\min} = 2\omega_0$ of the support of $g_{\text{unif}}(\omega)$, and the necessary bound (4.13) converges to half of that width. The exact value of K_{critical} given by (4.17)-(4.18) converges to $4(\omega_{\max} - \omega_{\min})/(2\pi) = 4\omega_0/\pi$ in agreement with condition (4.6) predicted for the continuum limit.

4.4.4 Frequency Synchronization of Multi-Rate Kuramoto Oscillators

In this section, we extend the results in Theorem 4.4.2 to the multi-rate Kuramoto model (3.2). As discussed in Subsection 3.1.1, the literature [2, 3, 57, 126,

127, 265, 266] on second-order Kuramoto oscillators reports partially controversial results on the inertial effects on synchronization. As a corollary of Theorem 4.4.2 together with the topological equivalence results in Theorems 3.3.1 and 3.3.3, we can show that frequency synchronization conditions for multi-rate Kuramoto oscillators (3.2) are indeed independent of the inertial coefficients:

Theorem 4.4.4 (Frequency Synchronization in the Multi-Rate Kuramoto Model).

Consider the multi-rate Kuramoto model (3.2) with $n \geq 2$ oscillators, natural frequencies $\omega \in \mathbf{1}_n^\perp$, coupling strength K , and positive inertial and damping coefficients $M_i > 0$ and $D_i > 0$, respectively. The following statements are equivalent:

- (i) *the coupling strength K is larger than a critical value, that is, $K > K_{\text{critical}} \triangleq \tilde{\omega}_{\max} - \tilde{\omega}_{\min}$; and*
- (ii) *there exists an arc length $\gamma_{\min} \in [0, \pi/2[$ such that each multi-rate Kuramoto model (3.2) satisfying $\tilde{\omega}_i = \omega_i - D_i \omega_{\text{sync}} \in [\tilde{\omega}_{\max}, \tilde{\omega}_{\min}]$, $i \in \{1, \dots, n\}$, has a locally exponentially stable synchronized solution with synchronization frequency ω_{sync} and arc invariant in $\overline{\text{Arc}}_n(\gamma_{\min})$.*

Moreover, in either of the two equivalent cases (i) and (ii), the ratio K_{critical}/K and the arc length $\gamma_{\min} \in [0, \pi/2[$ are related uniquely via $K_{\text{critical}}/K = \sin(\gamma_{\min})$.

Proof. By Theorem 3.3.3, a locally exponentially stable synchronized trajectory of the multi-rate Kuramoto model (3.2) exists if and only if there exists a lo-

cally exponentially stable equilibrium of the corresponding first-order Kuramoto model (1.2). By Theorem 4.4.2, the latter is true if and only if statement (i) holds. Moreover, Theorem 4.4.2 asserts that a synchronized solution is arc invariant in $\overline{\text{Arc}}_n(\gamma_{\min})$, where $\sin(\gamma_{\min}) = K_{\text{critical}}/K$. This concludes the proof. \square

The following remarks concerning Theorem 4.4.4 are in order. As noted in Theorem 3.3.3, the synchronization condition in statement (i) is independent of the inertial coefficients. Of course, the transient synchronization dynamics of multi-rate Kuramoto oscillators (3.2) strongly depend on the damping and the inertial coefficients, see the simulation in Figure 3.1. If the inertial coefficients are sufficiently small, then the contraction Lyapunov function (4.23) can be extended to second-order Kuramoto dynamics, which then show a similar transient behavior as the first-order Kuramoto dynamics (1.2), see [57] for further details.

Finally, as discussed in Section 4.4, the bound on K_{critical} presented in (i) is only sufficient and tight, and it may be conservative for a particular set of natural frequencies. Since the multi-rate Kuramoto model (3.2) is an instance of the parameterized system considered in Theorem 3.3.1, it has the same equilibria and the same stability properties as the Kuramoto model (1.2) (together with the frequency dynamics (4.19)). Hence, the implicit formulae (4.17)-(4.18) can also be applied to multi-rate Kuramoto oscillators (3.2) to find the exact critical coupling for a given set of natural frequencies.

4.5 Applications to Network-Reduced Power System Models

The author has adapted the analysis framework contained in this section to network-reduced power system models (3.16) and to the non-uniform Kuramoto model (3.17). Of course, the results have to be modified but the analysis methods can be applied nevertheless – provided that the network-reduced power system model features a complete coupling topology, such as the New England power grid illustrated in Figure 2.1. In fact, for most power networks the subgraph induced by the load buses \mathcal{V}_3 is connected, which implies that the coupling topology of the network-reduced model is complete [86, Theorem 3.4]. The singular perturbation approximation in Theorem 3.4.2 together with an adaption of the contraction-based proof of Theorem 4.4.2 lead to the following result [85, Theorem 2.4].

Theorem 4.5.1 (Synchronization in Network-Reduced Power Systems). *Consider the network-reduced power system model (3.16) and the non-uniform Kuramoto model (3.17) with a complete coupling graph, that is, $a_{ij} \geq 0$ for all distinct $i, j \in \{1, \dots, n\}$. Assume that the minimal lossless coupling of any oscillator to*

the network is larger than a critical value, that is,

$$\begin{aligned} \Gamma_{\min} &\triangleq n \min_{i \neq j} \left\{ \frac{a_{ij}}{D_i} \cos(\varphi_{ij}) \right\} \\ &> \Gamma_{\text{critical}} \triangleq \frac{1}{\cos(\varphi_{\max})} \left(\max_{i \neq j} \left| \frac{\omega_i}{D_i} - \frac{\omega_j}{D_j} \right| + 2 \max_{i \in \{1, \dots, n\}} \sum_{j=1}^n \frac{a_{ij}}{D_i} \sin(\varphi_{ij}) \right). \end{aligned} \quad (4.29)$$

Accordingly, define $\gamma_{\min} \in [0, \pi/2 - \varphi_{\max}[$ and $\gamma_{\max} \in]\pi/2, \pi]$ as unique solutions to the equations $\sin(\gamma_{\min}) = \sin(\gamma_{\max}) = \cos(\varphi_{\max}) \Gamma_{\text{critical}}/\Gamma_{\min}$.

For the non-uniform Kuramoto model,

- 1) **arc invariance:** the set $\overline{\text{Arc}}_n(\gamma)$ is positively invariant for all $\gamma \in [\gamma_{\min}, \gamma_{\max}]$, and each trajectory starting in $\text{Arc}_n(\gamma_{\max})$ asymptotically reaches $\overline{\text{Arc}}_n(\gamma_{\min})$;

and

- 2) **frequency synchronization:** for every $\theta(0) \in \Delta(\gamma_{\max})$, the frequencies $\dot{\theta}_i(t)$ synchronize exponentially to some frequency $\dot{\theta}_{\infty} \in [\dot{\theta}_{\min}(0), \dot{\theta}_{\max}(0)]$.

For the network-reduced power system model, for all $\theta(0) \in \text{Arc}_n(\gamma_{\max})$ and for all initial frequencies $\dot{\theta}(0)$,

- 3) **approximation errors:** there exists a constant $\epsilon^* > 0$ such that, if $\epsilon \triangleq M_{\max}/D_{\min} < \epsilon^*$, then the solution $(\theta(t), \dot{\theta}(t))$ of (3.16) exists for all $t \geq 0$, and it holds uniformly in t that

$$\begin{aligned} (\theta_i(t) - \theta_n(t)) &= (\bar{\theta}_i(t) - \bar{\theta}_n(t)) + \mathcal{O}(\epsilon), \quad \forall t \geq 0, \quad i \in \{1, \dots, n-1\}, \\ \dot{\theta}(t) &= h(\bar{\theta}(t)) + \mathcal{O}(\epsilon), \quad \forall t > 0, \end{aligned} \quad (4.30)$$

where $\bar{\theta}(t)$ is the solution to the non-uniform Kuramoto model (3.17) with initial condition $\bar{\theta}(0) = \theta(0)$ and $h(\theta)$ is defined in (3.22); and

- 4) **asymptotic approximation errors:** *there exists ϵ and φ_{\max} sufficiently small, such that the $\mathcal{O}(\epsilon)$ errors in equation (4.30) converge to zero as $t \rightarrow \infty$.*

The proof of can be found in the author's article [85] and will not be repeated here. We state the following remarks to Theorem 4.5.1:

Remark 4.5.2 (Physical interpretation and refinement of Theorem 4.5.1). *The right-hand side of condition (4.29) states the worst-case dissimilarity in natural frequencies (the difference in effective power inputs) and the worst-case lossy coupling of a generator to the network ($a_{ij} \sin(\varphi_{ij}) = E_i E_j \Re(-Y_{ij})$ is the transfer conductance), both of which are scaled with the rates D_i . The term $\cos(\varphi_{\max}) = \sin(\pi/2 - \varphi_{\max})$ corresponds to arc invariance in $\text{Arc}_n(\pi/2 - \varphi_{\max})$, which is necessary to apply Lemma 4.4.1. These negative effects have to be dominated by the left-hand side of (4.29), which is a lower bound for $\min_i \{ \sum_{j=1}^n (a_{ij} \cos(\varphi_{ij}) / D_i) \}$, the worst-case lossless coupling of a node to the network. The multiplicative gap $\Gamma_{\text{critical}} / \Gamma_{\text{min}}$ between the right- and the left-hand side in (4.29) can be understood as a robustness margin that additionally gives a practical stability result determining the admissible initial and the possible asymptotic lack of arc invariance.*

In summary, the conditions of Theorem 4.5.1 read as “the network connectivity has to dominate the network’s heterogeneity and the network’s losses.” In Theorem 4.5.1 we present the scalar synchronization condition (4.29), the estimate for the region of attraction $\text{Arc}_n(\gamma_{\max})$, and the ultimate phase cohesive set $\overline{\text{Arc}}_n(\gamma_{\min})$. In the derivations leading to Theorem 4.5.1 it is possible to trade off a tighter synchronization condition against a looser estimate of the region of attraction, or a single loose scalar condition against $n(n-1)/2$ tight pairwise conditions. These tradeoffs are explored in [81]. We remark that the coupling weights a_{ij} in condition (4.29) are not only the reduced power flows but reflect for uniform voltages E_i and phase shifts φ_{ij} also the effective resistance of the original (non-reduced) network topology [86]. Moreover, condition (4.29) indicates at which generator the damping torque has to be changed (for example, via local power system stabilizers) in order to meet the sufficient synchronization condition.

The network-reduced power system model (3.16) inherits the synchronization condition (4.29) in the (well-posed) relative coordinates $\theta_i - \theta_n$ and up to the approximation error (4.30) which is of order ϵ and eventually vanishes for ϵ and φ_{\max} sufficiently small. When specialized to the classic Kuramoto model (1.2), the sufficient condition (4.29) reduces to the sufficient and tight bound (4.24). \square

Chapter 5

Synchronization in Complex Oscillator Networks

The coupled oscillator model considered in this thesis is a variation of a well studied and still poorly understood spin glass model [245]:

Spin glasses: still complex after all these years?

Daniel Stein in *Decoherence and Entropy in Complex Systems* [256].

This chapter considers the first-order coupled oscillator model (3.1)

$$\dot{\theta}_i = \omega_i - \sum_{j=1}^n a_{ij} \sin(\theta_i - \theta_j), \quad \{1, \dots, n\}.$$

featuring de-synchronizing dissimilar natural frequencies $\omega \in \mathbf{1}_n^\perp$ and the synchronizing coupling through a graph $G(\mathcal{V}, \mathcal{E}, A)$ with a nontrivial topology. The network science and physics communities coined the term *complex* for such non-trivial topologies to distinguish them from long-range (that is, complete) and short-range (that is, lattice-type) interaction topologies. The interest of the control community in such complex oscillator networks has been sparked by the seminal arti-

cle [139] and the widespread scientific attention given to complex network studies [18, 31, 203, 259, 264], and consensus and its applications [37, 104, 180, 200, 221].

5.1 Introduction

5.1.1 Relevant Literature

The mechanical analog in Figure 1.1 and the formulation of the coupled oscillator model (3.1) as a forced gradient flow (3.5) clarifies the competition between the synchronization-enforcing coupling $a_{ij} \sin(\theta_i - \theta_j)$ and the synchronization-inhibiting dissimilar natural frequencies ω_i . For arbitrary network topologies and weights the equilibrium and potential landscape of the complex oscillator network (3.1) has been studied by different communities [16, 22, 179, 269]. We particularly recommend the article [16], where various surprising and counter-intuitive examples are reported. Loosely speaking, the oscillator network (3.1) achieves synchronization when the coupling dominates the dissimilarity in natural frequencies.

Various conditions have been proposed to quantify this trade-off for sparse graphs, both in theoretical studies as well as in power network applications. The coupling is typically quantified by the algebraic connectivity $\lambda_2(L)$ [18, 31, 85, 139, 193, 198, 215, 222, 299], the weighted nodal degree $\deg_i = \sum_{j=1}^n a_{ij}$ [40, 85, 86, 108, 153, 253, 298], or various metrics related to the notion of effective resistance

[86, 153, 298]. The dissimilarity among the natural frequencies is quantified either by absolute norms $\|\omega\|_p$ or by incremental norms¹ $\|B^T\omega\|_p$, for $p \in \mathbb{N}$. Here, we specifically consider the three incremental norms:

$$\begin{aligned}\|\omega\|_{\mathcal{E},\infty} &\triangleq \|B^T\omega\|_\infty = \max_{\{i,j\} \in \mathcal{E}} |\omega_i - \omega_j|, \\ \|\omega\|_{\mathcal{E},2} &\triangleq \|B^T\omega\|_2 = \left(\sum_{\{i,j\} \in \mathcal{E}} |\omega_i - \omega_j|^2 \right)^{1/2}, \\ \|\omega\|_{\mathcal{E}_{\text{cplt}},2} &\triangleq \|B_{\text{cplt}}^T\omega\|_2 = \frac{1}{2} \left(\sum_{i,j=1}^n |\omega_i - \omega_j|^2 \right)^{1/2},\end{aligned}$$

where the subscript *cplt* stands for the complete graph. With slight abuse of notation, we also adopt these incremental norms for angular differences. For example, for $\gamma \in [0, \pi[$, the incremental ∞ -norm ball $\{\theta \in \mathbb{T}^n \mid \|\theta\|_{\mathcal{E},\infty} \leq \gamma\}$ is identical to the phase cohesive set $\bar{\Delta}_G(\gamma)$. Some of the aforementioned conditions will be developed within this section.

As every review article on synchronization [3, 18, 31, 89, 258, 259], let us state here that the problem of finding sharp and provably correct synchronization conditions is not yet completely solved. Some of the proposed synchronization conditions for complex oscillator networks can be evaluated only numerically since they are state-dependent [298, 299] or arise from a non-trivial linearization process, such as the Master stability function formalism [18, 31, 193, 215]. In general, concise and accurate results are known only for specific topologies such as complete

¹More precisely, the incremental norms $\|B^T\omega\|_p$ are *seminorms* in \mathbb{R}^n and proper norms in the quotient space $\mathbf{1}_n^\perp$.

graphs discussed in the previous chapter, linear chains [262], highly symmetric ring graphs [40], acyclic graphs [75], and complete bipartite graphs [282] with uniform weights. For arbitrary coupling topologies, the literature contains only sufficient conditions [85, 139, 298, 299] as well as numerical and statistical investigations for large random networks indicating certain (for example, degree-dependent) scaling laws [108, 143, 192, 198, 222, 253]. Numerical studies indicate that all known and provably-correct synchronization conditions are conservative estimates on the threshold from incoherence to synchrony. Our recently-proposed condition [89] (see also Section 5.3) is provably correct for various extremal network topologies and weights, and is numerically accurate for a broad range of random networks; a complete analytic treatment is missing at this time. In this chapter, we present a set of provably correct synchronization conditions and analysis concepts.

5.1.2 Contributions and Organization

The remainder of this chapter is organized as follows:

Section 5.2: As summarized in Subsection 5.1.1, the quest for sharp and concise synchronization conditions is an important and outstanding problem emphasized in every review article on complex oscillator networks. The approaches known for phase synchronization in homogeneous oscillator networks or the contraction approach to frequency synchronization in heterogeneous Kuramoto os-

cillator networks do not generally extend to arbitrary network parameters and topologies, or do so only under extremely conservative conditions.

In this section, we present a set of necessary conditions (see Lemma 5.2.1) and a set of sufficient conditions for synchronization in the coupled oscillator model (3.1). The sufficient conditions are based on an analysis approach using two-norm-type metrics. In particular, Theorem 5.2.2 is based on a Lyapunov approach and results in a synchronization condition based on the algebraic connectivity. Additionally, the Lyapunov approach gives some insights into the transient dynamics of the oscillator network (3.1). Theorem 5.2.2 is based on a fixed-point approach and results in a sharper synchronization condition, which is also based on the algebraic connectivity. On the other hand, the stability result is only local. We conclude this section, by emphasizing the conservatism of these results. Even though, we present the best known – to the best of the author’s knowledge – conditions valid for arbitrary network parameters and topologies, they are fairly conservative.

Section 5.3: In this section, we improve upon the previously available necessary and sufficient conditions. Our approach is based on the fixed-point equations of the coupled oscillator model (3.1). We begin our analysis by stating a set of key insights in Lemma 5.3.1. The insights obtained from Lemma 5.3.1 emphasize the crucial role of cut-sets and cycles in the graph, they directly result in an optimal necessary condition (see Corollary 5.3.3), and they suggest the concise and scalar

synchronization condition $\|L^\dagger\omega\|_{\mathcal{E},\infty} < 1$. This condition relaxes the known conditions based on the algebraic connectivity, the effective resistance, and the nodal degree. For a complete and uniformly weighted graph, this condition reduces to the sufficient and tight condition (4.24) known for classic Kuramoto oscillators.

We prove that our proposed condition guarantees the existence of a locally exponentially stable synchronization manifold for the sparsest (acyclic) and densest (homogeneous) network topologies, for the best (phase synchronizing) and the worst (cut-set inducing) network parameters (see Theorem 5.3.5), for cycles with symmetric parameters or of length strictly less than five (see Theorem 5.3.7), and one-connected combinations of these networks (see Corollary 5.3.8). In all of these cases, our condition is either necessary and sufficient or at least sufficient and tight. Furthermore, by extensive Monte Carlo simulation studies, we establish the statistical correctness of our condition for a set of nominal random network topologies and parameters. As a negative result, we show the existence of possibly-thin sets of topologies and parameters for which our condition is not sufficiently tight.

Section 5.4: In this section, we demonstrate the applicability of the synchronization condition developed in Section 5.3 to complex and large-scale power network examples. In Subsection 5.4.1, we show how the proposed condition is connected to the well known DC power flow approximation, and how it can be effectively evaluated for large sparse networks by solving an associated set of

sparse and linear equations. We validate the predictive power and high accuracy of our condition for the IEEE power system test cases 14, RTS 24, 30, New England 39, 57, RTS 96, 118, 300, the 9 bus system by Chow, and the Polish 2383 bus system. In Subsection 5.4.2, we demonstrate the utility of our proposed synchronization condition for monitoring and contingency screening applications. We study the RTS 96 power network model under two severe contingencies and demonstrate that our condition accurately predicts a limit-induced bifurcation. Finally, in Subsection 5.4.3 we briefly outline further applications of our analysis and the proposed synchronization conditions.

5.2 Some Necessary or Sufficient Conditions

In this section, we present a set of necessary and a set of sufficient conditions for synchronization in the coupled oscillator model (3.1).

5.2.1 Absolute and Incremental Boundedness

We start our investigation from the basic observation that the sinusoidal interaction terms in equation (3.1) are upper bounded by the nodal degree $\deg_i = \sum_{j=1}^n a_{ij}$ of each oscillator. Hence, the natural frequencies ω have to satisfy certain bounds, relative to the nodal degree such that synchronized solutions exist.

Lemma 5.2.1 (Necessary sync condition). *Consider the coupled oscillator model (3.1) with graph $G(\mathcal{V}, \mathcal{E}, A)$ and natural frequencies $\omega \in \mathbf{1}_n^\perp$. If there is a synchronized solution $\theta \in \bar{\Delta}_G(\gamma)$ for some $\gamma \in [0, \pi/2]$, then the following conditions hold:*

1) **Absolute bound:** *For each node $i \in \{1, \dots, n\}$,*

$$\deg_i \sin(\gamma) \geq |\omega_i|; \quad (5.1)$$

2) **Incremental bound:** *For distinct $i, j \in \{1, \dots, n\}$,*

$$(\deg_i + \deg_j) \sin(\gamma) \geq |\omega_i - \omega_j|. \quad (5.2)$$

Lemma 5.2.1 follows from the fact that synchronized solutions must satisfy $\dot{\theta}_i = 0$ and $\dot{\theta}_i = \dot{\theta}_j$ for all $i, j \in \{1, \dots, n\}$, see [89, Lemma 3] for a proof along the lines of the proof of Lemma 4.3.2. Lemma 5.2.1 has long been known in the power systems community [269] since it defines the maximal nodal power injection $|\omega_i|$ in relation to the line capacities given by \deg_i . The necessary conditions (5.1) and (5.2) are conservative since they can be attained only if all angular distances $|\theta_i - \theta_k|$ and $|\theta_j - \theta_k|$ take the value γ , which is generally not possible. In Corollary 5.3.3, we show how to improve upon these necessary conditions.

5.2.2 Sufficient Synchronization Conditions

To the best of the authors' knowledge, the conditions (5.1)-(5.2) in Lemma 5.2.1 are the best known explicit necessary conditions for the existence of equilibria for

arbitrary topologies and weights. In what follows, we focus on sufficient conditions guaranteeing frequency synchronization and we restrict ourselves to phase cohesive synchronous solutions within the set $\Delta_G(\pi/2)$. There are three reasons for this choice. First, as discussed in Subsections 3.2.2 and 4.4.1, the equilibria in $\Delta_G(\pi/2)$ are exponentially stable, and the forward invariance of the set $\Delta_G(\pi/2)$ leads to stable synchronization by incremental stability or frequency dynamics arguments. Second, from a pragmatic point of view, there are few analysis results and conditions for equilibria outside $\Delta_G(\pi/2)$, with the treatment of (directed) ring graphs in [118, 227] being a notable exception. Third and finally, only equilibria in $\Delta_G(\pi/2)$ are of interest in power network applications.

The approaches to phase synchronization (in Theorems 2.4.2 and 3.3.4) and to frequency synchronization in complete graphs (in Chapter 4) are generally not applicable to dissimilar natural frequencies and sparse coupling graphs, or are so only under very conservative conditions. For example, in the presence of dissimilar natural frequencies $\omega \in \mathbf{1}_n^\perp$, a Lyapunov analysis of the forced gradient system (3.5) via the trigonometric potential $U(\theta)$ (as defined in (3.3)) is very involved since the level sets of $U(\theta)$ are hard to characterize. Likewise, the Lyapunov analysis based on the contraction Lyapunov function (4.23) inherently requires arc-invariance of *all* angles, and does not easily extend to arbitrary topologies. One quadratic Lyapunov function advocated by [58, 139] for classic Kuramoto

oscillators (1.2) is $W : \text{Arc}_n(\pi) \rightarrow \mathbb{R}$ defined by

$$W(\theta) = \frac{1}{4} \sum_{i,j=1}^n |\theta_i - \theta_j|^2 = \frac{1}{2} \|\theta\|_{\mathcal{E}_{\text{cpl},2}}^2. \quad (5.3)$$

This Lyapunov function is useful to analyze the more general oscillator network (3.1), and yields the following result.

Theorem 5.2.2 (Practical phase synchronization in sparse graphs I). *Consider the coupled oscillator model (3.1) with a connected graph $G(\mathcal{V}, \mathcal{E}, A)$ and frequencies $\omega \in \mathbf{1}_n^\perp$. There exists a locally exponentially stable equilibrium manifold $[\theta^*] \subset \Delta_G(\pi/2)$ if the algebraic connectivity is larger than a critical value, that is,*

$$\lambda_2(L) > \lambda_{\text{critical}} \triangleq \|\omega\|_{\mathcal{E}_{\text{cpl},2}}. \quad (5.4)$$

Moreover, if condition (5.4) holds, then the coupled oscillator model (3.1) achieves practical phase synchronization in the following sense. Given $\gamma_{\max} \in]\pi/2, \pi]$ and $\gamma_{\min} \in [0, \pi/2[$ as unique solutions to $(\pi/2) \cdot \text{sinc}(\gamma_{\max}) = \sin(\gamma_{\min}) = \lambda_{\text{critical}}/\lambda_2(L)$, the set $\{\theta \in \text{Arc}_n(\pi) \mid \|\theta\|_{\mathcal{E}_{\text{cpl},2}}^2 \leq \gamma\} \subseteq \bar{\Delta}_G(\gamma)$ is positively invariant for all $\gamma \in [\gamma_{\min}, \gamma_{\max}]$, and each trajectory starting in $\{\theta \in \text{Arc}_n(\pi) \mid \|\theta\|_{\mathcal{E}_{\text{cpl},2}}^2 < \gamma_{\max}\}$ asymptotically reaches $\{\theta \in \text{Arc}_n(\pi) \mid \|\theta\|_{\mathcal{E}_{\text{cpl},2}}^2 \leq \gamma_{\min}\}$.

The analysis leading to Theorem 5.2.2 is similar to the proof of Theorem 4.4.2: the Lyapunov function (5.3) is used to guarantee the ultimate boundedness of the phases in $\{\theta \in \text{Arc}_n(\pi) \mid \|\theta\|_{\mathcal{E}_{\text{cpl},2}} \leq \gamma_{\min}\} \subset \bar{\Delta}_G(\gamma_{\min})$, and the Jacobian

arguments in Lemma 4.4.1 guarantee frequency synchronization. We remark that the following proof can be extended to non-uniform Kuramoto oscillators (3.17) with multiple rates and phase shifts, see [85, Theorem 4.4] for details.

Proof of Theorem 5.2.2. Assume that $\theta(0) \in \overline{\text{Arc}_n(\rho)}$ for $\rho \in [0, \pi[$. Recall that the angular differences are well defined for θ in the open semi-circle $\text{Arc}_n(\pi)$, and define the vector of *all* phase differences $\delta \triangleq B_{\text{cplt}}^T \theta = (\theta_2 - \theta_1, \dots) \in [-\pi, +\pi]^{n(n-1)/2}$, where $B_{\text{cplt}} \in \mathbb{R}^{n \times (n(n-1)/2)}$ is the incidence matrix of the complete graph. By taking the derivative $d/dt \delta(t)$ the phase differences satisfy

$$\begin{aligned} \dot{\delta} &= B_{\text{cplt}}^T \omega - B_{\text{cplt}}^T B \text{diag}(\{a_{ij}\}_{i,j \in \mathcal{E}}) \mathbf{sin}(B^T \theta) \\ &= B_{\text{cplt}}^T \omega - B_{\text{cplt}}^T B_{\text{cplt}} \text{diag}(\{a_{ij}\}_{i,j \in \{1, \dots, n\}, i < j}) \mathbf{sin}(\delta), \end{aligned} \quad (5.5)$$

where $\mathbf{sin}(x) = (\sin(x_1), \dots, \sin(x_n))$ for a vector $x \in \mathbb{R}^n$. Notice that for $\theta(0) \in \text{Arc}_n(\pi)$ the δ -dynamics (5.5) are well-defined for an open interval of time. In the following, we will show that the set $\{\delta \in \mathbb{R}^n : \|\delta\|_2 < \gamma_{\max}\}$ is positively invariant under condition (5.4). As a consequence, the set $\{\delta \in \mathbb{R}^n : \|\delta\|_\infty < \gamma_{\max} \leq \pi\}$ is positively invariant as well, and the δ -coordinates are well defined for all $t \geq 0$.

The Lyapunov function (5.3) reads in δ -coordinates as $W(\delta) = \frac{1}{2} \|\delta\|^2$, and its derivative along trajectories of (5.5) is given by

$$\begin{aligned} \dot{W}(\delta) &= \delta^T B_{\text{cplt}}^T \omega - \delta^T B_{\text{cplt}}^T B_{\text{cplt}} \text{diag}(\{a_{ij}\}_{i,j \in \{1, \dots, n\}, i < j}) \mathbf{sin}(\delta) \\ &= \delta^T B_{\text{cplt}}^T \omega - n \delta^T \text{diag}(\{a_{ij}\}_{i,j \in \{1, \dots, n\}, i < j}) \mathbf{sin}(\delta), \end{aligned} \quad (5.6)$$

where the second equality follows from the identity

$$\delta^T B_{\text{cpl}}^T B_{\text{cpl}} = \theta^T B_{\text{cpl}} B_{\text{cpl}}^T B_{\text{cpl}} = \theta^T (nI_n - \mathbf{1}_{n \times n}) B_{\text{cpl}} = n\theta^T B_{\text{cpl}} = n\delta.$$

For $\|\delta_2\| \leq \rho$, $\rho \in [0, \pi[$, consider the following inequalities

$$\begin{aligned} n \delta^T \text{diag}(\{a_{ij}\}_{i < j}) \mathbf{sin}(\delta) &= n (B_{\text{cpl}}^T \theta)^T \text{diag}(\{a_{ij} \text{sinc}(\theta_i - \theta_j)\}_{i < j}) (B_{\text{cpl}}^T \theta) \\ &\geq n \text{sinc}(\rho) (B_{\text{cpl}}^T \theta)^T \text{diag}(\{a_{ij}\}_{i < j}) (B_{\text{cpl}}^T \theta) \\ &\geq \lambda_2(L) \text{sinc}(\rho) \|B_{\text{cpl}}^T \theta\|_2^2 = \lambda_2(L) \text{sinc}(\rho) \|\delta\|_2^2, \end{aligned}$$

where the last inequality follows from [85, Lemma 4.7]. Hence, the derivative (5.6) of $W(\delta)$ can be further upper-bounded as

$$\dot{W}(\delta) \leq \delta^T B_{\text{cpl}}^T \omega - \lambda_2(L) \text{sinc}(\rho) \|\delta\|_2^2. \quad (5.7)$$

In the following we regard $B_{\text{cpl}}^T \omega$ as external disturbance affecting the otherwise stable δ -dynamics (5.5) and apply ultimate boundedness arguments [146]. Note that the right-hand side of (5.7) is strictly negative for

$$\|\delta\|_2 > \mu_c \triangleq \frac{\|B_{\text{cpl}}^T \omega\|_2}{\lambda_2(L) \text{sinc}(\rho)} = \frac{\lambda_{\text{critical}}}{\lambda_2(L) \text{sinc}(\rho)}.$$

Pick $\epsilon \in]0, 1[$. If $\rho \geq \|\delta\|_2 \geq \mu_c/\epsilon$, then the right-hand side of (5.7) is upper-bounded by

$$\dot{W}(\delta) \leq -(1 - \epsilon) \cdot \lambda_2(L) \text{sinc}(\rho) W(\delta).$$

Now choose μ such that $\rho > \mu > \mu_c$ and let $\epsilon = \mu_c/\mu \in]0, 1[$. By standard ultimate boundedness arguments [146, Theorem 4.18], for $\|\delta(0)\|_2 \leq \rho$, there is

$T \geq 0$ such that $\|\delta(t)\|_2$ is exponentially decaying for $t \in [0, T]$ and $\|\delta(t)\|_2 \leq \mu$ for all $t \geq T$. For the choice $\mu = \gamma$ with $\gamma \in [0, \pi/2[$, the condition $\mu > \mu_c$ reduces to

$$\gamma \operatorname{sinc}(\rho) > \lambda_{\text{critical}}/\lambda_2(L). \quad (5.8)$$

Now, we perform a final analysis of the bound (5.8). The left-hand side of (5.8) is an increasing function of γ and a decreasing function of ρ . Therefore, there exists some (ρ, γ) in the convex set $\Lambda \triangleq \{(\rho, \gamma) : \rho \in [0, \pi[, \gamma \in [0, \pi/2[, \rho > \gamma\}$ satisfying equation (5.8) if and only if the inequality (5.8) is true at $\rho = \gamma = \pi/2$, where the left-hand side of (5.8) achieves its supremum in Λ . The latter condition is equivalent to inequality (5.4). Additionally, if these two equivalent statements are true, then there is an open set of points in Λ satisfying (5.8), which is bounded by the unique curve that satisfies inequality (5.8) with the equality sign, namely $f(\rho, \gamma) = 0$, where $f : \Lambda \rightarrow \mathbb{R}$, $f(\rho, \gamma) = \gamma \operatorname{sinc}(\rho) - \lambda_{\text{critical}}/\lambda_2(L)$. Consequently, for every $(\rho, \gamma) \in \{(\rho, \gamma) \in \Lambda : f(\rho, \gamma) > 0\}$, it follows for $\|\delta(0)\|_2 \leq \rho$ that there is $T \geq 0$ such that $\|\delta(t)\|_2 \leq \gamma$ for all $t \geq T$. The supremum value for ρ is given by $\rho_{\max} \in]\pi/2, \pi]$ solving the equation $f(\rho_{\max}, \pi/2) = 0$ and the infimum value of γ by $\gamma_{\min} \in [0, \pi/2[$ solving the equation $f(\gamma_{\min}, \gamma_{\min}) = 0$.

Hence, for $\|B_{\text{cplt}}^T \theta(0)\|_2 \leq \rho_{\max}$ and $\theta(0) \in \overline{\text{Arc}}_n(\rho_{\max})$, there is $T \geq 0$ such that $\|B_{\text{cplt}}^T \theta(t)\|_\infty \leq \|B_{\text{cplt}}^T \theta(t)\|_2 \leq \gamma_{\min} < \pi/2$ for all $t \geq T$, which proves the claimed statement on practical phase synchronization.² Since $\theta(t) \in \bar{\Delta}_G(\gamma_{\min})$ for $t \geq T$,

²In the statement of Theorem 5.2.2, we replaced ρ_{\max} by γ_{\max} .

exponential frequency synchronization follows from Lemma 4.4.1. Exponential frequency synchronization implies convergence of the phases, and boundedness of the phase differences in a subset of $\bar{\Delta}_G(\gamma_{\min})$ implies convergence of the phases to a locally exponentially stable synchronization manifold by Lemma 3.2.1. \square

For classic Kuramoto oscillators (1.2), the key condition (5.4) reduces to $K > \|\omega\|_{\mathcal{E}_{\text{cpt}},2}$. Clearly, this condition is more conservative than the tight bound (4.24) which reads $K > \|\omega\|_{\mathcal{E},\infty} = \omega_{\max} - \omega_{\min}$. One reason for this conservatism is that condition (5.4) guarantees that the two-norm of the vector of all phase differences $|\theta_i - \theta_j|$ is bounded. However, by Lemma 3.2.1, we know that bounded phase differences $|\theta_i - \theta_j|$ *only* for edges of the graph $\{i, j\} \in \mathcal{E}$ are sufficient to establish the existence of a locally exponentially stable synchronized solution.

In what follows, we adopt a fixed-point approach to study the equilibrium equations of the coupled oscillator model (3.1). In matrix notation, these equilibrium equations read as

$$\omega = B\mathcal{A}\sin(B^T\theta), \quad (5.9)$$

where $\mathcal{A} = \text{diag}(\{a_{ij}\}_{\{i,j\} \in \mathcal{E}})$ is the diagonal matrix of weights. We next follow the ingenious analysis of (5.9) suggested in [139, Section IIV.B]. For the sake of a streamlined presentation, we treat the angles θ as vectors in $\mathbf{1}_n^\perp$. Recall the state-dependent weights $c_{ij}(\theta) = a_{ij} \text{sinc}(\theta_i - \theta_j)$ from the consensus formulation (2.19), and define the state-dependent Laplacian $\mathcal{L}(B^T\theta) = B \text{diag}(\{c_{ij}(\theta)\}_{\{i,j\} \in \mathcal{E}})B^T$.

Hence, equations (5.9) can be rewritten compactly as $\omega = \mathcal{L}(B^T\theta)\theta$. Since $\omega \in \mathbf{1}_n^\perp$ (without loss of generality) and $\mathcal{L}(B^T\theta)^\dagger \cdot \mathcal{L}(B^T\theta) = I_n - \frac{1}{n}\mathbf{1}_{n \times n}$, we arrive at

$$\theta = \mathcal{L}(B^T\theta)^\dagger \omega. \quad (5.10)$$

The following result is obtained by applying to equation (5.10) a fixed point theorem in the incremental two norm $\|\cdot\|_{\mathcal{E},2}$. It has originally been presented by the author [84, Theorem 4.7], and the proof strategy is inspired by [139].

Theorem 5.2.3 (Practical phase synchronization in sparse graphs II). *Consider the coupled oscillator model (3.1) with a connected graph $G(\mathcal{V}, \mathcal{E}, A)$ and frequencies $\omega \in \mathbf{1}_n^\perp$. There exists a locally exponentially stable equilibrium manifold $[\theta^*] \subset \Delta_G(\pi/2)$ if the algebraic connectivity is larger than a critical value, that is,*

$$\lambda_2(L) > \lambda_{\text{critical}} \triangleq \|\omega\|_{\mathcal{E},2}. \quad (5.11)$$

Moreover, if condition (5.11) holds, then $[\theta^*]$ is phase cohesive in the following sense: $[\theta^*] \subset \{\theta \in \mathbb{T}^n \mid \|\theta\|_{\mathcal{E},2} \leq \gamma_{\min}\} \subseteq \bar{\Delta}_G(\gamma_{\min})$, where $\gamma_{\min} \in [0, \pi/2[$ satisfies $\sin(\gamma_{\min}) = \lambda_{\text{critical}}/\lambda_2(L)$.

Proof. By Lemma 3.2.1, existence of an equilibrium $\theta \in \bar{\Delta}_G(\gamma)$ implies local exponentially stability of the synchronization manifold $[\theta] \subset \bar{\Delta}_G(\gamma)$, $\gamma \in [0, \pi/2[$.

A multiplication of the fixed-point equations (5.10) from the left by B^T yields

$$B^T \mathcal{L}(B^T\theta)^\dagger \omega = B^T \theta. \quad (5.12)$$

Note that the left-hand side of equation (5.12) is a continuous³ function of $\theta \in \bar{\Delta}_G(\gamma)$. Consider the formal substitution $x = B^T\theta$, the compact and convex set $\mathcal{S}_\infty(\gamma) = \{x \in B^T\mathbb{R}^n : \|x\|_\infty \leq \gamma\}$, and the continuous map $f : \mathcal{S}_\infty(\gamma) \rightarrow \mathbb{R}$ given by $f(x) = B^T\mathcal{L}(x)^\dagger\omega$. Then equation (5.12) reads as $f(x) = x$, and we can invoke *Brouwer's Fixed Point Theorem* which states that every continuous map from a compact and convex set to itself has a fixed point, see [255, Section 7, Corollary 8].

Since the analysis of the map f in the ∞ -norm is very hard in the general case, we resort to a 2-norm analysis and restrict ourselves to the set $\mathcal{S}_2(\gamma) = \{x \in B^T\mathbb{R}^n : \|x\|_2 \leq \gamma\} \subseteq \mathcal{S}_\infty(\gamma)$. By Brouwer's Fixed Point Theorem, there exists a solution $x \in \mathcal{S}_2(\gamma)$ to the equations $x = f(x)$ if and only if $\|f(x)\|_2 \leq \gamma$ for all $x \in \mathcal{S}_2(\gamma)$, or equivalently if and only if

$$\max_{x \in \mathcal{S}_2(\gamma)} \|B^T\mathcal{L}(x)^\dagger\omega\|_2 \leq \gamma. \quad (5.13)$$

In the following we show that (5.11) is a sufficient condition for inequality (5.13).

First, we establish some identities. For a Laplacian matrix L , we obtain $L^\dagger = V\Lambda V^T$, where $\Lambda = \text{diag}(0, \{1/\lambda_i(L)\}_{i=2,\dots,n})$ is the diagonal matrix of zero and inverse positive eigenvalues of L , and $V \in \mathbb{R}^{n \times n}$ is an associated orthonormal matrix of eigenvectors. It follows that $V \text{diag}(0, 1, \dots, 1) V^T = I_n - (1/n)\mathbf{1}_{n \times n}$.

By means of these identities, the left-hand side of (5.13) can be simplified and

³The continuity can be established when re-writing equations (5.12) (or the equations $\omega = \mathcal{L}(B^T\theta)\theta$) in the quotient space $\mathbf{1}_n^\perp$, where $\mathcal{L}(\theta)$ is nonsingular, and using the fact that the inverse of a matrix is a continuous function of its elements.

upper-bounded for all $x \in \mathcal{S}_2(\gamma)$ as follows:

$$\begin{aligned}
 \|B^T \mathcal{L}(x)^\dagger \omega\|_2 &= \left\| B^T V(x) \operatorname{diag} \left(0, \frac{1}{\lambda_2(\mathcal{L}(x))}, \dots, \frac{1}{\lambda_n(\mathcal{L}(x))} \right) V(x)^T \omega \right\|_2 \\
 &\leq \frac{1}{\lambda_2(\mathcal{L}(x))} \cdot \|B^T V(x) \operatorname{diag} (0, 1, \dots, 1) V(x)^T \omega\|_2 \\
 &= (1/\lambda_2(\mathcal{L}(x))) \cdot \|B^T \omega\|_2, \tag{5.14}
 \end{aligned}$$

where the inequality arises from the transformation $y = V(x)^T \omega$ and the inequality $\|B^T V(x) \Lambda y\|_2^2 = (\Lambda y)^T (V(x)^T B B^T V(x)) (\Lambda y) \leq y^T (V(x)^T B B^T V(x)) y \cdot (1/\lambda_2(\mathcal{L}(x))) = (1/\lambda_2(\mathcal{L}(x))) \|B^T V(x) y\|_2^2$. Thus, by inequality (5.14), a sufficient condition for inequality (5.13) to hold can be derived as follows:

$$\begin{aligned}
 \max_{x \in \mathcal{S}_2(\gamma)} \|B^T \mathcal{L}(x)^\dagger \omega\|_2 &\leq \|B^T \omega\|_2 \max_{x \in \mathcal{S}_2(\gamma)} (1/\lambda_2(\mathcal{L}(x))) \\
 &\leq \|B^T \omega\|_2 \max_{x \in \{x \in \mathbb{R}^{|\mathcal{E}|} : \|x\|_\infty \leq \gamma\}} (1/\lambda_2(\mathcal{L}(x))) = \|B^T \omega\|_2 / (\lambda_2(L) \cdot \operatorname{sinc}(\gamma)) \stackrel{!}{\leq} \gamma,
 \end{aligned}$$

where we enlarged the domain $\mathcal{S}_2(\gamma)$ to $\{x \in \mathbb{R}^{|\mathcal{E}|} : \|x\|_\infty \leq \gamma\}$ and used⁴ $\lambda_2(\mathcal{L}(x)) \geq \lambda_2(L) \cdot \operatorname{sinc}(\gamma)$ for $\|x\|_\infty \leq \gamma$. In summary, there is a locally exponentially stable synchronization manifold $[\theta] \subset \{\theta \in \mathbb{T}^n : \|B^T \theta\|_2 \leq \gamma\} \subseteq \bar{\Delta}_G(\gamma)$ if

$$\lambda_2(L) \operatorname{sinc}(\gamma) \geq \|B^T \omega\|_2. \tag{5.15}$$

Since the left-hand side of (5.15) is a concave function of $\gamma \in [0, \pi/2[$, there exists an open set of $\gamma \in [0, \pi/2[$ satisfying equation (5.15) if and only if equation

⁴This fact follows from $\lambda_2(\mathcal{L}(x)) = \min_{v \in \mathbf{1}_n, \|v\|_2=1} (v^T B) \operatorname{diag}(\{a_{ij} \operatorname{sinc}(x)\}_{\{i,j\} \in \mathcal{E}}) (B^T v) \geq \operatorname{sinc}(\gamma) \cdot (v^T B) \operatorname{diag}(\{a_{ij}\}_{\{i,j\} \in \mathcal{E}}) (B^T v) = \operatorname{sinc}(\gamma) \lambda_2(L)$ for $\|x\|_\infty \leq \gamma$.

(5.15) is true with the strict equality sign at $\gamma^* = \pi/2$, which corresponds to condition (5.11). Additionally, if these two equivalent statements are true, then there exists a unique $\gamma_{\min} \in [0, \pi/2[$ that satisfies equation (4.26) with the equality sign, namely $\sin(\gamma_{\min}) = \|B^T \omega\|_2 / \lambda_2(L)$. This concludes the proof. \square

Clearly, condition (5.11) is sharper than condition (5.4), but the stability result is only local. The synchronization condition (5.11) is the sharpest sufficient condition for general graphs known to the authors, but it is still a conservative estimate for most network topologies and weights. Indeed, the necessary condition (5.2) and sufficient condition (5.11) are separated by a tremendous gap for $n > 2$ oscillators. The reasons for this conservatism are manifold. First, condition (5.11) guarantees the bound $\|\theta^*\|_{\mathcal{E},2} \leq \arcsin(\lambda_{\text{critical}}/\lambda_2(L))$. This incremental two-norm bound is a very strong property, and only the incremental ∞ -norm $\|\theta\|_{\mathcal{E},\infty}$ needs to be bounded to conclude synchronization by the Jacobian arguments in Lemma 3.2.1. Second, the derivation of the conditions (5.1), (5.2), (5.4), and (5.11) involves conservative bounding of the trigonometric nonlinearities and network interactions. Third, Lemma 3.2.1, Theorem 2.4.2, and Theorem 4.4.2 hint at the incremental ∞ -norm as a natural metric, whereas an analysis using two-norm type metrics inherently leads to more conservative results.

5.3 Towards an Exact Synchronization Condition

An analysis of the fixed-point equations (5.10) using two-norm bounding of $\|\mathcal{L}(B^T\theta)^\dagger\omega\|_{\mathcal{E},2}$ results in the condition $\|\omega\|_{\mathcal{E},2}/\lambda_2(L) < 1$ in Theorem 5.2.3. As discussed above, an ∞ -norm analysis of equations (5.10) and the term $\|\mathcal{L}(B^T\theta)^\dagger\omega\|_{\mathcal{E},\infty}$ should likely yield a less conservative condition, possibly of the form $\|L^\dagger\omega\|_{\mathcal{E},\infty} < 1$. Indeed, in this section, we derive the condition $\|L^\dagger\omega\|_{\mathcal{E},\infty} < 1$ for particular networks as well as rand network models.

5.3.1 Norm and Cycle Constraints

By formally replacing each term $\sin(\theta_i - \theta_j)$ in the fixed-point equations (5.9) by an auxiliary scalar variable ψ_{ij} we arrive at

$$\omega = B\mathcal{A}\psi, \quad (5.16)$$

$$\psi = \mathbf{sin}(B^T\theta), \quad (5.17)$$

where $\psi \in \mathbb{R}^{|\mathcal{E}|}$ is a vector with elements ψ_{ij} . We refer to equations (5.16) as the *auxiliary-fixed point equation*. It can be easily verified that every solution of the auxiliary fixed-point equations (5.16) is of the form

$$\psi = B^T L^\dagger \omega + \psi_{\text{hom}}, \quad (5.18)$$

where the homogeneous solution $\psi_{\text{hom}} \in \mathbb{R}^{|\mathcal{E}|}$ satisfies $\mathcal{A}\psi_{\text{hom}} \in \text{Ker}(B)$. Since the orthogonal vector spaces $\text{Ker}(B)$ and $\text{Ker}(B)^\perp = \text{Im}(B^T)$ are spanned by

vectors associated to cycles and cut-sets in the graph, see [29, 30], we arrive at a graph-theoretic characterization of the fixed points.

To state the following result, recall that $\arcsin:]-1, 1[\rightarrow]-\pi/2, \pi/2[$ is the unique inverse of the sine function in $]-\pi/2, \pi/2[$ (modulo 2π), that is, the roots of $x = \sin(\theta)$ for $x \in]-1, 1[$, are given by $\theta \in \{\arcsin(x) + k \cdot 2\pi, \pi - \arcsin(x) + k \cdot 2\pi\}$, where $k \in \mathbb{Z}$. We also define $\mathbf{arcsin}(x) = (\arcsin(x_1), \dots, \arcsin(x_n))$ for $x \in]-1, 1[^n \subset \mathbb{R}^n$, and the vector-valued modulo operation that identifies $x, y \in \mathbb{R}^n$ via $x = y \pmod{2\pi}$ if $x_i = y_i + k_i \cdot 2\pi$ for some $k_i \in \mathbb{Z}$ and for all $i \in \{1, \dots, n\}$.

Lemma 5.3.1 (Properties of the fixed-point equations). *Consider the coupled oscillator model (3.1) with graph $G(\mathcal{V}, \mathcal{E}, A)$ and $\omega \in \mathbf{1}_n^\perp$, its fixed-point equations (5.9), and the auxiliary fixed-point equations (5.16). The following statements hold:*

1) **Exact solution:** *Every solution of the auxiliary fixed-point equations (5.16)*

is of the form

$$\psi = B^T L^\dagger \omega + \psi_{\text{hom}}, \quad (5.19)$$

where the homogeneous solution $\psi_{\text{hom}} \in \mathbb{R}^{|\mathcal{E}|}$ satisfies $\mathcal{A} \psi_{\text{hom}} \in \text{Ker}(B)$.

2) **Exact synchronization condition:** *Let $\gamma \in [0, \pi/2[$. The following three statements are equivalent:*

(i) *There exists a solution $\theta^* \in \bar{\Delta}_G(\gamma)$ to the fixed-point equation (5.9);*

(ii) There exists a solution $\theta \in \bar{\Delta}_G(\gamma)$ to

$$B^T L^\dagger \omega + \psi_{\text{hom}} = \mathbf{sin}(B^T \theta). \quad (5.20)$$

for some $\psi_{\text{hom}} \in \mathcal{A}^{-1} \ker(B)$; and

(iii) There exists a solution $\psi \in \mathbb{R}^{|\mathcal{E}|}$ to the auxiliary fixed-point equation

$$(5.16) \text{ of the form (5.19) satisfying the norm constraint } \|\psi\|_\infty \leq \sin(\gamma)$$

and the cycle constraint $\mathbf{arcsin}(\psi) \in \text{Im}(B^T) \pmod{2\pi}$.

If the three equivalent statements (i), (ii), and (iii) are true, then we have the

identities $B^T \theta^* = B^T \theta = \mathbf{arcsin}(\psi) \pmod{2\pi}$. Additionally, $[\theta^*] \subset \bar{\Delta}_G(\gamma)$

is a locally exponentially stable synchronization manifold.

Proof. Statement 1): Every solution $\psi \in \mathbb{R}^{|\mathcal{E}|}$ to the auxiliary fixed-point equations (5.16) is of the form $\psi = \psi_{\text{hom}} + \psi_{\text{pt}}$, where ψ_{hom} is the homogeneous solution and ψ_{pt} is a particular solution. The homogeneous solution satisfies $B\mathcal{A}\psi_{\text{hom}} = \mathbf{0}_n$. One can easily verify that $\psi_{\text{pt}} = B^T L^\dagger \omega$ is a particular solution⁵, since $B\mathcal{A}\psi_{\text{pt}} = B\mathcal{A}B^T L^\dagger \omega = LL^\dagger \omega = (I_n - \frac{1}{n}\mathbf{1}_{n \times n})\omega = \omega$.

Statement 2), equivalence ((i) \Leftrightarrow (ii)) : If there exists a solution θ^* of the fixed-point equations (5.9), then θ^* can be equivalently obtained from equation

⁵Likewise, it can also be shown that $(B \text{diag}(\{a_{ij}\}_{\{i,j\} \in \mathcal{E}}))^\dagger \omega$ as well as $\text{diag}(\{a_{ij}\}_{\{i,j\} \in \mathcal{E}})^{-1} B^\dagger \omega$ are other possible particular solutions. All of these solutions differ only by addition of a homogenous solution. Each one can be interpreted as solution to a weighted least squares problem, see [110]. Further solutions can also be constructed in a graph-theoretic way by a spanning-tree decomposition, see [30]. Our specific choice $\psi_{\text{pt}} = B^T L^\dagger \omega$ has the property that $\psi_{\text{pt}} \in \text{Im}(B^T)$ lives in the cut-set space, and it is the most useful particular solution in order to proceed with our synchronization analysis.

(5.17) together with the solution (5.19) of the auxiliary equations (5.16). These two equations directly give equation (5.20).

Equivalence ((ii) \Leftrightarrow (iii)) : For $\theta^* \in \bar{\Delta}_G(\gamma)$, we have from equation (5.20) that $\|\psi\|_\infty \leq \sin(\gamma)$ and $\mathbf{arcsin}(\psi) = B^T \theta^* \pmod{2\pi}$, that is, $\mathbf{arcsin}(\psi) \in \text{Im}(B^T) \pmod{2\pi}$. Conversely, if the norm constraint $\|\psi\|_\infty \leq \sin(\gamma)$ and the cycle constraint $\mathbf{arcsin}(\psi) \in \text{Im}(B^T) \pmod{2\pi}$ are met, then equation (5.20) is solvable in $\bar{\Delta}_G(\gamma)$, and there is $\theta^* \in \bar{\Delta}_G(\gamma)$ such that $\mathbf{arcsin}(\psi) = B^T \theta^* \pmod{2\pi}$. Local exponential stability of the associated synchronization manifold $[\theta^*]$ follows then directly from Lemma 3.2.1. \square

Remark 5.3.2 (Parameterizations and the modulo operation). *The importance of the modulo operation in Lemma 5.3.1 can be illustrated by recalling the example in Remark 3.2.2. Consider a ring graph with $n \geq 5$ nodes, with identical unit weights, and with $\omega = \mathbf{0}_n$. In this case, the phase-synchronized set $[\theta^*] = \bar{\Delta}_G(0)$ and the set of uniformly spaced angles (or loop flow [154]) $[\tilde{\theta}^*] = [(0, 2\pi/n, \dots, (n-1) \cdot 2\pi/n)] \in \bar{\Delta}_G(2\pi/n)$ are two stable solutions in $\bar{\Delta}_G(\pi/2)$. Depending on the choice of coordinate chart (parameterization of the angles), the second solution $[\tilde{\theta}^*]$ has angular differences $B^T \tilde{\theta}^*$ given by $(2\pi/n, \dots, 2\pi/n, 2\pi/n)$ (which sum up to 2π) or by $(2\pi/n, \dots, 2\pi/n, 2\pi/n - 2\pi)$ (which sum up to 0). The latter is a vector in $\text{Im}(B^T)$ whereas the former one is not. Hence, the modulo operation is necessary*

to capture the solution $[\tilde{\theta}^*]$ independent of the parameterization. Otherwise, only the solution $[\theta^*] = \bar{\Delta}_G(0)$ is characterized by Lemma 5.3.1. \square

The particular solution $B^T L^\dagger \omega$ to the auxiliary fixed-point equations (5.16) lives in the cut-set space $\text{Ker}(B)^\perp$ and the homogenous solution ψ_{hom} lives in the weighted cycle space $\psi_{\text{hom}} \in \mathcal{A}^{-1} \text{Ker}(B)$. As a consequence, by statement (iii) of Lemma 5.3.1, for each cycle in the graph, we obtain one degree of freedom in choosing the homogeneous solution ψ_{hom} as well as one nonlinear constraint $c^T \mathbf{arcsin}(\psi) = 0 \pmod{2\pi}$, where $c \in \text{ker}(B)$ is a signed path vector corresponding to the cycle [29, 30]. Hence, the cycle space $\text{Ker}(B)$ of the graph serves as a degree of freedom to find a minimum ∞ -norm solution $\psi^* \in \mathbb{R}^{|\mathcal{E}|}$ to equations (5.16), which yields an *optimal* necessary synchronization condition.

Corollary 5.3.3 (Optimal necessary synchronization condition). *Consider the coupled oscillator model (3.1) with a connected graph $G(\mathcal{V}, \mathcal{E}, A)$ and $\omega \in \mathbf{1}_n^\perp$. Compute $\psi^* \in \mathbb{R}^{|\mathcal{E}|}$ as solution to the optimization problem*

$$\text{minimize}_{\psi \in \mathbb{R}^{|\mathcal{E}|}} \|\psi\|_\infty \quad \text{s.t.} \quad \omega = B\mathcal{A}\psi. \quad (5.21)$$

Let $\gamma \in [0, \pi/2[$. There exists a locally exponentially stable equilibrium manifold $[\theta^] \subset \bar{\Delta}_G(\gamma)$ only if $\|\psi^*\|_\infty \leq \sin(\gamma)$.*

The optimization problem (5.21) – the minimum ∞ -norm solution to an under-determined and consistent system of linear equations – is well studied in the

context of kinematically redundant manipulators. Its solution is known to be non-unique and contained in a disconnected solution space [110, 115]. Unfortunately, there is no “a priori” analytic formula to construct a minimum ∞ -norm solution, but the optimization problem is computationally tractable via its dual problem

$$\text{maximize}_{u \in \mathbb{R}^n} u^T \omega \quad \text{s.t.} \quad \|\mathcal{A}B^T u\|_1 = 1.$$

The optimal necessary condition $\|\psi^*\|_\infty \leq \sin(\gamma)$ improves upon the conditions (5.1)-(5.2) but it is still conservative since ψ^* does not necessarily satisfy the cycle constraint $\mathbf{arcsin}(\psi) \in \text{Im}(B^T) \pmod{2\pi}$ in Lemma 5.3.1.

5.3.2 Synchronization Assessment for Specific Networks

If the graph is acyclic, then there are no cycle constraints, and the norm constraint in Lemma 5.3.1 reduces to

$$\boxed{\|L^\dagger \omega\|_{\mathcal{E}, \infty} \leq \sin(\gamma)} \tag{5.22}$$

In this subsection we seek to establish that the condition (5.22) is sufficient for the existence of locally exponentially stable equilibria in $\bar{\Delta}_G(\gamma)$. Since the right-hand side of (5.22) is a concave function of $\gamma \in [0, \pi/2[$ that achieves its supremum value at $\gamma^* = \pi/2$, it follows that the condition

$$\boxed{\|L^\dagger \omega\|_{\mathcal{E}, \infty} < 1} \tag{5.23}$$

is sufficient for the existence of locally exponentially stable equilibria in $\Delta_G(\pi/2)$.

We establish the broad applicability of the proposed condition (5.22) to various classes of networks via analytical and statistical methods in this section. Before continuing our theoretical analysis, we summarize different interpretations of the conditions (5.23) and (5.22), provide some equivalent formulations, and compare them to existing synchronization conditions proposed in the literature.

Remark 5.3.4 (Interpretation of the sync condition). **Complex network interpretation:** *Surprisingly, topological or spectral connectivity measures such as nodal degree or algebraic connectivity are not key to synchronization. In fact, these often advocated [18, 31, 84, 85, 139, 298, 299] connectivity measures turn out to be conservative estimates of the synchronization condition (5.22). This statement can be seen by introducing the matrix V of orthonormal eigenvectors of the network Laplacian matrix L with corresponding eigenvalues $0 = \lambda_1 < \lambda_2 \leq \dots \leq \lambda_n$. From this spectral viewpoint, condition (5.22) can be equivalently written as*

$$\|V \operatorname{diag}(0, 1/\lambda_2, \dots, 1/\lambda_n) \cdot (V^T \omega)\|_{\mathcal{E}, \infty} \leq \sin(\gamma). \quad (5.24)$$

In words, the natural frequencies ω are projected on the network modes V , weighted by the inverse Laplacian eigenvalues, and $\|\cdot\|_{\mathcal{E}, \infty}$ evaluates the worst-case dissimilarity of this weighted projection. A sufficient condition for inequality (5.24) is $\lambda_2(L) > \|\omega\|_{\mathcal{E}, \infty}$, which strictly improves upon the algebraic connectivity conditions

Chapter 5. Synchronization in Complex Oscillator Networks

(5.4) and (5.11). Likewise, a necessary condition for (5.24) is $2 \cdot \max_{i \in \mathcal{V}} \deg_i \geq \lambda_n \geq \|\omega\|_{\mathcal{E}, \infty}$, resembling the degree-dependent conditions (5.1) and (5.2). When compared to (5.24), this sufficient condition and this necessary condition feature only one of $n - 1$ non-zero Laplacian eigenvalues and are overly conservative. We conclude that condition (5.23) strongly improves upon the conditions (5.1), (5.2), (5.4), and (5.11). On the other hand, as we will see later, a complete analytic characterization of its applicability is still open.

Kuramoto oscillator perspective: For classic Kuramoto oscillators (1.2) coupled in a complete graph with uniform weights $a_{ij} = K/n$, the synchronization condition (5.23) reduces to the condition $K > \max_{i,j \in \{1, \dots, n\}} |\omega_i - \omega_j|$, which equals the sufficient and tight condition (4.24) in Theorem 4.4.2.

Power network perspective: In power systems engineering, the equilibrium equations of the coupled oscillator model (3.1), given by $\omega_i = \sum_{j=1}^n a_{ij} \sin(\theta_i - \theta_j)$, are referred to as the AC power flow equations, and they are often approximated by their linearization $\omega_i = \sum_{j=1}^n a_{ij}(\theta_i - \theta_j)$, known as the DC power flow equations [16, 136, 257, 298, 299]. In vector notation the DC power flow equations are $\omega = L\theta$, and their solution satisfies $\max_{\{i,j\} \in \mathcal{E}} |\theta_i - \theta_j| = \|L^\dagger \omega\|_{\mathcal{E}, \infty}$. According to condition (5.22), the worst phase distance $\|L^\dagger \omega\|_{\mathcal{E}, \infty}$ obtained by the DC power flow needs to be less or equal than $\sin(\gamma)$, such that the solution to the AC power flow satisfies

$\max_{\{i,j\} \in \mathcal{E}} |\theta_i - \theta_j| \leq \gamma$. Hence, our condition extends the common DC power flow approximation from infinitesimally small angles $\gamma \ll 1$ to large angles $\gamma \in [0, \pi/2[$.

Auxiliary linear perspective: As detailed in the previous paragraph, the key term $L^\dagger \omega$ in condition (5.22) equals the phase differences obtained by the linear Laplacian equation $\omega = L\theta$. This linear interpretation is not only insightful but also practical since condition (5.22) can be quickly evaluated by numerically solving the linear system $\omega = L\theta$. This linear system is possibly of high dimension, but it inherits the sparsity of the graph $G(\mathcal{V}, \mathcal{E}, A)$. Thus, condition (5.22) can be verified efficiently even for large-scale sparse networks.

Energy landscape perspective: Condition (5.22) can also be understood in terms of an appealing energy landscape interpretation. The coupled oscillator model (3.1) is a system of particles that aim to minimize the energy function

$$\tilde{U}(\theta) = \sum_{\{i,j\} \in \mathcal{E}} a_{ij} (1 - \cos(\theta_i - \theta_j)) - \sum_{i=1}^n \omega_i \cdot \theta_i,$$

where the first term is the nonlinear spring potential $U(\theta)$ representing the pairwise nonlinear attraction among the particles, and the second term represents the external force driving the particles away from the “all-aligned” state. Since the energy function $\tilde{U}(\theta)$ is difficult to study, it is natural to look for a minimum of its second-order approximation $\tilde{U}_0(\theta) = \sum_{\{i,j\} \in \mathcal{E}} a_{ij} (\theta_i - \theta_j)^2 / 2 - \sum_{i=1}^n \omega_i \cdot \theta_i$, where the first term corresponds to a Hookean potential. Condition (5.22) is then restated as follows: $\tilde{U}(\theta)$ features a phase cohesive minimum with interacting particles no

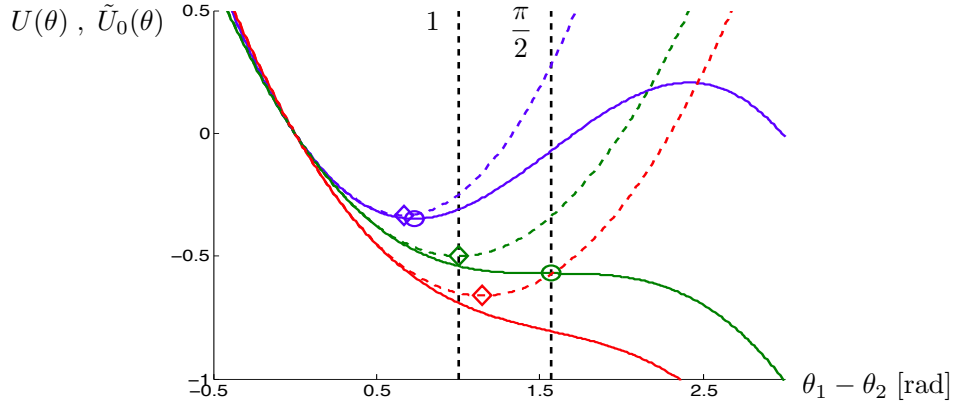


Figure 5.1: Energy landscape interpretation of the synchronization condition
 The energy function $\tilde{U}(\theta)$ and its quadratic approximation $\tilde{U}_0(\theta)$ for a two-particle system are shown as solid and dashed curves, respectively, for the stable (blue), marginal (green) and unstable (red) cases. The circles and diamonds represent stable critical points of $\tilde{U}(\theta)$ and $\tilde{U}_0(\theta)$, respectively.

further than γ apart if $\tilde{U}_0(\theta)$ features a minimum with interacting particles no further from each other than $\sin(\gamma)$, as illustrated in Figure 5.1.

Circuit-theoretic interpretation: In a power network, $\omega \in \mathbb{R}^n$ are the nodal power injections. Let $x \in \mathbb{R}^{|\mathcal{E}|}$ satisfy $Bx = \omega$, then x are the equivalent power injections along lines $\{i, j\} \in \mathcal{E}$.⁶ Condition (5.23) can then be rewritten as $\|B^T L^\dagger Bx\|_\infty < 1$. The matrix $B^T L^\dagger B \in \mathbb{R}^{|\mathcal{E}| \times |\mathcal{E}|}$ has elements $(e_n^i - e_n^j)^T L^\dagger (e_n^k - e_n^\ell)$ for $\{i, j\}, \{k, \ell\} \in \mathcal{E}$, its diagonal elements are the effective resistances R_{ij} , and its off-diagonal elements are the network distribution (sensitivity) factors [297, Appendix 11A]. Hence, from a circuit-theoretic perspective, condition (5.23) restricts the pair-wise effective resistances and the routing of power through the network

⁶Notice that x is not uniquely determined if the circuit features loops.

similar to the resistive synchronization conditions in [86, 153, 298]. For an acyclic graph, condition (5.23) simply corresponds to feasibility of the flow, see also [249].

Graph-theoretic interpretation: *With regards to the exact norm and cycle conditions in statement (iii) of Lemma 5.3.1, the proposed condition (5.22) is simply a norm constraint on the network parameters in cut-set space $\text{Im}(B^T)$ of the graph topology, and cycle components are discarded. For acyclic graphs, condition (5.23) is equivalent to the cut-set condition [75, Lemma 1].* \square

As it turns out, the norm and cycle conditions in Lemma 5.3.1 can be easily evaluated for the sparsest (acyclic) and densest (homogeneous) topologies and for “worst-case” (cut-set inducing) and “best” (identical) natural frequencies. For all of these cases the synchronization condition (5.22) is sharp. To quantify a “sharp” condition in the following theorem, we distinguish between *exact* (necessary and sufficient) conditions and *tight* conditions, which are sufficient in general and become necessary over a set of parametric realizations.

Theorem 5.3.5 (Synchronization condition for extremal network topologies and parameters). *Consider the coupled oscillator model (3.1) with connected graph $G(\mathcal{V}, \mathcal{E}, A)$ and $\omega \in \mathbf{1}_n^\perp$. Let $\gamma \in [0, \pi/2[$. The following statements hold:*

(G1) **Exact synchronization condition for acyclic graphs:** *Assume that $G(\mathcal{V}, \mathcal{E}, A)$ is acyclic. There exists a locally exponentially stable equilibrium*

manifold $[\theta^*] \subset \bar{\Delta}_G(\gamma)$ if and only if condition (5.22) holds. Moreover, in this case we have that $B^T \theta^* = \arcsin(B^T L^\dagger \omega) \in \bar{\Delta}_G(\gamma)$;

(G2) Tight synchronization condition for homogeneous graphs: Assume that $G(\mathcal{V}, \mathcal{E}, A)$ is a homogeneous graph, that is, there is $K > 0$ such that $a_{ij} = K$ for all distinct $i, j \in \{1, \dots, n\}$. Consider a compact interval $\Omega \subset \mathbb{R}$, and let $\mathbf{\Omega} = (\Omega_1, \dots, \Omega_n) \subset \mathbb{R}^n$ be the set of all vectors with components $\Omega_i \in \Omega$ for all $i \in \{1, \dots, n\}$. For all $\omega \in \mathbf{\Omega}$ there exists a locally exponentially stable equilibrium manifold $[\theta^*] \subset \bar{\Delta}_G(\gamma)$ if and only if condition (5.22) holds;

(G3) Exact synchronization condition for cut-set inducing frequencies: Let $\Omega_1, \Omega_2 \in \mathbb{R}$, and let $\mathbf{\Omega} = (\Omega_1, \dots, \Omega_n) \subset \mathbb{R}^n$ be the set of bipolar vectors with components $\Omega_i \in \{\Omega_1, \Omega_2\}$ for $i \in \{1, \dots, n\}$. For all $\omega \in L\mathbf{\Omega}$ there exists a locally exponentially stable equilibrium manifold $[\theta^*] \subset \bar{\Delta}_G(\gamma)$ if and only if condition (5.22) holds. Moreover, $\mathbf{\Omega}$ induces a cut-set: if $|\Omega_2 - \Omega_1| = \sin(\gamma)$, then for any particular $\mathbf{\Omega}^* \in \mathbf{\Omega}$ and $\omega = L\mathbf{\Omega}^*$ we obtain the equilibrium $\theta^* \in \bar{\Delta}_G(\gamma)$ satisfying $B^T \theta^* = \arcsin(B^T \mathbf{\Omega}^*)$, that is, for all $\{i, j\} \in \mathcal{E}$, $|\theta_i^* - \theta_j^*| = 0$ if $\Omega_i^* = \Omega_j^*$ and $|\theta_i^* - \theta_j^*| = \gamma$ if $\Omega_i^* \neq \Omega_j^*$; and

(G4) Asymptotic correctness: In the limit $\|B^T L^\dagger \omega\|_\infty \rightarrow 0$, that is, for identical natural frequencies and/or asymptotically strong network coupling, there

is a locally exponentially stable equilibrium manifold $[\theta^*]$ satisfying

$$\lim_{\|B^T L^\dagger \omega\|_\infty \rightarrow 0} \frac{(B^T \theta^*)_i}{(\mathbf{arcsin}(B^T L^\dagger \omega))_i} = 1, \quad i \in \{1, \dots, |\mathcal{E}|\}.$$

Proof. Statement (G1): For an acyclic graph, we have that $\text{Ker}(B) = \emptyset$. According to Lemma 5.3.1, there exists an equilibrium $\theta^* \in \bar{\Delta}_G(\gamma)$ if and only if condition (5.22) is satisfied. In this case, we obtain $B^T \theta^* = \mathbf{arcsin}(B^T L^\dagger \omega)$.

Statement (G2): In the homogeneous case, we have that $L = K(nI_n - \mathbf{1}_{n \times n})$ and $L^\dagger = \frac{1}{Kn}(I_n - \frac{1}{n}\mathbf{1}_{n \times n})$, see [86, Lemma 3.13]. Thus, the inequality condition (5.22) can be equivalently rewritten as $\sin(\gamma) \geq \|B^T L^\dagger \cdot \omega\|_\infty = \frac{1}{Kn} \|B^T \omega\|_\infty$. According to Theorem 4.4.2, the Kuramoto model (1.2) with homogenous coupling $a_{ij} = K$ features a locally exponentially stable equilibrium manifold $[\theta^*] \subset \bar{\Delta}_G(\gamma)$, $\gamma \in [0, \pi/2[$, for all $\omega \in \Omega$ if and only if the condition $K > \|B^T \omega\|_\infty / n$ is satisfied.

Statement (G3): For notational convenience, let $c \triangleq \Omega_1 - \Omega_2$. Then, for any $\Omega^* \in \Omega$ and for $\omega = L\Omega^*$, we have that $B^T L^\dagger \omega = B^T L^\dagger L\Omega^* = B^T \Omega^*$ is a vector with components $\{-c, 0, +c\}$. Now consider the solution $\psi = B^T L^\dagger \omega = B^T \Omega^*$ to the auxiliary fixed point equations (5.16), and notice that $\mathbf{arcsin}(\psi) = \mathbf{arcsin}(B^T \Omega^*)$ has components $\{-\arcsin(c), 0, +\arcsin(c)\}$. In particular, we have that $\mathbf{arcsin}(\psi) \in \text{Im}(B^T)$, and the exact synchronization condition from Lemma 5.3.1 is satisfied if and only if $\|\psi\|_\infty = c \leq \sin(\gamma)$, which corresponds

to condition (5.22). The cut-set property follows since $B^T \theta^* = \mathbf{arcsin}(\psi)$ has components $\{-\arcsin(c), 0, +\arcsin(c)\} = \{-\gamma, 0, +\gamma\}$.

Statement (G4): Since $\arcsin(x)/x = 1 + x^2/6 + \mathcal{O}(x)^4$, we have that

$$(\mathbf{arcsin}(B^T L^\dagger \omega))_i / (B^T L^\dagger \omega)_i = 1 + \mathcal{O}((B^T L^\dagger \omega)_i^2)$$

for each component $i \in \{1, \dots, |\mathcal{E}|\}$. Thus, in the limit $B^T L^\dagger \omega \rightarrow \mathbf{0}_{|\mathcal{E}|}$, it follows that $\mathbf{arcsin}(B^T L^\dagger \omega) \in \text{Im}(B^T)$, and the cycle constraint $\mathbf{arcsin}(\psi) = \mathbf{arcsin}(B^T L^\dagger \omega + \psi_{\text{hom}}) \in \text{Im}(B^T)$ is met with $\psi_{\text{hom}} = \mathbf{0}_{|\mathcal{E}|}$. For $B^T L^\dagger \omega \rightarrow \mathbf{0}_{|\mathcal{E}|}$ the norm constraint $\|B^T L^\dagger \omega\|_\infty \leq \sin(\gamma)$ is also satisfied with $\gamma \searrow 0$, and we obtain⁷ for each $i \in \{1, \dots, |\mathcal{E}|\}$ that $\lim_{B^T L^\dagger \omega \rightarrow \mathbf{0}_{|\mathcal{E}|}} (B^T \theta^*)_i / (\mathbf{arcsin}(B^T L^\dagger \omega))_i = 1$. \square

Lemma 5.3.1 shows that the solvability of the fixed-point equations (5.9) is inherently related to the *cycle constraints*. The following lemma establishes feasibility of a single cycle and offers a checkable condition.

Lemma 5.3.6 (Single cycle feasibility). *Consider the coupled oscillator model*

(3.1) *with a cycle graph $G(\mathcal{V}, \mathcal{E}, A)$ and $\omega \in \mathbf{1}_n^\perp$. Without loss of generality,*

assume that the edges are labeled by $\{i, i+1\} \pmod{n}$ for $i \in \{1, \dots, n\}$ and

$\text{Ker}(B) = \text{span}(\mathbf{1}_n)$. Define $x \in \mathbf{1}_n^\perp$ and $y \in \mathbb{R}_{>0}^n$ uniquely by $x \triangleq B^T L^\dagger \omega$ and

$y_i \triangleq a_{i, (i+1) \pmod{n}}^{-1} > 0$ for $i \in \{1, \dots, n\}$. Let $\gamma \in [0, \pi/2[$.

The following statements are equivalent:

⁷The limit $\|B^T L^\dagger \omega\|_\infty \rightarrow 0$ implies that the resulting equilibrium $\theta^* \in \bar{\Delta}_G(0)$ corresponds to phase synchronization $\theta_i = \theta_j$ for all $i, j \in \{1, \dots, n\}$. The converse statement $\theta^* \in \bar{\Delta}_G(0) \implies \omega = \mathbf{0}_n$ is also true and its proof can be found in Theorem 3.3.4.

(i) There is a locally exponentially stable equilibrium manifold $[\theta^*] \subset \bar{\Delta}_G(\gamma)$; and

(ii) The function $f : [\lambda_{\min}, \lambda_{\max}] \rightarrow \mathbb{R}$ defined by $f(\lambda) = (\sum_{i=1}^n \arcsin(x_i + \lambda y_i))$ and with the domain boundaries $\lambda_{\min} = \max_{i \in \{1, \dots, n\}} \frac{-\sin(\gamma) - x_i}{y_i}$ and $\lambda_{\max} = \min_{i \in \{1, \dots, n\}} \frac{\sin(\gamma) - x_i}{y_i}$ satisfies

$$f(\lambda_{\min}) < 0 < f(\lambda_{\max}) \pmod{2\pi}.$$

If both equivalent statements 1) and 2) are true, then we have that $B^T \theta^* = \mathbf{arcsin}(x + \lambda^* y) \pmod{2\pi}$, where $\lambda^* \in [\lambda_{\min}, \lambda_{\max}]$ satisfies $f(\lambda^*) = 0$.

Proof. According to Lemma 5.3.1, there exists an equilibrium $\theta^* \in \bar{\Delta}_G(\gamma)$ if and only if there exists a solution $\psi = x + \lambda y$, $\lambda \in \mathbb{R}$, to the auxiliary fixed-point equations (5.16) satisfying the norm constraint $\|\psi\|_\infty \leq \sin(\gamma)$ and the cycle constraint $\mathbf{arcsin}(\psi) \in \text{Im}(B^T) \pmod{2\pi}$. Equivalently, since $\text{Ker}(B) = \text{span}(\mathbf{1}_n)$, there is $\lambda \in \mathbb{R}$ satisfying the norm constraint $\|x + \lambda y\|_\infty \leq \sin(\gamma) < 1$ and the cycle constraint $\mathbf{1}_n^T \mathbf{arcsin}(x + y\lambda) = 0 \pmod{2\pi}$. Equivalently, the function $f(\lambda) = \mathbf{1}_n^T \mathbf{arcsin}(x + y\lambda)$ features a zero $\lambda^* \in [\lambda_{\min}, \lambda_{\max}]$ (modulo 2π) corresponding to the cycle constraint, where the constraints on λ_{\min} and λ_{\max} guarantee the norm constraints $x_i + y_i \lambda_{\max} \leq \sin(\gamma)$ and $x_i + y_i \lambda_{\min} \geq -\sin(\gamma)$ for all $i \in \{1, \dots, n\}$. Equivalently, by the intermediate value theorem and due to continuity and (strict) monotonicity of the function f , we have that $f(\lambda_{\min}) < 0 < f(\lambda_{\max}) \pmod{2\pi}$.

Finally, if $\lambda^* \in [\lambda_{\min}, \lambda_{\max}]$ is found such that $f(\lambda^*) = 0 \pmod{2\pi}$, then, by Lemma 5.3.1, $B^T \theta^* = \mathbf{arcsin}(\psi) = \mathbf{arcsin}(x + \lambda^* y) \pmod{2\pi}$. \square

Lemma 5.3.6 offers a simple condition for cycles, which leads to the next result.

Theorem 5.3.7 (Synchronization conditions for cycle graphs). *Consider the coupled oscillator model (3.1) with a cycle graph $G(\mathcal{V}, \mathcal{E}, A)$ and $\omega \in \mathbf{1}_n^\perp$. Consider the inequality condition (5.22) for $\gamma \in [0, \pi/2[$. The following statements hold.*

(C1) **Exact sync condition for symmetric natural frequencies:** *Assume that $\omega \in \mathbf{1}_n^\perp$ is such that $B^T L^\dagger \omega$ is a symmetric vector.⁸ There is a locally exponentially stable equilibrium manifold $[\theta^*] \subset \bar{\Delta}_G(\gamma)$ if and only if condition (5.22) holds. Moreover, in this case $B^T \theta^* = \mathbf{arcsin}(B^T L^\dagger \omega)$.*

(C2) **Tight sync condition for low-dimensional cycles:** *Assume the network contains $n \in \{3, 4\}$ oscillators. Consider a compact interval $\Omega \subset \mathbb{R}$, and let $\mathbf{\Omega} = (\Omega_1, \dots, \Omega_n) \subset \mathbb{R}^n$ be the set of vectors with components $\Omega_i \in \Omega$ for all $i \in \{1, \dots, n\}$. For all $\omega \in L\mathbf{\Omega}$ there exists a locally exponentially stable equilibrium manifold $[\theta^*] \subset \bar{\Delta}_G(\gamma)$ if and only if condition (5.22) holds.*

(C3) **General cycles and network parameters:** *In general for $n \geq 5$ oscillators, condition (5.23) does not guarantee existence of an equilibrium*

⁸A vector $x \in \mathbf{1}_n^\perp$ is symmetric if its histogram is symmetric, that is, up to permutation of its elements, x is of the form $x = [-c, +c]^T$ for n even and some vector $c \in \mathbb{R}^{n/2}$ and $x = [-c, 0, +c]^T$ for n odd and some $c \in \mathbb{R}^{(n-1)/2}$.

$\theta^* \in \Delta_G(\pi/2)$. As a sufficient condition, there exists a locally exponentially stable equilibrium manifold $[\theta^*] \subset \bar{\Delta}_G(\gamma)$, $\gamma \in [0, \pi/2[$, if

$$\|B^T L^\dagger \omega\|_\infty \leq \frac{\min_{\{i,j\} \in \mathcal{E}} a_{ij}}{\max_{\{i,j\} \in \mathcal{E}} a_{ij} + \min_{\{i,j\} \in \mathcal{E}} a_{ij}} \cdot \sin(\gamma). \quad (5.25)$$

We omit the proof of Theorem 5.3.7 here and refer to [89, Theorem 3] for details.

In the following, define a *patched network* $\{G(\mathcal{V}, \mathcal{E}, A), \omega\}$ as a collection of subgraphs and natural frequencies $\omega \in \mathbf{1}_n^\perp$, where (i) each subgraph is connected, (ii) in each subgraph one of the conditions (G1),(G2),(G3),(G4), (C1), or (C2) is satisfied, (iii) the subgraphs are connected to another through edges $\{i, j\} \in \mathcal{E}$ satisfying $\|(e_i^{|\mathcal{E}|} - e_j^{|\mathcal{E}|})^T L^\dagger \omega\|_\infty \leq \sin(\gamma)$, and (iv) the set of cycles in the overall graph $G(\mathcal{V}, \mathcal{E}, A)$ is equal to the union of the cycles of all subgraphs. Since a patched network satisfies the synchronization condition (5.22) as well the norm and cycle constraints, we can state the following result.

Corollary 5.3.8 (Synchronization condition for patched networks). *Consider the coupled oscillator model (3.1) with a patched network $\{G(\mathcal{V}, \mathcal{E}, A), \omega\}$, and let $\gamma \in [0, \pi/2[$. There is a locally exponentially stable equilibrium manifold $[\theta^*] \subset \bar{\Delta}_G(\gamma)$ if condition (5.22) holds.*

Example 1 (Cyclic counterexample). In the proof of Theorem 5.3.7 (see [89, Theorem 3] for details), we provide an analytic counterexample which demonstrates that condition (5.22) is not sufficiently tight for synchronization in sufficiently

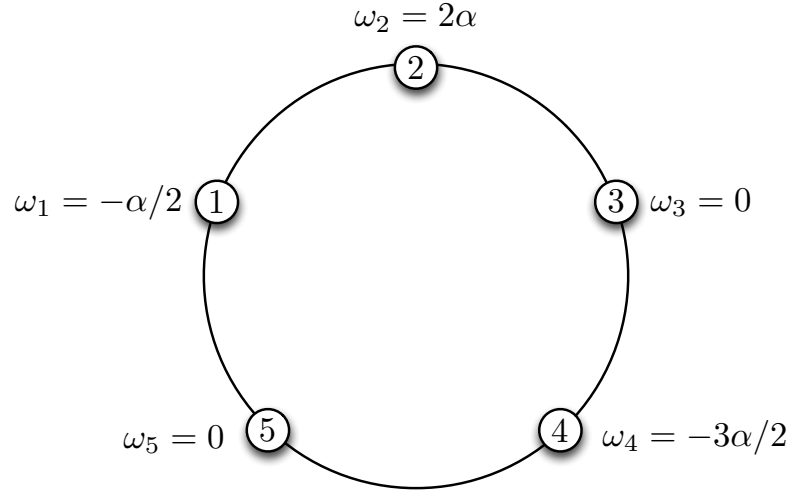


Figure 5.2: Cycle graph with $n = 5$ nodes and non-symmetric choice of ω .

large cyclic networks. Here, we provide an additional numerical counterexample. Consider a cycle family of length $n = 5 + 3 \cdot p$, where $p \in \mathbb{N}_0$ is a nonnegative integer. Without loss of generality, assume that the edges are labeled by $\{i, i + 1\} \pmod{n}$ for $i \in \{1, \dots, n\}$ such that $\text{Ker}(B) = \text{span}(\mathbf{1}_n)$. Assume that all edges are unit-weighted $a_{i, i+1 \pmod{n}} = 1$ for $i \in \{1, \dots, n\}$. Consider $\alpha \in [0, 1[$, and let

$$\omega = \alpha \cdot \begin{bmatrix} -1/2 & 2 & \mathbf{0}_{p+1} & 3/2 & \mathbf{0}_{2p+1} \end{bmatrix}^T.$$

For $n = 5$ ($p = 1$) the graph and the network parameters are illustrated in Figure 5.2. For the given network parameters, we obtain the non-symmetric vector

$$B^T L^\dagger \omega = \alpha \cdot \begin{bmatrix} 1 & -1 & -\mathbf{1}_{(n-2)/3} & 1/2 \cdot \mathbf{1}_{2(n-2)/3} \end{bmatrix}^T.$$

Analogously to the example provided in the proof of Theorem 5.3.7, $\|B^T L^\dagger \omega\|_\infty =$

α and $B^T L^\dagger \omega$ is the minimum ∞ -norm vector $B^T L^\dagger \omega + \lambda \mathbf{1}_n$ for $\lambda \in \mathbb{R}$. In the limit $\alpha \uparrow 1$, the necessary condition (5.1) is satisfied with equality. In Figure 5.2, for $\alpha \uparrow 1$, we have that $\omega_2 = 2$, and the necessary condition (5.1) reads as $a_{12} + a_{23} = |\omega_2| = 2$, and the corresponding equilibrium equation $\sin(\theta_1 - \theta_2) + \sin(\theta_3 - \theta_2) = 2$ can only be satisfied if $\theta_1 - \theta_2 = \pi/2$ and $\theta_3 - \theta_2 = \pi/2$. Thus, with two fixed edge differences there is no more “wobble room” to compensate for the effects of ω_i , $i \in \{1, 3, 4, 5\}$. As a consequence, there is no equilibrium $\theta^* \in \bar{\Delta}_G(\pi/2)$ for $\alpha = 1$ or equivalently $\|B^T L^\dagger \omega\|_\infty = 1$. Due to continuity of the equations (5.9) with respect to α , we conclude that for $\alpha < 1$ sufficiently large there is no equilibrium either. Numerical investigations show that this conclusion is true, especially for very large cycles. For the extreme case $p = 10^7$, we obtain the critical threshold $\alpha \approx 0.9475$ where $\theta^* \in \bar{\Delta}_G(\pi/2)$ ceases to exist. \square

Both the counterexample used in the proof of Theorem 5.3.7 and the one in Example 1 are at the boundary of the admissible parameter space, where the necessary condition (5.1) is marginally satisfied. In the next section, we establish through Monte Carlo simulation studies that such “degenerate” counterexamples almost never occur for generic network topologies and parameters.

To conclude this subsection, we remark that the main technical difficulty in proving sufficiency of the condition (5.22) for arbitrary graphs is the compact state space \mathbb{T}^n and the non-monotone sinusoidal coupling among the oscillators. Indeed,

if the state space was \mathbb{R}^n and if the oscillators were coupled via non-decreasing and odd functions, then the synchronization problem simplifies tremendously and the counterexamples in the proof of Theorem 5.3.7 and in Example 1 do not occur. We refer the reader to [38,39] for an elegant analysis based on optimization theory.

5.3.3 Statistical Synchronization Assessment

After having analytically established condition (5.22) for a variety of particular network topologies and parameters, we establish its correctness and predictive power for a broad range of networks.

Statistical Assessment of Correctness

Extensive simulation studies lead us to the conclusion that condition (5.22) is correct in general and guarantees the existence of a stable equilibrium $\theta^* \in \bar{\Delta}_G(\gamma)$. In order to validate this hypothesis we invoke probability estimation through Monte Carlo techniques, see [271, Section 9] and [41, Section 3] for a review.

We conducted Monte Carlo simulation studies over a wide range of natural frequencies ω_i , network sizes n , coupling weights a_{ij} , and different random graph models of varying degrees of sparsity and randomness. We select a set of *nominal network* models with topologies constructed from Erdős-Rényi graphs, random geometric graphs, and Watts-Strogatz small world networks, and the natural fre-

quencies and coupling weights are sampled from uniform distributions. In total, we constructed $1.2 \cdot 10^6$ samples of such nominal networks, each with a connected graph $G(\mathcal{V}, \mathcal{E}, A)$ and natural frequencies ω satisfying $\|L^\dagger \omega\|_{\mathcal{E}, \infty} \leq \sin(\gamma)$ for some $\gamma < \pi/2$. We will not detail the construction of the nominal network models here and refer to [89] for further information. For each sample, we numerically solve the fixed equation (5.9) with accuracy 10^{-6} and test the hypothesis

$$\mathcal{H} : \|L^\dagger \omega\|_{\mathcal{E}, \infty} \leq \sin(\gamma) \implies \exists \theta^* \in \bar{\Delta}_G(\gamma)$$

with an accuracy 10^{-4} . The results are reported in detail in [89] together with the *empirical probability* that the hypothesis \mathcal{H} is true:

$$\widehat{\text{Prob}}(\mathcal{H} \text{ is true}) = \frac{\text{number of samples satisfying } (\mathcal{H} \text{ is true})}{\text{total number of samples}}.$$

Given an accuracy level $\epsilon \in]0, 1[$ and a confidence level $\eta \in]0, 1[$, we ask for the number of samples N such that the true probability $\text{Prob}(\mathcal{H} \text{ is true})$ equals the empirical probability $\widehat{\text{Prob}}(\mathcal{H} \text{ is true})$ with confidence level greater than $1 - \eta$ and accuracy at least ϵ , that is,

$$\text{Prob} \left(\left| \text{Prob}(\mathcal{H} \text{ is true}) - \widehat{\text{Prob}}(\mathcal{H} \text{ is true}) \right| < \epsilon \right) > 1 - \eta.$$

By the Chernoff-Hoeffding bound (see [271, Equation (9.14)] and [125, Theorem 1]), the number of samples N for a given accuracy ϵ and confidence η is given as

$$N \geq \frac{1}{2\epsilon^2} \log \frac{2}{\eta}. \tag{5.26}$$

For $\epsilon = \eta = 0.01$, inequality (5.26) is satisfied for $N \geq 26492$ samples. By invoking the Chernoff-Hoeffding bound (5.26), our Monte Carlo simulations studies establish the following statement:

With 99% confidence level, there is at least 99% accuracy that the hypothesis \mathcal{H} is true with probability 99.97 % for a nominal network

From this statistical result, we deduce that the proposed synchronization condition (5.22) holds true for “almost all” topologies and parameters of the considered nominal network models. Indeed, in Subsection 5.3.2, we also show the existence of possibly-thin sets of “degenerate” network topologies and parameters for which our condition (5.22) is not sufficiently tight. Overall, our analytical and statistical results validate the correctness of the proposed condition (5.22).

We refer the interested reader to [89, Supplementary Information] for further details on the construction of the nominal network models, probability estimation through Monte Carlo techniques, and the detailed outcomes of our simulations.

Statistical Assessment of Accuracy

After having established the statistical correctness of condition (5.22), we now investigate its predictive power for arbitrary networks. Since we analytically establish in statement (G4) of Theorem 5.3.5 that condition (5.22) is exact for sufficiently small pairwise phase cohesiveness $|\theta_i - \theta_j| \ll 1$, we now investigate the

other extreme, $\max_{\{i,j\} \in \mathcal{E}} |\theta_i - \theta_j| = \pi/2$. To test the corresponding synchronization condition (5.23) in a low-dimensional parameter space, we consider a complex network of Kuramoto oscillators given by

$$\dot{\theta}_i = \omega_i - K \cdot \sum_{j=1}^n a_{ij} \sin(\theta_i - \theta_j), \quad i \in \{1, \dots, n\}, \quad (5.27)$$

where all coupling weights a_{ij} are either zero or one, and the coupling gain $K > 0$ serves as control parameter. If L is the corresponding unweighted Laplacian matrix, then condition (5.23) reads as $K > K_{\text{critical}} \triangleq \|L^\dagger \omega\|_{\mathcal{E}, \infty}$. Of course, the condition $K > K_{\text{critical}}$ is only sufficient and the critical coupling may be smaller than K_{critical} . In order to test the accuracy of the condition $K > K_{\text{critical}}$, we numerically found the smallest value of K leading to synchrony with phase cohesiveness $\pi/2$. In the following, we present only the main results and refer to [89, Supplementary Information] for the details of our numerical investigations.

Figure 5.3 reports our findings for various network sizes, connected random graph models, and sample distributions of the natural frequencies. First, notice from Subfigures (a),(b),(d), and (e) that condition (5.23) is extremely accurate for a sparse graph, that is, for small p and n , as expected from our analytical results. Second, for a dense graph with $p \approx 1$, Subfigures (a),(b),(d), and (e) confirm the results known for classic Kuramoto oscillators (1.2): for a bipolar distribution condition (5.23) is exact, and for a uniform distribution a small critical coupling is obtained. Third, Subfigures (c) and (d) show that condition (5.23) is scale-free

for a Watts-Strogatz small world network, that is, it has almost constant accuracy for various values of n and p . Fourth and finally, observe that condition (5.23) is always within a constant factor of the exact critical coupling, whereas other proposed conditions [18, 31, 84, 85, 139, 298, 299] on the nodal degree or on the algebraic connectivity scale poorly with respect to network size n .

5.4 Applications to Structure-Preserving Power

System Models

We envision that condition (5.22) can be applied to quickly assess synchronization and robustness in power networks under volatile operating conditions. In this section, we present a set of examples to demonstrate how the results in this chapter can be applied to power networks. We will only outline a few selected applications here, and refer to the corresponding articles for further details.

5.4.1 Synchronization and Security Assessment

Since real-world power networks are carefully engineered systems with particular network topologies and parameters, we do not extrapolate the statistical results from the previous section to power grids. Rather, we consider ten widely-established IEEE power network test cases provided by [111, 304].

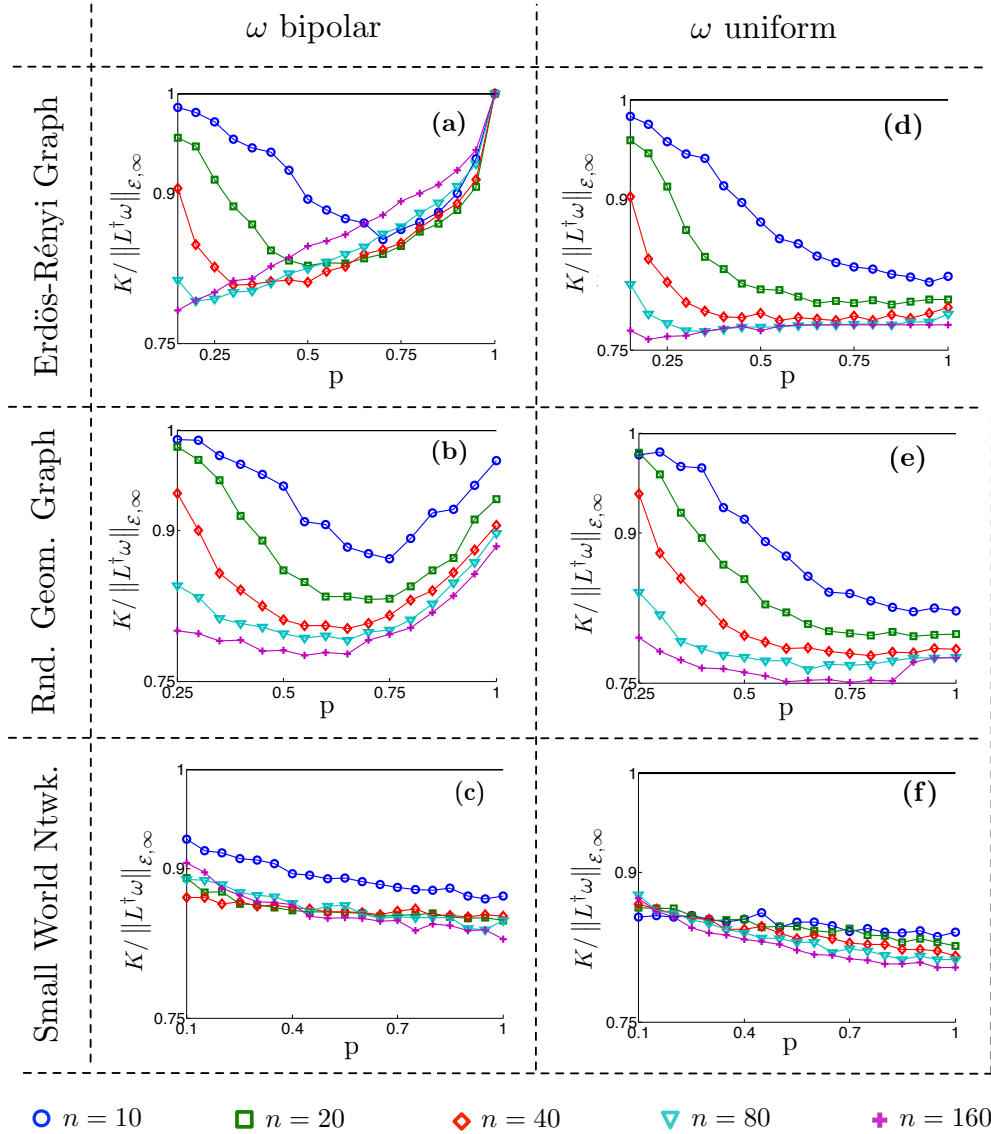


Figure 5.3: Synchronization threshold in a complex Kuramoto oscillator network. Numerical evaluation of the exact critical coupling K in a complex Kuramoto oscillator network. The subfigures show the critical coupling gain K normalized by $\|L^\dagger \omega\|_{\varepsilon, \infty}$ for an Erdős-Rényi graph with probability p of connecting two nodes, for a random geometric graph with connectivity radius p , and for a Watts-Strogatz small world network with rewiring probability p . Each data point is the mean over 100 samples of the respective random graph model, for values of ω_i sampled from a bipolar distribution or a uniform distribution supported on $[-1, 1]$, and for the network sizes $n \in \{10, 20, 40, 80, 160\}$, respectively.

Under nominal operating conditions, the power generation is optimized to meet the forecast demand, while obeying the AC power flow laws and respecting the thermal limits of each transmission line. Thermal limits constraints are precisely equivalent to phase cohesiveness requirements, and they are a subset of the so-called security constraints (limiting the branch power flows and the nodal voltages) which guarantee the robust operation of the power grid.

In order to test the synchronization condition (5.22) in a volatile smart grid scenario, we make the following changes to the nominal network: 1) We assume fluctuating demand and randomize 50% of all loads to deviate from the forecasted loads. 2) We assume that the grid is penetrated by renewables with severely fluctuating power outputs, for example, wind or solar farms, and we randomize 33% of all generating units to deviate from the nominally scheduled generation. 3) Following the paradigm of *smart operation of smart grids* [279], the fluctuations can be mitigated by fast-ramping generation, such as fast-response energy storage including batteries and flywheels, and controllable loads, such as large-scale server farms or fleets of plug-in hybrid electrical vehicles. Here, we assume that the grid is equipped with 10% fast-ramping generation and 10% controllable loads, and the power imbalance (caused by fluctuating demand and generation) is uniformly dispatched among these adjustable power sources. A detailed description of the simulation setup can be found in [89, Supplementary Information].

For each of the ten IEEE test cases, we construct 1000 random realizations of the scenario 1), 2), and 3) described above. For each realization, we numerically check for the existence of a solution $\theta^* \in \bar{\Delta}_G(\gamma)$, $\gamma \in [0, \pi/2[$ to the AC power flow equations, the right-hand side of the power network dynamics (2.1),(2.3), given by

$$P_i = \sum_{j=1}^n a_{ij} \sin(\theta_i - \theta_j), \quad i \in \{1, \dots, n\}, \quad (5.28)$$

where $P_i = P_{m,i}$ for generators $i \in \mathcal{V}_1$ and $P_i = P_{l,i}$ for loads $i \in \mathcal{V}_3$. The solution to the AC power flow equations (5.28) is found via the AC power flow solver provided by *MATPOWER* [304]. Notice that, by Lemma 3.2.1, if such a solution θ^* exists, then it is locally exponentially stable. Next, we compare the numerical solution θ^* with the results predicted by our synchronization condition (5.22). As discussed in Remark 5.3.4, a physically insightful and computationally efficient way to evaluate condition (5.22) is to solve the sparse and linear DC power flow:

$$P_i = - \sum_{j=1}^n a_{ij} (\delta_i - \delta_j), \quad i \in \{1, \dots, n\}. \quad (5.29)$$

In vector form, the DC power flow equations (5.29) read as $\omega = L\delta$, and their solution $\delta^* = L^\dagger \omega$ is defined uniquely up to translational invariance. Given the solution δ^* of the DC power flow equations (5.29), the left-hand side of our synchronization condition (5.22) evaluates to $\|L^\dagger \omega\|_{\mathcal{E}, \infty} = \|B^T L^\dagger \omega\|_\infty = \max_{\{i,j\} \in \mathcal{E}} |\delta_i^* - \delta_j^*|$.

Finally, we compare our prediction with the numerical results. If $\|L^\dagger \omega\|_{\mathcal{E}, \infty} \leq \sin(\gamma)$ for some $\gamma \in [0, \pi/2[$, then condition (5.22) predicts that there exists a

stable solution $\theta \in \bar{\Delta}_G(\gamma)$, or alternatively $\theta \in \bar{\Delta}_G(\arcsin(\|L^\dagger\omega\|_{\mathcal{E},\infty}))$. To validate this hypothesis, we compare the numerical solution θ^* to the AC power flow equations (5.28) with our prediction $\theta \in \bar{\Delta}_G(\arcsin(\|L^\dagger\omega\|_{\mathcal{E},\infty}))$.

Randomized test case (1000 instances)	Numerical worst-case angle differences: $\max_{\{i,j\} \in \mathcal{E}} \theta_i^* - \theta_j^* $	Analytic prediction of angle differences: $\arcsin(\ L^\dagger\omega\ _{\mathcal{E},\infty})$	Accuracy of condition: $\arcsin(\ L^\dagger\omega\ _{\mathcal{E},\infty})$ – $\max_{\{i,j\} \in \mathcal{E}} \theta_i^* - \theta_j^* $
9 bus system	0.12889 rad	0.12893 rad	$4.1218 \cdot 10^{-5}$ rad
IEEE 14 bus system	0.16622 rad	0.16650 rad	$2.7995 \cdot 10^{-4}$ rad
IEEE RTS 24	0.22309 rad	0.22480 rad	$1.7089 \cdot 10^{-3}$ rad
IEEE 30 bus system	0.16430 rad	0.16456 rad	$2.6140 \cdot 10^{-4}$ rad
New England 39	0.16821 rad	0.16828 rad	$6.6355 \cdot 10^{-5}$ rad
IEEE 57 bus system	0.20295 rad	0.22358 rad	$2.0630 \cdot 10^{-2}$ rad
IEEE RTS 96	0.24593 rad	0.24854 rad	$2.6076 \cdot 10^{-3}$ rad
IEEE 118 bus system	0.23524 rad	0.23584 rad	$5.9959 \cdot 10^{-4}$ rad
IEEE 300 bus system	0.43204 rad	0.43257 rad	$5.2618 \cdot 10^{-4}$ rad
Polish 2383 bus system (winter peak '99/'00)	0.25144 rad	0.25566 rad	$4.2183 \cdot 10^{-3}$ rad

Table 5.1: Evaluation of the synchronization condition (5.22) for ten IEEE power network test cases under volatile operating conditions. The results are averaged over 1000 instances of randomized load and generation.

Our findings and the detailed statistics are reported in Table 5.4.1. It can be observed that condition (5.22) predicts the worst-case phase cohesiveness $|\theta_i^* - \theta_j^*|$ along all transmission lines $\{i, j\} \in \mathcal{E}$ with extremely high accuracy even for large-scale networks, such as the Polish power grid model featuring 2383 nodes.

The results given in Table 5.4.1 are averaged over 1000 instances of randomized load and generation. The detailed histograms of the prediction errors

$$\arcsin(\|L^\dagger \omega\|_{\mathcal{E}, \infty}) - \max_{\{i,j\} \in \mathcal{E}} |\theta_i^* - \theta_j^*| \quad (5.30)$$

are shown in Figure 5.4 for two representative large-scale models – the IEEE 118 bus system and the Polish 2383 bus system. It can be observed that the error histogram is very narrow, it has very thin tails, and our synchronization condition (5.22) predicts the correct phase cohesiveness with high accuracy and few outliers.

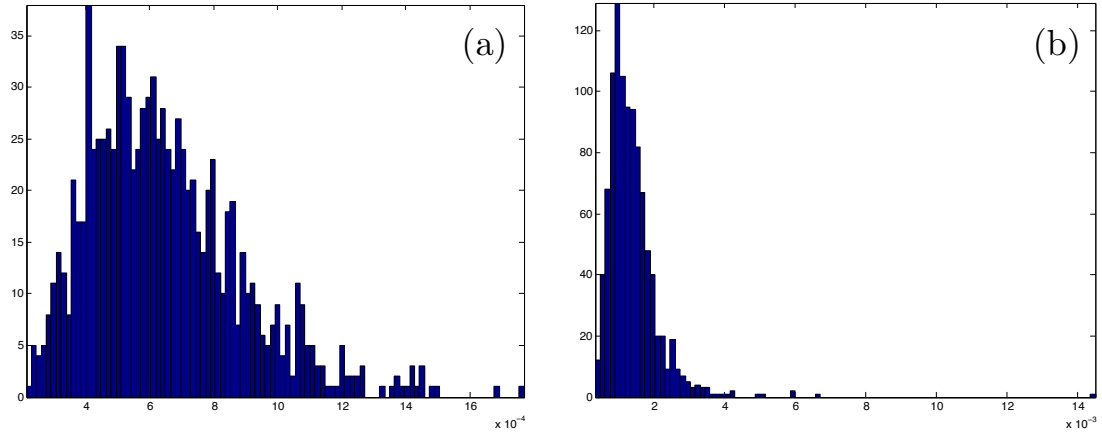


Figure 5.4: Histogram of the prediction errors

This figure shows the detailed histogram of the prediction errors (5.30) for 1000 instances of randomized load and generation. Panel (a) shows the error histogram for the the IEEE 118 bus system and the Polish 2383 bus system, and panel (b) shows the error histogram for the Polish 2383 bus system.

These conclusions can also be extended to power network models with variable parameters which account for uncertainty in load power demand or unmodeled voltage dynamics. We refer to the author’s articles [87, 89] for further details.

5.4.2 Monitoring and Contingency Screening

As a final test, we validate the synchronization condition (5.22) in a stressed power grid case study. We consider the *IEEE Reliability Test System 96* (RTS 96) illustrated in Figure 5.5. The RTS 96 is a widely adopted and relatively large-scale power network test case featuring 40 load buses and 33 generation buses. The RTS 96 has been designed as a benchmark model for power flow and stability studies, and its network and dynamic generator parameters can be found in [111].

The dynamic power system model of the RTS 96 can be obtained as structure-preserving power network model (2.1),(2.3), which is a particular instance of the coupled oscillator model (1.1), as discussed in Subsection 2.2.1. The quantities a_{ij} in the coupled oscillator model (1.1) correspond to the product of the voltage magnitudes at buses i and j as well the susceptance of the transmission line connecting buses i and j . For a given set of power injections at the buses and branch parameters, the voltage magnitudes and initial phase angles were calculated using the optimal power flow solver provided by *MATPOWER* [304]. The quantities ω_i , $i \in \mathcal{V}_3$, are the real power demands at loads, and ω_i , $i \in \mathcal{V}_1$, are the real power injections at the generators, which were found through the optimal power flow solver provided by *MATPOWER* [304].

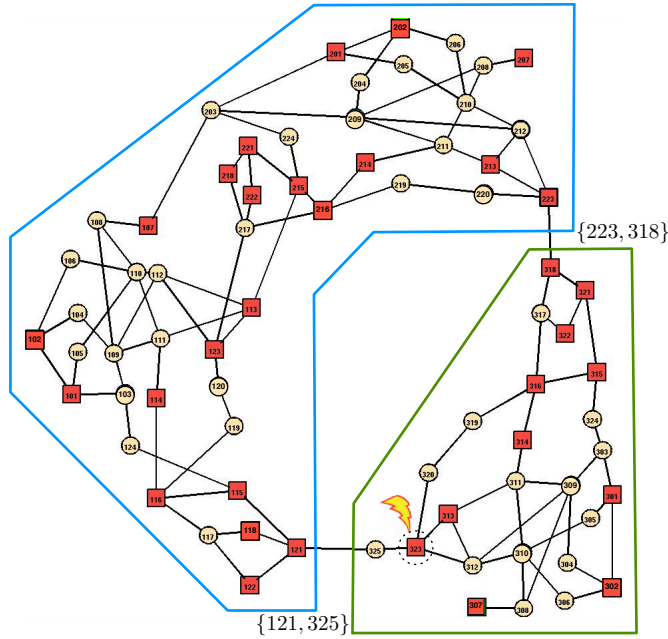


Figure 5.5: Illustration of contingencies the RTS 96 power network. This figure illustrates the RTS 96 power network and two contingencies. Here, the square nodes are generators and the round nodes are loads, large amounts of power are exported from the Northwestern (blue) area to the Southeastern (red) area, and generator 323 is tripped.

We made the following changes in order to adapt the detailed RTS 96 model to the classic structure-preserving power network model (2.1),(2.3). First, we replaced the synchronous condenser in the original RTS 96 model [111] by a U50 hydro generator. Second, since the numerical values of the damping coefficients D_i are not contained in the original RTS 96 description [111], we chose the following values to be found in [156]: for the generator damping, we chose the uniform damping coefficient $D_i = 1$ in per unit system and for $i \in \mathcal{V}_1$, and for the load

frequency coefficient we chose $D_i = 0.1$ s for $i \in \mathcal{V}_2$. Third and finally, we discarded an optional high voltage DC link for the branch $\{113, 316\}$.

We assume the following two contingencies have taken place and we characterize the remaining safety margin. First, we assume generator 323 is disconnected, possibly due to maintenance or failure events. Second, we consider the following imbalanced power dispatch situation: the power demand at each load in the Southeastern (red) area deviates from the nominally forecasted demand by a uniform and positive amount, and the resulting power deficiency is compensated by uniformly increasing the generation in the Northwestern (blue) area. This imbalance can arise, for example, due to a shortfall in predicted load and renewable energy generation. Correspondingly, power is exported from the Northwestern to the Southeastern area via the transmission lines $\{121, 325\}$ and $\{223, 318\}$.

At a nominal operating condition, the RTS 96 power network is sufficiently robust to tolerate each single one of these two contingencies, but the safety margin is now minimal. When both contingencies are combined, then our synchronization condition (5.22) predicts that the thermal limit of the transmission line $\{121, 325\}$ is reached at an additional loading of 22.20%. Indeed, the dynamic simulation scenario shown in Figure 5.6 validates the accuracy of this prediction. It can be observed, that synchronization is lost for an additional loading of 22.33%, and the areas separate via the transmission line $\{121, 325\}$. This separation triggers a

cascade of events, such as the outage of the transmission line {223, 318}, and the power network is en route to a blackout.

In the power system literature, the above scenario is sometimes referred to as a *limit-induced bifurcation* [79, 113] since the loss of synchrony is triggered by the thermal constraints limiting the maximal power transfer. We remark that, if generator 323 is not disconnected and there are no thermal limit constraints, then, by increasing the loading, we observe the classic loss of synchrony through a saddle-node bifurcation [78]. Also this bifurcation can be predicted accurately by our synchronization condition (5.22), see the the author's article [89] for a detailed description. In summary, this transmission line scenario illustrates the accuracy and applicability of the proposed synchronization condition (5.22)

5.4.3 Further Applications

The results in this section confirm the validity, the applicability, and the accuracy of the synchronization condition (5.22) in complex power network scenarios.

We envision that our analysis and the proposed synchronization condition (5.22) finds further applications in power networks. Together with collaborators the author further exploited the insights obtained in Section 5.3 to develop new control and analysis methods for power network applications. In particular, we identified a tight connection between the solutions of the AC power flow

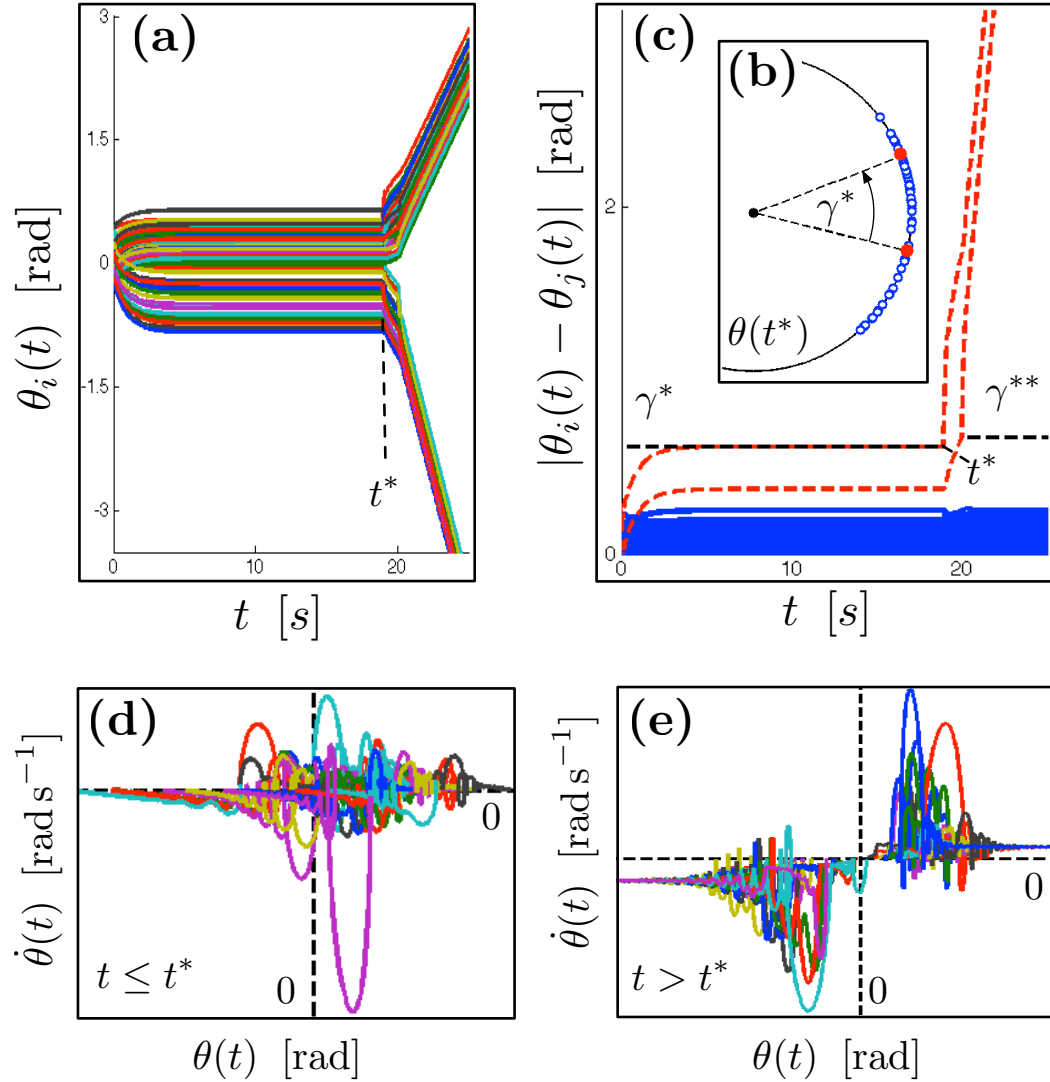


Figure 5.6: The RTS 96 dynamics at the transition to instability. The RTS 96 dynamics for a continuous load increase from 22.19% to 22.24%. Subfigure (a) shows the angles $\theta(t)$ which lose synchrony at $t^* = 18.94$ s, when the thermal limit $\gamma^* = 0.1977$ rad of the transmission line $\{121, 325\}$ is reached. Subfigure (b) shows the angles $\theta(t)$ at $t = t^*$. Subfigure (c) depicts the angular distances and the thermal limits γ^* and γ^{**} , where the lines $\{121, 325\}$ and $\{223, 318\}$ are plotted as dashed curves. Subfigures (d) and (e) show the generator phase space $(\theta(t), \dot{\theta}(t))$ before and after t^* , where the loss of a common synchronization frequency can be observed.

equations (5.28) and the DC power flow equations (5.29) through the arcsin-nonlinearity. These insights can be further exploited to develop an improved DC power flow approximation, see [87] for details. Our analysis of coupled oscillator models and the resulting synchronization condition (5.22) can be directly exploited in the analysis and control design of drooped-controlled inverters in microgrids. We refer the reader to [32, 248–251] for further details on primary and secondary control design strategies and connections to coupled oscillator networks.

Finally, we envision further applications of the results developed in this chapter to the following power network problems: security-constrained optimal power flow, design of remedial action schemes (in particular islanding and load shedding), online contingency screening, continuous control design for FACTS (flexible AC transmission system) devices, and primary and secondary control strategies.

Chapter 6

Conclusions

In this thesis we studied synchronization in complex oscillator networks and applications in electric power grids. On the theory side, we studied homogeneous and heterogeneous oscillator networks, with finite or infinite-dimensional oscillator populations, and with complete or complex interaction topologies. Additionally, we showed how our theoretic results can be applied to different power system problems and different dynamic power network models.

In the following two sections, we summarize the contributions of this thesis, we briefly summarize a few of the author's side projects related to the contents of this thesis, and we suggest a few directions for future research.

6.1 Summary

Synchronization in networks of coupled oscillators is a pervasive topic in various scientific disciplines. Within the rich modeling phenomenology on synchro-

nization among coupled oscillators and within the broad range of application domains, we focused on the coupled oscillator model

$$\begin{aligned} M_i \ddot{\theta}_i + D_i \dot{\theta}_i &= \omega_i - \sum_{j=1}^n a_{ij} \sin(\theta_i - \theta_j), & i \in \mathcal{V}_1, \\ D_i \dot{\theta}_i &= \omega_i - \sum_{j=1}^n a_{ij} \sin(\theta_i - \theta_j), & i \in \mathcal{V}_2 \end{aligned}$$

and its applications in electric power networks.

In Chapter 1, we gave a broad motivation for the study of complex oscillator networks, we emphasized the importance of the synchronization problem in power networks, and we outlined the contents and contributions of this thesis.

In Chapter 2, we reviewed several applications of the coupled oscillator model and showed how dynamic power network models can be naturally cast as coupled oscillators. Additionally, we discussed different synchronization notions and introduced some analysis methods from algebraic graph theory and consensus protocols, which proved to be valuable tools throughout this thesis.

In Chapter 3, we studied static and dynamic relationships between mechanical and kinematic oscillator models. We established the local topological equivalence between these models and proved that they feature the same synchronization conditions independent of the inertial terms. Next, we showed that mechanical oscillator networks can be dynamically approximated by kinematic oscillator networks, provided that the mechanical oscillators are strongly overdamped. We concluded

our analysis in Chapter 3 with a word of caution and demonstrated that the qualitative dynamic behavior of the two models can be severely different in some cases. Finally, we discussed the applicability of these results to power network models.

In Chapter 4, we studied the classic Kuramoto model. We discussed different synchronization notions, we related different synchronization metrics, and reviewed various estimations on the critical coupling strength. We also established an explicit, necessary, and sufficient synchronization condition for Kuramoto oscillators with natural frequencies supported on a compact interval. Our main result also included tight estimates of the region of attraction and the asymptotic performance metrics achieved by the oscillator network. We further extended this result to higher-order multi-rate Kuramoto oscillators. Finally, we presented an extension of the results and the analysis framework contained in this chapter to non-uniform Kuramoto models and network-reduced power system models.

In Chapter 5, we analyzed heterogeneous oscillators interacting through a complex network. We reviewed numerous synchronization conditions based on different metrics quantifying the coupling and the heterogeneity in the network. We presented a set of necessary and a set of sufficient conditions for synchronization. We proposed a novel algebraic analysis approach emphasizing the role of cycles and cut-sets in the graph. Our approach suggests a novel synchronization condition, which significantly improves upon the existing conditions advocated thus far.

The proposed condition is provably exact for various interesting network topologies and parameters, and it is statistically correct for a broad range of nominal random network models. Finally, we illustrated the practical applicability of our proposed condition in complex networks scenarios and in smart grid applications.

6.2 Tangential and Related Contributions

In this subsection, we briefly summarize the author's side projects that are related to the contributions of this thesis.

Kron reduction: In order to relate synchronization conditions in network-reduced power system models (2.5)-(2.6) and in the associated structure-preserving model, we studied the Kron reduction process relating the two models [80,82]. On the matrix-theoretic side, Kron reduction is based on a Schur complement of the graph Laplacian matrix. Since graph-theoretic modeling and model reduction is an interesting topic in its own right, we also studied the Kron reduction process in a more general framework and from a purely theoretic perspective [86].

Control of inverters in microgrids: Microgrids are autonomously managed low-voltage distribution networks that can operate in an islanded mode, that is, disconnected from the main transmission grid. Microgrids typically feature multiple small heterogeneous power sources (possibly of DC type) that are interfaced

with the microgrid through power converters (or simply inverters). These inverters are controlled voltage sources. In Subsection 2.2.1, we showed that the classic frequency droop control [46,275] gives rise to the closed-loop dynamics (2.2), which are an instance of the coupled oscillator model (1.1). In subsequent work, we investigated the stability of this closed loop [248], designed secondary controllers for frequency restoration [32,249], implemented them in simulations and experimental testbeds [251], and also studied voltage droop control strategies [250].

Slow Coherency and Wide-Area Control: Bulk power systems typically exhibit multiple electromechanical oscillations. Of particular interest are inter-area oscillations, which are associated with the dynamics of power transfers and involve groups of generators oscillating relative to each other. In the classic slow coherency and area aggregation problem [59,60], groups of coherently swinging generators are aggregated to equivalent machines and a reduced model is constructed. Given our insights into the power network dynamics, we revisited this model reduction process using consensus methods and algebraic graph theory [229]. Since inter-area oscillations are only poorly controllable by means of local control, we further designed a distributed wide-area controllers. The design relies on simultaneous optimization of the communication architecture and the closed-loop performance, and it yields optimal controllers with sparse communication structures [90,91].

Monitoring and cyber-physical security: Distributed control strategies are enabled and complemented by distributed estimation, monitoring, and information fusion. We developed a distributed estimation algorithm based on local continuous-time filtering and information fusion at discrete time instants, and we applied it to sensor and power transmission networks [92,93]. Finally, a major concern in the implementation of distributed algorithms is cyber-physical security. We proposed a mathematical framework for cyber-physical systems subject to attacks affecting their control, communication, and monitoring system. We established the fundamental limitations of attack detection and identification systems, we designed centralized and distributed attack detection and identification monitors, and we applied our results to sensor, water, and power networks [212–214].

6.3 Future Research Directions

Despite the vast literature, the countless applications, and the numerous theoretical results on the synchronization properties of model (1.1), many interesting and important problems are still open. In the following, we summarize limitations of the existing analysis approaches and present a few worthwhile directions for future research with particular emphasis on power network applications.

Asymmetric interactions: Most of the results presented in this thesis can be extended to more general anti-symmetric and 2π -periodic coupling functions as long as the coupling is diffusive and bidirectional. In some applications, the coupling topology is inherently directed, such as transcriptional, metabolic, or neuronal networks [176]. In this case, there are only a few theoretical investigations including ring graphs [118, 227], results on the synchronization frequency [19, 85], and statistical analysis of large graphs [223]. Also, in many applications the coupling between the oscillators is not purely diffusive. For instance, mutual excitatory or inhibitory synaptic organizations in neuroscience [70], time delays in sensor networks [247], or transfer conductances in power networks [50] lead to a shifted coupling of the form $\sin(\theta_i - \theta_j - \varphi_{ij})$ with $\varphi_{ij} \in [-\pi/2, \pi/2]$. In these cases and also for other “skewed” or “symmetry-breaking” interactions among the oscillators, many of the presented analysis schemes either fail or lead to overly conservative results. In summary, the extension of the present work to symmetry-breaking coupling functions is a challenging yet tremendously important problem.

Pulse coupling: Though not related to power network applications, another interesting class of oscillator networks are systems of pulse-coupled oscillators featuring hybrid dynamics: impulsive coupling at discrete time instants and uncoupled continuous dynamics otherwise [184]. This class of oscillator networks displays a very interesting phenomenology which is qualitatively different from

diffusive and continuous coupling, see [177]. For instance, the behavior of identical oscillators coupled in a complete graph strongly depends on the curvature of the uncoupled dynamics. As discussed in Subsection 2.2.2, such pulse-coupled oscillator models can be reduced to the canonical model (2.12) through a phase reduction and averaging analysis. For certain pulse-coupled oscillators the coupling functions $h_{ij}(\cdot)$ turn out to be monotone and discontinuous, and they result in finite-time convergent dynamics [161, 178]. Most of the results and analysis methods known for continuously-coupled oscillators still need to be extended to pulse-coupled oscillators, especially in the case of dissimilar natural frequencies.

Transient dynamics: For dissimilar oscillators, most results presented here pertain to existence, uniqueness, and local stability of synchronous solutions, with the exception of Theorems 4.4.2 and 5.2.2. In a next major step, the rich transient dynamics in oscillator networks need to be analyzed. Such an investigation is of tremendous value for transient stability problems in volatile power grids. The on-line assessment of transient stability (in real-time) is one of the major outstanding problems in power system stability studies and in industrial applications [48, 50].

Even for the classic Kuramoto model (1.2), many problems pertaining to the transient dynamics still need to be fully resolved. For instance, most known estimates on the region of attraction of a synchronized solution are conservative, such as the semi-circle estimates given in Theorems 2.4.2 and 4.4.2. We refer

to [50, 293] for a set of interesting results and conjectures on the region of attraction. As shown in Theorem 4.4.2, for complete graphs, the region of attraction of a synchronous solution always includes $\Delta_G(\pi/2)$ for any $K > K_{\text{critical}}$. It is unclear if an analogous result holds for sparse graphs or if the region of attraction severely depends on the topology. When the Kuramoto dynamics (1.2) are subject to additive noise, they can be analyzed through Fokker-Planck equations similar to the continuum-limit model (4.3)-(4.4) or in the limit of small stochastic perturbations, see [21, 76]. In this case, there are various interesting transitions between wells of the potential landscape and only few analytic investigations. Also the sub-synchronous regime for $K < K_{\text{critical}}$ is vastly unexplored, and partial synchronization or clustering (similar to the partially-synchronized state for infinite-dimensional models) [5, 74] or chaotic motion [172, 218, 264, 273] can occur.

Finally, the incremental stability results referenced in Subsection 4.4.1 appear to be a promising direction that still needs to be fully explored.

Higher-order and state space oscillators: For the mechanical analog in Figure 1.1, the power network models detailed in Subsection 2.2.1, and the previously listed applications [26, 96, 117, 120, 130, 144, 211, 224, 246, 261, 292, 303], the coupled oscillator dynamics are of second order as in (1.1a). The analysis of second-order oscillator networks has also received a lot of attention and many tools can be extended from first to second-order dynamics, see Chapter 3 for the local

topological equivalence of first and second-order oscillator networks, the singular perturbation approximation, and a comprehensive literature overview.

As shown in Subsection 3.3.4, the transient dynamics of second-order oscillator networks have their own characteristics, especially for large inertia and small damping. Thus, many of the presented results and the analysis of the transient dynamics still need to be extended to second-order oscillator networks. In other oscillator network models, there is no readily available phase variable to describe the limit cycle dynamics of the coupled system, and the model (1.1) is valid only after a phase reduction and averaging analysis. Since features of the original model may be poorly preserved in the canonical model (2.12), a direct analysis of the state space model is preferred. In the case of linear or passive systems, state or output synchronization are well understood [17, 38, 171, 289], but the analysis of synchronization problems in more general heterogeneous state space oscillator networks remains a challenging and important problem.

Sparse and heterogeneous networks: Despite the vast scientific interest the quest for sharp, concise, and closed-form synchronization conditions for arbitrary connected graphs has been so far in vain. As suggested by our discussion in Chapter 5, the proper metric for the analysis of synchronization problem appears to be the incremental ∞ -norm. In the author's opinion, an analysis with the incremental ∞ -norm will most likely deliver the sharpest possible conditions. We

believe that the norm and cycle constraints developed in Section 5.3 are a fruitful approach towards a more complete understanding of sparse topologies.

For the transient analysis, the ℓ_∞ -type contraction Lyapunov function (4.23) is a powerful analysis concept for complete graphs and still needs to be extended to arbitrary connected graphs. Regarding the potential and equilibrium landscape, a few interesting and still unresolved conjectures can be found in [16, 22, 154, 179, 269] and pertain to the number of (stable) equilibria and topological properties of the equilibrium set. Finally, the complex networks and statistical physics communities found various interesting scaling laws in their statistical and numerical analyses of random graph models, such as conditions depending on the spectral ratio λ_2/λ_n of the Laplacian eigenvalues, interesting results for correlations between the degree deg_i and the natural frequency ω_i , and degree-dependent synchronization conditions [18, 31, 108, 143, 192, 198, 222, 253]. It is unclear which of these results and findings are amenable to an analytic and quantitative investigation.

Specific applications in power networks: This thesis focused primarily on the analysis of synchronization in complex oscillator networks and power grids. In Subsection 5.4.2, we also showed how our results can be used for contingency screening. We believe that there is great potential to use our results not only for online monitoring purposes but also for remedial action schemes, such as islanding and load shedding. In Subsection 5.4.1, we outlined how our proposed

synchronization condition can be related to predict solutions to the AC power flow equations via the DC power flow equations, see also [87]. We believe that these insights are of great value in applications, where the numerical solution to the AC power flow is computationally expensive or even unfeasible, such as real-time security assessment, transmission planning, or large-scale power flow optimization, among others. Finally, we recently turned our analysis insights into control design strategies for inverters in microgrids [32, 248–250]. We found that synchronization theory provides a valuable tool for the analysis and control of microgrids. Some open and important problems include analysis and control of network models with conductances and with coupled active and reactive power flows.

We sincerely hope that the results contained in this thesis stimulate further research on synchronization in coupled oscillators. We believe that the identified connection between coupled oscillators and electric power networks provides a fruitful ground for exciting interdisciplinary research problems, both on the theoretical side as well as in the challenging and inspiring power network applications.

Bibliography

- [1] A. A. Abidi and L. O. Chua. On the dynamics of Josephson-junction circuits. *IEE Journal on Electronic Circuits and Systems*, 3(4):186–200, 1979.
- [2] J. A. Acebrón, L. L. Bonilla, and R. Spigler. Synchronization in populations of globally coupled oscillators with inertial effects. *Physical Review E*, 62(3):3437–3454, 2000.
- [3] J. A. Acebrón, L. L. Bonilla, C. J. P. Vicente, F. Ritort, and R. Spigler. The Kuramoto model: A simple paradigm for synchronization phenomena. *Reviews of Modern Physics*, 77(1):137–185, 2005.
- [4] Robert Adler. A study of locking phenomena in oscillators. *Proceedings of the IRE*, 34(6):351–357, 1946.
- [5] D. Aeyels and J. A. Rogge. Existence of partial entrainment and stability of phase locking behavior of coupled oscillators. *Progress on Theoretical Physics*, 112(6):921–942, 2004.
- [6] L. F. C. Alberto and N. G. Bretas. Synchronism versus stability in power systems. *Electrical Power and Energy Systems*, 21(4):261–267, 1999.
- [7] L. F. C. Alberto and N. G. Bretas. Required damping to assure multiswing transient stability: the SMIB case. *International Journal of Electrical Power & Energy Systems*, 22(3):179–185, 2000.
- [8] L. F. C. Alberto, F. H. J. R. Silva, and N. G. Bretas. Direct methods for transient stability analysis in power systems: state of art and future perspectives. In *IEEE Power Tech Proceedings*, Porto, Portugal, September 2001.
- [9] LFC Alberto and NG Bretas. Damping estimation for multi-swing transient stability analysis: the omib case. In *International Conference on Power System Technology*, volume 2, pages 1383–1387. IEEE, 1998.
- [10] F. Alvarez. On the minimizing property of a second order dissipative system in Hilbert spaces. *SIAM Journal on Control and Optimization*, 38(4):1102–1119, 2000.

- [11] P. M. Anderson and A. A. Fouad. *Power System Control and Stability*. Iowa State University Press, 1977.
- [12] P. M. Anderson and A. A. Fouad. *Power System Control and Stability*. Wiley, 2 edition, 2002.
- [13] G. Andersson, P. Donalek, R. Farmer, N. Hatziargyriou, I. Kamwa, P. Kundur, N. Martins, J. Paserba, P. Pourbeik, J. Sanchez-Gasca, R. Schulz, A. Stankovic, C. Taylor, and V. Vittal. Causes of the 2003 major grid blackouts in North America and Europe, and recommended means to improve system dynamic performance. *IEEE Transactions on Power Systems*, 20(4):1922–1928, 2005.
- [14] D. Angeli. A Lyapunov approach to incremental stability properties. *IEEE Transactions on Automatic Control*, 47(3):410–421, 2002.
- [15] S. Aoi and K. Tsuchiya. Locomotion control of a biped robot using nonlinear oscillators. *Autonomous Robots*, 19(3):219–232, 2005.
- [16] A. Araposthatis, S. Sastry, and P. Varaiya. Analysis of power-flow equation. *International Journal of Electrical Power & Energy Systems*, 3(3):115–126, 1981.
- [17] M. Arcak. Passivity as a design tool for group coordination. *IEEE Transactions on Automatic Control*, 52(8):1380–1390, 2007.
- [18] A. Arenas, A. Díaz-Guilera, J. Kurths, Y. Moreno, and C. Zhou. Synchronization in complex networks. *Physics Reports*, 469(3):93–153, 2008.
- [19] A. E. Ati and E. Panteley. On frequency synchronization of kuramoto model with non-symmetric interconnection structure. In *Int. Conf. on Communications, Computing and Control Applications*, Hammamet, Tunisia, March 2012.
- [20] H. Attouch and P.E. Maingé. Asymptotic behavior of second-order dissipative evolution equations combining potential with non-potential effects. *ESAIM: Control, Optimisation and Calculus of Variations*, 2010. To appear.
- [21] B. C. Bag, K. G. Petrosyan, and C. K. Hu. Influence of noise on the synchronization of the stochastic Kuramoto model. *Physical Review E*, 76(5):056210, 2007.
- [22] J. Baillieul and C. I. Byrnes. Geometric critical point analysis of loss-less power system models. *IEEE Transactions on Circuits and Systems*, 29(11):724–737, 1982.

- [23] R. Baldoni, A. Corsaro, L. Querzoni, S. Scipioni, and S. T. Piergiovanni. Coupling-based internal clock synchronization for large-scale dynamic distributed systems. *IEEE Transactions on Parallel and Distributed Systems*, 21(5):607–619, 2010.
- [24] N. J. Balmforth and R. Sassi. A shocking display of synchrony. *Physica D: Nonlinear Phenomena*, 143(1):21–55, 2000.
- [25] S. Barbarossa and G. Scutari. Decentralized maximum-likelihood estimation for sensor networks composed of nonlinearly coupled dynamical systems. *IEEE Transactions on Signal Processing*, 55(7):3456–3470, 2007.
- [26] M. Bennett, M. F. Schatz, H. Rockwood, and K. Wiesenfeld. Huygens’s clocks. *Proceedings: Mathematical, Physical and Engineering Sciences*, 458(2019):563–579, 2002.
- [27] A. R. Bergen and D. J. Hill. A structure preserving model for power system stability analysis. *IEEE Transactions on Power Apparatus and Systems*, 100(1):25–35, 1981.
- [28] D. S. Bernstein. *Matrix Mathematics*. Princeton University Press, 2 edition, 2009.
- [29] N. Biggs. *Algebraic Graph Theory*. Cambridge University Press, 2 edition, 1994.
- [30] N. Biggs. Algebraic potential theory on graphs. *Bulletin of the London Mathematical Society*, 29(6):641–683, 1997.
- [31] S. Boccaletti, V. Latora, Y. Moreno, M. Chavez, and D. U. Hwang. Complex networks: Structure and dynamics. *Physics Reports*, 424(4-5):175–308, 2006.
- [32] H. Bouattour, J. W. Simpson-Porco, F. Dörfler, and F. Bullo. Further results on distributed secondary control in microgrids. In *IEEE Conf. on Decision and Control*, Florence, Italy, December 2013. To appear.
- [33] J. C. Bronski, L. DeVille, and M. Jip Park. Fully synchronous solutions and the synchronization phase transition for the finite- n Kuramoto model. *Chaos: An Interdisciplinary Journal of Nonlinear Science*, 22(3):033133, 2012.
- [34] E. Brown, P. Holmes, and J. Moehlis. Globally coupled oscillator networks. In E. Kaplan, J. E. Marsden, and K. R. Sreenivasan, editors, *Perspectives and Problems in Nonlinear Science: A Celebratory Volume in Honor of Larry Sirovich*, pages 183–215. Springer, 2003.

- [35] E. Brown, J. Moehlis, and P. Holmes. On the phase reduction and response dynamics of neural oscillator populations. *Neural Computation*, 16(4):673–715, 2004.
- [36] J. Buck. Synchronous rhythmic flashing of fireflies. II. *Quarterly Review of Biology*, 63(3):265–289, 1988.
- [37] F. Bullo, J. Cortés, and S. Martínez. *Distributed Control of Robotic Networks*. Princeton University Press, 2009.
- [38] M. Bürger, D. Zelazo, and F. Allgöwer. Hierarchical clustering of dynamical networks using a saddle-point analysis. *IEEE Transactions on Automatic Control*, 2012. to appear.
- [39] Mathias Bürger, Daniel Zelazo, and Frank Allgöwer. Duality and network theory in passivity-based cooperative control. *arXiv preprint arXiv:1301.3676*, 2013.
- [40] L. Buzna, S. Lozano, and A. Diaz-Guilera. Synchronization in symmetric bipolar population networks. *Physical Review E*, 80(6):66120, 2009.
- [41] G. C. Calafiore, F. Dabbene, and R. Tempo. Research on probabilistic methods for control system design. *Automatica*, 47(7):1279–1293, 2011.
- [42] E. Canale and P. Monzón. Almost global synchronization of symmetric Kuramoto coupled oscillators. In *Systems Structure and Control*, chapter 8, pages 167–190. InTech Education and Publishing, 2008.
- [43] E. A. Canale, P. Monzón, and F. Robledo. On the complexity of the classification of synchronizing graphs. In *Grid and Distributed Computing, Control and Automation*, pages 186–195, Jeju Island, Korea, December 2010.
- [44] E. A. Canale, P. A. Monzón, and F. Robledo. The wheels: an infinite family of bi-connected planar synchronizing graphs. In *IEEE Conf. Industrial Electronics and Applications*, pages 2204–2209, Taichung, Taiwan, June 2010.
- [45] D. Carlson and H. Schneider. Inertia theorems for matrices: The semidefinite case. *Journal of Mathematical Analysis and Applications*, 6:430–446, 1963.
- [46] M. C. Chandorkar, D. M. Divan, and R. Adapa. Control of parallel connected inverters in standalone AC supply systems. *IEEE Transactions on Industry Applications*, 29(1):136–143, 1993.
- [47] K. S. Chandrashekar and D. J. Hill. Cutset stability criterion for power systems using a structure-preserving model. *International Journal of Electrical Power & Energy Systems*, 8(3):146–157, 1986.

- [48] H.-D. Chiang. *Direct Methods for Stability Analysis of Electric Power Systems*. Wiley, 2011.
- [49] H.-D. Chiang and C. C. Chu. Theoretical foundation of the BCU method for direct stability analysis of network-reduction power system models with small transfer conductances. *IEEE Transactions on Circuits and Systems I: Fundamental Theory and Applications*, 42(5):252–265, 1995.
- [50] H.-D. Chiang, C. C. Chu, and G. Cauley. Direct stability analysis of electric power systems using energy functions: Theory, applications, and perspective. *Proceedings of the IEEE*, 83(11):1497–1529, 1995.
- [51] H. D. Chiang and F. F. Wu. Stability of nonlinear systems described by a second-order vector differential equation. *IEEE Transactions on Circuits and Systems*, 35(6):703–711, 2002.
- [52] H.-D. Chiang, F. F. Wu, and P. P. Varaiya. Foundations of the potential energy boundary surface method for power system transient stability analysis. *IEEE Transactions on Circuits and Systems*, 35(6):712–728, 1988.
- [53] H.D. Chiang and M.E. Baran. On the existence and uniqueness of load flow solution for radial distribution power networks. *IEEE Transactions on Circuits and Systems*, 37(3):410–416, 1990.
- [54] H. Chiba. A proof of the Kuramoto’s conjecture for a bifurcation structure of the infinite dimensional Kuramoto model, August 2010. Available at <http://arxiv.org/abs/1008.0249>.
- [55] Y. P. Choi, S. Y. Ha, S. Jung, and Y. Kim. Asymptotic formation and orbital stability of phase-locked states for the Kuramoto model. *Physica D: Nonlinear Phenomena*, 241(7):735–754, 2011.
- [56] Y. P. Choi, S. Y. Ha, M. Kang, and M. Kang. Exponential synchronization of finite-dimensional Kuramoto model at critical coupling strength. *Communications in Mathematical Sciences*, 11(2):385–401, 2013.
- [57] Y.-P. Choi, S.-Y. Ha, and S.-B. Yun. Complete synchronization of Kuramoto oscillators with finite inertia. *Physica D*, 240(1):32–44, 2011.
- [58] N. Chopra and M. W. Spong. On exponential synchronization of Kuramoto oscillators. *IEEE Transactions on Automatic Control*, 54(2):353–357, 2009.
- [59] J. H. Chow, J. J. Allemong, and P. V. Kokotović. Singular perturbation analysis of systems with sustained high frequency oscillations. *Automatica*, 14(3):271–279, 1978.
- [60] J. H. Chow and P. Kokotović. Time scale modeling of sparse dynamic networks. *IEEE Transactions on Automatic Control*, 30(8):714–722, 1985.

- [61] C. C. Chu. *Transient Dynamics of Electric Power Systems: Direct Stability Assessment and Chaotic Motions*. PhD thesis, Cornell University, 1996.
- [62] C.C. Chu and H.D. Chiang. Constructing analytical energy functions for lossless network-reduction power system models: Framework and new developments. *Circuits, Systems, and Signal Processing*, 18(1):1–16, 1999.
- [63] C.C. Chu and H.D. Chiang. Boundary properties of the BCU method for power system transient stability assessment. In *IEEE Int. Symposium on Circuits and Systems*, pages 3453–3456, Paris, France, May 2010.
- [64] S. J. Chung and J. J. Slotine. On synchronization of coupled Hopf-Kuramoto oscillators with phase delays. In *IEEE Conf. on Decision and Control*, pages 3181–3187, Atlanta, GA, USA, December 2010.
- [65] E. A. Coayla-Teran, S. E. A. Mohammed, and P. R. C. Ruffino. Hartman-Grobman theorems along hyperbolic stationary trajectories. *Dynamical Systems*, 17(2):281–292, 2007.
- [66] George Constable and Bob Somerville. *A Century of Innovation: The Engineering That Transformed Our Lives*. Joseph Henry Pr, 2003.
- [67] L. Contevelle and E. Panteley. Linear reformulation of the Kuramoto model: Asymptotic mapping and stability properties. In *Int. Conf. on Communications, Computing and Control Applications*, Hammamet, Tunisia, March 2012.
- [68] S. Corsi and C. Sabelli. General blackout in Italy Sunday September 28, 2003, h. 03: 28: 00. In *IEEE Power & Energy Society General Meeting*, pages 1691–1702, Denver, CO, June 2004.
- [69] J. D. Crawford. Amplitude expansions for instabilities in populations of globally-coupled oscillators. *Journal of statistical physics*, 74(5):1047–1084, 1994.
- [70] S. M. Crook, G. B. Ermentrout, M. C. Vanier, and J. M. Bower. The role of axonal delay in the synchronization of networks of coupled cortical oscillators. *Journal of Computational Neuroscience*, 4(2):161–172, 1997.
- [71] D. Cumin and C. P. Unsworth. Generalising the Kuramoto model for the study of neuronal synchronisation in the brain. *Physica D: Nonlinear Phenomena*, 226(2):181–196, 2007.
- [72] H. Daido. Quasientrainment and slow relaxation in a population of oscillators with random and frustrated interactions. *Physical Review Letters*, 68(7):1073–1076, 1992.

- [73] R. De Luca. Strongly coupled overdamped pendulums. *Revista Brasileira de Ensino de Física*, 30:4304–4304, 2008.
- [74] F. De Smet and D. Aeyels. Partial entrainment in the finite Kuramoto–Sakaguchi model. *Physica D: Nonlinear Phenomena*, 234(2):81–89, 2007.
- [75] A. H. Dekker and R. Taylor. Synchronization properties of trees in the Kuramoto model. *SIAM Journal on Applied Dynamical Systems*, 12(2):596–617, 2013.
- [76] L. DeVille. Transitions amongst synchronous solutions for the stochastic Kuramoto model. *Nonlinearity*, 25(5):1–20, 2011.
- [77] A. L. Do, S. Boccaletti, and T. Gross. Graphical notation reveals topological stability criteria for collective dynamics in complex networks. *Physical Review Letters*, 108(19):194102, 2012.
- [78] I. Dobson. Observations on the geometry of saddle node bifurcation and voltage collapse in electrical power systems. *IEEE Transactions on Circuits and Systems I: Fundamental Theory and Applications*, 39(3):240–243, 1992.
- [79] Ian Dobson and Liming Lu. Voltage collapse precipitated by the immediate change in stability when generator reactive power limits are encountered. *Circuits and Systems I: Fundamental Theory and Applications, IEEE Transactions on*, 39(9):762–766, 1992.
- [80] F. Dörfler and F. Bullo. Spectral analysis of synchronization in a lossless structure-preserving power network model. In *IEEE Int. Conf. on Smart Grid Communications*, pages 179–184, Gaithersburg, MD, USA, October 2010.
- [81] F. Dörfler and F. Bullo. Synchronization and transient stability in power networks and non-uniform Kuramoto oscillators. In *American Control Conference*, pages 930–937, Baltimore, MD, USA, June 2010. Extended version available at <http://arxiv.org/abs/0910.5673>.
- [82] F. Dörfler and F. Bullo. Synchronization of power networks: Network reduction and effective resistance. In *IFAC Workshop on Distributed Estimation and Control in Networked Systems*, pages 197–202, Annecy, France, September 2010.
- [83] F. Dörfler and F. Bullo. On the critical coupling for Kuramoto oscillators. *SIAM Journal on Applied Dynamical Systems*, 10(3):1070–1099, 2011.
- [84] F. Dörfler and F. Bullo. Exploring synchronization in complex oscillator networks. In *IEEE Conf. on Decision and Control*, pages 7157–7170, Maui, HI, USA, December 2012.

- [85] F. Dörfler and F. Bullo. Synchronization and transient stability in power networks and non-uniform Kuramoto oscillators. *SIAM Journal on Control and Optimization*, 50(3):1616–1642, 2012.
- [86] F. Dörfler and F. Bullo. Kron reduction of graphs with applications to electrical networks. *IEEE Transactions on Circuits and Systems I: Regular Papers*, 60(1):150–163, 2013.
- [87] F. Dörfler and F. Bullo. Novel insights into lossless AC and DC power flow. In *IEEE Power & Energy Society General Meeting*, Vancouver, BC, Canada, July 2013. To appear.
- [88] F. Dörfler and F. Bullo. Synchronization in complex oscillator networks: A survey. *Automatica*, April 2013. Submitted.
- [89] F. Dörfler, M. Chertkov, and F. Bullo. Synchronization in complex oscillator networks and smart grids. *Proceedings of the National Academy of Sciences*, 110(6):2005–2010, 2013.
- [90] F. Dörfler, M. Jovanović, M. Chertkov, and F. Bullo. Sparse and optimal wide-area damping control in power networks. In *American Control Conference*, pages 4295–4300, Washington, DC, USA, June 2013.
- [91] F. Dörfler, M. Jovanović, M. Chertkov, and F. Bullo. Sparsity-promoting optimal wide-area control of power networks. *IEEE Transactions on Power Systems*, July 2013. Submitted.
- [92] F. Dörfler, F. Pasqualetti, and F. Bullo. Distributed detection of cyber-physical attacks in power networks: A waveform relaxation approach. In *Allerton Conf. on Communications, Control and Computing*, pages 1486–1491, Allerton, IL, USA, September 2011.
- [93] F. Dörfler, F. Pasqualetti, and F. Bullo. Continuous-time distributed observers with discrete communication. *IEEE Journal of Selected Topics in Signal Processing*, 7(2):296–304, 2013.
- [94] P. G. Doyle and J. L. Snell. *Random Walks and Electric Networks*. Mathematical Association of America, 1984.
- [95] G. B. Ermentrout. Synchronization in a pool of mutually coupled oscillators with random frequencies. *Journal of Mathematical Biology*, 22(1):1–9, 1985.
- [96] G. B. Ermentrout. An adaptive model for synchrony in the firefly *pteroptyx malaccae*. *Journal of Mathematical Biology*, 29(6):571–585, 1991.
- [97] G. B. Ermentrout and N. Kopell. Frequency plateaus in a chain of weakly coupled oscillators, I. *SIAM Journal on Mathematical Analysis*, 15(2):215–237, 1984.

- [98] M. Fiedler. Algebraic connectivity of graphs. *Czechoslovak Mathematical Journal*, 23(2):298–305, 1973.
- [99] G. Filatrella, A. H. Nielsen, and N. F. Pedersen. Analysis of a power grid using a Kuramoto-like model. *The European Physical Journal B*, 61(4):485–491, 2008.
- [100] V. Fioriti, S. Ruzzante, E. Castorini, E. Marchei, and V. Rosato. Stability of a distributed generation network using the Kuramoto models. In *Critical Information Infrastructure Security*, Lecture Notes in Computer Science, pages 14–23. Springer, 2009.
- [101] F. Forni and R. Sepulchre. A differential Lyapunov framework for contraction analysis, 2012. Available at <http://arxiv.org/abs/1208.2943>.
- [102] A. Franci, A. Chaillet, and W. Pasillas-Lépine. Phase-locking between Kuramoto oscillators: Robustness to time-varying natural frequencies. In *IEEE Conf. on Decision and Control*, pages 1587–1592, Atlanta, GA, USA, December 2010.
- [103] B. A. Francis. Distributed control of autonomous mobile robots. Course Notes, Version 1.01, University of Toronto, Canada, May 2006.
- [104] F. Garin and L. Schenato. A survey on distributed estimation and control applications using linear consensus algorithms. In A. Bemporad, M. Heemels, and M. Johansson, editors, *Networked Control Systems*, LNCIS, pages 75–107. Springer, 2010.
- [105] A. Ghosh, S. Boyd, and A. Saberi. Minimizing effective resistance of a graph. *SIAM Review*, 50(1):37–66, 2008.
- [106] A. K. Ghosh, B. Chance, and E. K. Pye. Metabolic coupling and synchronization of NADH oscillations in yeast cell populations. *Archives of Biochemistry and Biophysics*, 145(1):319–331, 1971.
- [107] C. D. Godsil and G. F. Royle. *Algebraic Graph Theory*, volume 207 of *Graduate Texts in Mathematics*. Springer, 2001.
- [108] J. Gómez-Gardeñes, Y. Moreno, and A. Arenas. Paths to synchronization on complex networks. *Physical Review Letters*, 98(3):34101, 2007.
- [109] X. Goudou and J. Munier. The gradient and heavy ball with friction dynamical systems: the quasiconvex case. *Mathematical Programming*, 116(1):173–191, 2009.
- [110] I. A. Gravagne and I. D. Walker. On the structure of minimum effort solutions with application to kinematic redundancy resolution. *IEEE Transactions on Robotics and Automation*, 16(6):855–863, 2000.

- [111] C. Grigg, P. Wong, P. Albrecht, R. Allan, M. Bhavaraju, R. Billinton, Q. Chen, C. Fong, S. Haddad, S. Kuruganty, W. Li, R. Mukerji, D. Patton, N. Rau, D. Reppen, A. Schneider, M. Shahidehpour, and C. Singh. The IEEE Reliability Test System - 1996. A report prepared by the Reliability Test System Task Force of the Application of Probability Methods Subcommittee. *IEEE Transactions on Power Systems*, 14(3):1010–1020, 1999.
- [112] S. Grijalva and P. W. Sauer. A necessary condition for power flow Jacobian singularity based on branch complex flows. *IEEE Transactions on Circuits and Systems I: Fundamental Theory and Applications*, 52(7):1406–1413, 2005.
- [113] Santiago Grijalva. Individual branch and path necessary conditions for saddle-node bifurcation voltage collapse. *IEEE Transactions on Power Systems*, 27(1):12–19, 2012.
- [114] I. Gutman and W. Xiao. Generalized inverse of the Laplacian matrix and some applications. *Bulletin: Classe des Sciences Mathématiques et Naturelles, Sciences Mathématiques*, 129(29):15–23, 2004.
- [115] I. Ha and J. Lee. Analysis on a minimum infinity-norm solution for kinematically redundant manipulators. *ICASE Transaction on Control, Automation and Systems Engineering*, 4(2):130–139, 2002.
- [116] S.-Y. Ha, T. Ha, and J.-H. Kim. On the complete synchronization of the Kuramoto phase model. *Physica D: Nonlinear Phenomena*, 239(17):1692–1700, 2010.
- [117] S. Y. Ha, E. Jeong, and M. J. Kang. Emergent behaviour of a generalized Viscek-type flocking model. *Nonlinearity*, 23(12):3139–3156, 2010.
- [118] S. Y. Ha and M. J. Kang. On the basin of attractors for the unidirectionally coupled Kuramoto model in a ring. *SIAM Journal on Applied Mathematics*, 72(5):1549–1574, 2012.
- [119] S. Y. Ha and M. Slemrod. A fast-slow dynamical systems theory for the Kuramoto type phase model. *Journal of Differential Equations*, 251(10):2685–2695, 2011.
- [120] S.Y. Ha, C. Lattanzio, B. Rubino, and M. Slemrod. Flocking and synchronization of particle models. *Quarterly Applied Mathematics*, 69:91–103, 2011.
- [121] M. M. Hamada, M. A. A. Wahab, and N. G. A. Hemdan. Simple and efficient method for steady-state voltage stability assessment of radial distribution systems. *Electric Power Systems Research*, 80(2):152–160, 2010.

- [122] Maria A. Hanley. Frequency instability problems in North American interconnections. *Department of Energy report*, DOE/NETL-2011/1473, June 2011.
- [123] D. J. Hill and G. Chen. Power systems as dynamic networks. In *IEEE Int. Symposium on Circuits and Systems*, pages 722–725, Kos, Greece, May 2006.
- [124] I. A. Hiskens. Analysis tools for power systems—contending with nonlinearities. *Proceedings of the IEEE*, 83(11):1573–1587, 2002.
- [125] W. Hoeffding. Probability inequalities for sums of bounded random variables. *Journal of the American Statistical Association*, 58(301):13–30, 1963.
- [126] H. Hong, M. Y. Choi, J. Yi, and K. S. Soh. Inertia effects on periodic synchronization in a system of coupled oscillators. *Physical Review E*, 59(1):353, 1999.
- [127] H. Hong, G. S. Jeon, and M. Y. Choi. Spontaneous phase oscillation induced by inertia and time delay. *Physical Review E*, 65(2):026208, 2002.
- [128] Y. W. Hong and A. Scaglione. A scalable synchronization protocol for large scale sensor networks and its applications. *IEEE Journal on Selected Areas in Communications*, 23(5):1085–1099, 2005.
- [129] F. C. Hoppensteadt and E. M. Izhikevich. *Weakly Connected Neural Networks*. Springer, 1997.
- [130] F. C. Hoppensteadt and E. M. Izhikevich. Synchronization of laser oscillators, associative memory, and optical neurocomputing. *Physical Review E*, 62(3):4010–4013, 2000.
- [131] F. C. Hoppensteadt and E. M. Izhikevich. Synchronization of MEMS resonators and mechanical neurocomputing. *IEEE Transactions on Circuits and Systems I: Fundamental Theory and Applications*, 48(2):133–138, 2001.
- [132] R. A. Horn and C. R. Johnson. *Matrix Analysis*. Cambridge University Press, 1985.
- [133] C. Huepe, R. F. Cadiz, and M. Colasso. Generating music from flocking dynamics. In *American Control Conference*, pages 4339–4344, Montréal, Canada, June 2012.
- [134] C. Huygens. *Oeuvres Complètes De Christiaan Huygens*. Societe Hollandaise des Sciences, The Hague, Netherlands, 1893. M. Nijhoff, ed.
- [135] A. J. Ijspeert. Central pattern generators for locomotion control in animals and robots: A review. *Neural Networks*, 21(4):642–653, 2008.

- [136] M. Ilić. Network theoretic conditions for existence and uniqueness of steady state solutions to electric power circuits. In *IEEE International Symposium on Circuits and Systems*, pages 2821–2828, San Diego, CA, USA, May 1992.
- [137] E. M. Izhikevich. *Dynamical Systems in Neuroscience: The Geometry of Excitability and Bursting*. MIT Press, 2007.
- [138] E. M. Izhikevich and Y. Kuramoto. Weakly coupled oscillators. *Encyclopedia of Mathematical Physics*, 5:448, 2006.
- [139] A. Jadbabaie, N. Motesharref, and M. Barahona. On the stability of the Kuramoto model of coupled nonlinear oscillators. In *American Control Conference*, pages 4296–4301, Boston, MA, USA, June 2004.
- [140] J. Jarjis and F. D. Galiana. Quantitative analysis of steady state stability in power networks. *IEEE Transactions on Power Apparatus and Systems*, 100(1):318–326, 1981.
- [141] G. Jongen, J. Anemüller, D. Bollé, A. C. C. Coolen, and C. Perez-Vicente. Coupled dynamics of fast spins and slow exchange interactions in the XY spin glass. *Journal of Physics A: Mathematical and General*, 34(19):3957–3984, 2001.
- [142] E. W. Justh and P. S. Krishnaprasad. Equilibria and steering laws for planar formations. *Systems & Control Letters*, 52(1):25–38, 2004.
- [143] A. C. Kalloniatis. From incoherence to synchronicity in the network Kuramoto model. *Physical Review E*, 82(6):066202, 2010.
- [144] M. Kapitaniak, K. Czolczynski, P. Perlikowski, A. Stefanski, and T. Kapitaniak. Synchronization of clocks. *Physics Reports*, 517:1–69, 2012.
- [145] WH Kersting. Radial distribution test feeders. In *Power Engineering Society Winter Meeting, 2001. IEEE*, volume 2, pages 908–912. IEEE, 2001.
- [146] H. K. Khalil. *Nonlinear Systems*. Prentice Hall, 3 edition, 2002.
- [147] I. Z. Kiss, Y. Zhai, and J. L. Hudson. Emerging coherence in a population of chemical oscillators. *Science*, 296(5573):1676–1678, 2002.
- [148] D. J. Klein. *Coordinated Control and Estimation for Multi-agent Systems: Theory and Practice*. PhD thesis, University of Washington, 2008.
- [149] D. J. Klein, P. Lee, K. A. Morgansen, and T. Javidi. Integration of communication and control using discrete time Kuramoto models for multivehicle coordination over broadcast networks. *IEEE Journal on Selected Areas in Communications*, 26(4):695–705, 2008.

- [150] D. E. Koditschek. Strict global Lyapunov functions for mechanical systems. In *American Control Conference*, pages 1770–1775, Atlanta, GA, USA, June 1988.
- [151] D. E. Koditschek. The application of total energy as a Lyapunov function for mechanical control systems. In J. E. Marsden, P. S. Krishnaprasad, and J. C. Simo, editors, *Dynamics and Control of Multibody Systems*, volume 97, pages 131–157. AMS, 1989.
- [152] N. Kopell and G. B. Ermentrout. Coupled oscillators and the design of central pattern generators. *Mathematical Biosciences*, 90(1-2):87–109, 1988.
- [153] G. Korniss, M. B. Hastings, K. E. Bassler, M. J. Berryman, B. Kozma, and D. Abbott. Scaling in small-world resistor networks. *Physics Letters A*, 350(5-6):324–330, 2006.
- [154] Andrew J Korsak. On the question of uniqueness of stable load-flow solutions. *Power Apparatus and Systems, IEEE Transactions on*, (3):1093–1100, 1972.
- [155] G. Kozyreff, A. G. Vladimirov, and P. Mandel. Global coupling with time delay in an array of semiconductor lasers. *Physical Review Letters*, 85(18):3809–3812, 2000.
- [156] P. Kundur. *Power System Stability and Control*. McGraw-Hill, 1994.
- [157] P. Kundur, J. Paserba, V. Ajjarapu, G. Andersson, A. Bose, C. Canizares, N. Hatziargyriou, D. Hill, A. Stankovic, C. Taylor, et al. Definition and classification of power system stability. IEEE/CIGRE joint task force on stability terms and definitions. *IEEE Transactions on Power Systems*, 19(3):1387–1401, 2004.
- [158] Y. Kuramoto. Self-entrainment of a population of coupled non-linear oscillators. In H. Araki, editor, *Int. Symposium on Mathematical Problems in Theoretical Physics*, volume 39 of *Lecture Notes in Physics*, pages 420–422. Springer, 1975.
- [159] Y. Kuramoto. *Chemical Oscillations, Waves, and Turbulence*. Springer, 1984.
- [160] Y. Kuramoto. Cooperative dynamics of oscillator community. *Progress of Theoretical Physics Supplement*, 79:223–240, 1984.
- [161] Y. Kuramoto. Collective synchronization of pulse-coupled oscillators and excitable units. *Physica D: Nonlinear Phenomena*, 50(1):15–30, 1991.

- [162] J. Lavaei, D. Tse, and B. Zhang. Geometry of power flows in tree networks. In *IEEE Power & Energy Society General Meeting*, San Diego, CA, USA, 2012. To appear.
- [163] N. E. Leonard, T. Shen, B. Nabet, L. Scardovi, I. D. Couzin, and S. A. Levin. Decision versus compromise for animal groups in motion. *Proceedings of the National Academy of Sciences*, 109(1):227–232, 2012.
- [164] B. C. Lesieutre, P. W. Sauer, and M. A. Pai. Existence of solutions for the network/load equations in power systems. *IEEE Transactions on Circuits and Systems I: Fundamental Theory and Applications*, 46(8):1003–1011, 1999.
- [165] Z. Lin, B. Francis, and M. Maggiore. Necessary and sufficient graphical conditions for formation control of unicycles. *IEEE Transactions on Automatic Control*, 50(1):121–127, 2005.
- [166] Z. Lin, B. Francis, and M. Maggiore. State agreement for continuous-time coupled nonlinear systems. *SIAM Journal on Control and Optimization*, 46(1):288–307, 2007.
- [167] W. C. Lindsey, F. Ghazvinian, W. C. Hagmann, and K. Dessouky. Network synchronization. *Proceedings of the IEEE*, 73(10):1445–1467, 1985.
- [168] C. Liu, D. R. Weaver, S. H. Strogatz, and S. M. Reppert. Cellular construction of a circadian clock: period determination in the suprachiasmatic nuclei. *Cell*, 91(6):855–860, 1997.
- [169] W. Lohmiller and J.-J. E. Slotine. On contraction analysis for non-linear systems. *Automatica*, 34(6):683–696, 1998.
- [170] J. Lunze. Complete synchronization of Kuramoto oscillators. *Journal of Physics A: Mathematical and Theoretical*, 44:425102, 2011.
- [171] J. Lunze. Synchronization of heterogeneous agents. *IEEE Transactions on Automatic Control*, 57(11):2885–2890, 2012.
- [172] Y. L. Maistrenko, O. V. Popovych, and P. A. Tass. Desynchronization and chaos in the Kuramoto model. In J.-R. Chazottes and B. Fernandez, editors, *Dynamics of Coupled Map Lattices and of Related Spatially Extended Systems*, volume 671 of *Lecture Notes in Physics*, pages 285–306. Springer, 2005.
- [173] E. Mallada and A. Tang. Synchronization of phase-coupled oscillators with arbitrary topology. In *American Control Conference*, pages 1777–1782, Baltimore, MD, USA, June 2010.

- [174] E. Mallada and A. Tang. Distributed clock synchronization: Joint frequency and phase consensus. In *IEEE Conf. on Decision and Control and European Control Conference*, pages 6742–6747, Orlando, FL, USA, December 2011.
- [175] E. A. Martens, E. Barreto, S. H. Strogatz, E. Ott, P. So, and T. M. Antonsen. Exact results for the Kuramoto model with a bimodal frequency distribution. *Physical Review E*, 79(2):26204, 2009.
- [176] O. Mason and M. Verwoerd. Graph theory and networks in biology. *IET Systems Biology*, 1(2):89–119, 2007.
- [177] A. Mauroy, P. Sacré, and R. J. Sepulchre. Kick synchronization versus diffusive synchronization. In *IEEE Conf. on Decision and Control*, pages 7171–7183, Maui, HI, USA, December 2012.
- [178] A. Mauroy and R. Sepulchre. Contraction of monotone phase-coupled oscillators. *Systems & Control Letters*, 61(11):1097–1102, 2012.
- [179] D. Mehta and M. Kastner. Stationary point analysis of the one-dimensional lattice Landau gauge fixing functional, aka random phase XY Hamiltonian. *Annals of Physics*, 326(6):1425–1440, 2011.
- [180] M. Mesbahi and M. Egerstedt. *Graph Theoretic Methods in Multiagent Networks*. Princeton University Press, 2010.
- [181] C. D. Meyer. *Matrix Analysis and Applied Linear Algebra*. SIAM, 2001.
- [182] D. C. Michaels, E. P. Matyas, and J. Jalife. Mechanisms of sinoatrial pacemaker synchronization: a new hypothesis. *Circulation Research*, 61(5):704–714, 1987.
- [183] R. Mirollo and S. H. Strogatz. The spectrum of the partially locked state for the Kuramoto model. *Journal of Nonlinear Science*, 17(4):309–347, 2007.
- [184] R. E. Mirollo and S. H. Strogatz. Synchronization of pulse-coupled biological oscillators. *SIAM Journal on Applied Mathematics*, 50(6):1645–1662, 1990.
- [185] R. E. Mirollo and S. H. Strogatz. The spectrum of the locked state for the Kuramoto model of coupled oscillators. *Physica D: Nonlinear Phenomena*, 205(1-4):249–266, 2005.
- [186] A. Mirzaei, M. E. Heidari, R. Bagheri, S. Chehrazi, and A. A. Abidi. The quadrature LC oscillator: A complete portrait based on injection locking. *IEEE Journal of Solid-State Circuits*, 42(9):1916–1932, 2007.
- [187] T. Mizumoto, T. Otsuka, K. Nakadai, T. Takahashi, K. Komatani, T. Ogata, and H. G. Okuno. Human-robot ensemble between robot thereminist and human percussionist using coupled oscillator model. In *IEEE/RSJ Int. Conf.*

- on *Intelligent Robots & Systems*, pages 1957–1963, Taipei, Taiwan, October 2010.
- [188] B. Mohar. The Laplacian spectrum of graphs. In Y. Alavi, G. Chartrand, O. R. Oellermann, and A. J. Schwenk, editors, *Graph Theory, Combinatorics, and Applications*, volume 2, pages 871–898. Wiley, 1991.
- [189] P. Monzón and F. Paganini. Global considerations on the Kuramoto model of sinusoidally coupled oscillators. In *IEEE Conf. on Decision and Control*, pages 3923–3928, San Diego, CA, USA, December 2005.
- [190] L. Moreau. Stability of continuous-time distributed consensus algorithms. In *IEEE Conf. on Decision and Control*, pages 3998–4003, Nassau, Bahamas, 2004.
- [191] L. Moreau. Stability of multiagent systems with time-dependent communication links. *IEEE Transactions on Automatic Control*, 50(2):169–182, 2005.
- [192] Y. Moreno and A. F. Pacheco. Synchronization of Kuramoto oscillators in scale-free networks. *Europhysics Letters*, 68:603, 2004.
- [193] A. E. Motter, S. A. Myers, M. Anghel, and T. Nishikawa. Spontaneous synchrony in power-grid networks. *Nature Physics*, February 2013.
- [194] U. Münz, A. Papachristodoulou, and F. Allgöwer. Consensus reaching in multi-agent packet-switched networks with non-linear coupling. *International Journal of Control*, 82(5):953–969, 2009.
- [195] A. Nabi and J. Moehlis. Single input optimal control for globally coupled neuron networks. *Journal of Neural Engineering*, 8:065008, 2011.
- [196] Z. Néda, E. Ravasz, T. Vicsek, Y. Brechet, and A.-L. Barabási. Physics of the rhythmic applause. *Physical Review E*, 61(6):6987–6992, 2000.
- [197] NERC. Final Report on the August 14, 2003 Blackout in the United States and Canada: Causes and Recommendations, April 2004. Available at <http://www.nerc.com/filez/blackout.html>.
- [198] T. Nishikawa, A. E. Motter, Y. C. Lai, and F. C. Hoppensteadt. Heterogeneity in oscillator networks: Are smaller worlds easier to synchronize? *Physical Review Letters*, 91(1):14101, 2003.
- [199] R. Olfati-Saber. Swarms on sphere: A programmable swarm with synchronous behaviors like oscillator networks. In *IEEE Conf. on Decision and Control*, pages 5060–5066, San Diego, CA, USA, 2006.

- [200] R. Olfati-Saber, J. A. Fax, and R. M. Murray. Consensus and cooperation in networked multi-agent systems. *Proceedings of the IEEE*, 95(1):215–233, 2007.
- [201] R. Olfati-Saber and R. M. Murray. Consensus problems in networks of agents with switching topology and time-delays. *IEEE Transactions on Automatic Control*, 49(9):1520–1533, 2004.
- [202] R. E. O’Malley. *Singular Perturbation Methods for Ordinary Differential Equations*. Springer, 1991.
- [203] G. V. Osipov, J. Kurths, and C. Zhou. *Synchronization in Oscillatory Networks*. Springer, 2007.
- [204] E. Ott and T. M. Antonsen. Low dimensional behavior of large systems of globally coupled oscillators. *Chaos: An Interdisciplinary Journal of Non-linear Science*, 18(3):037113, 2008.
- [205] F. Paganini and B. C. Lesieutre. Generic properties, one-parameter deformations, and the BCU method. *IEEE Transactions on Circuits and Systems I: Fundamental Theory and Applications*, 46(6):760–763, 1999.
- [206] M. A. Pai. *Power System Stability*. North-Holland, 1981.
- [207] M. A. Pai. *Energy Function Analysis for Power System Stability*. Kluwer Academic Publishers, 1989.
- [208] MA Pai, Peter W Sauer, Bernard C Lesieutre, and Rambabu Adapa. Structural stability in power systems-effect of load models. *IEEE Transactions on Power Systems*, 10(2):609–615, 1995.
- [209] D. A. Paley, N. E. Leonard, R. Sepulchre, D. Grunbaum, and J. K. Parrish. Oscillator models and collective motion. *IEEE Control Systems Magazine*, 27(4):89–105, 2007.
- [210] J. Pantaleone. Stability of incoherence in an isotropic gas of oscillating neutrinos. *Physical Review D*, 58(7):073002, 1998.
- [211] J. Pantaleone. Synchronization of metronomes. *American Journal of Physics*, 70:992, 2002.
- [212] F. Pasqualetti, F. Dörfler, and F. Bullo. Cyber-physical attacks in power networks: Models, fundamental limitations and monitor design. In *IEEE Conf. on Decision and Control and European Control Conference*, pages 2195–2201, Orlando, FL, USA, December 2011.
- [213] F. Pasqualetti, F. Dörfler, and F. Bullo. Attack detection and identification in cyber-physical systems. *IEEE Transactions on Automatic Control*, August 2012. to appear.

- [214] F. Pasqualetti, F. Dörfler, and F. Bullo. Cyber-physical security via geometric control: Distributed monitoring and malicious attacks. In *IEEE Conf. on Decision and Control*, pages 3418–3425, Maui, HI, USA, December 2012.
- [215] L. M. Pecora and T. L. Carroll. Master stability functions for synchronized coupled systems. *Physical Review Letters*, 80(10):2109–2112, 1998.
- [216] A. Pluchino, S. Boccaletti, V. Latora, and A. Rapisarda. Opinion dynamics and synchronization in a network of scientific collaborations. *Physica A: Statistical Mechanics and its Applications*, 372(2):316–325, 2006.
- [217] A. Pluchino, V. Latora, and A. Rapisarda. Compromise and synchronization in opinion dynamics. *The European Physical Journal B - Condensed Matter and Complex Systems*, 50(1):169–176, 2006.
- [218] O. V. Popovych, Y. L. Maistrenko, and P. A. Tass. Phase chaos in coupled oscillators. *Physical Review E*, 71(6):065201, 2005.
- [219] P. Pourbeik, P. S. Kundur, and C. M. Taylor. The anatomy of a power grid blackout - root causes and dynamics of recent major blackouts. *IEEE Power and Energy Magazine*, 4(5):22–29, 2006.
- [220] M. M. U. Rahman, R. Mudumbai, and S. Dasgupta. Consensus based carrier synchronization in a two node network. In *IFAC World Congress*, pages 10038–10043, Milan, Italy, August 2011.
- [221] W. Ren, R. W. Beard, and E. M. Atkins. Information consensus in multi-vehicle cooperative control: Collective group behavior through local interaction. *IEEE Control Systems Magazine*, 27(2):71–82, 2007.
- [222] J. G. Restrepo, E. Ott, and B. R. Hunt. Onset of synchronization in large networks of coupled oscillators. *Physical Review E*, 71(3):036151, 2005.
- [223] J. G. Restrepo, E. Ott, and B. R. Hunt. Synchronization in large directed networks of coupled phase oscillators. *Chaos*, 16(1):015107–015107, 2006.
- [224] L. Righetti and A. J. Ijspeert. Programmable central pattern generators: an application to biped locomotion control. In *IEEE Int. Conf. on Robotics and Automation*, pages 1585–1590, Orlando, FL, USA, May 2006.
- [225] D. C. Roberts. Linear reformulation of the Kuramoto model of self-synchronizing coupled oscillators. *Physical Review E*, 77(3):031114, 2008.
- [226] C. Robinson. *Dynamical Systems: Stability, Symbolic Dynamics, and Chaos*. CRC Press, 1999.
- [227] J. A. Rogge and D. Aeyels. Stability of phase locking in a ring of unidirectionally coupled oscillators. *Journal of Physics A*, 37:11135–11148, 2004.

- [228] M. Rohden, A. Sorge, M. Timme, and D. Witthaut. Self-organized synchronization in decentralized power grids. *Physical Review Letters*, 109(6):064101, 2012.
- [229] D. Romeres, F. Dörfler, and F. Bullo. Novel results on slow coherency in consensus and power networks. In *European Control Conference*, Zürich, Switzerland, July 2013. To appear.
- [230] G. Russo, M. Di Bernardo, and E. D. Sontag. Stability of networked systems: A multi-scale approach using contraction. In *IEEE Conf. on Decision and Control*, pages 6559–6564, Atlanta, GA, USA, 2010.
- [231] P. Sacré and R. Sepulchre. System analysis of oscillator models in the space of phase response curves, 2012. Available at <http://arxiv.org/abs/1206.4144>.
- [232] A. Sarlette. *Geometry and Symmetries in Coordination Control*. PhD thesis, University of Liège, Belgium, January 2009.
- [233] A. Sarlette and R. Sepulchre. Consensus optimization on manifolds. *SIAM Journal on Control and Optimization*, 48(1):56–76, 2009.
- [234] S. Sastry and P. Varaiya. Hierarchical stability and alert state steering control of interconnected power systems. *IEEE Transactions on Circuits and Systems*, 27(11):1102–1112, 1980.
- [235] P. W. Sauer, B. C. Lesieutre, and M. A. Pai. Maximum loadability and voltage stability in power systems. *International Journal of Electrical Power & Energy Systems*, 15(3):145–153, 1993.
- [236] P. W. Sauer and M. A. Pai. *Power System Dynamics and Stability*. Prentice Hall, 1998.
- [237] L. Scardovi. Clustering and synchronization in phase models with state dependent coupling. In *IEEE Conf. on Decision and Control*, pages 627–632, Atlanta, GA, USA, December 2010.
- [238] L. Scardovi, A. Sarlette, and R. Sepulchre. Synchronization and balancing on the N -torus. *Systems & Control Letters*, 56(5):335–341, 2007.
- [239] G. S. Schmidt, U. Münz, and F. Allgöwer. Multi-agent speed consensus via delayed position feedback with application to Kuramoto oscillators. In *European Control Conference*, pages 2464–2469, Budapest, Hungary, August 2009.
- [240] G. S. Schmidt, A. Papachristodoulou, U. Münz, and F. Allgöwer. Frequency synchronization and phase agreement in Kuramoto oscillator networks with delays. *Automatica*, 48(12):3008–3017, 2012.

- [241] R. Sepulchre. Consensus on nonlinear spaces. *Annual Reviews in Control*, 35(1):56–64, 2011.
- [242] R. Sepulchre, D. A. Paley, and N. E. Leonard. Stabilization of planar collective motion: All-to-all communication. *IEEE Transactions on Automatic Control*, 52(5):811–824, 2007.
- [243] R. Sepulchre, D. A. Paley, and N. E. Leonard. Stabilization of planar collective motion with limited communication. *IEEE Transactions on Automatic Control*, 53(3):706–719, 2008.
- [244] R. Sepulchre, A. Sarlette, and P. Rouchon. Consensus in non-commutative spaces. In *IEEE Conf. on Decision and Control*, pages 6596–6601, Atlanta, GA, USA, December 2010.
- [245] D. Sherrington and S. Kirkpatrick. Solvable model of a spin-glass. *Physical Review Letters*, 35(26):1792–1796, 1975.
- [246] S. B. Shim, M. Imboden, and P. Mohanty. Synchronized oscillation in coupled nanomechanical oscillators. *Science*, 316(5821):95–99, 2007.
- [247] O. Simeone, U. Spagnolini, Y. Bar-Ness, and S. H. Strogatz. Distributed synchronization in wireless networks. *IEEE Signal Processing Magazine*, 25(5):81–97, 2008.
- [248] J. W. Simpson-Porco, F. Dörfler, and F. Bullo. Droop-controlled inverters are Kuramoto oscillators. In *IFAC Workshop on Distributed Estimation and Control in Networked Systems*, pages 264–269, Santa Barbara, CA, USA, September 2012.
- [249] J. W. Simpson-Porco, F. Dörfler, and F. Bullo. Synchronization and power sharing for droop-controlled inverters in islanded microgrids. *Automatica*, 49(9):2603–2611, 2013.
- [250] J. W. Simpson-Porco, F. Dörfler, and F. Bullo. Voltage stabilization in microgrids using quadratic droop control. In *IEEE Conf. on Decision and Control*, Florence, Italy, December 2013. To appear.
- [251] J. W. Simpson-Porco, F. Dörfler, Q. Shafiee, J. M. Guerrero, and F. Bullo. Stability, power sharing, & distributed secondary control in droop-controlled microgrids. In *IEEE Int. Conf. on Smart Grid Communications*, Vancouver, BC, Canada, October 2013. To appear.
- [252] Sherwin J Skar. Stability of multi-machine power systems with nontrivial transfer conductances. *SIAM Journal on Applied Mathematics*, 39(3):475–491, 1980.

- [253] P. S. Skardal, J. Sun, D. Taylor, and J. G. Restrepo. Effects of degree-frequency correlations on network synchronization: Universality and full phase-locking. *Europhysics Letters*, 101(2):20001, 2013.
- [254] E. D. Sontag. Contractive systems with inputs. In J. C. Willems, S. Hara, Y. Ohta, and H. Fujioka, editors, *Perspectives in Mathematical System Theory, Control, and Signal Processing*, pages 217–228. Springer, 2010.
- [255] E. H. Spanier. *Algebraic Topology*. Springer, 1994.
- [256] Daniel L Stein. Spin glasses: still complex after all these years? In *Decoherence and Entropy in Complex Systems*, pages 349–361. Springer, 2004.
- [257] B. Stott, J. Jardim, and O. Alsac. DC power flow revisited. *IEEE Transactions on Power Systems*, 24(3):1290–1300, 2009.
- [258] S. H. Strogatz. From Kuramoto to Crawford: Exploring the onset of synchronization in populations of coupled oscillators. *Physica D: Nonlinear Phenomena*, 143(1):1–20, 2000.
- [259] S. H. Strogatz. Exploring complex networks. *Nature*, 410(6825):268–276, 2001.
- [260] S. H. Strogatz. *SYNC: The Emerging Science of Spontaneous Order*. Hyperion, 2003.
- [261] S. H. Strogatz, D. M. Abrams, A. McRobie, B. Eckhardt, and E. Ott. Theoretical mechanics: Crowd synchrony on the Millennium Bridge. *Nature*, 438(7064):43–44, 2005.
- [262] S. H. Strogatz and R. E. Mirollo. Phase-locking and critical phenomena in lattices of coupled nonlinear oscillators with random intrinsic frequencies. *Physica D: Nonlinear Phenomena*, 31(2):143–168, 1988.
- [263] D. Subbarao, R. Uma, B. Saha, and M. V. R. Phanendra. Self-organization on a power system. *IEEE Power Engineering Review*, 21(12):59–61, 2001.
- [264] J. A. K. Suykens and G. V. Osipov. Introduction to focus issue: Synchronization in complex networks. *Chaos*, 18(3):037101–037101, 2008.
- [265] H. A. Tanaka, A. J. Lichtenberg, and S. Oishi. First order phase transition resulting from finite inertia in coupled oscillator systems. *Physical Review Letters*, 78(11):2104–2107, 1997.
- [266] H. A. Tanaka, A. J. Lichtenberg, and S. Oishi. Self-synchronization of coupled oscillators with hysteretic responses. *Physica D: Nonlinear Phenomena*, 100(3-4):279–300, 1997.

- [267] P. A. Tass. A model of desynchronizing deep brain stimulation with a demand-controlled coordinated reset of neural subpopulations. *Biological Cybernetics*, 89(2):81–88, 2003.
- [268] C. J. Tavora and O. J. M. Smith. Characterization of equilibrium and stability in power systems. *IEEE Transactions on Power Apparatus and Systems*, 91(3):1127–1130, 1972.
- [269] C. J. Tavora and O. J. M. Smith. Equilibrium analysis of power systems. *IEEE Transactions on Power Apparatus and Systems*, 91(3):1131–1137, 1972.
- [270] C. J. Tavora and O. J. M. Smith. Stability analysis of power systems. *IEEE Transactions on Power Apparatus and Systems*, 91(3):1138–1144, 1972.
- [271] R. Tempo, G. Calafiore, and F. Dabbene. *Randomized Algorithms for Analysis and Control of Uncertain Systems*. Springer, 2005.
- [272] A. K. Tilton, E. T. Hsiao-Wecksler, and P. G. Mehta. Filtering with rhythms: Application to estimation of gait cycle. In *American Control Conference*, pages 3433–3438, Montréal, Canada, June 2012.
- [273] R. Tönjes. *Pattern formation through synchronization in systems of non-identical autonomous oscillators*. PhD thesis, Universitäts Potsdam, Germany, 2007.
- [274] N. Tsofas, A. Arapostathis, and P. Varaiya. A structure preserving energy function for power system transient stability analysis. *IEEE Transactions on Circuits and Systems*, 32(10):1041–1049, 1985.
- [275] A. Tuladhar, H. Jin, T. Unger, and K. Mauch. Parallel operation of single phase inverter modules with no control interconnections. In *Applied Power Electronics Conference and Exposition*, pages 94–100, Atlanta, GA, USA, February 1997.
- [276] T. Van Cutsem and C. Vournas. *Voltage Stability of Electric Power Systems*. Springer, 1998.
- [277] J. L. van Hemmen and W. F. Wreszinski. Lyapunov function for the Kuramoto model of nonlinearly coupled oscillators. *Journal of Statistical Physics*, 72(1):145–166, 1993.
- [278] P. Varaiya, F. F. Wu, and R. L. Chen. Direct methods for transient stability analysis of power systems: Recent results. *Proceedings of the IEEE*, 73(12):1703–1715, 1985.
- [279] P. P. Varaiya, F. F. Wu, and J. W. Bialek. Smart operation of smart grid: Risk-limiting dispatch. *Proceedings of the IEEE*, 99(1):40–57, 2011.

- [280] F. Varela, J. P. Lachaux, E. Rodriguez, and J. Martinerie. The brainweb: Phase synchronization and large-scale integration. *Nature Reviews Neuroscience*, 2(4):229–239, 2001.
- [281] M. Verwoerd and O. Mason. Global phase-locking in finite populations of phase-coupled oscillators. *SIAM Journal on Applied Dynamical Systems*, 7(1):134–160, 2008.
- [282] M. Verwoerd and O. Mason. On computing the critical coupling coefficient for the Kuramoto model on a complete bipartite graph. *SIAM Journal on Applied Dynamical Systems*, 8(1):417–453, 2009.
- [283] M. Verwoerd and O. Mason. A convergence result for the Kuramoto model with all-to-all coupling. *SIAM Journal on Applied Dynamical Systems*, 10(3):906–920, 2011.
- [284] T. J. Walker. Acoustic synchrony: two mechanisms in the snowy tree cricket. *Science*, 166(3907):891–894, 1969.
- [285] W. Wang and B. Ghosh. Kuramoto models, coupled oscillations and laser networks. In *SICE Annual Conference*, pages 130–135, Kagawa, Japan, September 2007.
- [286] W. Wang and J.-J. E. Slotine. On partial contraction analysis for coupled nonlinear oscillators. *Biological Cybernetics*, 92(1):38–53, 2005.
- [287] Y. Wang and F. J. Doyle. Optimal phase response functions for fast pulse-coupled synchronization in wireless sensor networks. *IEEE Transactions on Signal Processing*, 60:5583–5588, 2012.
- [288] Y. Wang, F. Núñez, and F. J. Doyle. Increasing sync rate of pulse-coupled oscillators via phase response function design: theory and application to wireless networks. *IEEE Transactions on Control Systems Technology*, 2012. To appear.
- [289] P. Wieland. *From static to dynamic couplings in consensus and synchronization among identical and non-identical systems*. PhD thesis, Universität Stuttgart, 2010.
- [290] N. Wiener. *Cybernetics; or Control and Communication in the Animal and the Machine*. Wiley, 1948.
- [291] N. Wiener. *Nonlinear Problems in Random Theory*. MIT Press, 1958.
- [292] K. Wiesenfeld, P. Colet, and S. H. Strogatz. Frequency locking in Josephson arrays: Connection with the Kuramoto model. *Physical Review E*, 57(2):1563–1569, 1998.

- [293] D. A. Wiley, S. H. Strogatz, and M. Girvan. The size of the sync basin. *Chaos*, 16(1):015103, 2006.
- [294] A. T. Winfree. Biological rhythms and the behavior of populations of coupled oscillators. *Journal of Theoretical Biology*, 16(1):15–42, 1967.
- [295] A. T. Winfree. *The Geometry of Biological Time*. Springer, 2 edition, 2001.
- [296] Dirk Witthaut and Marc Timme. Braess’s paradox in oscillator networks, desynchronization and power outage. *New Journal of Physics*, 14(8):083036, 2012.
- [297] A. J. Wood and B. F. Wollenberg. *Power Generation, Operation, and Control*. Wiley, 2 edition, 1996.
- [298] F. Wu and S. Kumagai. Steady-state security regions of power systems. *IEEE Transactions on Circuits and Systems*, 29(11):703–711, 1982.
- [299] F. F. Wu and S. Kumagai. *Limits on Power Injections for Power Flow Equations to Have Secure Solutions*. Electronics Research Laboratory, College of Engineering, University of California, 1980.
- [300] H. Yin, P. G. Mehta, S. P. Meyn, and U. V. Shanbhag. Synchronization of coupled oscillators is a game. *IEEE Transactions on Automatic Control*, 57(4):920–935, 2012.
- [301] R. A. York and R. C. Compton. Quasi-optical power combining using mutually synchronized oscillator arrays. *IEEE Transactions on Microwave Theory and Techniques*, 39(6):1000–1009, 2002.
- [302] F. Zhang. *The Schur Complement and Its Applications*. Springer, 2005.
- [303] M. Zhang, G. S. Wiederhecker, S. Manipatruni, A. Barnard, P. McEuen, and M. Lipson. Synchronization of micromechanical oscillators using light. *Physical Review Letters*, 109(23):233906, 2012.
- [304] R. D. Zimmerman, C. E. Murillo-Sánchez, and D. Gan. MATPOWER: Steady-state operations, planning, and analysis tools for power systems research and education. *IEEE Transactions on Power Systems*, 26(1):12–19, 2011.
- [305] Y. Zou, M. H. Yin, and H.-D. Chiang. Theoretical foundation of the controlling UEP method for direct transient-stability analysis of network-preserving power system models. *IEEE Transactions on Circuits and Systems I: Fundamental Theory and Applications*, 50(10):1324–1336, 2003.